Solvent Manipulation, Dielectric Spectroscopy, and Rheological Analysis in the Electrospinning of a Rigid Rod Polymer

by Karmann Cressman Mills

SOLVENT MANIPULATION, DIELECTRIC SPECTROSCOPY, AND RHEOLOGICAL ANALYSIS IN THE ELECTROSPINNING OF A RIGID ROD POLYMER

A Thesis

Presented to the Faculty of the Graduate School

of Cornell University

In Partial Fulfillment of the Requirements for the Degree of

Master of Science

by

Karmann Cressman Mills

August 2010

ABSTRACT

The main contribution of this research work is the demonstration that a highly rigid polymer can be electrospun into nanofibers using judicious combining of a good and a bad solvent. This research project is also a comprehensive examination of the dielectric and rheological properties of binary solvent poly(etherimide) (PEI) solutions and the influence of these properties in the formation of nanofibers via the electrospinning process. PEI is a high heat resistant polymer with rigid-rod chain orientation. Electrospun nanofiber mats of PEI have potential to be used in a myriad of applications including high efficiency air filtration in high temperature environments, such as industrial smokestacks as well as fire resistant layering. Through carefully structured combinations of polymer, good solvent and bad solvent a full range of electrospun morphologies were created, evolving from beads to uniform fibers, which were mapped to the polymer and solvent concentrations.

Previous work has shown that rigid-rod PEI nanofibers could be electrospun by blending PEI with more flexible polymers, such as poly(etheretherketone) (PEEK). It is proposed that a positive alternative to polymer blending would be the replacement of a percentage of the good solvent with a miscible bad solvent. The advantage of the proposed approach is that the resulting fibers are composed of 100% PEI hence avoiding the compromise on the PEI's thermal and mechanical properties induced by a polymer blend with a flexible polymer.

This projected used dimethylacetamide (DMAc) as the good solvent and tetrahydrofuran (THF) as the bad solvent. Dynamic rheological measurements were used to evaluate how the addition of a bad solvent to polymer-good solvent solutions modified the resulting electrospun nanofibers. Also, the bad solvent was used to dissolve polymer into the good solvent at percentages higher than the good solvent

super saturation point. It was demonstrated that although THF lowers the viscosity of PEI/DMAc solutions, the addition of THF produces better PEI electrospun nanofibers. Because of THF's effect on the PEI chain volume and dissolution, and its high evaporation rate, the addition of THF and other "bad" solvents may add a new degree of freedom to the formation of nanofibers from rig-rod polymers via electrospinning.

BIOGRAPHICAL SKETCH

Karmann Cressman Mills, born July 1983, grew up in the Raleigh/Cary, North Carolina area, where she graduated from Southeast Raleigh High School (2001). She graduated from North Carolina State University (2005) with a Bachelor of Science degree in Polymer and Color Chemistry and a minor in Journalism. She is wife to Brandon and mother to Adelaide Frances.

This work is dedicated to my husband, Brandon, who sacrificed of himself so that I could take this two year opportunity. I aspire to be as equal a blessing to you in return, and could not have accomplished this degree without your loving support.

ACKNOWLEDGMENTS

Many thanks to Dr. Juan Hinestroza, Dr. Martin Wells and Dr. Margaret Frey for your time and advisement and to my research lab mates in the Hinestroza group from ’06 to ’08 for your immense support and care.

TABLE OF CONTENTS

LIST OF FIGURES

LIST OF TABLES

CHAPTER 1

INTRODUCTION

This research project is a comprehensive examination of the dielectric and rheological properties of binary solvent poly(etherimide) (PEI) solutions and their influences in the formation of nanofibers via the electrospinning process. It is proposed that understanding the relationships between dielectric and mechanical relaxation behaviors in polymeric solutions can provide a new perspective on the fundamentals of the electrospinning process. The hypothesis of this work is that cooperating electrical and mechanical behaviors control fiber formation during electrospinning. Because electrospinning involves the application of a high electric field, it is proposed that electrical analysis, by way of dielectric spectroscopy, will lead to better understanding of the electrospinning process. Emphasis was placed on evaluating dielectric spectroscopy as a prediction tool for fiber formation. Because both dielectric and rheological analyses can evaluate molecular relaxations, this thesis employs rheological analysis – a method with well established connections to electrospinning – as the mechanical comparison to the dielectric results.

Also, emphasis is placed on understanding the influence of adding a bad solvent to a polymer-good solvent system. A good solvent is that which successfully dissolves the solute in question, while a bad solvent is repelled by the solute. Through carefully structured combinations of polymer, good solvent and bad solvent in this work, a full range of electrospun morphologies, from beads to uniform fibers, is created and these morphologies were "mapped" to the polymer concentration as well as the solvent ratio.

PEI is a high heat resistant polymer with rigid-rod chain orientation. Electrospun nanofiber mats of PEI have the potential to provide high efficiency air filtration in

many high temperature environments, such as industrial smokestacks. Previous researchers showed the blending of rigid polymers, like PEI, with more flexible polymers in order to form electrospun nanofibers. This thesis work proposes that a positive alternative to added polymers is the replacement of a percentage of the good solvent with a miscible bad solvent. This project uses dimethylacetamide (DMAc) as the good solvent and tetrahydrofuran (THF) as the bad solvent.

Rheological analysis is an essential tool for understanding viscosity and viscoelastic properties. For this reason, dynamic rheological measurements are used to also evaluate how adding a bad solvent to polymer-good solvent solutions modifies the electrospinning process. In this research work, through electron microscopy, the fiber formation of PEI solutions is characterized. Then, with the help of dielectric spectroscopy and rheology, the influence of adding a bad solvent to a polymer-good solvent system is investigated. In this paper, the principles of both dielectric and rheological analyses are covered, along with a discussion of previous work on poly(etherimide) (PEI). The effect of polymer molecular weight and the effect of solvent combinations on dielectric properties of PEI solutions have not previously been investigated.Results of this research work showed that increasing either or both polymer and bad solvent concentrations produced uniform fibers. Statistical analysis of the dielectric data showed that permittivity of the polymer solutions could not be directly related to electrospun morphology. However, rheological data were successfully correlated via statistical modeling to electrospun morphology. A new dimensionless number was created to express the morphology regions of electrospun PEI/DMAc/THF systems. This electrospinning number, E, is capable of predicting the electrospun morphology given the solution's concentrations and viscosity.

CHAPTER 2

LITERATURE REVIEW

2.1 Poly(etherimide)

Poly(etherimide) (PEI) is an amorphous polymer that can be obtained from the condensation of bisphenol A, phthalic acid anhydride and m-phenylenediamine.[1] PEI is commercially known as Ultem®. Its synthesis was first reported by White *et al.* [20] The class of structures for this condensation polymer was initially explored at General Electric (GE) and first reported in 1984. [2]

GE's Ultem (Figure 2.1), now sold by SABIC Innovative Plastics, is produced through an imidization polymerization, which is presented in Figure 2.2. This process uses bis-ether-dianhydride monomers which are prepared in several steps, a critical part being the aromatic nucleophilic nitro-displacement. In this key step it is crucial to eliminate water from the system, because any water will turn the nitro-imide groups into nitro-amic-acid salt (Figure 2.3), thus restricting the nitro group from later being displaced in the polymerization process and ruining the possibility for high molecular weight chains.

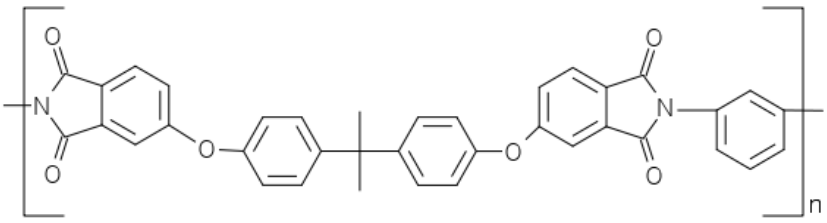

Figure 2.1 GE Ultem (Ultem 1000 MW ~ 41,000 g/mol, Ultem 1010 MW ~ 33,000 g/mol) [1]

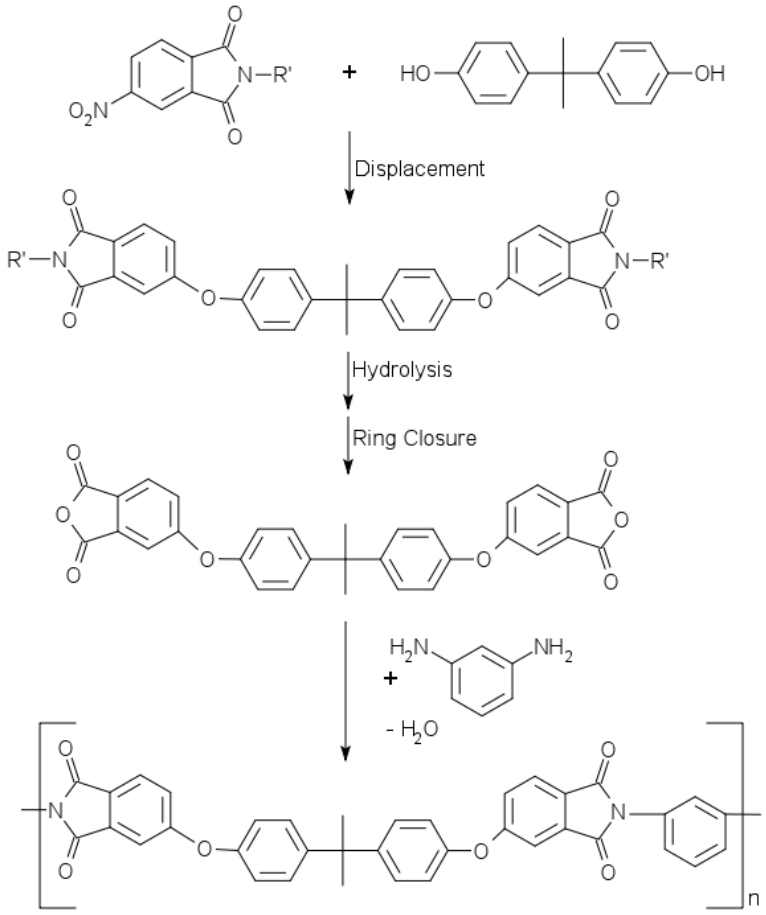

Figure 2.2 Synthesis of GE's Ultem [2]

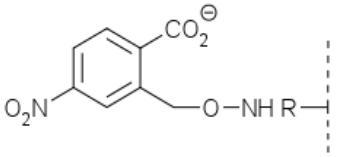

Figure 2.3 Nitro-amic-acid salt a casualty of the presence of water in the synthesis of PEI [2]

2.1.1 Applications

PEI, most frequently Ultem 1000 (41,000 g/mol), is used in many applications, the majority of which are composite resin materials. These end uses are chosen because PEI exhibits excellent mechanical properties, fire-retardancy, and thermo-stability.

Poly(etherimide) composites have been investigated using several methods. Recent investigations have included reinforcing PEI resin with nanotubes and nanoparticles [21-23], and blending PEI with poly(etheretherketone) (PEEK) [24-26] and montmorillonite. [27-30]

Yudin *et al.* combined Ultem 1000 melt with magnesium hydrosilicate nanotubes. [23] Previous success improving the physical properties using nanofillers for reinforcement of polymers motivated this experiment with PEI. The nanotubes used in Yudin *et al.*'s study were of a lower dielectric constant than that of neat films of PEI. The resulting composite reduced the dielectric constant from neat PEI as much as 24% (2.9 to 2.2) as well as improved stiffness and strength. Researchers predicted incentives for end use of this material as protective coatings for microelectronics and applications needing flammability reductive coatings. Moon *et al.*[26] tested the adhesion between composite seams of PEI and carbon fiber poly-etheretherketone (CF PEEK). Results indicated an adhesive bond of PEI and CF PEEK was stronger than that of other amorphous polymers. Huang *et al.* [28] melt blended montmorillonite with PEI which, because of the dispersion of the clay and the strong interaction between polymer and clay, resulted in a composite with higher glass transition temperature (T_g) as well as a higher thermal decomposition temperature than that of neat PEI. Naskar and Edie [31] utilized Ultem powder to coat and link carbon fibers. Because of inherent storage limitations for support structures in outer space use, researchers were looking for a crosslinkable thermoplastic polymer with good radiation resistance to use in strengthening the currently used collapsible carbon fiber structures. By heat-cross-

linking the Ultem powder around the poly(acrilonitrile)-based carbon fibers, a sturdy composite was created. Naskar and Edie's goal was to create a rigidization method through the application of electrical current to a powder coating. Based on the characterization by SEM and tensile testing of the electrified PEI coated carbon fibers, it was concluded that the composite exhibited potential for providing rigidity to inflatable structures for outer space.

2.1.2 Mechanical Properties

Results from Relles' testing of Ultem resin's typical mechanical properties can be found in Table 2.1. [2]

Table 2.1 Typical mechanical properties of Ultem resin (received from manufacturer)

ASTM Test	Mechanical Property	Ultem 1000	Ultem 1010
D638	Tensile strength, Yield	110 N/mm^2	110 N/mm^2
	Tensile Elongation, Yield	7 %	7 %
	Tensile Elongation, Ultimate	60%	60%
D790	Flexural Strength	165 N/mm^2	165 N/mm^2
	Flexural Modulus, Tangent	3,509 N/mm^2	3,509 N/mm^2
D695	Compressive Strength (2)	140 N/mm^2	-
	Compressive Modulus (2)	2,900 N/mm^2	-
	Shear Strength, Ultimate (2)	100 N/mm^2	-
D785	Rockwell Hardness	M109	M109

Belana *et al.* have described PEI's properties by its chemical structure. [1] Aromatic ring groups are inflexible and produce a very rigid chemical structure. The high content of aromatic rings provides PEI with superb thermal stability, while the

phthalimide groups provide the polymer with high heat resistance as well as good mechanical properties. The ether units connecting the aromatic groups allow PEI to be flexible and also have good melt flow behavior. Belana *et al.* performed differential scanning calorimetry (DSC) at different heating rates to determine the T_g of Ultem 1000. [1] Results showed a T_g ~ 220°C (Figure 2.4), which supports results published by H.M. Relles as well as results obtained in this research work. [2]

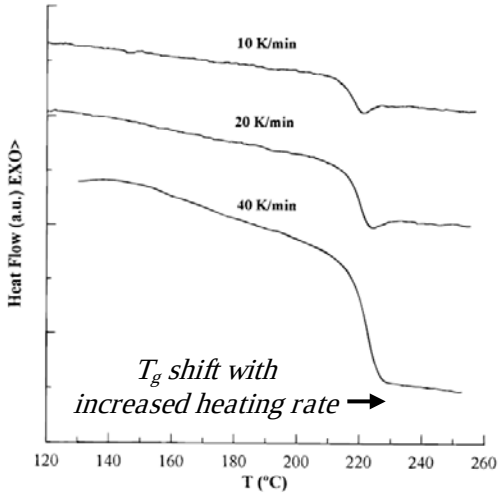

Figure 2.4 DSC of Ultem 1000 at different heating rates. The glass transition subtly shifts to higher temperatures when heating rate is increased. Because the T_g involves the motion of large chain segments in the sample, it is logical to see the chains not be able to respond when rate is increased. [1]

Belana *et al.*[1] also measured PEI films using dynamic mechanical analysis (DMA) and compared this data with results from dielectric analysis. These scans were performed at 3 Hz with temperature ranges from -150 – 250°C are compared in Figure 2.5.

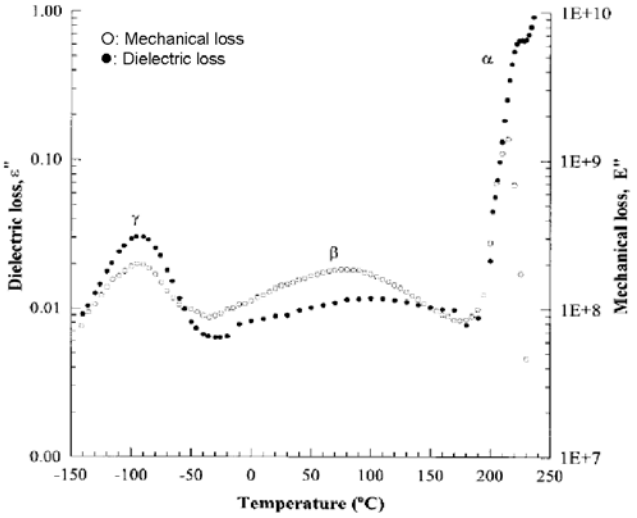

Figure 2.5 TSDC of PEI film at 3 Hz [1]

The activation energies of the relaxation peaks from DMA and dielectric analysis using thermally stimulated depolarization currents (TSDC) were shown to be similar, giving concurrence to the conclusion that the relaxations seen in mechanical analysis appear to be similar to those measured with dielectric spectroscopy. Table 2.2 lists the activation energies of each peak using mechanical and dielectric analyses. The *γ-relaxation* was found to be related to the hydration of a PEI sample. This was discovered through drying of the PEI film and retesting with TSDC. The *α-relaxation*, as with other polymers, was found to be strongly related to the glass transition, or bulk chain motion. Polymer relaxations are further discussed in Section 2.2.1. The *β-relaxation* of PEI has not been fully explained, but is thought to be the result of subtle chain reorientations involving the ether linkages. This broad peak is traditionally associated with dipole partial reorientation to the applied stress. [4, 32]

Table 2.2 Activation energies (E_a) associated with relaxation peaks of mechanical (DMA) and dielectric (DS) analyses [4]

Relaxation	E_a (kJ/mol)	
	DMA	DS
γ	48 ± 5	42 ± 5
β	212 ± 10	163 ± 10
α	706 ± 50	703 ± 50

As a factor in dielectric properties, chemical composition was analyzed for polymer thin film blends of PEI and PEEK by Goodwin and Simon. [54] The focus of the measurements was to determine the glass transition relaxation (*α -relaxation*). The samples showed a dramatic decrease in dielectric loss (ε″) magnitude of the 50/50 blend compared to the curves of each polymer, neat. The authors proposed this to be a result of the new molecular interactions, given the polymer blend. Also, PEEK had a relaxation peak at much lower frequencies than that of PEI. The 50/50 blend showed a relaxation between the two peaks of the neat polymers, but was decidedly closer to that of PEI. Goodwin and Simon concluded that this occurred because PEI has a longer relaxation time and because PEI also exists within the blend in small crystalline domains between PEEK.

Thermo-gravimetric analysis of PEI was performed by Choi *et al.* and was compared to that of their electrospun PEI fibers (Figure 2.6A). A dramatic change in thermostability was attributed to the presence of solvent, 1,1,2-trichloroethane, which remained attached to the polymer after electrospinning. Choi *et al.* were able to rectify this through heat treatment, as shown in Figure 2.6B.

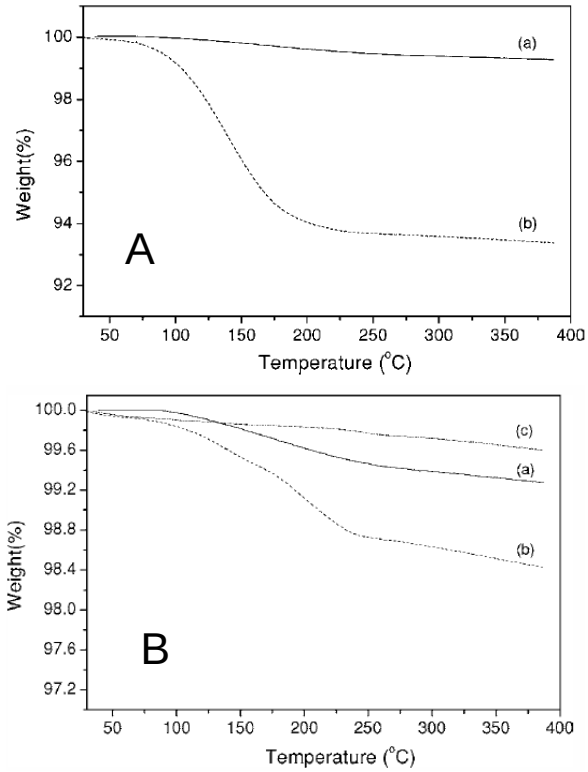

Figure 2.6 Thermogravimetric analysis of PEI. Graph A - (a): PEI as received, (b): electrospun PEI. Graph B – (a): PEI as received, (b): electrospun PEI after heat treatment at 150ºC, (c): electrospun PEI after heat treatment at 240ºC [3]

2.1.3 Electrical Properties

Typical electrical properties for Ultem 1000 are listed in Table 2.3. Dielectric constants at similar frequency for PEI solutions in DMAc and THF from this research are shown in Figure 4.17.

Table 2.3 Typical electrical properties of Ultem resin (as received from manufacturer)

ASTM Test	Electrical Property	Ultem 1000	Ultem 1010
D149	Dielectric strength (1/16")		
	In air	831 V/mil	830 V/mil
	In oil	710 V/mil	710 V/mil

Table 2.3 (Continued)

ASTM Test	Electrical Property	Ultem 1000	Ultem 1010
D150	Dielectric constant (1 kHz, 50% RH)	3.15	3.15
	Dissipation factor		
	1 kHz, 50% RH, 23ºC	0.0012	0.0013
	2450 kHz, 50% RH, 23ºC	0.0025	0.0025
D257	Volume resistivity (1/16")	10^{17} ohm.cm	10^{17} ohm.cm
D495	Arc resistance	128 sec	128 sec

Díaz-Calleja *et al.* investigated the dielectric relaxations of Ultem 1000 thin films. Figure 2.7 shows that PEI was found to exhibit three relaxations which were synonymous with that of the mechanical relaxation tests performed by Belana *et al.* The dielectric relaxations were measured by temperature sweeps and at varying frequencies. The relaxations were shown to be dependent on temperature and shifted to higher temperatures with an increase in frequency.

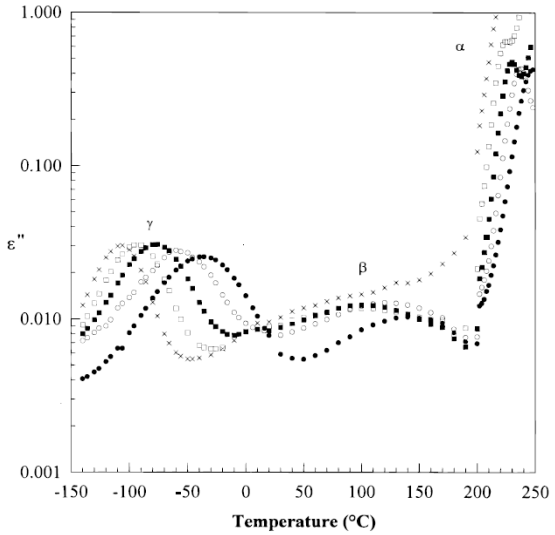

Figure 2.7 Dielectric loss (ε″) of PEI at several frequencies (x: 1 Hz, □: 10 Hz, ■: 100 Hz, ○: 1000 Hz, ●: 10,000 Hz) [4]

2.1.4 Previous Work – Converting PEI into Fiber

A fiber form is ideal to maximize surface area to volume ratio, thus providing a more effective product for applications such as filtration and sensors. For a fiber-form PEI, conventional melt-spinning and wet-spinning have been extensively investigated as methods to produce filtration membranes. [5, 33-37] Xu *et al.* [5] examined the morphologies of wet-spun PEI hollow fibers from solutions with DMAc as a solvent. DMAc was mixed with water to act as an inner coagulant. An example of the membrane is shown in Figure 2.8.

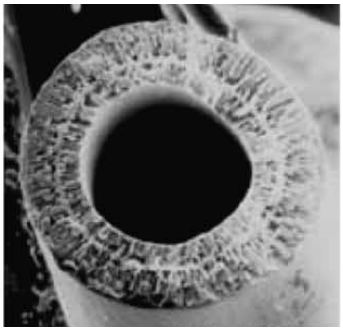

Figure 2.8 PEI hollow fiber membrane produced by wet-spinning for possible use in gas phase separation [5]

The electrospinnability of PEI has been explored previously for several reasons. Choi *et al.* used PEI for its thermoset-ability and, after electrospinning, produced interfiber bonds by heating the fiber mat up to 240°C (Figure 2.9). [3] The solvent used by Choi *et al.* was 1,1,2-trichloroethane and average fiber diameters for PEI at 14 wt% solution were between 500 and 700 nm. The fibers were formed using an applied voltage of 15 kV and a pipette-to-collector distance of 15 cm. They were collected onto a rotating drum covered in aluminum foil which was set in a vertical alignment under the loaded pipette.

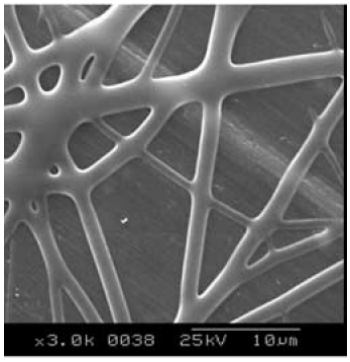

Figure 2.9 Scanning electron micrograph of electrospun PEI from a solution with 1,1,2-trichloroethane, heated to 240°C [3]

In an investigation of electrospun fiber shapes, Koombhongse *et al.* [6] produced ribbon-like nanofibers from a solution of 10 wt% Ultem 1000 in hexafluoro-2-propanol. The electrospinning set-up was vertically oriented, with a collector distance of 20 cm and an electric potential difference of 20 kV. The cause of the ribbon formation was rapid solvent evaporation from the outside of the jet, which formed a polymer 'skin,' leaving the rest of the solvent to diffuse through the skin in order to evaporate. This skin formation resulted in the collapse of the jet cylinder (Figure 2.10).

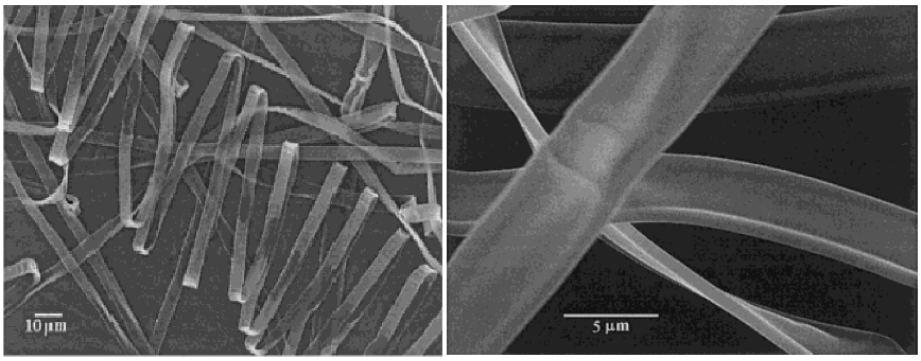

Figure 2.10 Scanning electron micrographs of electrospun PEI from a solution with hexafluoro-2-propanol [6]

Han *et al.* [7] electrospun blended solutions of PEI in chloroform with solutions of poly(3-hydroxybutyrate-*co*-3-hydroxyvalerate) (PHBV) in chloroform (Figure 2.11). These two polymers are not miscible, but when the solutions are combined, the polymers were found to electrospin together. The fiber mats were then thermally treated to degrade the PHBV, which has a much lower thermal resistance. The result was porous fibers with diameters ranging from 2.6-15.1 μm.

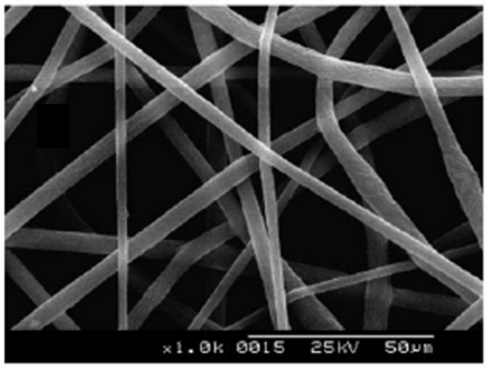

Figure 2.11 Scanning electron micrographs of electrospun PEI/PHBV (50/50) blend [7]

2.2 Dielectric Spectroscopy

Because electrospinning requires the application of a high electric field to a liquid sample, this thesis work investigated the electrical properties of PEI precursor solutions using dielectric spectroscopy. Through dielectric analysis, a greater understanding of the behavior of PEI solutions during electrospinning by determining the sample relaxations was sought.

2.2.1 Theory

Dielectric spectroscopy is used for measuring relaxation behavior of electrical dipoles when the sample is subjected to an electric field. The polarity of the applied electric field is typically alternated at a known frequency and is applied to the sample

over a desired range of frequencies or temperatures. This impact of the electric field is akin to that of a mechanical stress but does not physically deform the sample. Also, mechanical stress analysis only considers responses of a sample to physical forces, while dielectric analysis is able to examine more discrete motions in a sample not related to mechanics. The theories of mechanical and dielectric behavior for a sample have analogous values allowing for the comparison between the two. The shear stress on a sample (σ) is comparable to the stress from an electric field (E) and the strain of a sample (γ) is similar to the dissipation (D), while the complex shear compliance (J^*) is comparable to the complex permittivity of a sample to the electric field (ε^*). [16, 38]

$$\gamma = J^* \times \sigma \tag{1}$$

$$D = \varepsilon^* \times E \tag{2}$$

Complex permittivity,

$$\varepsilon^*(\omega) = \varepsilon'(\omega) - i\varepsilon''(\omega) \tag{3}$$

contains a real part, $\varepsilon'(\omega)$, which is the part of a sample's polarization in line with the electric field strength, $\underline{E}(t)$, and an imaginary part, $\varepsilon''(\omega)$, the contribution with a phase shift, where ω is angular frequency in rad/s ($\omega = 2\pi\upsilon$; υ in Hz). [39]

The majority of experimental uses for dielectric analysis involve simple samples of one or two components, usually in solid state. A basic reasoning for the lack of extensive study with complex samples was given by Kaatze and Feldman. [39] Because systems like solutions and emulsions show relaxation behavior on the mesoscopic scale and exhibit complicated behavior, they are only recently being investigated in this way. A liquid disperse system, like a polymer solution, is able to be analyzed by dielectric spectroscopy given its accumulation of charges at system boundaries. [40-43] The investigations cited by Kaatze and Feldman aimed toward a greater understanding of the molecular dynamics governing macroscopic properties of their systems.

In terms of a concentrated solution or melt, the applied electric field used in dielectric analysis is able to force the dipoles on a willing polymer chain to orient with the electric field. The time taken for these dipoles to reorient is considered to be one type of molecular relaxation. Different times are seen with disperse liquid systems, due to the additional components and their own interactions with the electric field. There are three levels of molecular relaxation (or movement) at which these adjustments take place, and each shows different relaxation times. [8, 44, 45] These three levels (Figure 2.12) are: (A) Local motion, or a rotation within a monomer unit, (B) Segment motion, like a flexing of a short side chain, and (C) Bulk chain motion, where a polymer chain fully exits its original occupying space and enters a new space.

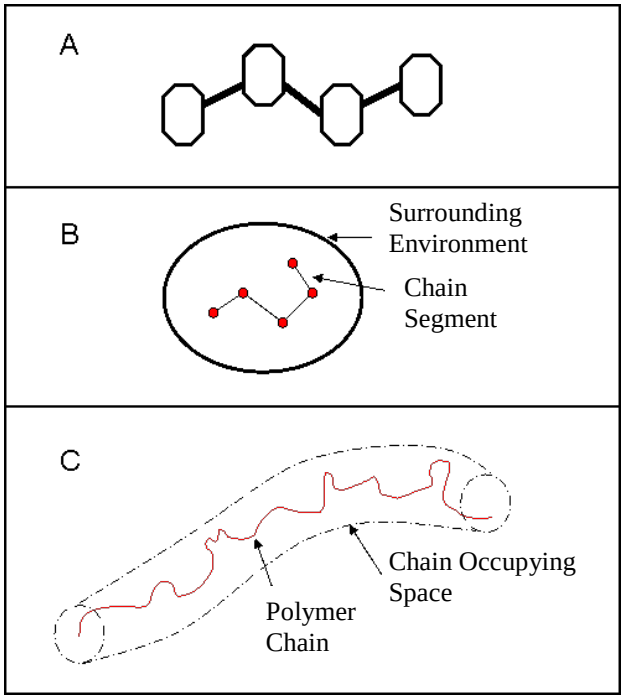

Figure 2.12 Relaxation behavior in a polymer chain. Figure adapted from Blythe (2005) [8]

This last motion also has the longest relaxation time, τ_{max}, and in a concentrated/entangled solution is generally related to the molecular weight of the

polymer chain (M) such that $\tau_{max} \propto M^3$. This time relationship was determined by de Gennes [45], and is called reptation time. When time is less than τ_{max} the solution will behave elastically, while flow occurs at time greater than τ_{max} because chains are given time to continue moving through space. However, with dilute polymer solutions, where chain entanglement does not govern the behavior of the liquid and solubility becomes an issue, a more complicated relationship between molecular weight and relaxation time is seen. Rouse's theory for dilute solutions suggests that $\tau \propto M^2$. [45] Zimm also developed a model for dilute polymer solution relaxations which predicts $\tau \propto M^{1.5}$. [46] Rouse and Zimm later amended both models of this relationship, while Adachi and Kotaka [47] established its validity with experimental work on a stiff polymer, *cis*-polyisoprene (*cis*-PI), in benzene (a good solvent) and dioxane (a theta solvent). Both Rouse and Zimm's independent theories did predict the relationship in theta solvent, but did not predict the correct relationship to molecular weight of a relaxation time in the benzene. However, the Rouse-Zimm theory,

$$\tau = \frac{1.4 M \eta_s [\eta]}{RT}, \tag{4}$$

where η_s is the viscosity of the solvent and $[\eta]$ is the intrinsic viscosity, was able to fit the double-log plots of relaxation time versus molecular weight for cis-PI in both polymers as well as with several other polymer solvent combinations. [32, 46, 48]

Polymer solutions have been shown to exhibit long-time relaxations, which are seen at low frequencies. [44, 49] Frequency domain dielectric spectroscopy is used for low frequency measurements and is a main focus of dielectric measurements in this project.

2.2.2 Modes of Operations

2.2.2.1 Frequency Domain

In each frequency domain measurement, a constant voltage is applied through the desired frequency range and temperature is held constant. The type of electrical circuit analyzer used in this research work is categorized as a lumped-circuit method of measurement, and it is always used in low frequency measurements (below 10^9 Hz). [8, 16] The lumped-circuit method (Figure 2.13) retrieves the equivalent electrical circuit of a sample at the frequencies used in the measurement.

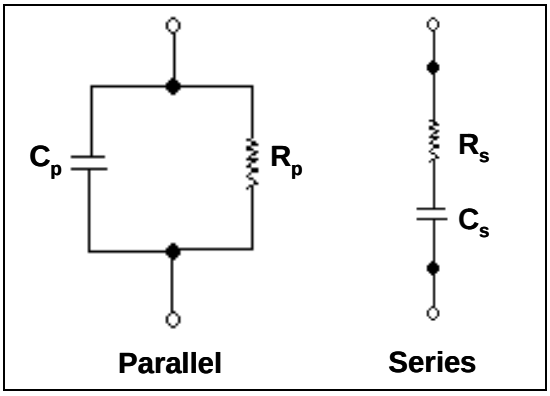

Figure 2.13 Lumped circuit in parallel and series alignment: C = Capacitance, R = Resistance

A solid sample measured by a dielectric spectrometer is placed between two plates of a capacitor and the relationship between the applied voltage and the related current is

$$I = \varepsilon^* C_0 \frac{dV}{dt} \tag{5}$$

where C_0 is the empty cell capacitance. To achieve the components of complex permittivity ($\varepsilon^* = \varepsilon' + i\varepsilon''$) the properties of the parallel circuit can be followed. The total impedance of the circuit, Z^*, is a complex number and is a relationship between the complex current and the complex voltage of the circuit,

$$Z^* = \frac{V^*}{I^*} \tag{6}$$

When an alternating voltage is applied to the sample, the real part of an out-of-phase, or capacitive, current (represented by $V = V_0 e^{i\omega t}$) will be produced. This can be referred to as the imaginary part of complex current, with $[V/Z]$, and is

$$I_c = i\omega C_p V \tag{7}$$

While the in-phase current (or the real part/resistive current, $\left[\frac{V}{R}\right]$) is

$$I_R = \frac{V}{R_p} \tag{8}$$

So, by these relationships it can be seen how the sample capacitance, C_p, is related to the sample impedance:

$$Z = R_p + \frac{1}{i\omega C_p} \tag{9}$$

By these circuit relationships, the components of permittivity can be seen (equations 10 and 11).

$$\varepsilon' = \frac{C_p}{C_0} \tag{10}$$

$$\varepsilon'' = \frac{1}{R_p C_0 \omega} \tag{11}$$

Permittivity mathematically connects the applied electric field and the electric displacement of that field by a sample as seen in equation 2. [8]

$$E = E_0 \cos \omega t \tag{12}$$

where E is an alternating electric field and E_0 is the amplitude of that field.

$$D = D_0 \cos(\omega t - \delta) \tag{13}$$

where D is the electrical displacement and δ is the phase lag. This phase lag is important, because in any application of an electric field to a sample, the orientation of

the sample dipoles will inevitably lag behind the applied field. [16] When D is expanded by the trigonometric addition and subtraction theorem,

$$D = D_0 \cos\delta \cos\omega t + D_0 \sin\delta \sin\omega t\,, \tag{14}$$

we can then see that D relates to permittivity by

$$\varepsilon' = \frac{D_0 \cos\delta}{\varepsilon_0 E_0} \tag{15}$$

$$\varepsilon'' = \frac{D_0 \sin\delta}{\varepsilon_0 E_0} \tag{16}$$

Also, from these two equations the components of ε^* can be related by δ as

$$\frac{\varepsilon''}{\varepsilon'} = \tan\delta \tag{17}$$

The quantity tan δ is commonly called the dissipation factor. Looking back at the first discussion of permittivity by the parallel circuit it is evident that

$$\tan\delta = \frac{\varepsilon''}{\varepsilon'} \propto \frac{energy\,dissipated\,/\,cycle}{energy\,/\,cycle}.$$

In the frequency domain of measurement where the independent variable is frequency, ε* can connect many variables in dielectric analysis. [16, 32, 39] It is also dependant on temperature, pressure and chemical structure of the sample. This complex permittivity is calculated through a relation of capacitance by

$$\varepsilon^*(\upsilon) = \frac{C}{C_0} \tag{18}$$

where C_0 is the empty cell capacitance and C is the capacitance of the sample. [49] Electric conductivity, σ, is a parameter measured by dielectric analysis and can translate to permittivity by

$$\varepsilon^* = \frac{\sigma}{i\omega\varepsilon_0} \tag{19}$$

where ε_0 is the permittivity in a vacuum (or the electric field constant) $8.85\times10^{-12} Fm^{-1}$. [8] Permittivity can also be related to the complex electric modulus, which is a less interpretable term in dielectric analysis.

$$G^* = \frac{1}{\varepsilon^*} = \frac{\varepsilon'}{\varepsilon'^2 + \varepsilon''^2} + i\frac{\varepsilon'}{\varepsilon'^2 + \varepsilon''^2} = G' + iG'' \tag{20}$$

Finally, permittivity is a value which relates the electric polarization ($\underline{P}$) of a sample to the electric field strength ($\underline{E}$).

$$\underline{P} = \left(\varepsilon^* - 1\right)\varepsilon_0 \underline{E} \tag{21}$$

$$\varepsilon^*(\upsilon) = \varepsilon'(\upsilon) - i\varepsilon''(\upsilon) = \frac{1}{\varepsilon_0}\frac{P(\upsilon)}{E(\upsilon)} + 1 \tag{22}$$

2.2.2.2 Time Domain

Time domain spectroscopy has been be used for analysis at higher frequencies (10^5-10^{10} Hz) and for samples that have low conductivity. [32, 50-53] In the typical case, a voltage step is applied to the sample for a set time. This voltage, V_{pol}, is related to the sample permittivity along with the polarization current through the sample. [32]

$$\frac{d\varepsilon}{dt} = \frac{I(t)}{C_0 V_{pol}} \tag{23}$$

$$\varepsilon(t) = \frac{C(t)}{C_0} \tag{24}$$

2.2.3 Previous Work on Dielectric Spectroscopy

2.2.3.1 Effect of Temperature, Polymer Molecular Weight, and Solvent

Many investigations in dielectric analysis have been done through temperature domain, with frequency set as a constant through the measurement. [1, 4, 9, 54-56] After measurements at different frequencies, a shift was seen of the relaxation peaks (ex: Figure 2.14). When temperature was kept constant over a range of frequencies, a

similar shift in relaxation peaks was seen. This shift over temperature was also observed in this thesis research when temperature effect was being tested.

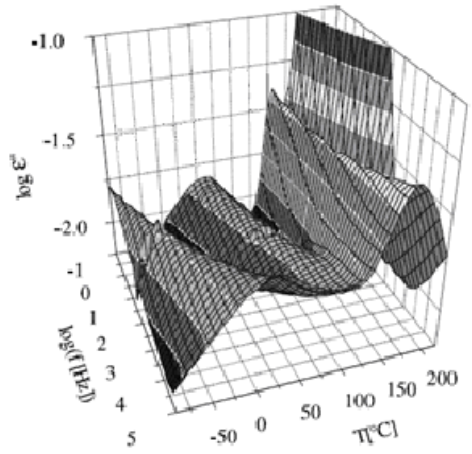

Figure 2.14 Dielectric analysis of biaxially stretched poly(ethylene naphthalene 2,6 dicarboxylate) (PEN) film shows [9]

Dielectric comparisons of solvents were performed by Wurm *et al.* [57, 58] Examinations of ion interactions in amide solvents, like those used to dissolve PEI, were done by dissolving salts into the solvents. This comparison of relaxation times for several solvents containing similar salts showed different relaxation behavior for the solutions with solvent-ion interaction (formamide and N,N-methylformamide) from those that did not interact with the salts (dimethylformamide and dimethylacetamide). Dimethylacetamide, being the primary good solvent for the current research, was a focus of the dielectric analysis in this thesis work.

Theron *et al.* previously used dielectric analysis in relation to electrospinning. [18] They calculated the conductivity and permittivity of polymer solutions by measuring the complex impedance of a small cylinder of each solution, similar to the method employed in this thesis. The five polymers measured were polyethylene oxide (PEO), polyacrylamide (PAA), polyvinyl acetate (PVA), polyurethane (PU), and

polycaprolactone (PCL), each in a suitable solvent. From relative permittivity measurements, Theron *et al.* concluded that the solvent properties dominated the permittivity of the solutions. Also, while conductivities of solvents increased with the addition of polymer, all solutions had very low conductivities. This led to the conclusion that the magnitude of conductivity measured was mostly due to the ionic conductivity of the solvent, which was assumed to be slightly impure. Table 2.4 shows the results measured by Theron *et al.* with PEO in ethanol and water. There was neither trend in permittivity nor in conductivity as PEO concentration was increased.

Table 2.4 Relative permittivity and conductivity of PEO solutions, by Theron et al. [18] Neither values changed in trend with the change in PEO concentration. The conclusion being that these numbers are a result of solvent properties only. Ethanol/Water (40/60) properties: $\varepsilon_r = 69.47$, $\sigma = 0.15$ mS/m

Polymer	Solvent	Conc. (%)	ε_r	σ (mS/m)
PEO	Ethanol/Water (40/60)	2	67.09	0.85
		3	61.44	1.38
		4	66.57	1.15
		6	57.63	1.67

It was also observed that conductivity and relative permittivity values for solutions with the same polymer and solvent combination did not show trends through increased polymer content. This is most likely due to the standard error of the meter used. The lack of linear trend through polymer addition was also seen in the current research, which is elaborated upon in Section 4.2.

2.2.3.2 Dielectric Analysis of PEI

The PEIs used in this investigation were Ultem 1000 and 1010. Dielectric relaxations of Ultem 1000 were previously investigated in the thin film state. [1, 4] A spectrum of PEI's relaxations is shown in Figure 2.15, measured by Díaz-Calleja *et al.* By measuring the PEI film at different moisture contents, it was determined that the γ - *relaxation* was highly water dependant (Figure 2.16). In a fully dry sample, this peak disappeared from the DMA curve and reduced dramatically in the dielectric analysis curve in the full range of frequencies tested.

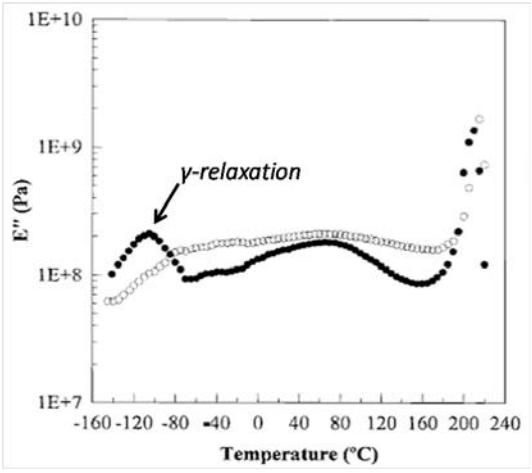

Figure 2.15 Loss modulus of PEI film, at 0.3 Hz, showing hydration dependence of γ-*relaxation* (peak at -120°C), measured with dynamic mechanical analysis (DMA). [4]
●: Sample at climate hydration, ○: Sample dried in vacuo

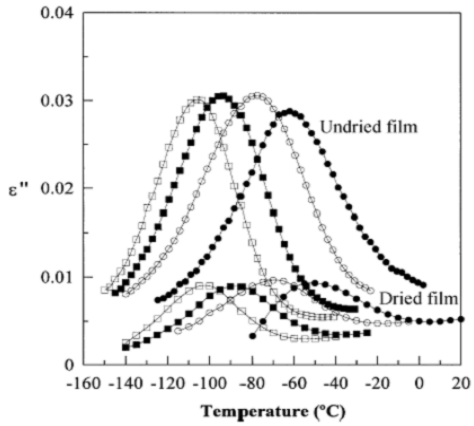

Figure 2.16 Dielectric loss of PEI film at various frequencies, showing hydration dependence of γ*-relaxation.* [4] □: 1 Hz, ■: 10 Hz, ○: 100 Hz, ●: 1000 Hz

Following examination of PEI's dielectric relaxations with TSDC, Belana *et al.*[1] were able to determine probable mechanisms for the α, β, and γ*-relaxations*. In all cases, the α*-relaxation* occurs at the glass transition temperature, which implies that this relaxation is related to the bulk chain motion in the sample (relaxation type C of Figure 2.12). The other relaxations were examined based on the generally held view that relaxations below T_g occur by molecular motions of chain side groups or from lateral chain vibrations coupled with local motions along single chains (relaxation types A and B of Figure 2.12). The γ*-relaxation* was shown to be highly water dependent and PEI's connection with water likely creates a 'false' relaxation unrelated to the pure PEI chain. The β*-relaxation* was attributed to more subtle molecular motions, based on the wideness of the peak. The suggested mechanism for this relaxation by Belana *et al.* was the vibration mobility of the aromatic and benzimide rings on the PEI chain around equilibrium positions.

2.3 Rheology

Rheology, the study of matter deformation and flow, can evaluate many variables of the flow or deformation of interest, including velocity and pressure gradients,

stresses, and strains. To evaluate any isothermal flow of a liquid or solid three principles must be addressed. They are: the conservation of mass, the conservation of momentum, and a constitutive equation. The first two principles are universal equations dealing with the laws of thermodynamics and are only mathematically modified for specific experimental set-ups by the 3-D space chosen for calculation and by the type of liquid being measured. Theoretically, there are innumerable constitutive equations. The appropriate one should be chosen through an examination of best fit to the experiment. Caution must be taken when choosing a constitutive equation because it is possible to perform an analysis of a flow with an equation too simple for the system. The result of this being numbers which look acceptable, but are not taking into account the specific system, and are therefore less reliable.

The first equation addressed in the evaluation of a flow is the law of mass conservation. [59-61] When an experimental system is chosen, the system can be thought of as a controlled volume. This volume has a control surface at which material can enter and leave the control volume. The change in mass of the control system over time is equal to zero because all changes in the area of the surface are accounted for in a double integration of the control surface (making it a closed integral), and is therefore, the opposite in the control volume's change by the time rate. In other words, this control volume can have any motion with velocity V and time rate d/dt as long as they are measured relative to the control volume. So, the total outward flow rate of mass through this control surface will equal the rate at which mass is decreasing from the control volume, or

$$\oiint_{CS} \rho V \cdot dA = -\frac{d}{dt} \iiint_{CV} \rho \, dv \tag{25}$$

The scalar version of this concept is arrived upon through evaluation of the equation above, where the volume is fixed. The balance of mass in the system is then shown to be,

$$0 = \frac{\partial \rho}{\partial t} + \nabla \cdot (\rho \underline{v}). \tag{26}$$

This equation applies to all substances: incompressible, compressible, Newtonian and non-Newtonian. In regard to an incompressible Newtonian fluid, equation 26 becomes

$$0 = \nabla \cdot \underline{v} \tag{27}$$

So, in a steady-state flow in the horizontal, a fluid's velocity rate

$$\frac{dv_x}{dx} = 0 \tag{28}$$

Newton's second law of motion is called the conservation of momentum. [10, 62] This law operates similarly to the law of mass conservation, except here the involved forces of a control volume and its control surface are balanced.

$$\rho \left(\frac{dv}{dt} + \underline{v} \cdot \nabla \underline{v} \right) = -\nabla \cdot \underline{\underline{\Pi}} + \rho \underline{g}\,, \tag{29}$$

where $\underline{\underline{\Pi}}$ is the total stress tensor, which incorporates all stresses at a point, and $\underline{g}$ is the gravitational force vector. To specify $\underline{\underline{\Pi}}$ for a flow or deformation, part of the stresses it includes need to be taken out. This is done by

$$\underline{\underline{\Pi}} - p\underline{\underline{I}} = \underline{\underline{T}}\,, \tag{30}$$

which takes out the thermodynamic pressure in the system (by multiplying pressure by the Identity matrix) and leaves us with all other stresses, $\underline{\underline{T}}$. The result of this action is the Navier-Stokes equation [10, 63]:

$$\rho \left(\frac{dv}{dt} + \underline{v} \cdot \nabla \underline{v} \right) = -\nabla p - \nabla \cdot \underline{\underline{T}} + \rho \underline{g}\,, \tag{31}$$

where for an incompressible Newtonian fluid, $-\nabla \cdot \underline{\underline{T}} = \mu \nabla^2 \underline{v}$. Finally by breaking the Navier-Stokes equation into parts, the flow is able to be analyzed by using boundary conditions of the experiment and the continuity equation from above (equation 31). Through this analysis of a system, the velocity profile, pressure profile, flow rate, torque required to produce a flow, and the stress profile can all be determined.

A fluid that is considered non-Newtonian is one with elastic properties and a flow behavior influenced by stress memory, which does not follow the Generalized Newtonian Flow (GNF) model. [63] In the simplest non-Newtonian case, the GNF model is modified and μ is changed to η, where $\eta(\dot{\gamma})$,

$$\eta = m\dot{\gamma}^{n-1}, \tag{32}$$

and m and n are constants dictated by the fluid sample. [62] In a log-log plot of viscosity (η) versus shear rate ($\dot{\gamma}$) the power-law of equation 32 characterizes the linear region of viscosity where m is the intercept with units Pa.s^n, and $n-1$ is the slope. By a relationship of elastic modulus and angular frequency, zero-shear viscosity, η_0, may be obtained through oscillatory measurements of the flow, when the oscillating frequency is small[64], given

$$G' = \eta_0 \omega \tag{33}$$

The number of mechanical relaxations in a polymer depends on its molecular weight distribution, or polydispersity index (PDI). Longer relaxations occur at smaller frequencies, so a model which fits a set of data only at low frequencies may be adequate to see the longest relaxation, or that of the longest polymer chains. The generalized Maxwell model provides material functions for small amplitude oscillatory shear (SAOS), which in the simplest form will fit modulus data at low frequencies.

$$G'(\omega) = \frac{g_1 \omega^2 \lambda_1^2}{1+\omega^2 \lambda_1^2} \tag{34}$$

$$G''(\omega) = \frac{g_1 \omega \lambda_1}{1 + \omega^2 \lambda_1^2} \tag{35}$$

These functions provide a single average relaxation time as $G' = G''$ or when $\omega = 1/\lambda_1$. In these functions λ_1 is the relaxation time and $g_1 = \eta_1 / \lambda_1$. Realistically, most polymers are not of uniform molecular weight, so there will be more than one relaxation. To expand the generalized Maxwell model to fit full spectrums of data, the subscript in the single-relaxation functions is changed to a sum-able term

$$G'(\omega) = \sum_{k=1}^{N} \frac{g_k \omega^2 \lambda_k^2}{1 + \omega^2 \lambda_k^2} \tag{36}$$

$$G''(\omega) = \sum_{k=1}^{N} \frac{g_k \omega \lambda_k}{1 + \omega^2 \lambda_k^2} \tag{37}$$

where $g_k = \eta_k / \lambda_k$, and the longest relaxation time is the largest value of λ_k, which will also be the λ_k that applies to the lowest frequency range. The number of parameters (N) used is arbitrary and can be chosen merely based on purpose of study. However, too many parameters would be akin to over-saturating a statistical model. Therefore, calculating the least number of parameters possible for an adequate fit of the data is recommended.

2.3.1 Principles of Polymer-Solvent Interaction

The effect of solvent in a polymer solution can primarily be seen through a variation in viscosity described by Figure 2.17. [8]

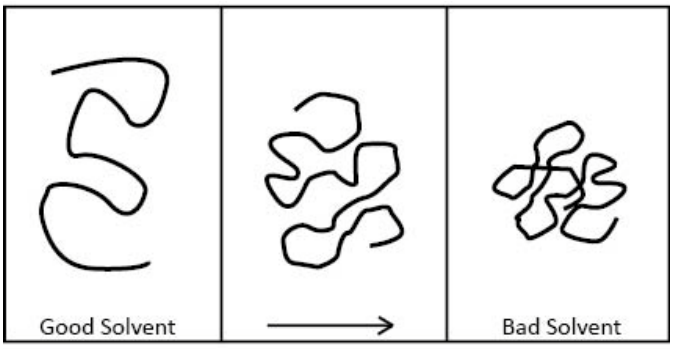

Figure 2.17 The effect of polymer-solvent interaction on chain spacing. [8]

The orientation of a polymer chain is greatly affected by the quality of the solvent and can be described in a change of root-mean-square end-to-end distance $\langle R^2 \rangle^{1/2}$. $\langle R^2 \rangle^{1/2}$ can be derived through several polymer analysis techniques, such as small-angle X-ray scattering or light scattering. [19] In a good solvent $\langle R^2 \rangle^{1/2}$ will be larger than in the polymer melt because polymer and solvent interaction is more favorable than polymer and polymer interaction. The opposite will occur in a bad solvent, and $\langle R^2 \rangle^{1/2}$ will decrease. If the solvent is poor enough for the polymer, phase separation will occur. Also, if the solvent is of a certain quality, the $\langle R^2 \rangle^{1/2}$ of the polymer will be the same as if the polymer were just in melt state. This type of solvent is referred to as a theta solvent.

2.3.2 Double Cylinder Geometry

To determine the rheological geometry appropriate for a given sample, a summary of the three most common geometries, by F. Morrison, was referred. [10] To draw trustworthy data from rheology measurements, a geometry must be chosen that has an appropriate stress range. The parallel plate and cone-plate geometries are good for high viscosity samples, while the double cylinder is good for low viscosity samples. This is because the double cylinder geometry allows for more surface contact with the

sample, hence, better accuracy of data at low viscosities. With respect to sample shear rate, each geometry has issues as rates increase to certain levels. The parallel plate and cone-plate exhibit sample fracturing (or leaving the geometry) at the edges when moderate rates are used. The double cylinder will see Taylor cells form in the bottom of the couette with high Reynolds numbers because of inertia. The double cylinder geometry, however, will have uniform sample behavior during stable measurements, due to the narrow gap, as will the cone-plate because of the small angle of the cone. The parallel plate will not have homogeneous behavior, though, as the shear rate and stress will vary with plate radius. Pressure is not an issue with the latitudinal geometries of the parallel plate and cone-plate, but the double cylinder should be kept within a temperature range of about 0 – 60°C because of the narrow gap and the importance of keeping the same cylinder spacing throughout.

The geometry chosen for the samples in this thesis was the Couette. It was made up of two concentric metal cylinders. To measure a liquid's flow in this way both cylinders must have a relatively large radius and the gap between the two cylinders must be very narrow. This allows the shear rate to the liquid sample to be virtually equal everywhere in the gap. [64]

Simplistic, less accurate designs of the double cylinder geometry use a 'bob and cup' method with a stationary bob set in the sample fluid, in a movable cup. [63-68] The cup is rotated at various rates, the required torque for each rate is measured, and the flow parameters are extrapolated from these tests. In a complex computer-driven measurement, control of a ramped stress may be performed in one measurement.

The double cylinder Couette geometry (Figure 2.18) with an incompressible fluid in cylindrical coordinates is considered to provide a full examination of the shear stress and function of viscosity of the polymer solutions in this thesis. [10, 61, 67-69]

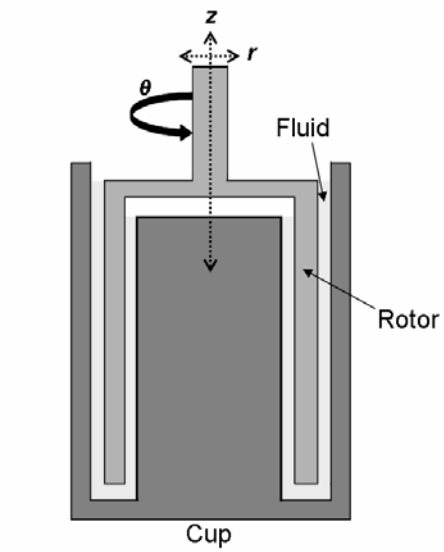

Figure 2.18 Center cross section of double cylinder Couette geometry. Adapted from bob and cup geometry described by Morrison [10]

If the rotor, with length, L, is rotating at a constant speed, the angular velocity Φ for the system can be expressed as

$$\underline{v} = \begin{pmatrix} 0 \\ v_\theta \\ 0 \end{pmatrix} \tag{38}$$

Equation 38 can be transposed to see that the gradient of flow for v_θ is in the r-direction. Also if the rotor is rather long, any variation of flow over the z-direction can be overlooked. So, the continuity equation yields:

$$0 = \frac{\partial v_\theta}{\partial \theta} \tag{39}$$

The shear viscosity is then given by

$$\eta = \frac{2\pi R^2 \tau}{4\pi\left[\left(\frac{\alpha^2 R^2}{\alpha^2 - 1}\right)\left(\Phi_O - \Phi_i\right)\right]}, \tag{40}$$

where R is the radius of the inner cylinder (rotor), α is the ratio of the outer cylinder radius to that of the inner cylinder, and τ is the shear stress per unit length of the

rotor. [69] The angular velocities of the outer cylinder and the inner cylinder (rotor) are represented by Φ_O and Φ_i, respectively. The viscosity is a ratio of the torque to the angular velocity of the geometry. Thus, it is concluded that a rheometer, which measures the necessary torque for a flow, can use equation 40 to calculate other values (e.g. G' and G'').

In order to compare the dielectric analysis to that of the rheometer, their common independent variable, frequency, was used. To achieve this with the rheometer, procedures in oscillation mode were used, where instead of the inner cylinder rotating at a given angular velocity, it was oscillated about a reference point, through a range of frequencies. Also, the geometry used in this project had a bob which was hollowed out. This did not change the measurements for torque, but doubled the measurement surface. The fluid sample then had twice the surface area for interaction, giving the rheometer greater precision.

Since rheological models are accurate only when using small rates of deformation, the frequency driven measurements for rheological analysis are done in what is called small amplitude oscillatory-shear flow. If these measurements are performed within the sample's linear viscoelastic region, the oscillation flow can be described with the complex viscosity, which is frequency-dependant. [63]

2.3.3 Previously Reported Rheology Data for PEI

As the majority of current end-uses for PEI are composites, the majority of rheological work involving PEI is also in this area. [70-76] In the work of Bonnet *et al.*[70], the phase separation in various thermoplastic epoxy composites was examined as bisphenol A diglycidil ether cured with 4,4´-methylenebis[3-chloro,2,6-diethylaniline] was combined with various amounts of PEI. Results showed a strong rheological dependence at phase separation on the initial concentration of PEI, while a large

interdependence of morphology and initial composition of the composite was seen through rheological analysis.

Early research into controlling the results of electrospinning focused on the polymer concentrations used in precursor solutions. Typically with an increase of polymer concentration, there is an increased likelihood of uniform fiber formation. [12, 77, 78] This is reasonable considering the inevitable increase of viscosity with increased polymer concentration. Rheological analysis can be used to analyze viscosity and other properties of liquid polymeric samples. Previous rheological analyses in regards to electrospinning have been performed on many polymers. For example, McKee *et al.* [11] studied various molecular weights of a PET-*co*-PEI polymer in various linear and branched forms. McKee *et al.* found the critical entanglement concentration (C_e) of the copolymer by examining the change in slope of specific viscosity as concentration increased. They used the C_e to understand the range of fiber diameters that were electrospun. Figure 2.19 shows the critical entanglement concentration to be approximately 10.8 wt%.

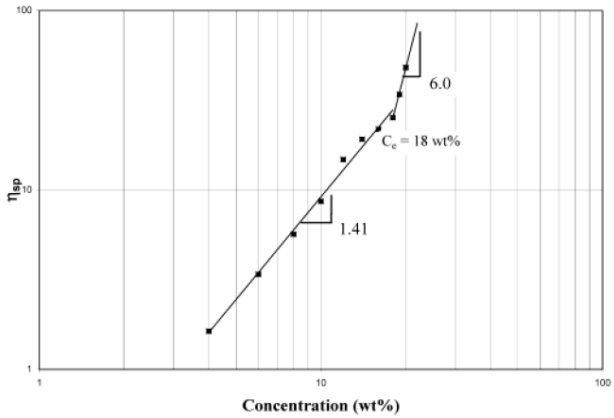

Figure 2.19 Specific viscosity of PET-*co*-PEI with MW ~ 11,700 g/mol as a function of polymer concentration showing the change in slope of viscosity, also called the critical entanglement concentration. [11]

The comparison of average electrospun fiber diameter to specific viscosity for the copolymer in Figure 2.20 revealed that with increasing viscosity an increase in fiber diameter was seen, progressing from beads to bead-on-string to uniform fibers with increasing diameter.

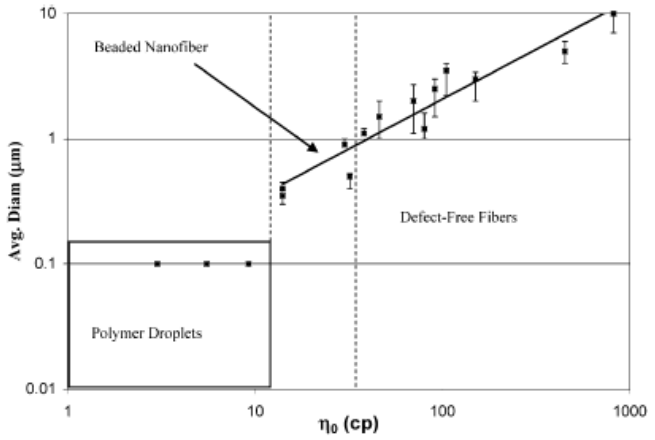

Figure 2.20 Average diameter of electrospun PET-*co*-PEI (MW ~ 11,700 g/mol) as a function of solution specific viscosity showing the change in morphology of electrospun PET-*co*-PEI, with regimes of product identified [11]

When the polymer concentration was standardized by the critical entanglement concentration, C_e, the authors were able to formulate an equation for average fiber diameter, which can be seen in Figure 2.21.

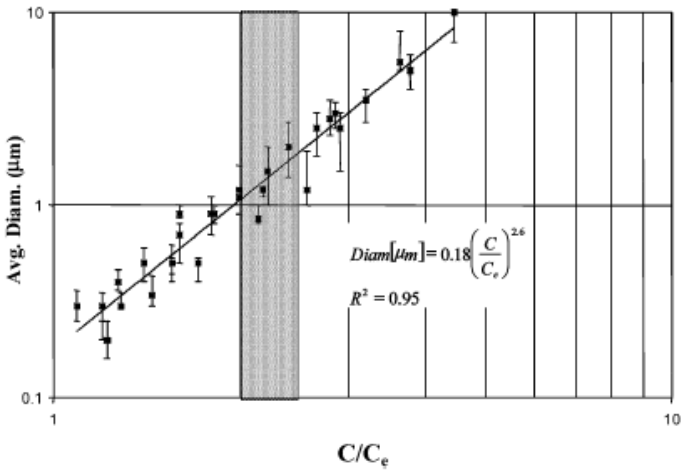

Figure 2.21 Average diameter of various electrospun PET-co-PEI versus polymer concentration, *C*, standardized by the critical entanglement concentration, C_e [11]

Below the C_e, the solutions either formed beads or beaded fibers when electrospun, but above the C_e, formed uniform fibers. A similar phenomenon was seen in the research presented in this thesis. However, the relationship of nanofiber diameter to polymer concentration is not seen. It is proposed that this behavior is induced by THF and the mechanisms by which its addition changes the system.

2.4 Electrospinning

Nanofibers, with their large surface area to volume ratio are the next step of evolution in technologies ranging from air filtration to drug delivery and sensors. [78] Electrospinning is a very popular process for manufacturing fibers with submicron diameters, but it is filled with control parameters which are often hard to optimize. This makes electrospinning a complicated process in which it is difficult to consistently reproduce a quality product. Controlling factors in electrospinning include: polymer and solvent combination, component concentrations, syringe needle diameter, conductivity of the collector, distance from the needle to the collector, applied voltage, and rate of solution pumping. [15, 77, 79, 80] The solution properties

which vary based on solution components include viscosity, conductivity, surface tension, and solvent evaporation rate. Given the potential of extremely thin, continuous fibers, many researchers have focused on more fully understanding the effects of these parameters, thereby creating a mass producible commercial product.

Recently, J. Yu *et al.* [12] investigated solution elasticity and the responsibility it carries during electrospinning. They used a capillary breakup extensional rheometer (CaBER) for measuring the extensional viscosity and longest relaxation time for each PEO aqueous solution to which they compared the morphology of the PEO nanofibers. From their measurements they also calculated the Deborah number, which is a descriptor term for the flow of a substance, and is the ratio of the relaxation time scale and the observation time scale (lower Deborah numbers indicate a more fluid behavior): $De = \lambda_p \omega_{\max} / t^*$, where λ_p is the relaxation time, $\omega_{\max}$ is the frequency for the maximum relaxation, $t^* = r_0^2 / \nu$, ν is the characteristic viscosity, and r_0 is the characteristic length. The characteristic length used was the initial radius of the jet when electrospinning and it was the same for all solutions (0.8 mm). They observed that if the solution relaxation time was greater than the instability growth time, or having a De > 1, the elastic response of the solution would begin to overcome the Rayleigh instability of the jet, and fibrous morphologies would start to form. Once the instability was completely suppressed, uniform fibers would form. To fully understand the relationship of elasticity to electrospinning, Yu *et al.* graphed Deborah numbers of their samples against the Ohnesorge numbers, which are a relation of the shear viscosity and the surface tension of a substance: $Oh = \mu / (\rho \sigma r_0)^{1/2}$, where μ is the shear viscosity, ρ is the density, and σ is the surface tension as shown in Figure 2.22.

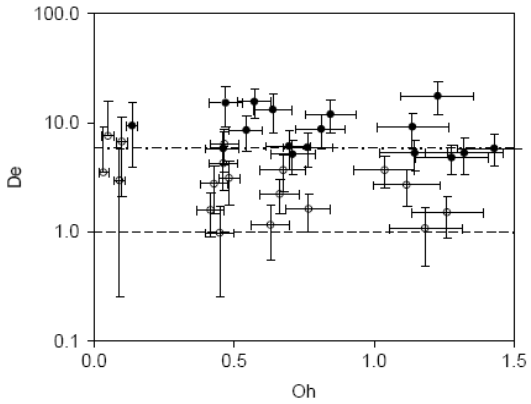

Figure 2.22 Relation of electrospun PEO/PEG morphology to elasticity by plot of the Deborah number by the Ohnesorge number. ●: uniform fibers, ○: beads-on-string [12]

Because the Ohnesorge number did not show regimes of bead-on-string and uniform fibers, it was concluded that shear viscosity does not establish fiber morphology. However, with at least a Deborah number of 6, the solutions formed uniform fibers, and below 6 were bead-on-string. Below De = 1, no fibers were present in samples. This showed the relationship of relaxation time (a major component of elasticity) and fiber morphology. Because elastic behavior influences morphology more than viscous behavior, it can be concluded that elastic modulus (G´) and complex viscosity (η^*) will be important parameters to examine through the current research work.

P. Gupta *et al.* [13] explored the relationship of polymer content and solution viscosity to fiber formation by electrospinning. The primary parameter explored was polymer chain entanglement. Dynamic light scattering (DLS) was used to measure the radius of gyration (R_g) for each sample. These data were then used to compute the critical entanglement concentration of narrow molecular weight PMMA. It was determined, as shown in Figure 2.23, that for all molecular weights of PMMA tried, there were two regimes of semidilute solution: unentangled and entangled.

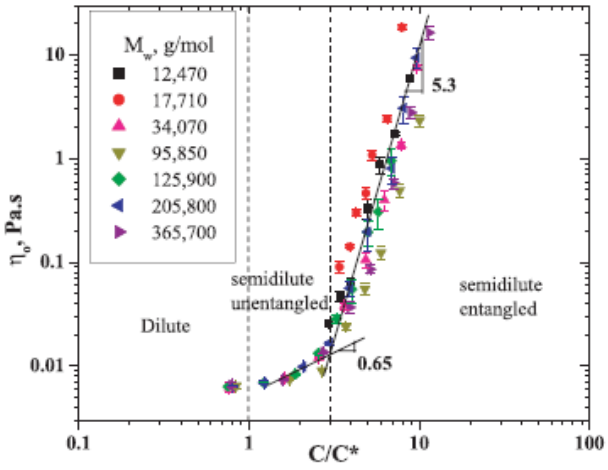

Figure 2.23 Zero shear viscosities of PMMA of differing molecular weights in different concentrations, standardized by the critical entanglement concentration. Fibrous structures formed when C/C* > 3, uniform fibers when C/C* ≥ 6.8. [13]

According to SEM results, above a standardized concentration (C/C*) of 3, fibers began to form, and by a C/C* value of 6.8, uniform fibers formed. This work shows that at a certain concentration, not just a certain molecular weight, uniform fibers can be formed. Similar results were seen in this thesis work.

Carroll and Joo [81] created model systems of viscoelastic Boger fluids as well. One of their focuses was on the influence of solution conductivity on the initial jet, and solution electrospinability. The researchers imaged Taylor cones of glycerol solutions, containing varied salt amounts, put through a vertical electrospinning setup. In this way, they were able to conclude that the initial jet of a higher conductivity sample thinned at a slower rate than did the initial jet of a lower conductivity sample. Also, after a certain salt content was reached the salt caused the solution to become harder to spin, if it spun at all, in that they needed higher voltages to spin the solutions well. Their analysis of this phenomenon was to say that with the lower conductivity solutions the charge was held, carried by the fluid, and was satisfied by the fluids movement through the electric field. However, with a higher conductivity sample, the

higher charges "slipped" through the fluid to respond to the electric field and, therefore, did not pull the fluid along. This analysis satisfied an observation by Theron *et al.* [18], that many polymer solvent combinations used for good electrospinning have quite low conductivities.

Thompson *et al.* [14] produced a theoretical model for electrospinning, taking into account thirteen parameters which may affect the fibrous product of the electrospinning process. One major conclusion of the work was that a larger diameter of the initial jet, after the Taylor cone, resulting in larger fiber diameter on the collector. The size of the Taylor cone was also related to the amount of applied voltage. So, the interaction of these two parameters is a contributor to fiber diameter. Figure 2.24 shows theoretical model results of jet radius distributions by jet distance from the collector, over several volumetric charge densities.

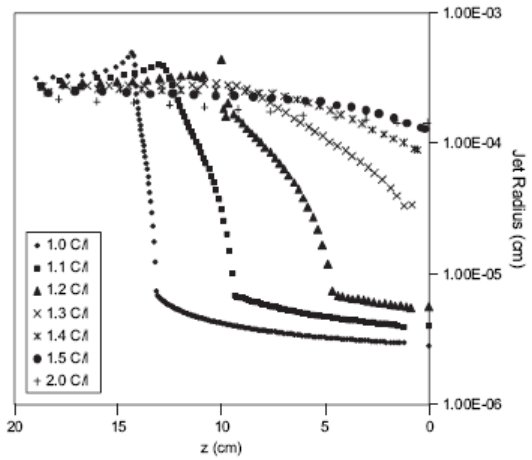

Figure 2.24 Electrospinning jet radius by distance from collector, at varied volumetric charge densities (coulomb/liter) [14]

Figure 2.25 shows that dimethylformamide (DMF), with a boiling point of 150°C, produced fibers much thinner than did THF, with a boiling point of 60°C. In a study

on the effects of solvent to the electrospinnability of a system, Wannatang *et al.* used six different solvents to electrospin polystyrene (PS).

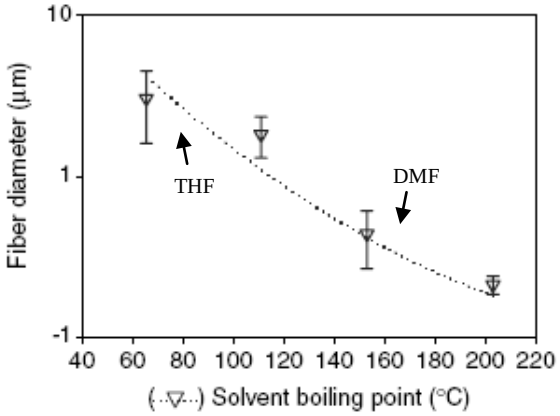

Figure 2.25 Effect of solvent boiling point on the diameter of electrospun PS. [15] Both THF and DMF are good solvents for PS.

When the difference in the solubility parameter of the solvent and that of PS was lower, the percentage of polymer bead area, relative to the whole product, was smaller. This was also the case with dielectric constants. When solvents with high boiling points were used, the resulting electrospun PS fiber diameter decreased.

CHAPTER 3

EXPERIMENTAL APPROACH

3.1 Materials

Poly(etherimide) (PEI), Ultem 1000 (MW ~ 41,000 g/mol) and Ultem 1010 (MW ~ 33,000 g/mol), was obtained from GE Plastics (Pittsfield, MA). N,N-Dimethylacetamide (DMAc) and Tetrahydrofuran (THF), obtained from Sigma Aldrich (Milwaukee, WI), were used as the "good" and "bad" solvents for PEI, respectively. PEI was ground, using a bench-top polymer grinder, for quicker dissolution.

3.2 Instruments

The Broadband Dielectric Spectrometer used in this project was made by Novocontrol (Hundsangen, Germany). The spectrometer used a sample measurement circuit called the Alpha-A Analyzer. A Novocontrol BDS 1308 vacuum sealed parallel electrode cell with a spring for sealing out air was used as the sample containment apparatus. The circuit and electrode cell are illustrated in Figure 3.1.

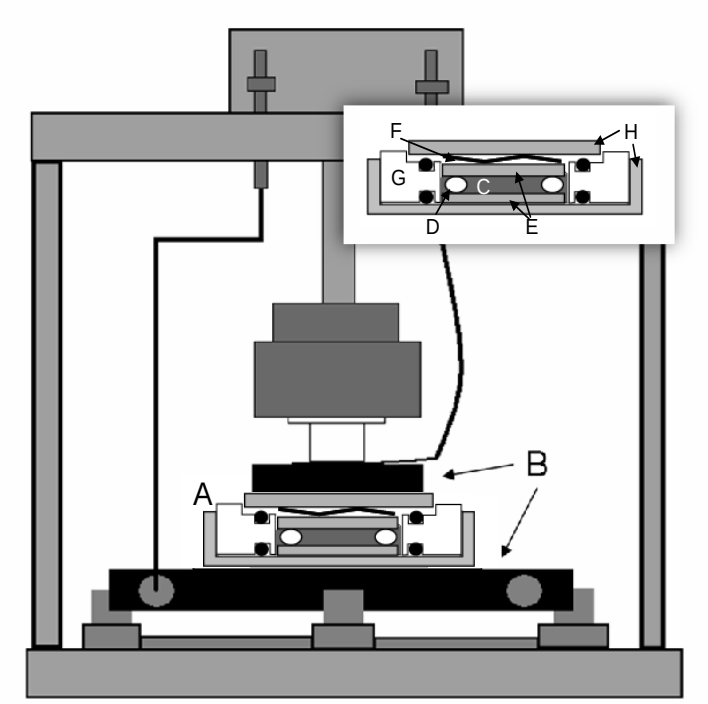

Figure 3.1 Schematic of Novocontrol's Alpha-A Analyzer circuit and BDS 1308 sample cell, for dielectric analysis: (A) sample capacitor cell, (B) upper and lower electrodes of circuit. Inset – liquid sample capacitor cell: (C) sample, (D) non-conductive spacer ring (ex: Teflon), (E) upper and lower electrodes, (F) spring, (G) non-conductive ring (ex: Teflon) with sealing rubber o-rings, (H) casing electrodes

For conductivity measurements of solvents at room temperature, an IQ170 meter (IQ Scientific Instruments, Carlsbad, CA) was used.

An AR2000 stress-controlled rheometer from TA Instruments (New Castle, DE) was used for rheological analysis. The concentric cylinder geometry with an external fluid circulator for temperature control was chosen for reasons listed in Section 2.3.2. Comparison measurements were taken with a Physica MCR 301 rheometer (Anton Paar, Graz, Austria). The double gap couette geometry was used here as well, with a C-PTD 200 cylinder system for temperature control.

Medical syringes and hypodermic needles from Fisher Scientific (Pittsburgh, PA) were used for solution containment during electrospinning experiments. A NE-500

syringe pump from New Era Pump Systems, Inc. (Wantagh, NY) was used for feeding the solution. Aluminum foil was used as a replaceable collector, which was wrapped onto a sheet of copper flashing; both metals were obtained from Fisher Scientific (Pittsburgh, PA). An electrical power supply unit, series EH 0 – 60kV, from Glassman High Voltage, Inc. (High Bridge, NJ) was used. Electrospun sample imaging was performed using a Leica 440 Scanning Electron Microscope. Fiber diameters were measured using ImageJ, a public domain Java image processing program written by Wayne Rasband (Research Services Branch, National Institute of Mental Health, Bethesda, MD).

3.3 Experimental Procedures

This work focused on understanding the relationship between electrical and mechanical properties of polymer solutions as well as the effect of the components of the polymer solutions and their influence on the electrospun product. PEI concentration levels, solvents and solvent ratios were varied. Dimethylacetamide (DMAc) is a well known solvent for PEI, and was used as the primary solvent of the samples in this work. Tetrahydrofuran (THF) is not a solvent for PEI and has an extremely high volatility. By adding a bad solvent to a good solvent-polymer system, the aim was to manipulate the physical properties of the system in order to improve morphology in the electrospun fibers. Figure 3.2 displays the experimental design for this thesis.

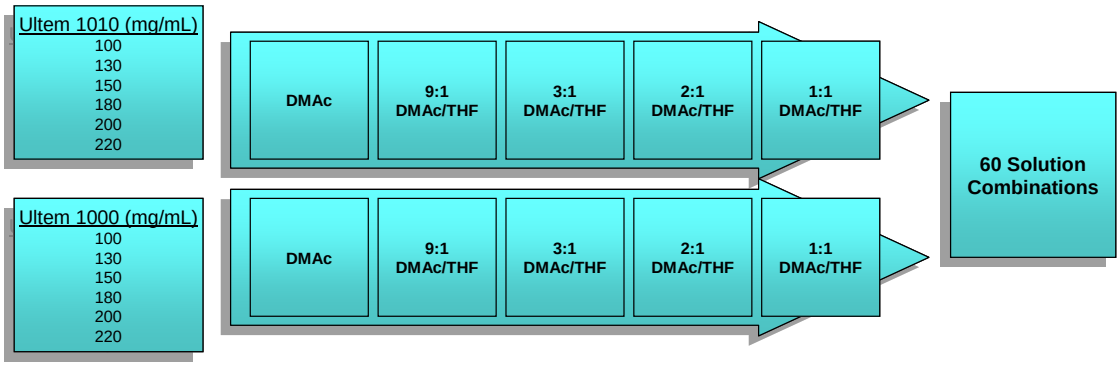

Figure 3.2 Schematic of the sample compositions tested in this research work. Increasing THF content in solvent system was tested with two molecular weights of PEI which were tested at a range of concentrations.

Five solvent ratios were tested, including 9:1 DMAc/THF, 3:1 DMAc/THF, 2:1 DMAc/THF, 1:1 DMAc/THF, as well as pure DMAc. The concentrations of PEI evaluated included 100, 130, 150, 180, 200, and 220 mg/mL.

3.3.1 Dielectric Experiments

For dielectric spectroscopy, the polymer solution was placed within the measurement cell so that the sample area was fully covered and minutely overflowing, keeping air out of the sample. After tightening the sample cell into the spectrometer's circuit and bringing the system to 25°C, a frequency sweep measurement was taken. The spectrometer was set to a bias of 3 volts and each sample was measured between $0.1 – 10^7$ Hz. Also, measurements were set up so that, from $1 – 10^7$ Hz, each output data point was an average of 3 measurements. Each combination of polymer and solvent system was loaded and measured several times. A statistical analysis of measurement repeatability is presented in Section 4.3.2. While the operating software from Novocontrol provides automatic calculation of many variables, this study focused on results of conductivity and complex electrical permittivity components. Conductivity is an important descriptor of a sample's behavior in an electric field. Permittivity components express sample polarization and charge carry ability. If there

is a polymer relaxation present, peaks will be observed in ε″ signal, as well as in the tan δ values. With these variables, the molecular dynamics of the system during electric field application were examined.

3.3.2 Rheological Experiments

The double cylinder couette geometry used in this study was a conduction temperature control system, which was programmed to keep the samples at 25°C through all measurements.

3.3.2.1 Stress Sweep Measurement

The stress sweep measurement of a TA Instruments AR2000 rheometer is an oscillation test, run at a range of stresses at a set frequency value. All stress sweeps in this work were conducted between 0.03 – 100 Pa. The stress sweep was used to determine the sample's linear viscoelastic region.

3.3.2.2 Frequency Sweep Measurement

Data was acquired for all samples in the range of 0.05 – 100 rad/s (0.0079 – 15.92 Hz). Frequency sweep tests are used to evaluate the viscous and elastic components of a sample under oscillatory stress. Characteristic relaxation times as well as the complex parameters of viscosity, η^*, and modulus, G^*, can be obtained using this measurement,. This research focused on understanding the relationships between η^*, elastic modulus, G′, and storage modulus, G". Results of frequency sweeps for each sample may be found in Section 4.3.

3.3.2.3 Steady State Flow Measurement

A steady state flow measurement, a shear flow measurement, was performed on each sample in the frequency range of 0.05 – 100 rad/s. This steady shear

measurement is used to collect the shear viscosity of a sample. The shear viscosity measurements were compared to the complex viscosity values for a more complete understanding of the viscoelastic behavior of the solution systems.

3.3.3 Electrospinning Experiments

A horizontal electrospinning setup was used in this work, a schematic of which can be seen in Figure 3.3. During electrospinning, the room temperature was between 21°C – 22°C and the relative humidity was approximately 24%. A plastic disposable syringe was used with a 20 gauge hypodermic needle (1.5 inches long). The mechanical pump was set to 0.9 mL/hr for all solutions. The needle-to-collector distance was kept at 25 cm, while the applied electrical difference was 20,000 volts. The grounded collector was a copper sheet base with aluminum foil cover. In each experiment approximately 10 minutes elapsed after voltage and pump were turned on before visible collection of electrospun PEI was observed. Voltage and pump were continued until collection of product was thick enough to fully cover an area of the foil.

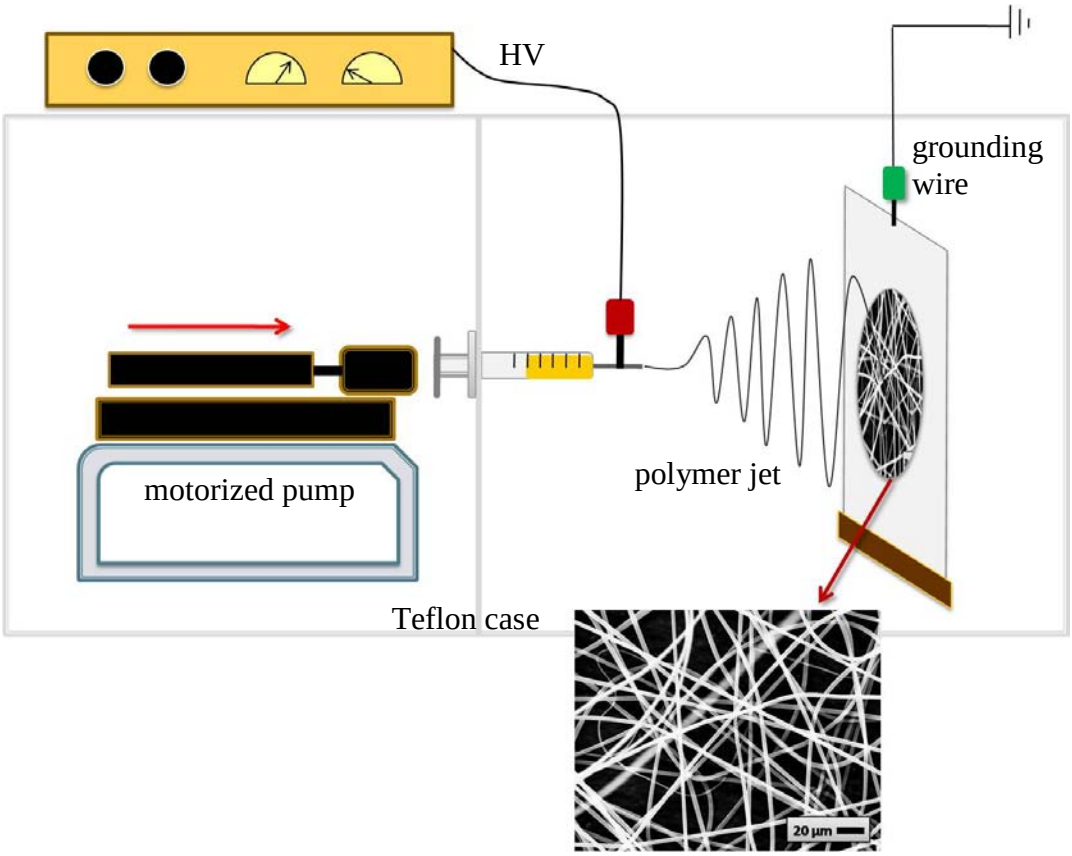

Figure 3.3 Schematic of electrospinning setup used in this project. Solutions were pumped out of syringes at 0.9 mL/hr and an electric field of 80,000 V/m was used. (Schematic by A. Andere Jones)

3.3.4 SEM Image Analysis

Scanning electron micrographs (SEMs) were obtained for each sample at several magnifications in order to accurately characterize the morphologies of electrospun PEI nanofibers. When uniform fibers were obtained, at least 40 – 50 fiber diameters were measured in the SEMs. The average diameters for each polymer-solvent combination are included in Section 4.1. A grading system was created in order to qualitatively categorize the PEI morphologies. The scale of 1 – 5 and each level's visual equivalent is given in Table 3.1.

Table 3.1 Morphology grading system. Half steps were also used in the scale to introduce more continuity of relationships between morphologies. Examples of grades are shown at appropriate magnifications for best morphology summary.

Visual Description	Morphology Grade	Example of Grade
Beads	5	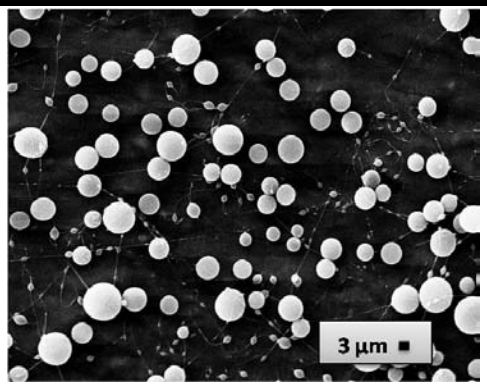 130 mg/mL Ultem 1000 in DMAc
Too many beads to be fibers	4	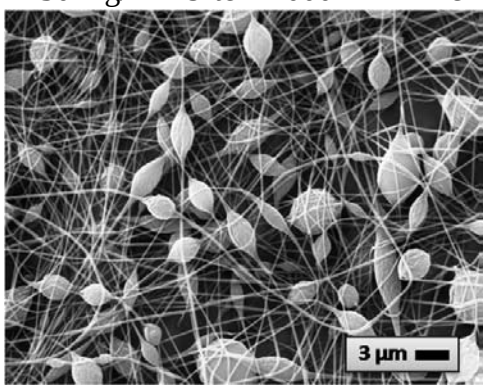 130 mg/mL Ultem 1010 3:1 DMAc/THF
Beady fibers	3	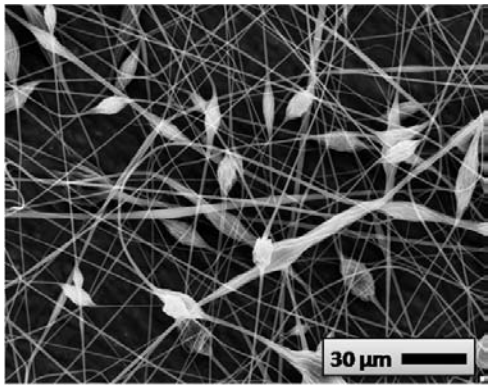 200 mg/mL Ultem 1010 2:1 DMAc/THF

Table 3.1 (Continued)

Fibers with few beads	2
Uniform fibers	1

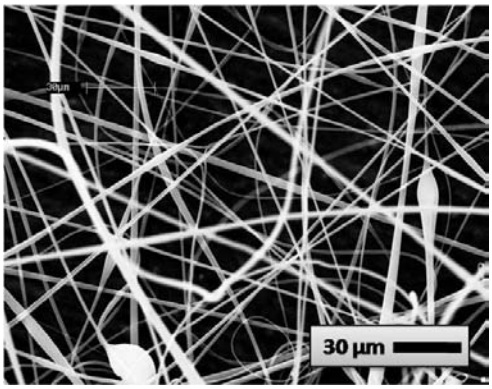

220 mg/mL Ultem 1000
9:1 DMAc/THF

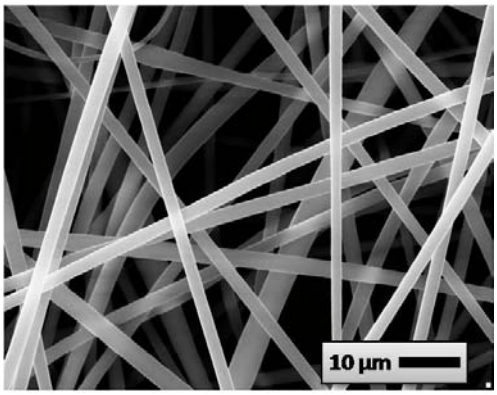

220 mg/mL Ultem 1010
1:1 DMAc/THF

For a more statistically continuous grading, half levels were also used if deemed necessary.

CHAPTER 4

RESULTS AND DISCUSSION

In order to electrospun PEI, a rigid, short-chained polymer, a combination of good solvent and bad solvent was used which produced the highly concentrated polymer chain-to-chain interactions and entanglements needed to create uniform fibers. The electrospinning of polymers which are unable to produce fibers when electrospun from a single solvent was studied via manipulation of, not only good and bad solvent ratio, but also polymer concentration and polymer molecular weight.

The following sections report the physical properties of both classes of PEI, Ultem 1000 and Ultem 1010 as well as the solvents, DMAc and THF; the array of morphologies produced via combinations of PEI, DMAc and THF; the results of dielectric analysis on these solutions and the rheological behaviors of the solutions. The experimental results are evaluated statistically, gleaning any relationships between dielectric and rheological behavior with solution concentrations and polymer molecular weight.

Thermogravimetric analysis (TGA) was performed on samples of Ultem 1010 and 1000. TGA indicated that PEI degrades at approximately 500°C, without the presence of a melting temperature (T_m) (Figure 4.1). This behavior means that PEI polymer chains do not have a crystalline (or semi-crystalline) transition to amorphous solid before they degrade. Analysis by polarized light microscopy confirmed that PEI was not crystalline in solution with DMAc or DMAc/THF blends.

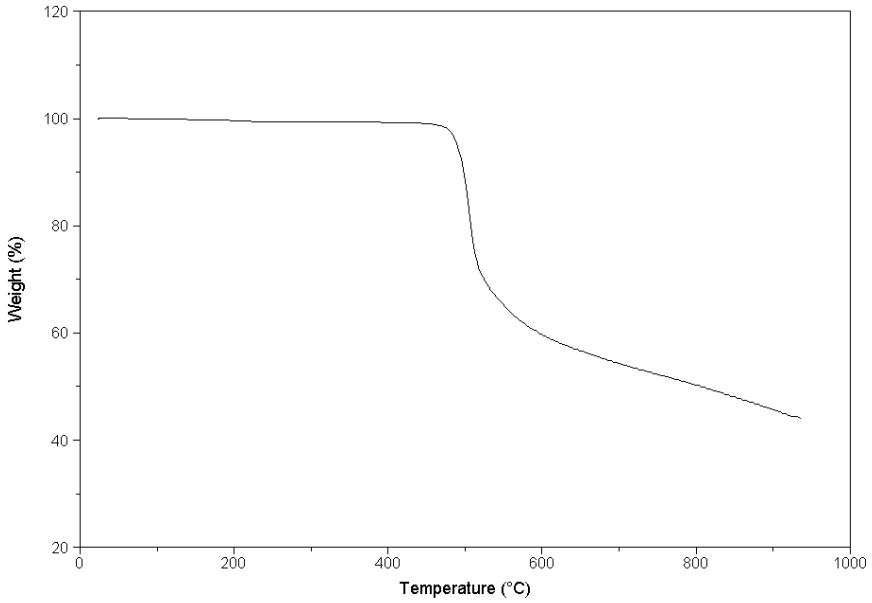

Figure 4.1 TGA of Ultem 1000 shows degradation at 500°C with no melting point

Differential scanning calorimetry (DSC) experiments performed on both specimens of PEI indicated a slightly lower T_g for Ultem 1010 than for Ultem 1000 (Figure 4.2). This behavior may be indicative of their molar mass difference, as Ultem 1010 has a molar mass of approximately 33,000 g/mol and Ultem 1000 is approximately 41,000 g/mol [19].

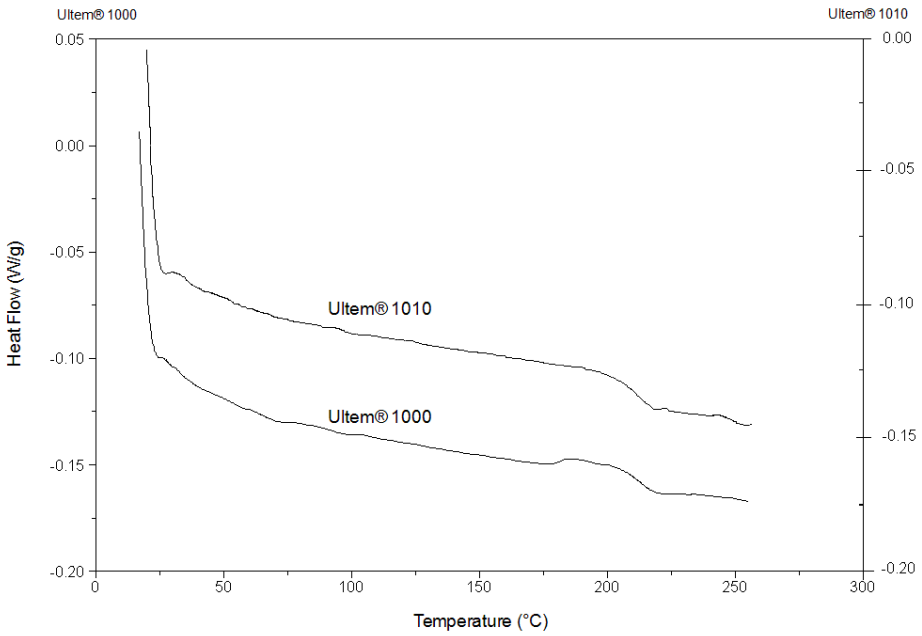

Figure 4.2 DSC of PEI shows the T_g to be approximately 215-220°C

Conductivity measurements were taken of the solvents with a conductivity meter (Figure 4.3) as well as a dielectric spectrometer (Section 4.2) using experimental procedures described in Chapter 3.

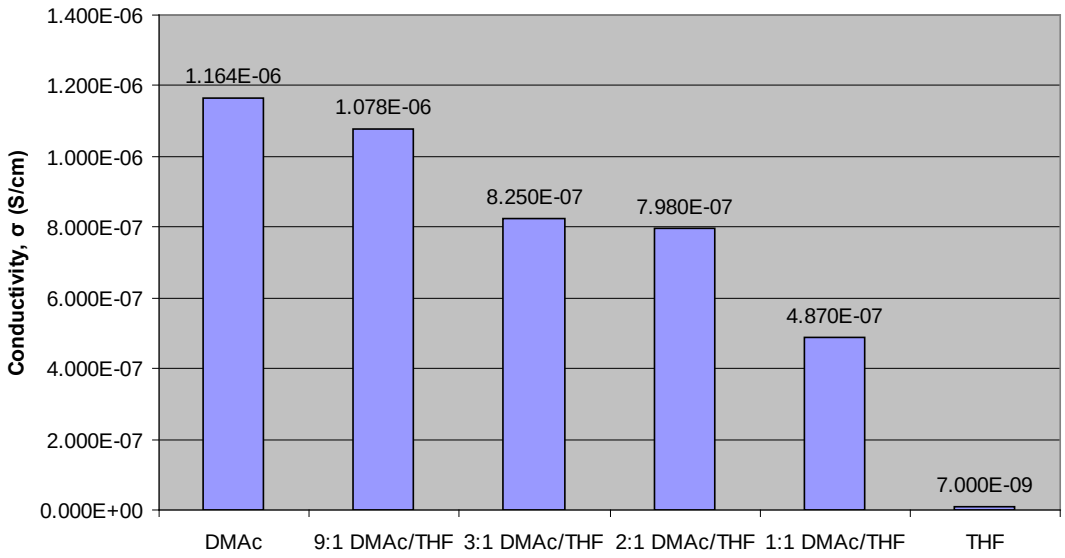

Figure 4.3 Electrical conductivity of DMAc/THF solvent ratios, taken with conductivity meter at room temperature.

4.1 Electrospinning

Electrospinning of PEI was performed at several concentrations of polymer, with several different ratios of good and bad solvent and with two molecular weights of PEI. Figure 4.4 reveals that Ultem 1010 will produce uniform fibers in a 1:1 DMAc/THF solvent mix once the polymer concentration is increased to 180 mg/mL. Also, at the highest concentration of Ultem 1010, 220 mg/mL, uniform fibers are not produced until the ratio of DMAc to THF is 2:1. Of the thirty polymer solvent combinations for Ultem 1010, only five combinations produced mostly fibrous electrospun product. Ultem 1000, at only a slightly higher molecular weight, produced a dramatically larger fibrous range. Figure 4.5 shows that, with the same polymer concentrations and solvent ratios as Ultem 1010, fourteen of the thirty combinations produced mostly fibrous electrospun product. The numbers in the upper left corner of each SEM in Figures 4.4 and 4.5 are the carefully chosen fiber grades, which were used in Figure 4.6, the ternary comparison of electrospun products. These fiber grades were also used in the statistical analysis (Sections 4.2.1 and 4.3.4).

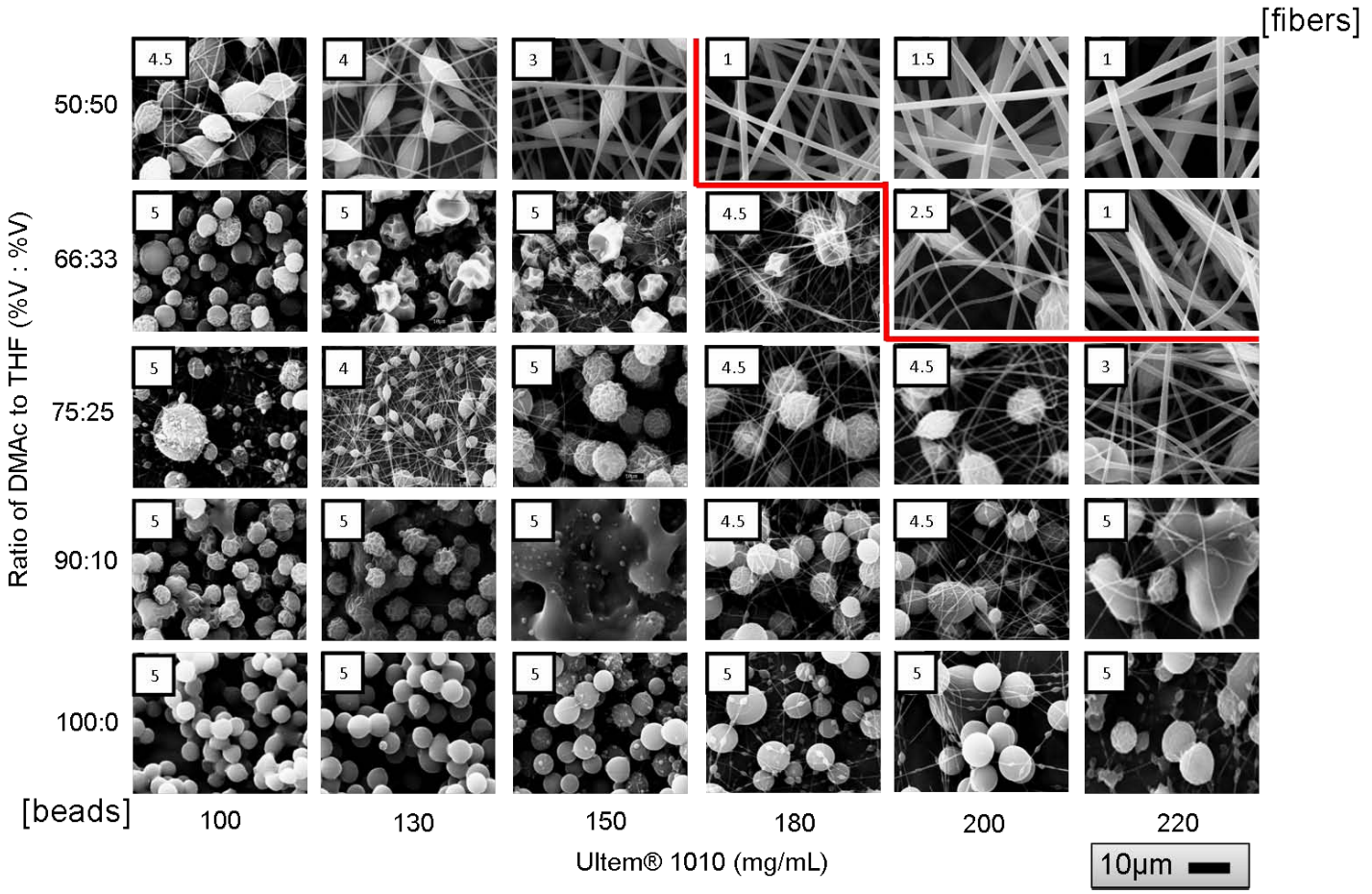

Figure 4.4 Scanning electron micrographs of electrospun Ultem 1010 (MW ~ 33,000 g/mol) from precursor solutions in various DMAc and THF combinations. The micrographs show the evolution in fiber formation from beads in the lower left to fully uniform fibers in the upper right. The red line defines the region where the vastly dominant morphology is fibers. The fiber formation grade is in the upper left corner of each micrograph. Scale bars indicate 10 µm.

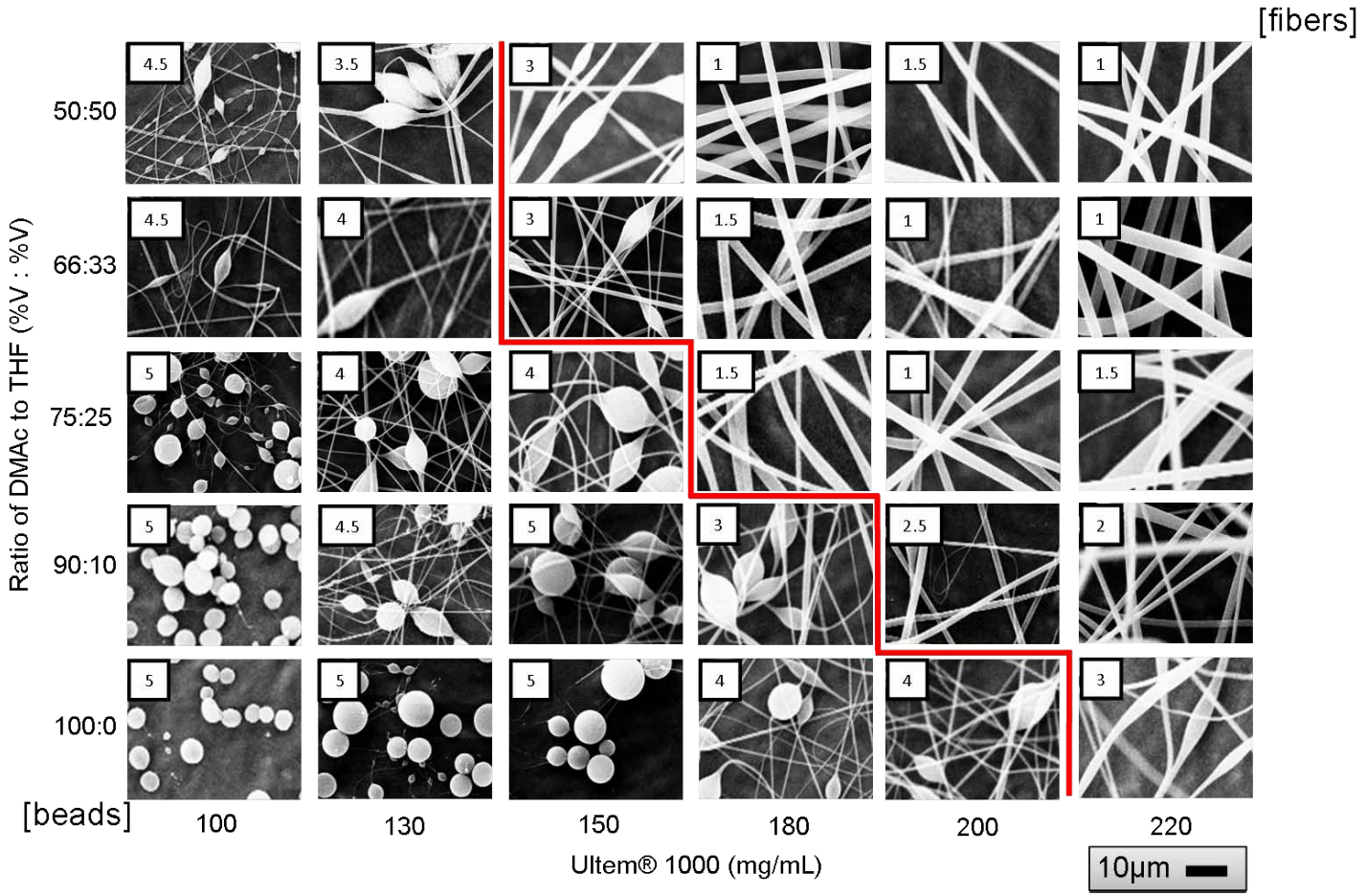

Figure 4.5 Scanning electron micrographs of electrospun Ultem 1000 (MW ~ 41,000) from precursor solutions in various DMAc and THF combinations. The micrographs show the evolution in fiber formation from beads in the lower left to fully uniform fibers in the upper right. The red line defines the region where the vastly dominant morphology is fibers. The fiber formation grade is in the upper left corner of each micrograph. Scale bars indicate 10 µm.

Figure 4.6 shows that the uniform fibers electrospun from PEI had average diameters between 1.3 and 3.8 µm, and generally increased in diameter with greater THF content. Previous results for electrospun PEI reported diameters between 500 and 700 nm when using 1,1,2-trichloroethane as the solvent, but had overall variability between 100 nm and 1.2 µm. [3]

According to previously reported experiments, the diameter of electrospun fibers is affected by many process parameters, including applied voltage, solution feed rate and needle diameter. The system used in this project could be optimized to create thinner fibers. However, for the purposes of this project, a feed rate and voltage were held constant so that a wide variation of solution concentrations could be compared, not necessarily optimized. From Figure 4.6, it was concluded that if THF % and PEI % were each increased further, the range of solution composition possibilities for fiber formation would likely broaden.

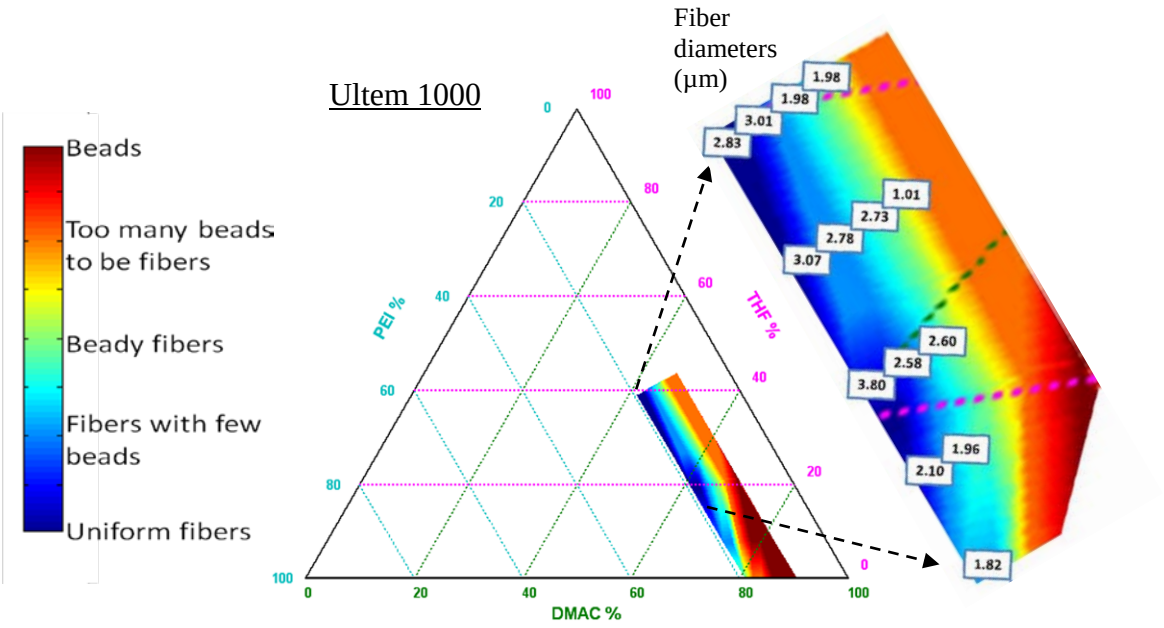

Figure 4.6 Morphology map of electrospun Ultem 1000 and 1010 in DMAc/THF.

Figure 4.6 (Continued)

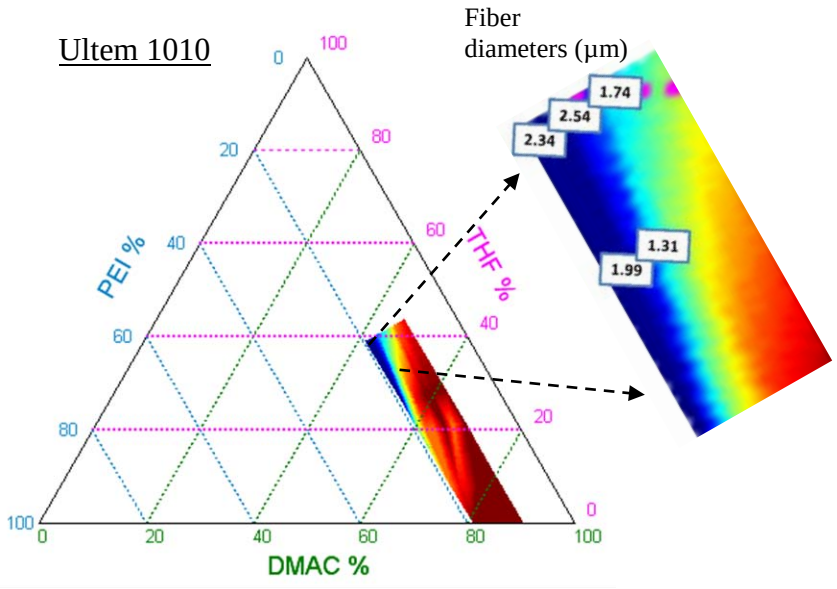

4.2 Dielectric Analysis

The pursuit of evaluating dielectric spectroscopy as a method of understanding electrospinning was undertaken with the hypothesis that if the dielectric data were to organize based upon changes in solution components – polymer or solvent – a concise comparison of the electrospun PEI morphologies to the dielectric data could be made.

Dielectric response data of poly(vinyl pyrrolidone) and poly(vinyl alcohol) (PVP/PVA) blend aqueous solutions, measured by Sengwa and Sankhla, showed very similar permittivity signals to that of PEI solutions in this project. [82] The authors found that changes in polymer concentration induced distinct frequency shifts in the permittivity signal and the location of the tan δ peak. Independent dielectric trials performed for this thesis work on aqueous PVP solutions also showed frequency shifts as the polymer concentration varied. These experiments were performed to validate

the performance of the instrument and the reproducibility of the data obtained using the Novocontrol Broadband Dielectric Spectrometer located in the Cornell Center for Materials Research Hudson Mesoscale Processing Facility. It is important to note that the interactions between PVP, a hydrophilic polymer, and the water's high conductivity amount to a much different system than that used in this project. Figure 4.7 shows the ε′, ε″, and tan δ of PVP in deionized water at various PVP concentrations, illustrating the dramatic difference in dielectric spectroscopy a polymer solution exhibit with just changes in polymer concentration.

A typical polymer relaxation from a solid polymer sample will show a distinctive relationship between the elements of permittivity. A model representation of a single polymer relaxation is shown in Figure 4.8. [16] The ε′ signals in the experimental results (Figure 4.9) looked very similar to that of the model ε′. In the experimental results, a peak in tan δ similar to that in the model relaxation was also seen. However, the ends of the tan δ peak in the experimental results did not descend to zero as is commonly seen, due to the ratio of ε″ and ε′. Also, a polymer relaxation is known to exhibit a peak in ε″, but in the experimental results the ε″ signal had a slope of approximately -1 through almost the entire frequency range and was lacking a peak.

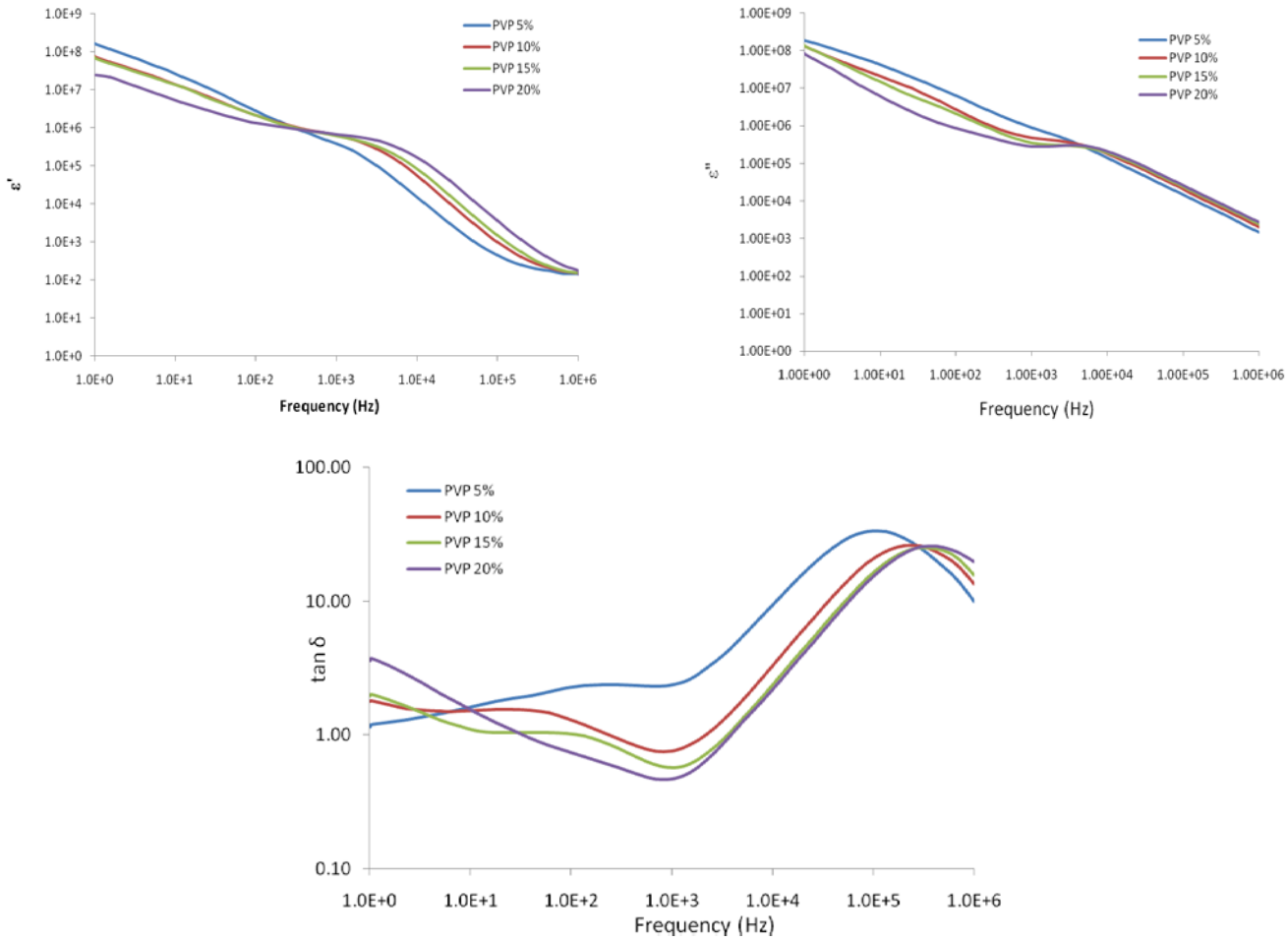

Figure 4.7 Permittivity and tan δ of PVP aqueous solutions showing an influence of PVP concentration on dielectric behavior. ε″ signals exhibit an increased curvature at 1000 Hz as PVP concentration is increased, revealing an increasing influence of ε″ to be attributed to polymer chain behavior.

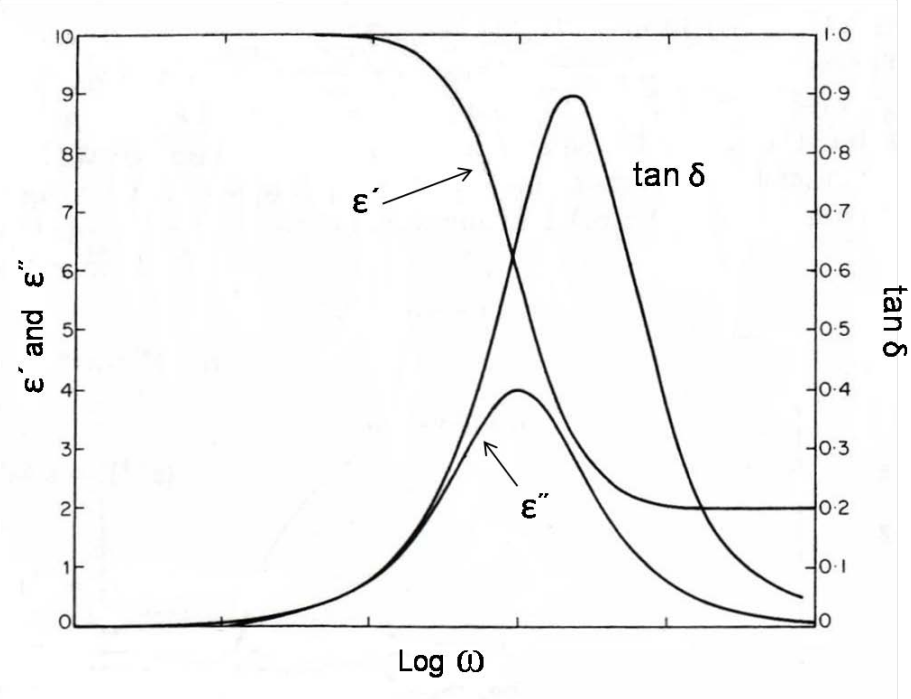

Figure 4.8 Typical permittivity curves for a polymer relaxation (solid polymer sample). [16]

Results of dielectric spectroscopy of neat solvent and polymer solutions in Figure 4.9 indicate that a polymeric relaxation does not occur over the tested range of frequencies. Figure 4.10 shows the dielectric analysis of the solvents minus polymer.

Dielectric data for PEI solutions in DMAc/THF solvent systems indicated that the solution behavior being measured may primarily originate from the solvents, and not from the PEI. The signals from pure solvent, shown in Figure 4.9, were almost no different compared to those from samples *with* PEI.

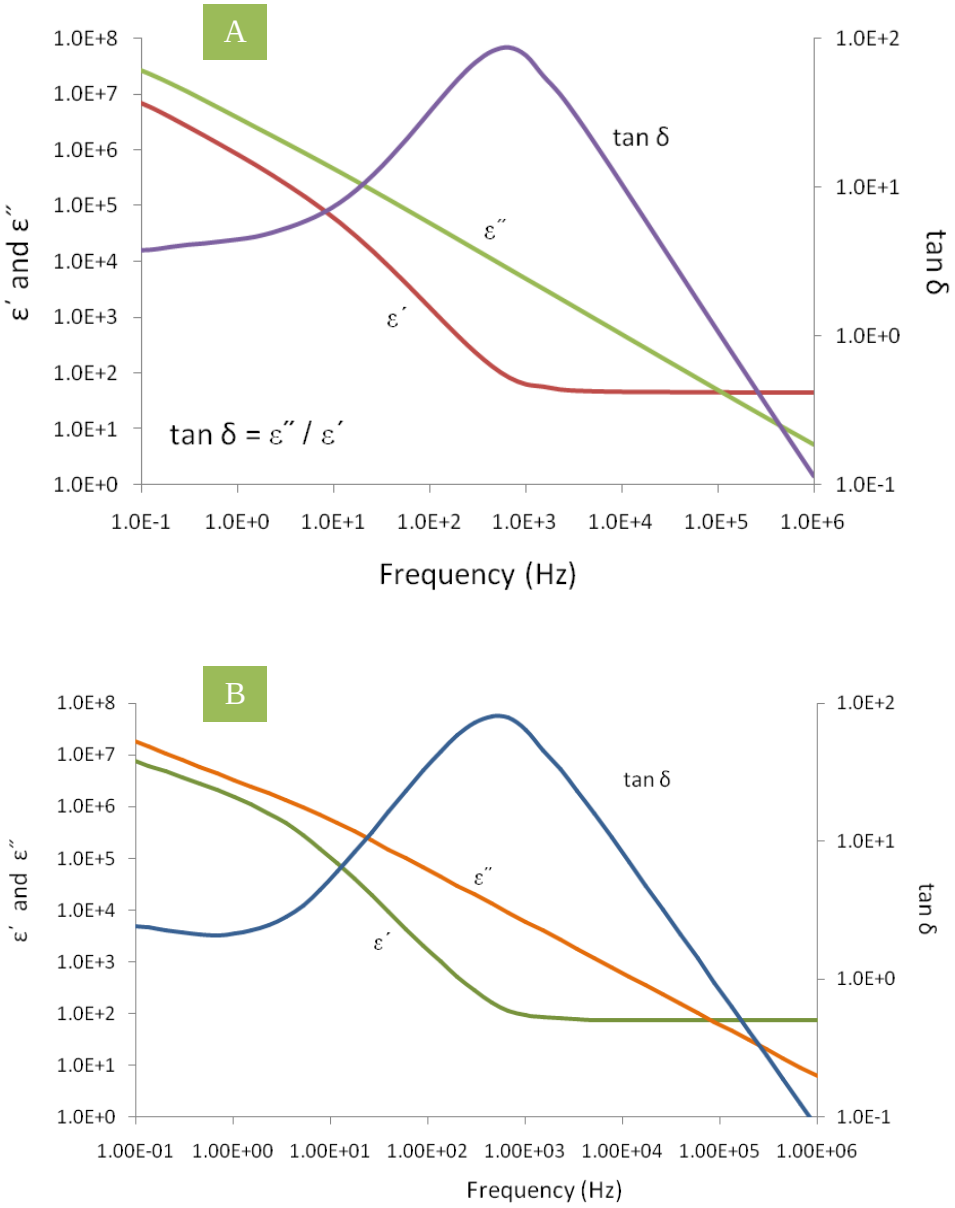

Figure 4.9 Graph A: Typical permittivity curves from PEI/DMAc/THF solutions during this project. ε˝ signals did not exhibit the characteristic peak. This behavior appears to indicate that the dielectric signal mostly originated from the solvents (Graph B: typical dielectric signals from just solvent, DMAc).

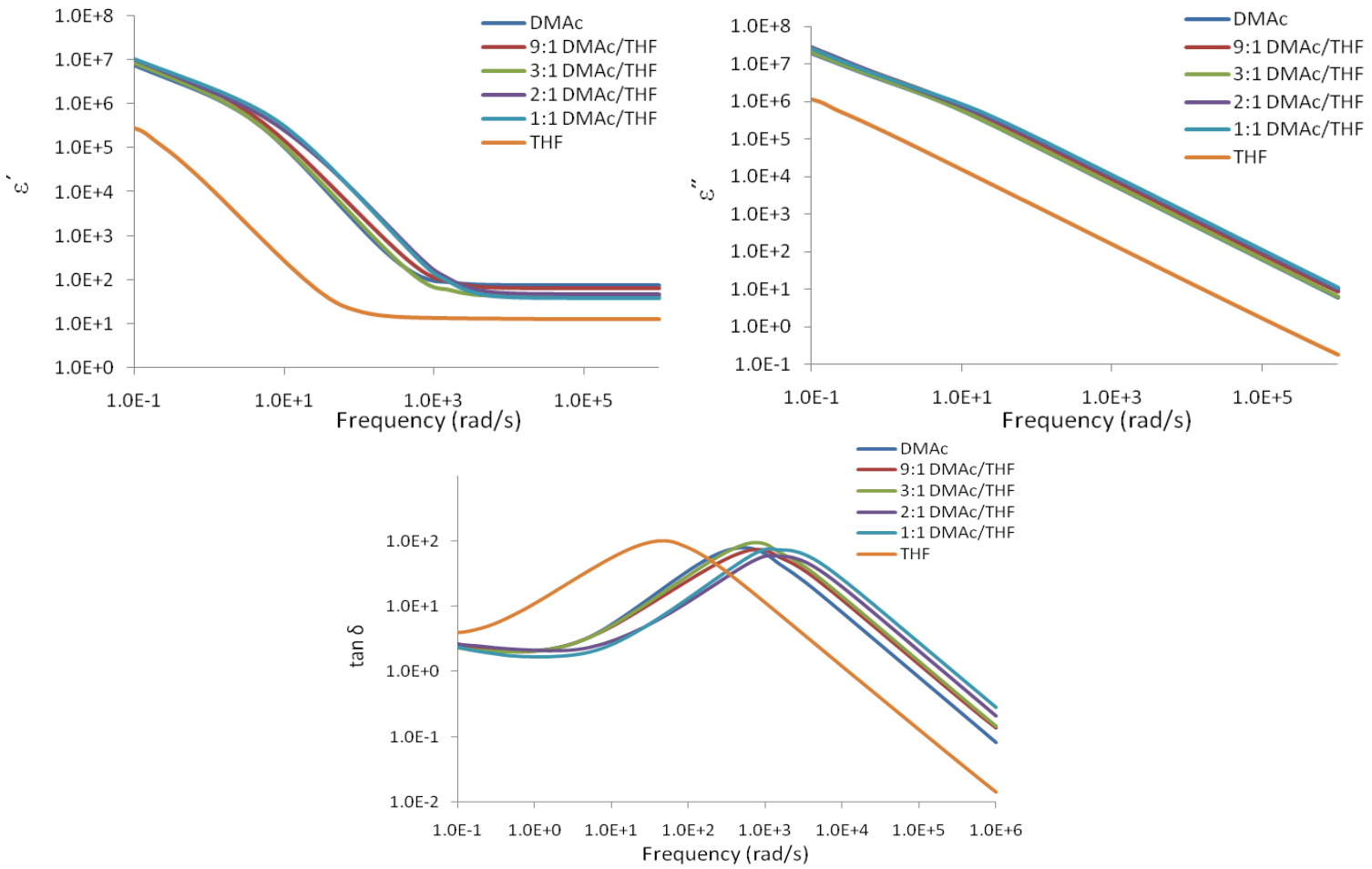

Figure 4.10 Dielectric measurements of solvents and solvent combinations used in this work. Signals show shifts in ε and t an δ when the THF content is higher than 25% of the solvent ratio. The magnitudes of the signals for solvent mixtures are very similar to signals from PEI solutions, indicating that the signals from the solvent dominate the behavior of the polymer solution.

The components of complex permittivity represent different elements of the sample system, which can reveal what part of the sample is changing with the applied electric field. For example, the curvature and inflections of ε′ are caused by the polarization of the sample. Also, the contour of the ε″ signal is due to the presence of charge carriers in the sample. Therefore, the ε″ curve will be influenced if there is a space charge contribution. In relatively entropic polymer systems, like the solutions used in this work, there is more chance for ionic conductivity and, therefore, space charge contribution. The slope of -1 seen in ε″ curves of this research shows that the signals from dielectric measurements are based significantly on the sample conductivity, and not polymer molecule relaxations. [83] It was therefore concluded that permittivity of the solutions is related to the ionic transport in the "slightly impure" solvents (reported previously by Theron *et al.* [18]). It was also concluded that the conductivity signal is related only to the conductivity of the solvent in each solution. Solvent conductivities measured by dielectric spectrometer can be seen in Figure 4.11, while conductivity meter results are in Figure 4.3.

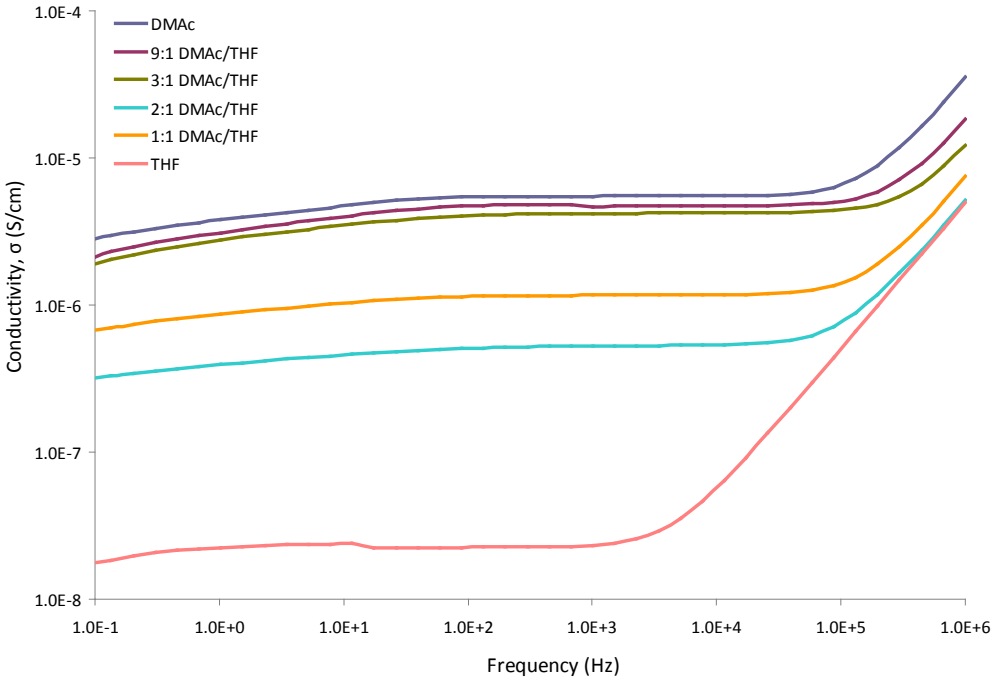

Figure 4.11 Solvent conductivities, |σ|, collected from dielectric measurements at 25°C. Conductivity signals are known to increase to an asymptote as frequency increases, so conductivity differences are evaluated in lower frequency. As DMAc was replaced with THF, the conductivity decreased.

Conductivities of PEI-containing solutions were also measured using dielectric spectroscopy. Figure 4.12 shows all conductivity signals increasing to an asymptote as frequency increases. Therefore, differences between solutions were evaluated at lower frequencies. Conductivity values did not show a trend over polymer concentration, but was generally lower when the solvent was 1:1 DMAc/THF. This is expected based on conductivity values of pure solvents.

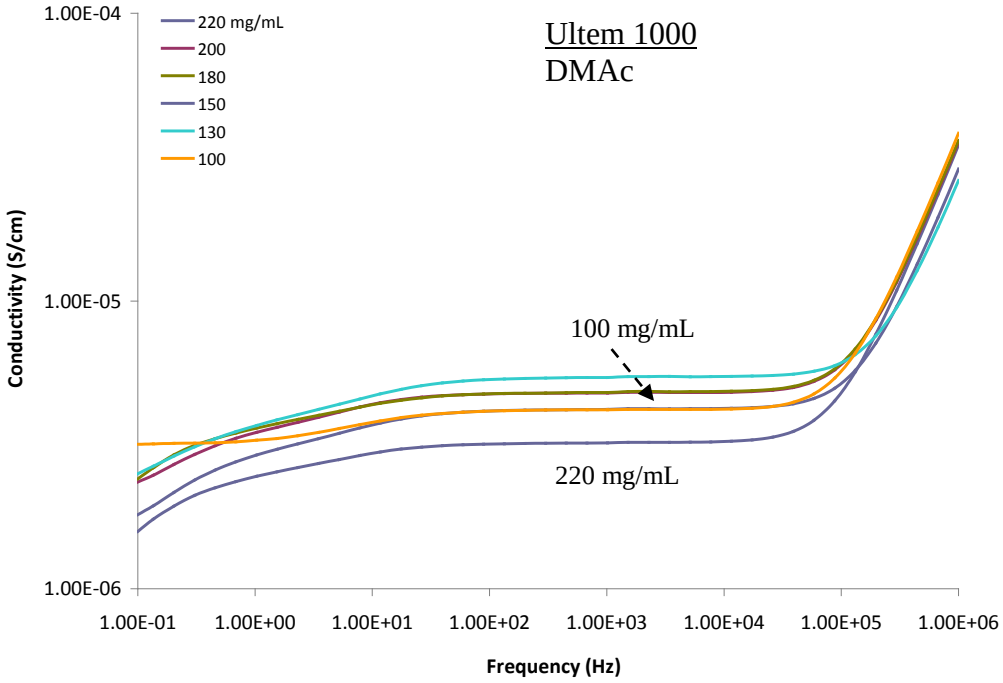

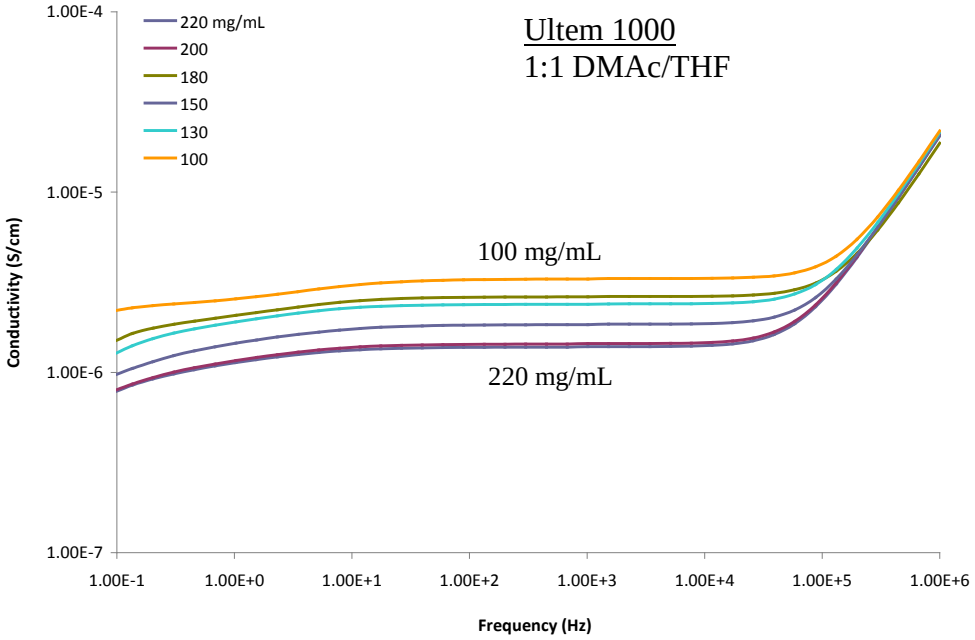

Figure 4.12 Conductivity measurements of Ultem 1000 in DMAc and Ultem 1000 in 1:1 DMAc/THF collected from dielectric measurements at 3V and 25°C. The asymptotic behavior is attributed to the calculation of conductivity from permittivity signals, $\sigma^* = i2\pi f\varepsilon_0\left(\varepsilon^* - 1\right)$. ε′ and ε″ approach a similar slope in the lower frequencies.

Since THF exhibited essentially no ionic or electrical conductivity, most of the dielectric signal of solvent mixes and polymer solutions originated from the DMAc component. In general, the samples with 1:1 DMAc/THF exhibited lower conductivities than those dissolved in DMAc. However, the dielectric data showed no statistically valid trends over PEI concentration, or solvent ratio at the same PEI concentration.

In early trials, the standard setting of 1 volt was used for the dielectric spectroscopy. The data collected at this voltage did not show the hypothesized trending, so in order to increase the signal/noise ratio, the voltage was changed to 3 volts. Also in initial trials, temperature control was not used, with the hypothesis that room temperature (approximately 20°C) was stable enough for measuring all samples. After unsuccessful data comparisons between samples, tests were run to assess change in data caused by temperature. Results from this analysis can be seen in Figures 4.13 and 4.14. It was evident from these trials that temperature induces a frequency shift in dielectric data, and should be controlled in order to be ruled out as a variable in this study. Time and temperature are related when referring to molecular movement dynamics. As temperature is increased, signals from the sample shift to higher frequencies because the motions require shorter time to occur. Specific discussion on the molecular dynamics is included later in this section.

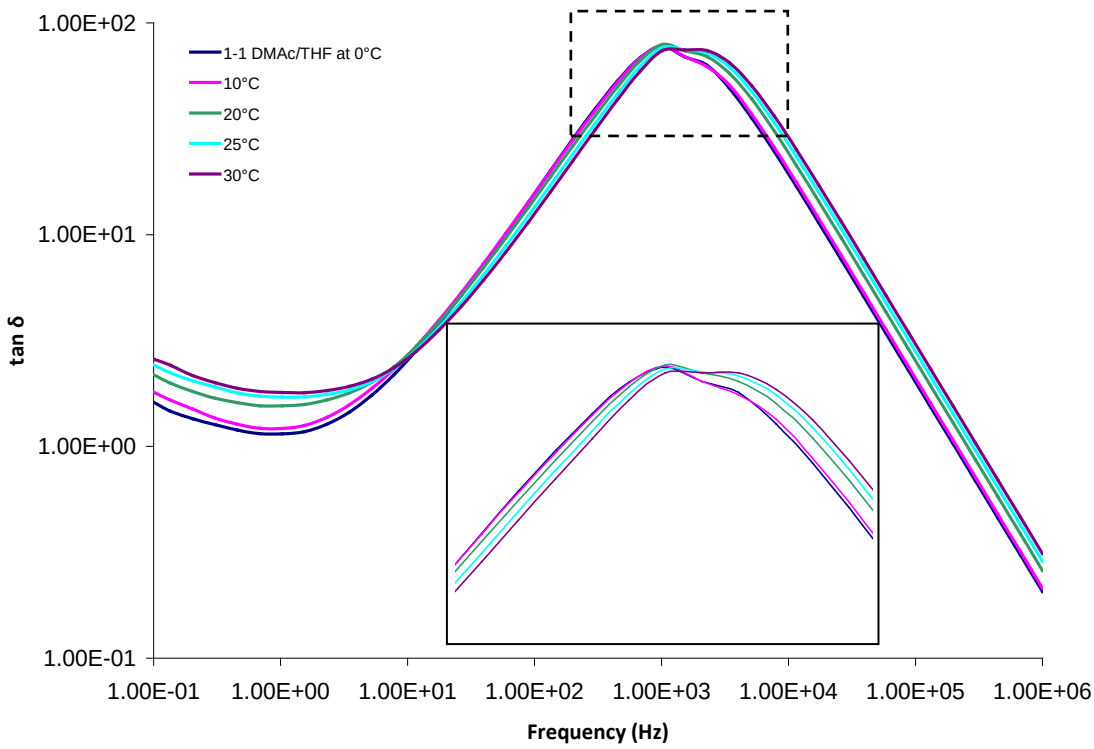

Figure 4.13 1:1 DMAc/THF tan δ at varied temperature, 0 – 30°C. Time and temperature have a similar influence on molecular movement dynamics. As temperature is increased, signals shift to higher frequencies because the motions require shorter time to occur. In this case the motion being measured is charge transport through the solvent. Inset is outlined in dashed line on larger graph. Tan δ peaks became wider as temperatures were increased.

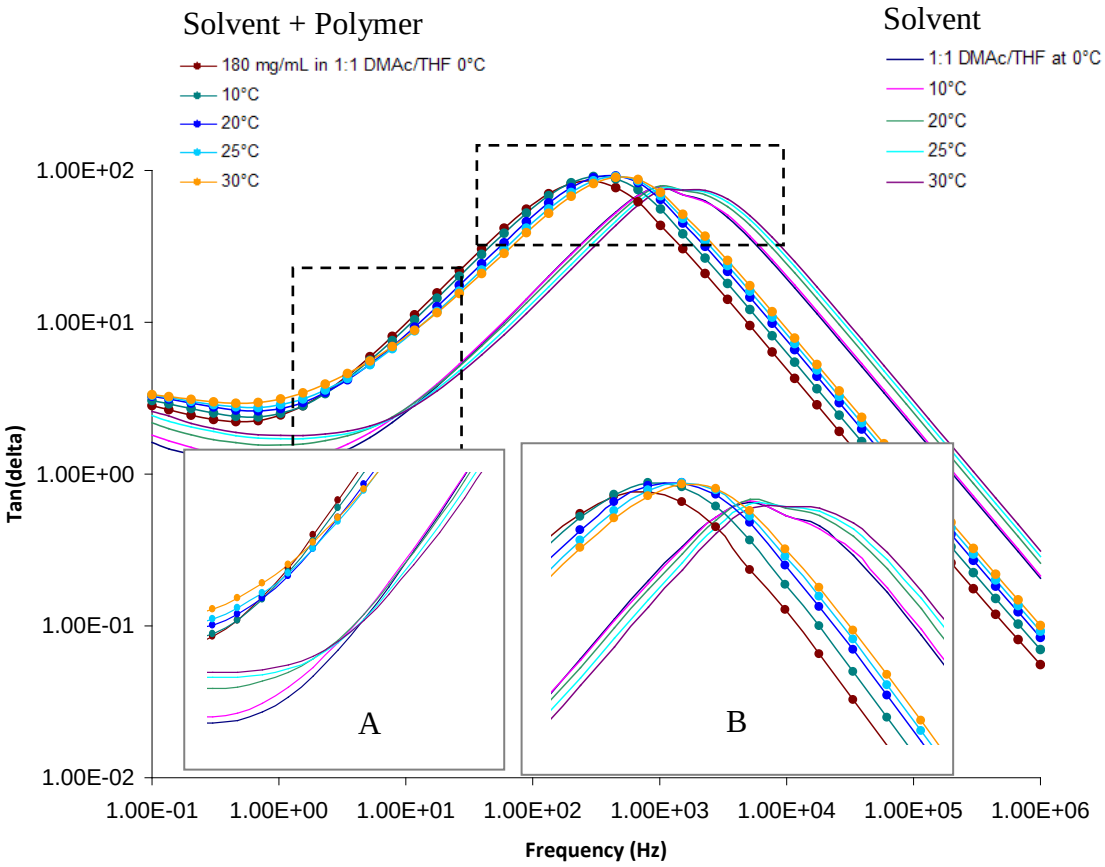

Figure 4.14 Tan δ of 1:1 DMAc/THF solvent mixture and 1:1 DMAc/THF solutions containing 180 mg/mL Ultem 1000 at varied temperature, 0 – 30°C. Sub-figures A and B show key areas of difference between solvent and solution. The temperature curves for solvent and solution change order in low frequencies. This inflection point happens at lower frequencies with the solution. Also, when polymer is present, the magnitude at the tan δ maximum is higher and occurs at lower frequencies. Both of these behaviors show that there is a change in dielectric signal when polymer is involved.

This dielectric spectroscopy analysis also revealed the change in signal induced by the presence of PEI. Compared to the 1:1 DMAc/THF solvent signals, the PEI solutions showed tan δ maximum points occurring at lower frequencies and higher tan δ magnitudes prior to the crossover of solution signals and pure solvent signals. This relationship was not the same for other solvent ratios. While DMAc did not have molecular relaxations during the dielectric analysis, it did transport charges through the system from one electrode to the other. PEI's presence appeared to affect this signal, but mostly the frequencies at which transitions in the data occur, and not the overall shapes of the curves (see Figure 4.15).

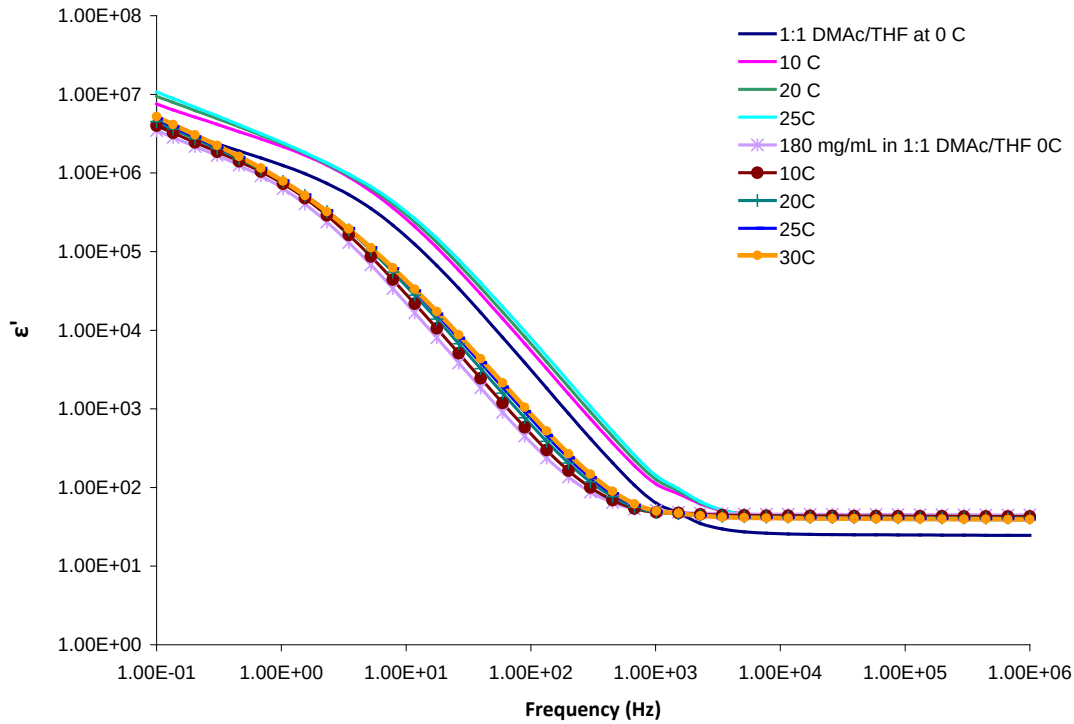

Figure 4.15 ε´ of 1:1 DMAc/THF and 1:1 DMAc/THF with 180 mg/mL Ultem 1000 at temperatures from 0 – 30°C shows a decrease in magnitude through most frequencies when PEI is present. There is an increase in magnitude and a frequency shift when temperature is increased. Conventionally used dielectric constants for PEI in all solvent ratios, shown in Figure 4.17, are ε´ values gathered at 1000 Hz.

After controlling for temperature, repeated measures of dielectric properties still showed variable results, even within a single specimen. This variation is addressed in Section 4.3.2.

Figure 4.16 shows that there were no consistent trends of frequency shift in the data as functions of solvent concentration or polymer concentration. Further comparisons for $|\sigma|$, ε'', ε', and tan δ at other concentration levels showed very similar results. These data for dielectric signal comparisons are continued in Appendix B.

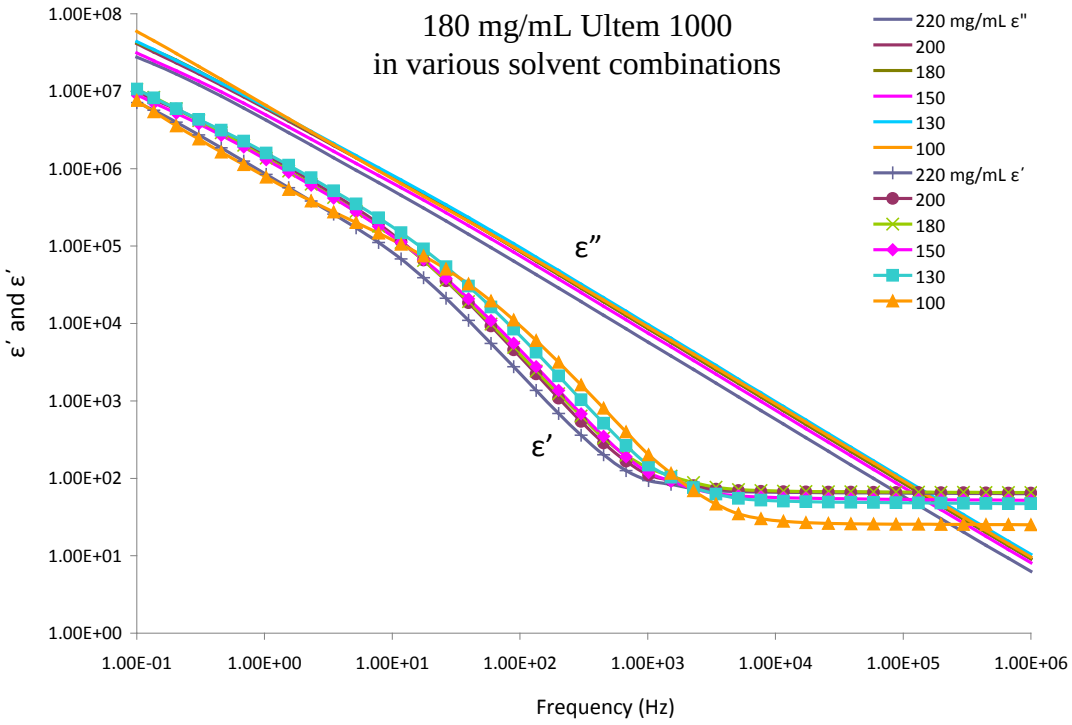

Figure 4.16 Permittivity from measurements of Ultem 1000 in DMAc and permittivity of solvent variations with 180 mg/mL Ultem 1000 show that there are no statistically significant trends of dielectric signals based on solvent ratio or polymer concentration.

Figure 4.16 (Continued)

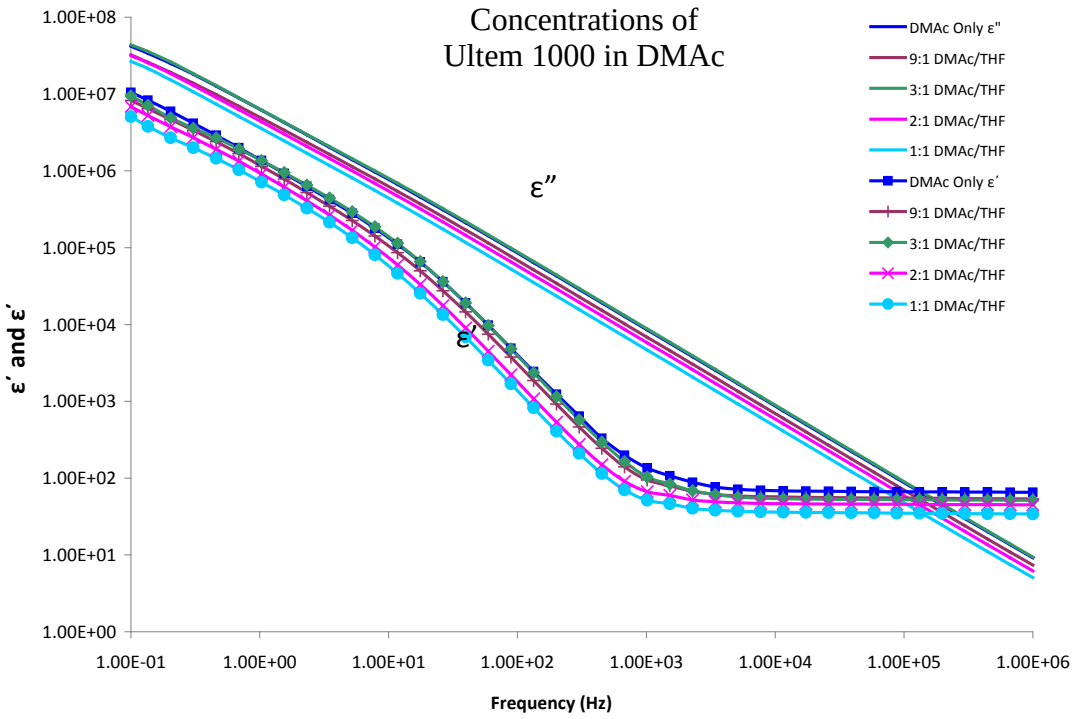

The typically communicated 'dielectric constant' of a molecule is ε′ measured at 1000 Hz. Figure 4.17 shows the ε′ values of Ultem 1000 measured in the thesis which are at the closest frequency, 1075 Hz, to the dielectric constant frequency.

It is evident from Figures 4.14 and 4.15 that PEI's presence does significantly influenced the dielectric signal of the solution. However, significantly different shifts with PEI solutions, similar to those of the PVP/water solutions in Figure 4.7, were not seen in this work. In the PEI system, the dielectric constant was generally lower with THF concentration greater than 25% (Figure 4.17).

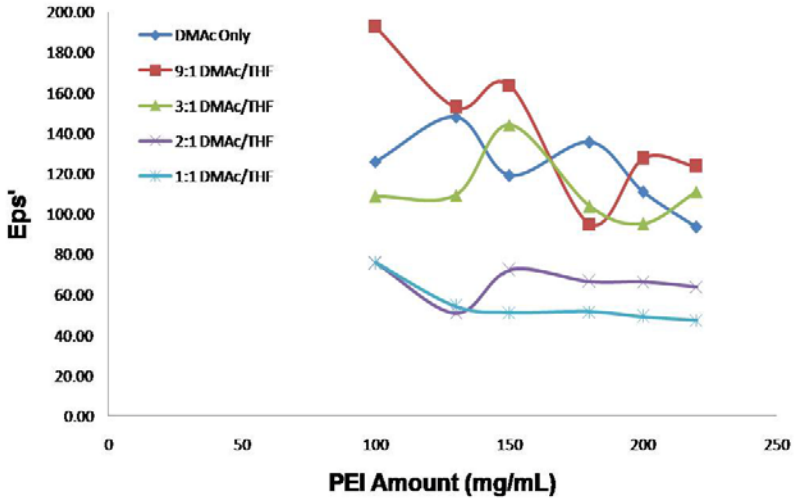

Figure 4.17 Dielectric constants, from ε´ data measured with the dielectric spectrometer, of Ultem 1000 in all DMAc/THF combinations, at 1015 Hz and 3V. The dielectric constant of PEI films was measured to be 3.15 at 1000 Hz and 50% RH.

The spectrometer sensitivity may be partly responsible for the lack of repeatability of the data. The reported region of good performance in the frequency range tested is limited to sample capacitance ranging from 50 picoFarads (pF) to 200 pF, but the spectrometer can measure capacitances up to 1 F. The range of capacitance for the samples in this work was approximately 10 nF – 0.01 F. While this is higher than the prescribed range of the spectrometer, there is only mention in the Novocontrol literature on the lack of accuracy when sample capacities are lower than the accuracy range. All samples in this work have higher capacitance than the ideal range for the spectrometer.

There was a noticeable lack of shifting or stacking of the data in this work relatable to molecular interactions between PEI and DMAc or PEI chain relaxations.

4.2.1 Statistical Analysis of Dielectric Data

Several factors contributed to the standard deviation of the dielectric measurements taken in this work. Primarily, the capacitance signal from the samples was quite small. The signal was not big enough to cause a significant and repeatable difference in data when factors of the sample are being changed (polymer concentration or solvent composition). In order to test the precision of dielectric analysis for this system, the effect of polymer concentration on solutions containing only DMAc was initially analyzed. Each specimen was measured three times. Graphing the maximum and minimum values for each specimen's repeated measurements shows that ranges of all concentrations overlap each other. Figure 4.18 shows the range in tan δ at all PEI concentrations. Figure 4.19 uses 5% confidence intervals via spline fits on the means of the ε″ signals of each PEI concentration. The confidence intervals about the ε″ means as well as the ranges of tan δ data overlap each other, indicating a lack of significant difference between dielectric measurements at varied PEI content. The conclusion from this is that there are no statistically significant differences between dielectric measurements at varied PEI concentration.

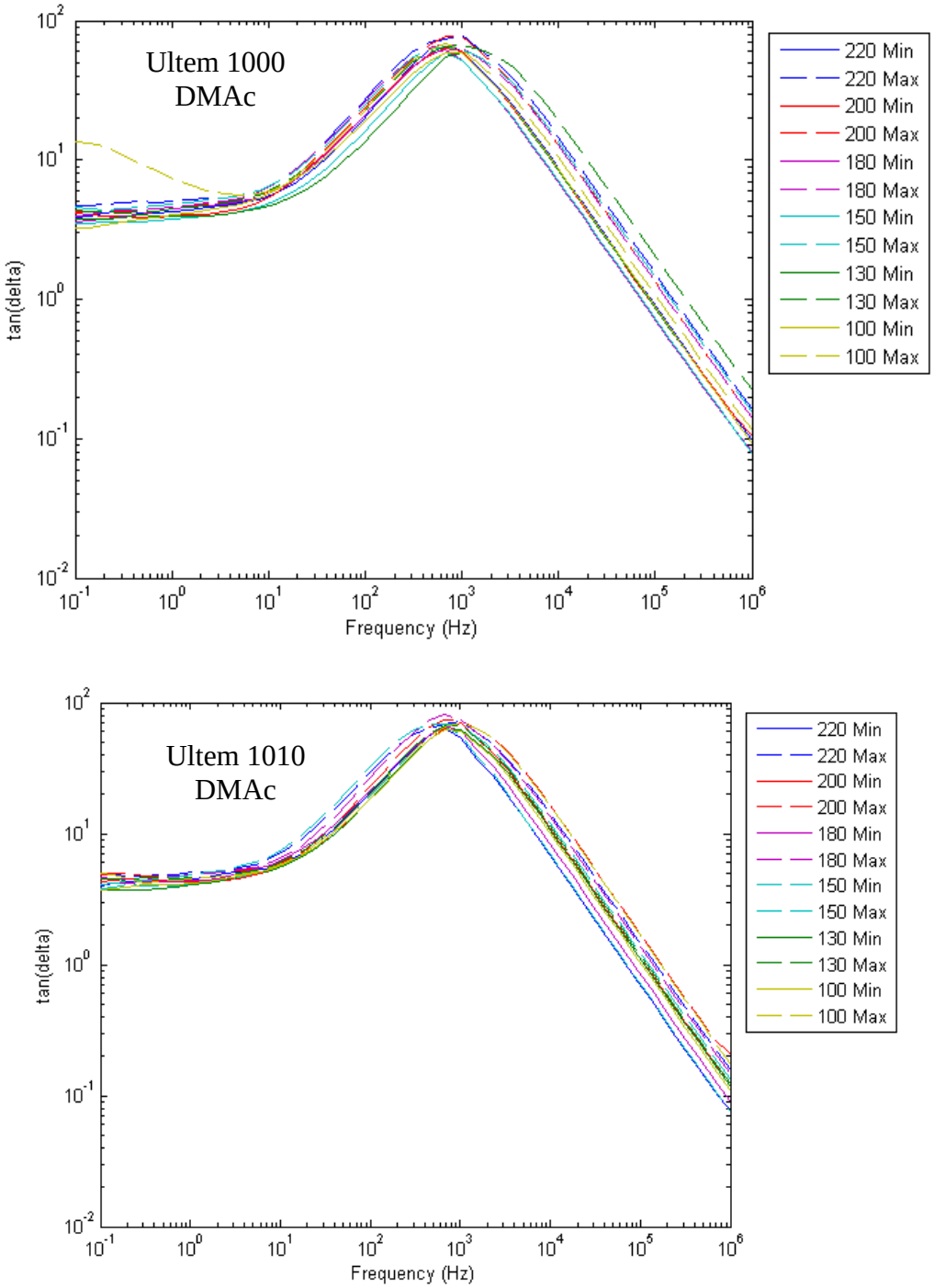

Figure 4.18 Maximum and minimum tan δ values for Ultem 1000 and Ultem 1010 in DMAc measurement repeats. Three measurements were taken at each polymer concentration (mg/mL).

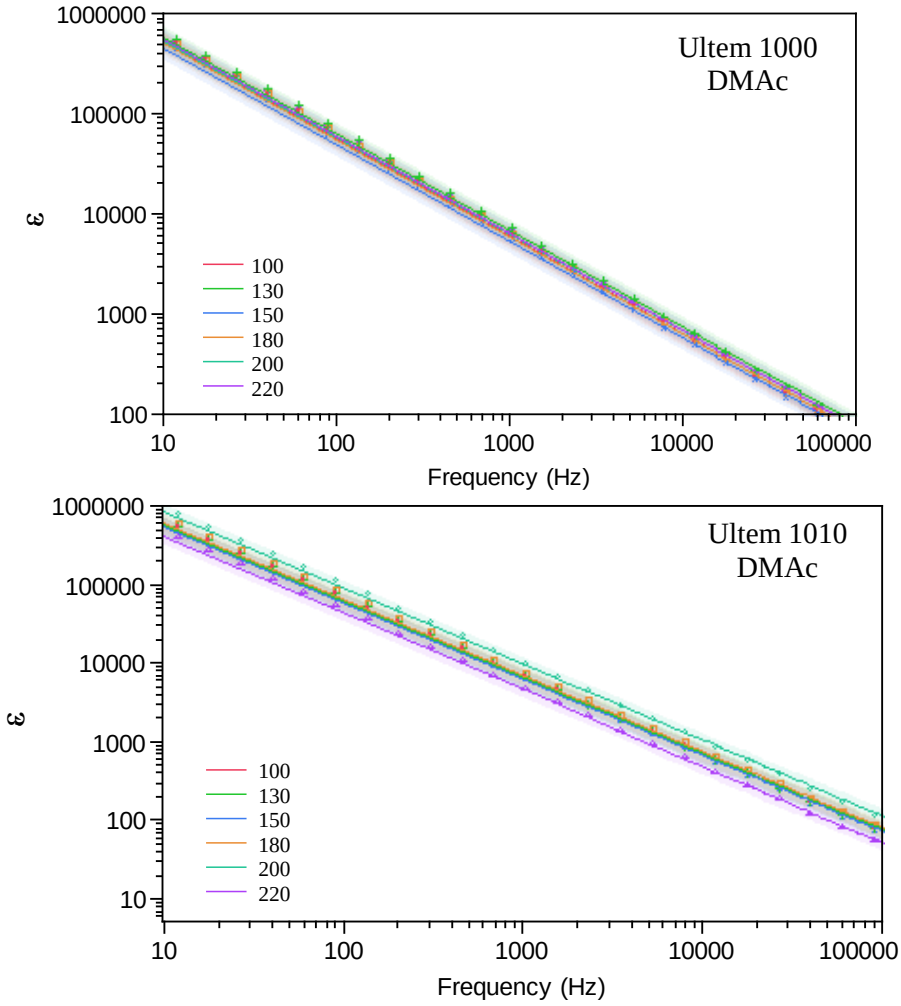

Figure 4.19 Means of repeated ε″ data with shaded 5% confidence intervals (CI) around spline fits. PEI concentrations are in mg/mL. All CI are overlapped by at least one other CI(s), so it cannot be said that measurements of different PEI concentrations are significantly different.

To confirm that the measurements were not significantly different, a standard least squares regression was fit to the ε″ repeat data at the highest frequency and then lowest frequency with the amount of PEI as the predictor, with a 95% level of confidence (Table 4.1). The t-test on the differences between the least squared means showed only two or three different groups of means and not six, which would be preferable. Table 4.2 shows the results from the t-test. Because ε′ and tan δ are directly related to

ε″, it was concluded that these data sets would show similar lacks in significant difference over polymer concentration.

Table 4.1 Spline fit equations for ε″ means of DMAc solution repeat measurements, where ν is frequency in Hz. All fit lines had R^2 values of 0.999 or better.

PEI	Concentration (mg/mL)	Equation of Fit Line	R^2
Ultem 1000	100	$\log(\varepsilon'') = 15.40 - 0.9696 * \log(\nu)$	0.999
	130	$\log(\varepsilon'') = 15.46 - 0.9609 * \log(\nu)$	0.999
	150	$\log(\varepsilon'') = 15.24 - 0.9629 * \log(\nu)$	0.999
	180	$\log(\varepsilon'') = 15.36 - 0.9657 * \log(\nu)$	0.999
	200	$\log(\varepsilon'') = 15.40 - 0.9637 * \log(\nu)$	0.999
	220	$\log(\varepsilon'') = 15.46 - 0.9670 * \log(\nu)$	0.999
Ultem 1010	100	$\log(\varepsilon'') = 15.45 - 0.9657 * \log(\nu)$	0.999
	130	$\log(\varepsilon'') = 15.44 - 0.9648 * \log(\nu)$	0.999
	150	$\log(\varepsilon'') = 15.41 - 0.9664 * \log(\nu)$	0.999
	180	$\log(\varepsilon'') = 15.53 - 0.9680 * \log(\nu)$	0.999
	200	$\log(\varepsilon'') = 15.85 - 0.9648 * \log(\nu)$	0.999
	220	$\log(\varepsilon'') = 15.13 - 0.9712 * \log(\nu)$	0.999

Table 4.2 Student's t-test of Least Squared Means Differences of ε″ for DMAc solution dielectric measurement repeats

Ultem 1010 in DMAc at 10^6 Hz	Significant Difference Grouping*			Least Squared Mean
200 mg/mL	A			2.4909397
180		B		2.0489749
130		B	C	1.9917879
150		B	C	1.9551229
100		B	C	1.9261456
220			C	1.6279525
Ultem 1010 in DMAc at 10^{-1} Hz				
200 mg/mL	A			17.763851
180	A	B		17.394187
130		B		17.277438
150		B		17.245272
100		B		17.231836
220		B		17.040924

Table 4.2 (Continued)

Ultem 1000 in DMAc at 10^6 Hz				
200 mg/mL	A			2.0816635
180	A			2.019187
130	A			1.9843538
150	A			1.901483
100	A			1.8976297
220	A			1.8107085
Ultem 1000 in DMAc at 10^{-1} Hz				
200 mg/mL	A			17.306649
180	A			17.278059
130	A			17.275605
150	A			17.253101
100	A			17.149834
220	A			17.092831

* Different letters mean significant difference

Another statistical analysis was performed against the fiber formation gradient created from SEM images. This model was run to achieve a reasonable evaluation of fiber grade effect, if any. Tests performed on measurement repeats with DMAc samples showed the dielectric data to be unreliable for comparisons between polymer content, but this did not describe the change over solvent ratio. ε′, ε″, and conductivity data were used at a single frequency (1 Hz) as the predictors in a standard least squares regression of the fiber form gradient. A general decrease occured in permittivity when THF concentration was increased, because charge transport through the sample was less when less DMAc was present in the solution (Figure 4.17). The regression formulated for fiber form grades using dielectric data as the independent variables, Figure 4.20, showed a general clustering of predicted fiber form grades by solvent ratio. The 1:1 DMAc/THF data were grouped in the lower fiber formation grades (both actual and predicted) and DMAc data were grouped in the upper fiber formation grades (again, both actual and predicted).

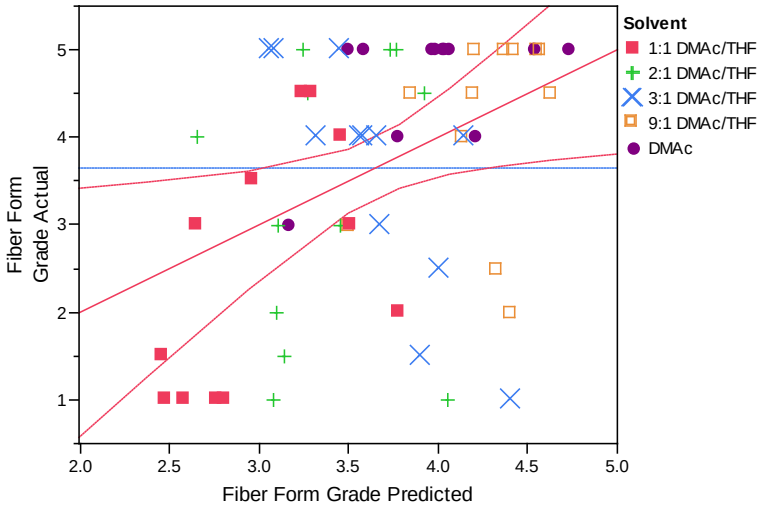

Figure 4.20 Standard least squares regression of fiber form grades for both Ultem 1000 and 1010. The ε′, ε″, and conductivity data at 1 Hz were used as the predictors. The regression showed dielectric analysis to not be significant in the prediction of fiber form grade. The p-values for ε′, ε″, and conductivity were 0.3998, 0.3359, and 0.3327, respectively. The model had a R^2 of 0.174, and only explains 17% of the variation in the fiber form grade. The red dashed lines are the 95% confidence interval around the spline fit for the data, while the blue dashed line represents the model if no predictors were used.

However, the regression showed dielectric analysis to not be significant in the prediction of fiber form grade. The p-values for ε′, ε″, and conductivity were 0.3998, 0.3359, and 0.3327, respectively. The model had a R^2 of 0.174, meaning the values of dielectric permittivity and conductivity only explained 17% of the variation in the fiber form grade.

While repeat dielectric measurements of DMAc solutions did not show significant differences between polymer concentrations, measurements at solutions with THF content higher than 33% showed a subtle decrease of ε′ values, as in Figure 4.17. The goal of this part of the project was to determine the usefulness of dielectric spectroscopy as a direct help in understanding morphology differences during electrospinning. For the polymer/solvent system used in this project it was concluded,

based on lack of statistical significance, that dielectric spectroscopy could not definitively help predict fiber formation during electrospinning. Additional systems should be evaluated, with higher polymer/solvent molecular interactions and possibly a more conductive solvent to increase the signal.

4.2.2 Time Domain Dielectric Analysis

This method was employed briefly during this thesis project. The resulting data showed conductivities too high (currents were measured in the milliamp range) for reasonably precise evaluations of the dielectric properties in the time domain (Figure 4.21). Typically, the recommended scale of current for this method is picoamp.

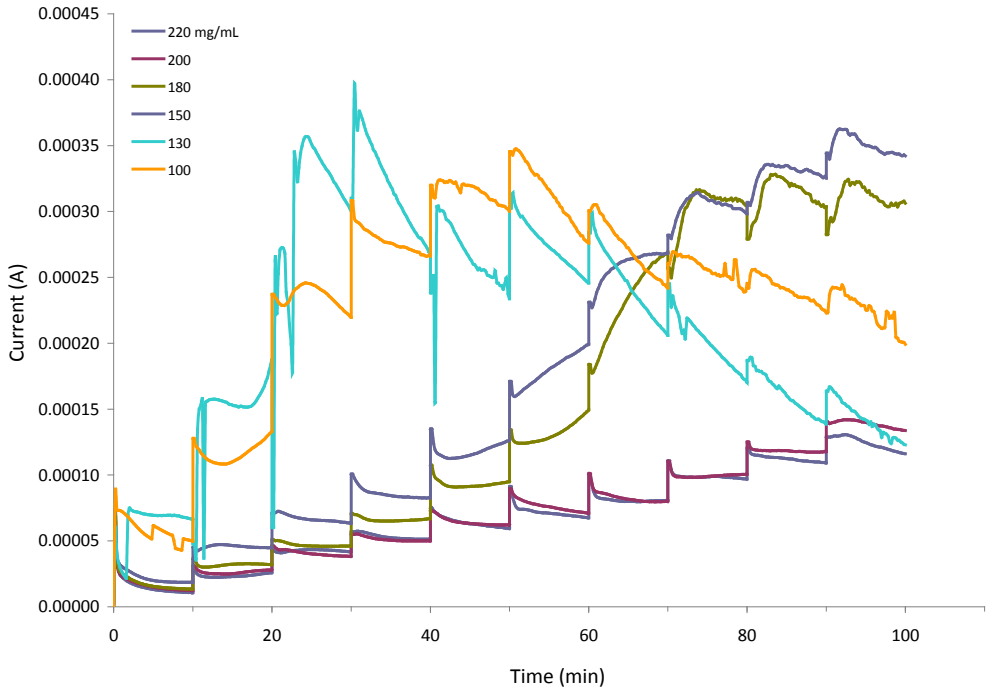

Figure 4.21 Time domain currents from dielectric measurement of Ultem 1000 in 1:1 DMAc/THF. Direct current was used at 10 minute intervals for a total of 100 minutes. Samples with lower concentrations of PEI showed current too high for reasonable time domain dielectric analysis. Samples with higher concentrations showed lower conductivity values.

4.3 Rheological Analysis

The rheological results of all specimens were compared with respect to variations of PEI and THF concentrations. All samples had constant shear viscosities (See Figure 4.22), which indicated Newtonian behavior.

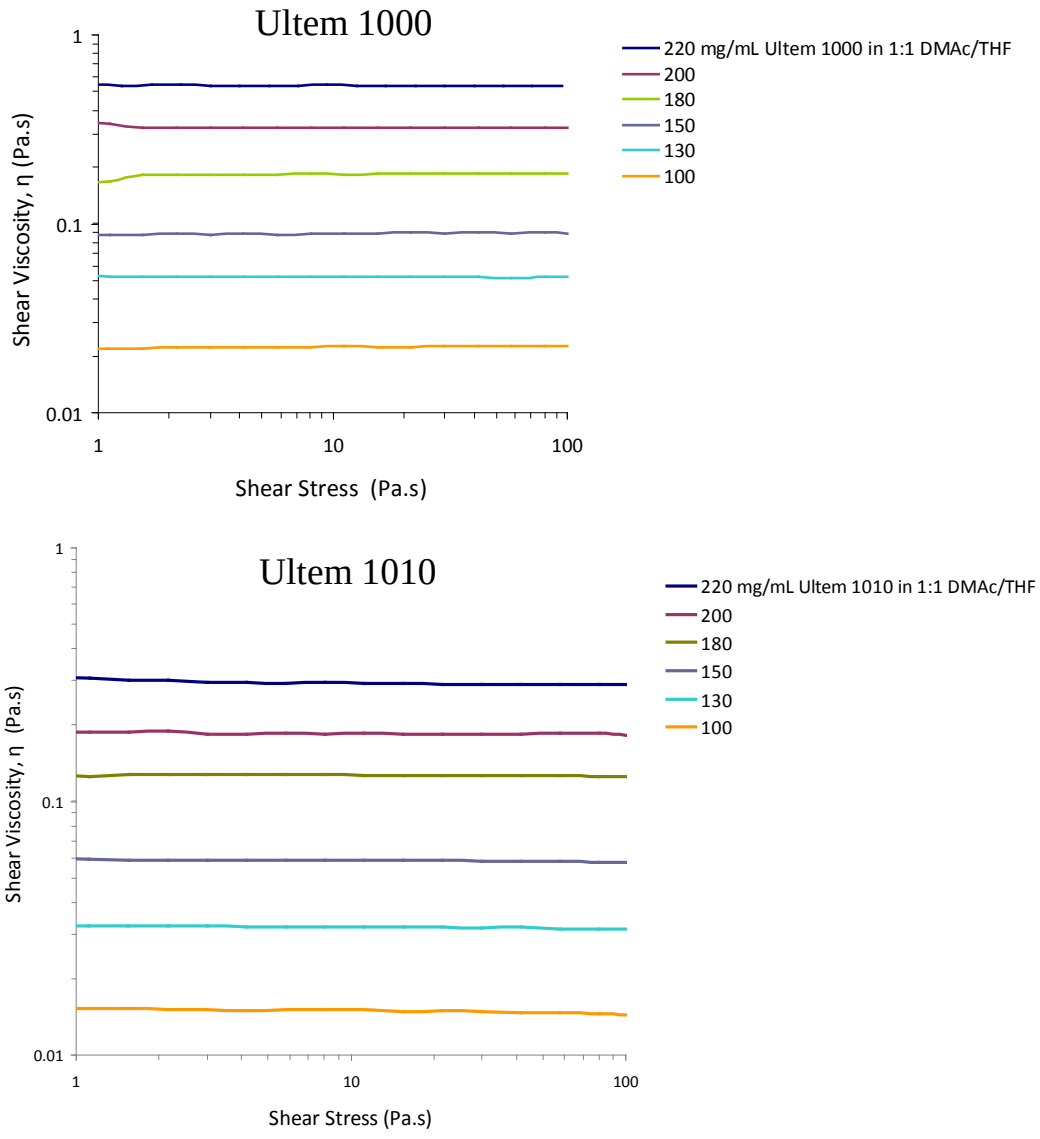

Figure 4.22 Shear viscosities of Ultem 1000 and 1010 in 1:1 DMAc/THF show that the solutions exhibit Newtonian behavior. Deviations from constant viscosity are attributed to THF evaporation from the unsealed geometry, and not the actual viscosity of the solution. For comparison of unsealed and sealed geometries see Section 4.3.1.

Newtonian behavior of solutions were also confirmed using dynamic rheological measurements (complex moduli) (See Figure 4.23). The loss modulus, G″, was found to be approximately two orders of magnitude higher than the storage modulus, G´.

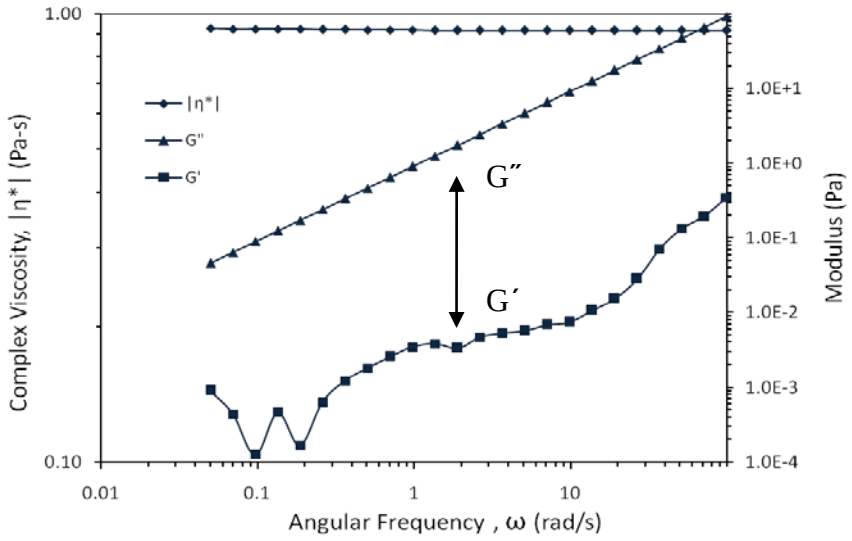

Figure 4.23 Complex viscosity and modulus data for 220 mg/mL Ultem 1000 in 3:1 DMAc/THF shows that even at the highest concentration of PEI used, the loss (liquid) modulus was more than 2 orders of magnitude higher than the storage (solid) modulus, indicating that liquid properties dominated the behavior of the solutions.

Also, the G´ values were low and often even gave negative points at lower frequencies. These negative values resulted from machine and sample limitations, and were interpreted as revealing that G´ data in low frequencies were negligible, especially at lower PEI concentrations. Stress sweep measurements looked like Figure 4.24, and the stress point chosen for each sample was in the middle of the linear region of the G´. Each sample's G´ also descended as the stress was increased. The point when this happened was the point at which the sample was instable against the "high" stresses and was not shear thinning. This instability point was related to network formation within the sample and occurred at higher stresses as the polymer

concentration was increased. Specimen with different solvent ratios showed very similar results for G″, G′, and η*. Data for all frequency sweep comparisons is continued in Appendix C.

The values of G″ for Ultem 1010 and 1000 are in Figure 4.25. Increase in PEI concentration increased the G″ of the solution. The values of G″ for Ultem 1000 were higher in magnitude than those for Ultem 1010 data at the same concentration. This behavior can be attributed to their difference in molecular weight. Because G″ reveals the energy dissipated from a stressed sample, when more polymer is present in a solution, there is more potential energy to dissipate during a response to the applied stress. [19] Similar relationships are seen with specimens of different solvent ratios.

G′ of Ultem 1010 and 1000 are shown in Figure 4.26. With low concentrations of polymer in the solution, and therefore a lack of chain entanglements, the rheometer detected less elastic behavior. Therefore, the G′ data were mostly negative in the lower and higher frequencies. Also, the PEI concentrations for all solutions were too low to have quality signals in elastic modulus. Ideally, the signals would have been linear and exhibited signal magnitudes which stacked in order of the PEI concentration.

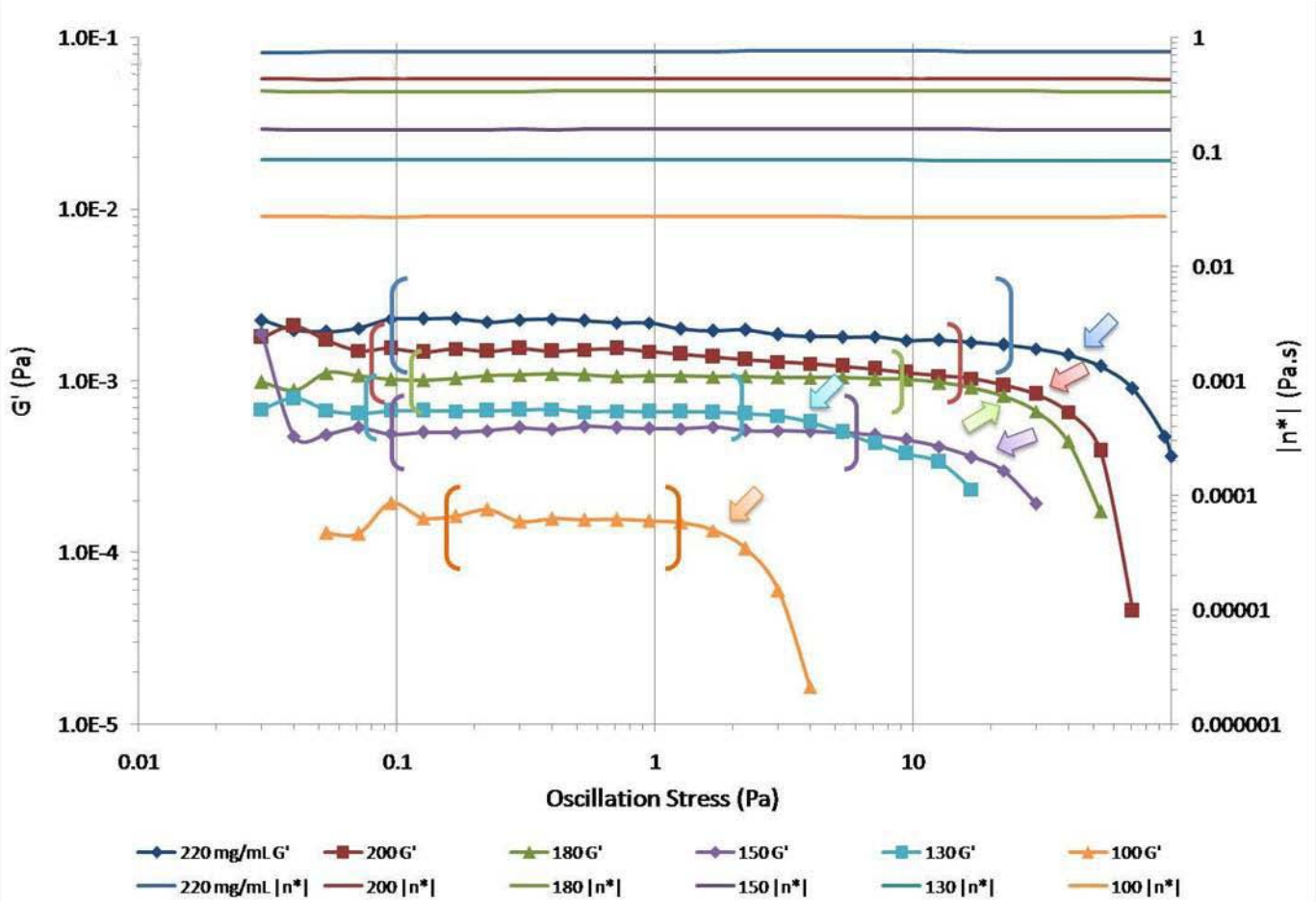

Figure 4.24 Stress sweep measurements as a function of PEI concentration for DMAc solutions. Brackets show linear viscoelastic regions, while arrows point to the critical strength points of the micro domains and the subsequent instability of the measurements. Complex viscosity shows all samples to exhibit Newtonian behavior. Average values of complex

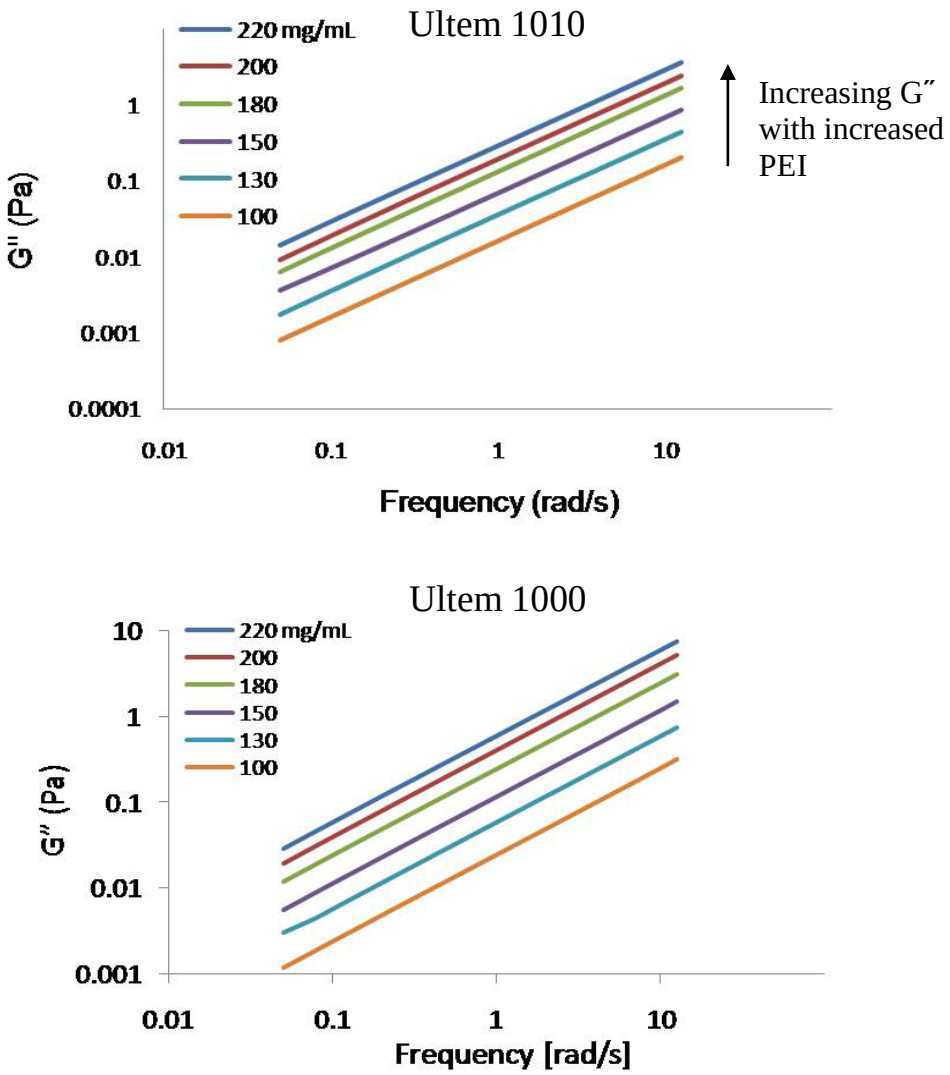

Figure 4.25 Loss modulus of Ultem 1010 and 1000 in 1:1 DMAc/THF. Increase in PEI concentration induces and increase the G″ of the solution. The values of G″ for Ultem 1000 are higher in magnitude than those for Ultem 1010 data at the same concentration. This behavior can be attributed to their difference in molecular weight.

Ultem 1010

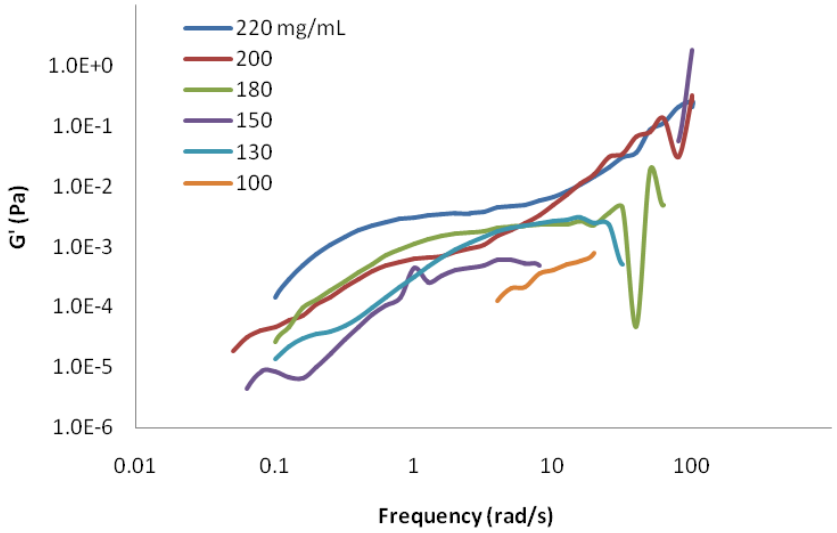

Ultem 1000

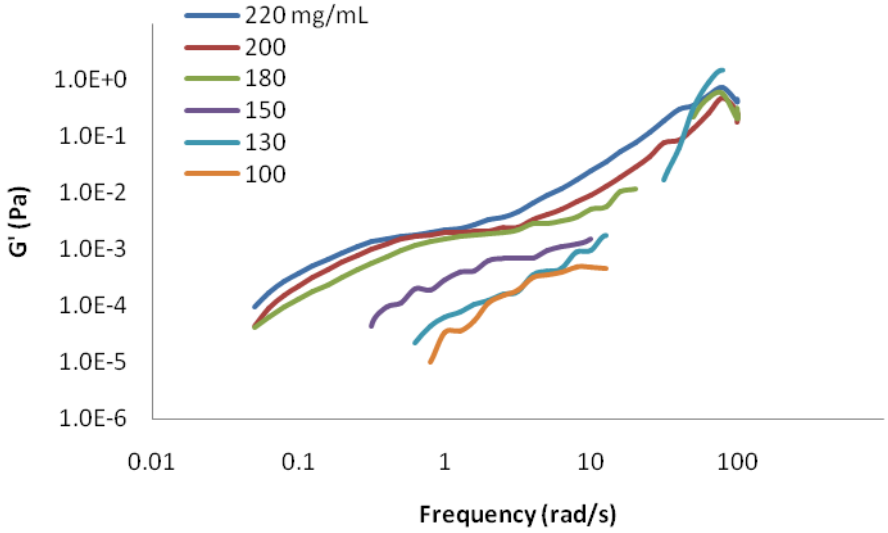

Figure 4.26 Storage modulus of Ultem 1010 and 1000 in 1:1 DMAc/THF. With lower concentrations of polymer in the solution, there is less elastic behavior detected by the rheometer. Therefore, the G´ data are mostly negative in the lower and higher frequencies. Also, the concentrations for all solutions are too low to have quality signals in elastic modulus. Ideally the signals would be linear and have magnitudes stacking in order of the PEI concentration.

Viscosities of the PEI solutions are displayed in Figure 4.27. Both the shear and complex viscosities showed that the solutions in this thesis were Newtonian in flow behavior. With increasing PEI at both molecular weights, the solution viscosities increased. Also, as DMAc was increased in the solvent ratio, the viscosity increased. This can be seen in Figure 4.28.

The average viscosities in Figure 4.28 reveal that as both DMAc and PEI were increased there was a distinct inflection point in average viscosity of the solution at around 150 mg/mL. This, however, cannot be considered the critical entanglement concentration because this was not the concentration of Ultem 1010 at which the solutions begin to form fibers. It was observed that the range in viscosities of solutions with the same PEI concentration, but varying solvent ratio, was more pronounced as PEI was increased (see arrows on graphs in Figure 4.28).

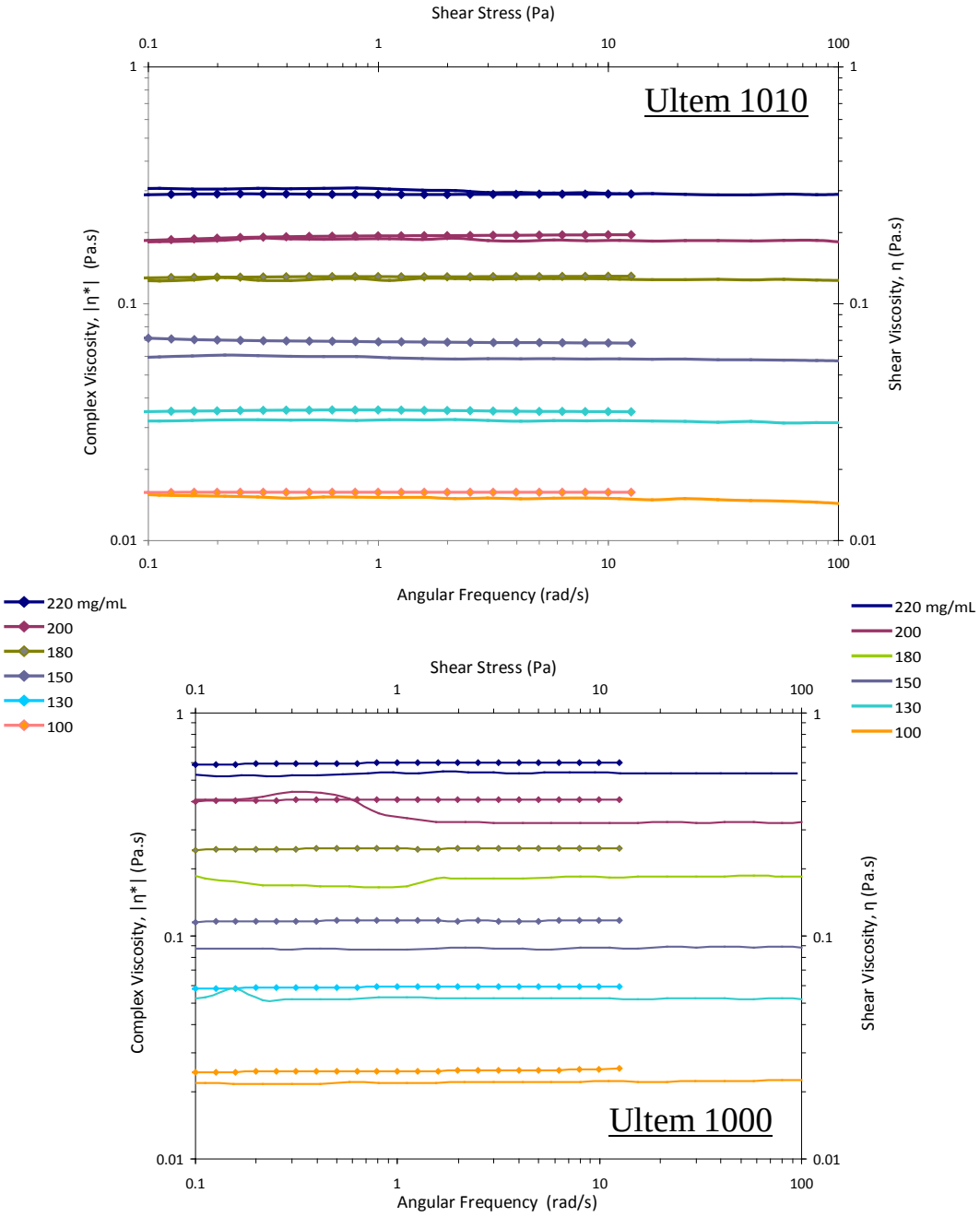

Figure 4.27 Complex and shear viscosities of Ultem 1010 and 1000 in 1:1 DMAc/THF. Shear viscosity was measured before the complex viscosity while the solution was in the rheometer. Complex viscosity being slightly higher than shear reveals that viscosity is time dependant, due to solvent evaporation. Each increase in PEI concentration increases the viscosity of the solution. Identical relationships are seen with specimen of different solvent ratios.

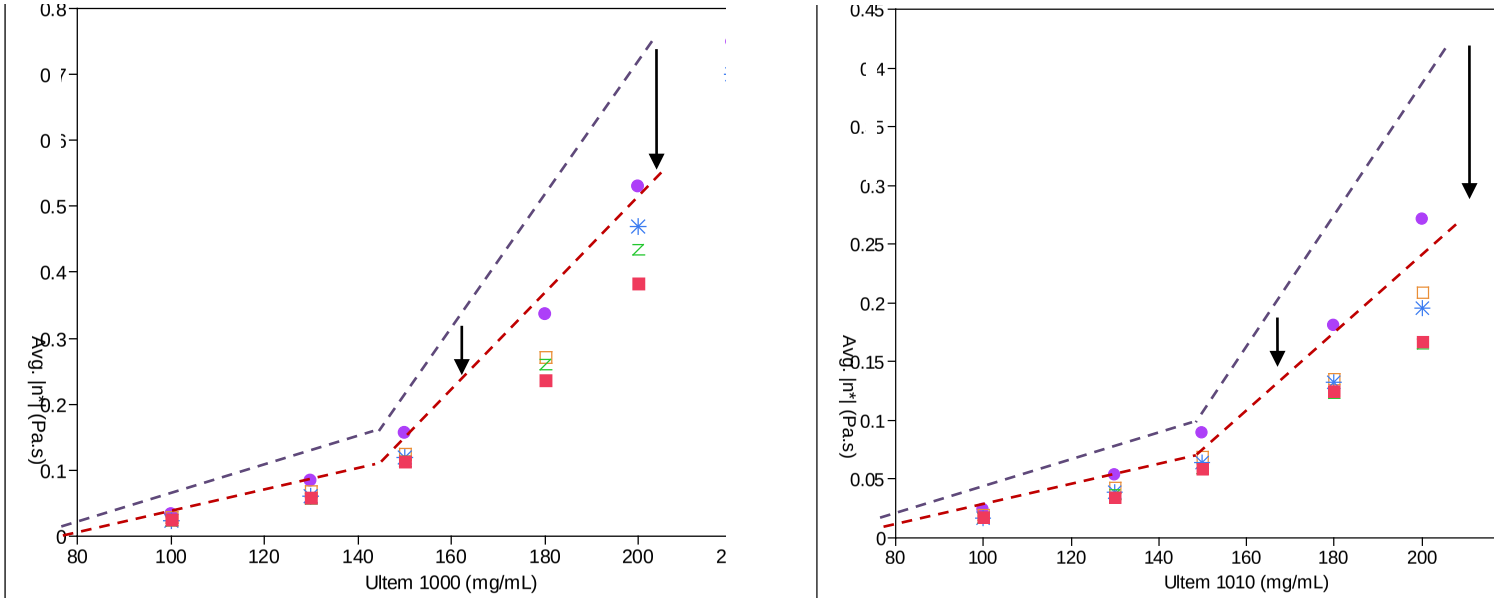

Figure 4.28 Average complex viscosity, |η*|, of PEI solutions as a function of polymer concentration and solvent ratio. Dashed lines indicate a change in slope occurring between 150 and 180 mg/mL. In Ultem 1000 solutions, this is the threshold at which fibers begin to be formed during electrospinning. This inflection also occurs with Ultem 1010, but the overall viscosity for Ultem 1010 is lower and the molecular weight is not high enough to create the necessary entanglements when electrospun. The difference in viscosity between DMAc solutions and 1:1 DMAc/THF solutions increases with increased PEI content (indicated by arrows) indicating that the addition of THF has a greater effect on solution behavior and

The average viscosities were analyzed by separating them via PEI concentration and graphing by THF concentration (Figure 4.29). This method was also employed for analysis of G″ (Figure 4.30). Red trend lines trace the Ultem 1000 data while blue trend lines follow the Ultem 1010 data. Figures 4.29 and 4.30 show that Ultem 1000 has higher viscosity and G″ at all concentrations. Also, as THF content was increased, the values of viscosity and G″ decreased in all cases.

The Buckingham Pi Theorem was used to create a dimensionless number which related the rheological properties of a polymeric solution to the electrospinning parameters of that solution. By using variables which characterized the flow, internal chain networking and elasticity of the solution – viscosity and polymer concentration – and variables which characterized the electrospinning of the solution – radius of the electrospinning needle and feed rate of the solution – a phase diagram was created describing the relationships of solution and electrospinning parameters to the resulting electrospun morphologies. For all variations of a polymer/solvent system being electrospun, if the voltage, gap distance, solution feed rate and needle gauge remain constant, a characteristic number can be evaluated based upon the polymer concentration and viscosity of each solution.

$$E = \frac{\mu \cdot r_0}{C_p f} \ , \tag{41}$$

where μ is the solution viscosity, r_0 is the initial radius of the electrospinning jet, or the inner radius of the needle used for electrospinning, f is the feed rate of the solution as it's electrospun and C_p is the concentration of polymer in the solution. In this thesis work, for example, the solution that contains 220 mg/mL of Ultem 1010 in DMAc only, having a viscosity of 0.419 kg/(m*s), using a needle gauge of 20 (3.015×10^{-4} m), and a feed rate of 0.9 mL/hr (2.50000E-10 m/s), the solution will have an E number of 2.3×10^{3}.

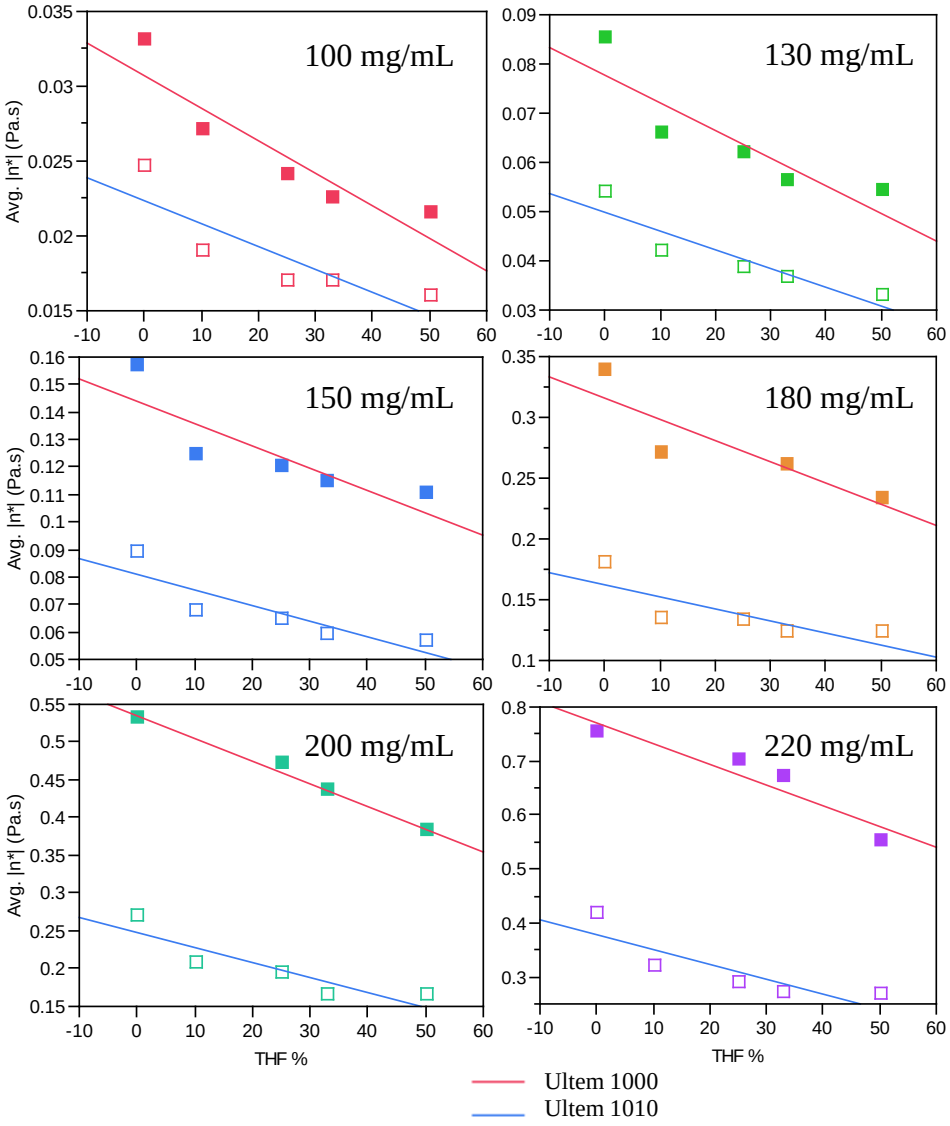

Figure 4.29 Average complex viscosities by PEI molecular weight. At all concentrations of PEI and THF, Ultem 1010 has lower viscosity than 1000. This shows the effect of molecular weight on rheological behavior. Also, as THF is increased, the viscosity at each PEI concentration decreases. The average complex viscosities are summarized in Figure 4.26.

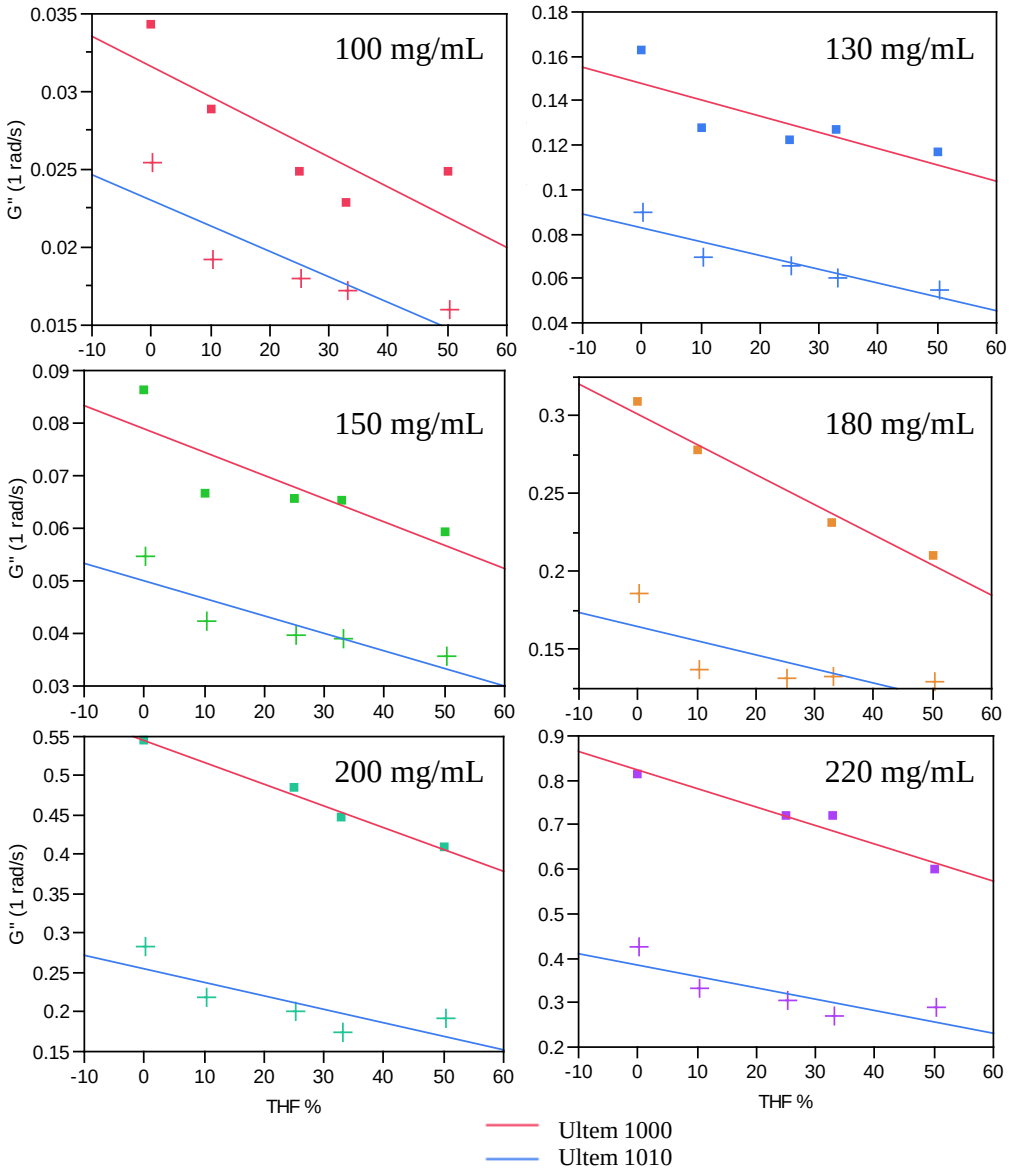

Figure 4.30 G″ at 1 rad/s shows that for all concentrations and all solvent ratios Ultem 1010 has lower G″ than Ultem 1000. This is due to the principle of G″. As the loss modulus, G″ shows the energy dissipated from a sample in response to a stress. A solution with higher polymer content, whether it is molecular weight or concentration, has more potential energy for dissipation in response to the stress. [19]

Figure 4.31 examines the contributions of polymer concentration and THF concentration in the solvent system on the resulting *E* values. The *E* number increased with the increase in polymer concentration and decreased at each polymer

concentration with the increase in THF, via the value of viscosity. This is why the slopes at each polymer concentration were negative.

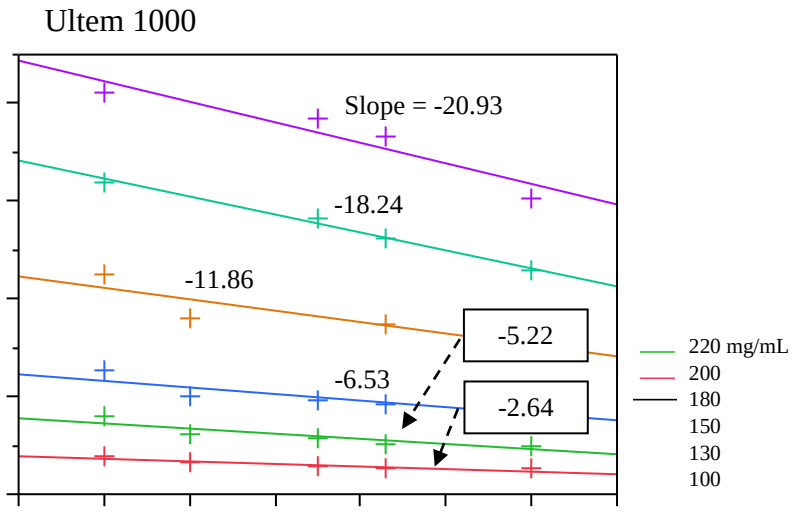

Figure 4.31 Electrospinning numbers, *E*, based on PEI concentration as THF concentration is varied. The dimensionless numbers were calculated for each sample using equation 41. Based on PEI concentration, the change in *E* with increase in THF is greater as the concentration of PEI is increased. The *E* value represents the flow properties of a solution. As PEI concentration is increased, the magnitudes of *E* increase, which indicates the influence of PEI concentration on polymer networking in solution. Also, the slope of *E* at a single PEI concentration reflects the decrease in viscosity as THF is increased.

Figure 4.31 (Continued)

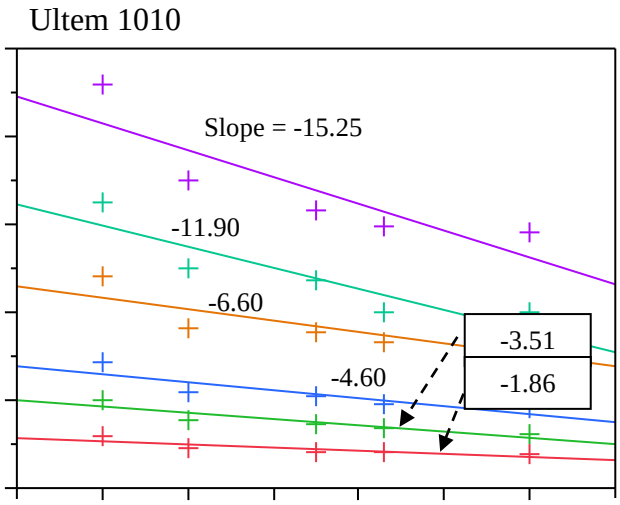

As polymer concentration was increased, there were more chain interactions and entanglements in the solution. As THF concentration was increased for each polymer concentration, the effect on the polymer network was greater, as illustrated in the increase in slope as the polymer concentration was increased. For example, if a solution contained 100 mg/mL Ultem 1000, because the polymer chains were able to disperse quite well into all solvent combinations, there was only a minute increase in polymer networking as THF was increased and, therefore, only a very small slope in *E* number. If a solution contained 220 mg/mL of Ultem 1000, as THF was increased, there were many more polymer chain entanglements. Therefore, the slope for the *E* number at 220 mg/mL was much greater, 10 times that of 100 mg/mL solutions. Figure 4.32 shows the regions of morphology found in each PEI molecular weight. When the *E* numbers of Ultem 1000 and 1010 were combined in the same graph (Figure 4.33) the regions of fiber, beads-on-string and bead formation were the same. The example solution mentioned previously, containing 220 mg/mL of Ultem 1010 in

DMAc only, with an *E* number of $2.3x10^3$ would be placed in the beads region. When electrospun, this solution did create beads, confirming the relationship between the *E* number and electrospun morphology of the PEI/DMAc/THF system.

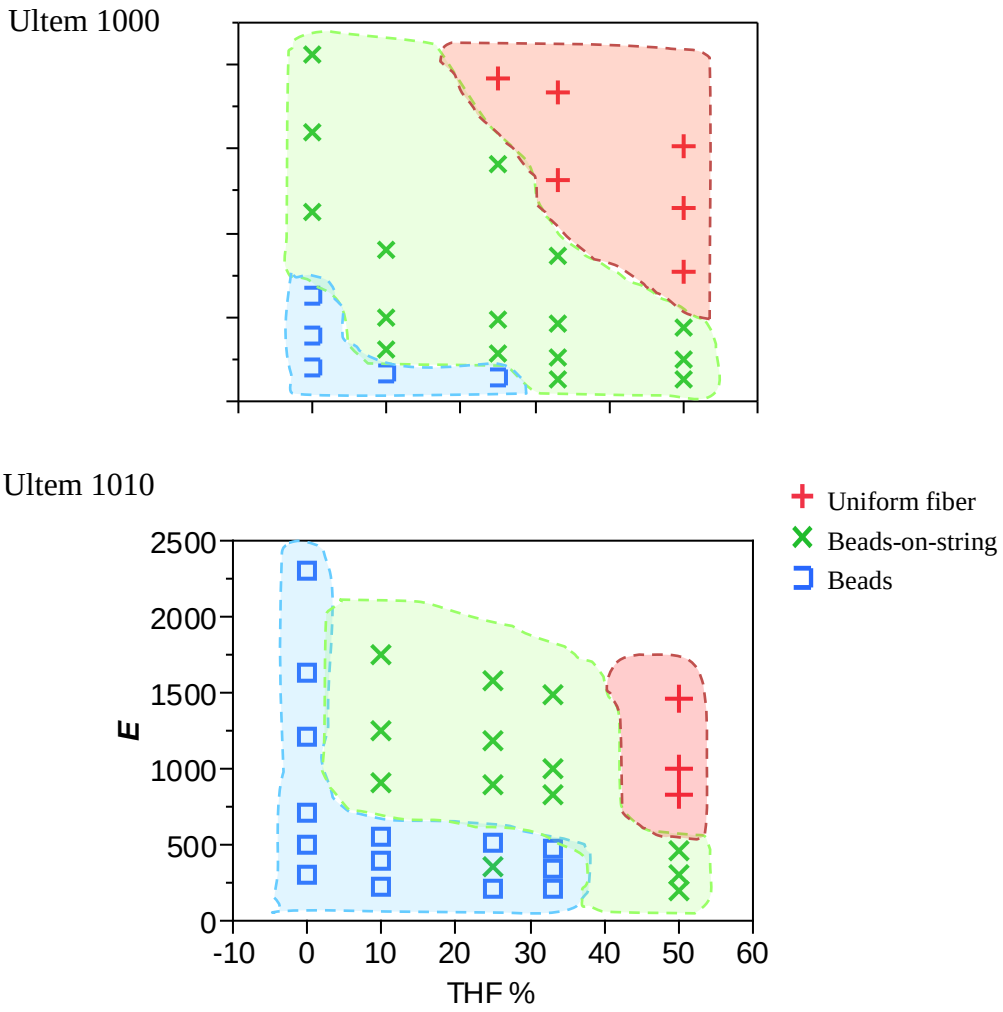

Figure 4.32 The Electrospinning number, *E*, as a function of solution concentrations and electrospun morphologies. *E* values were calculated to compare fiber formation to solvent ratio and polymer concentration. By evaluating influential factors of both rheology and electrospinning, a value representing flow properties and polymer network effect on solution electrospinnability was achieved with the *E* value. In this work distinct regions of *E* for each solvent system where each morphology is formed as well as the universality of comparing *E* with morphology were seen.

Combined:

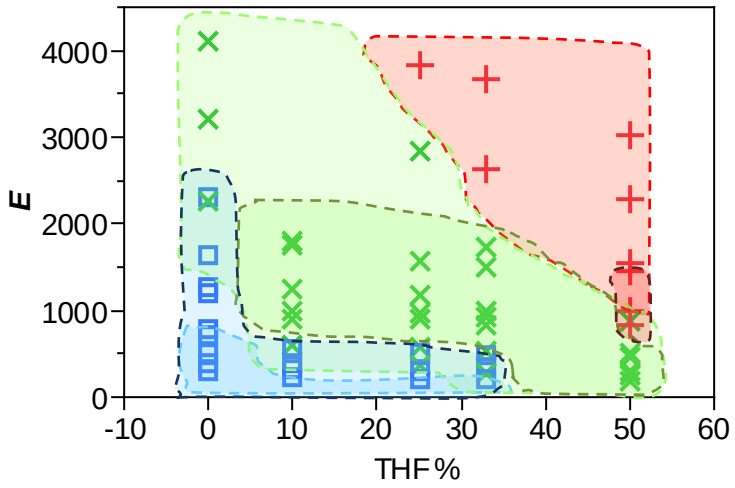

Figure 4.33 The combined Electrospinning numbers of both PEI types as functions of solution concentrations and electrospun morphologies. When the two molecular weights of PEI are combined, the regions of morphology remain almost identical to those in the Ultem 1000 graph. In this combined graph, darker outlined regions are for Ultem 1010. The morphology zones for each type of PEI line up, showing that the Electrospinning number may be used to predict morphology of electrospun PEI regardless of the molecular weight.

By keeping electrospinning parameters constant for each sample, a spectrum of morphologies was reached by simply varying the solution components' concentrations. Results of the *E* calculation showed that fiber formation depends strongly on viscosity and polymer networking within the solution. By comparing the *E* number calculations to actual morphology results it was concluded that each solvent combination has its own regions of fiber formation. Based on the calculations of the *E*, it was also concluded that regardless of the molecular weight, *E* can show the fiber formation ability of PEI. The *E* number phase diagram in Figure 4.32 indicates that having a high *E* number does not necessarily mean high quality fibers will be electrospun. The solvent system, when taken into account, must interact with the polymer network in a favorable enough way to produce fibers. Figure 4.32 illustrates

that while having a higher *E* number value is necessary, in a PEI/THF/DMAc system, one must also use at least 20% THF (or bad solvent) in the solvent mix. The required *E* number for good fiber formation decreases as THF is increased.

4.3.1 Sealed versus Non-Sealed Rheological Fixtures

The evaporation of THF from the rheological geometry was unavoidable because the solvent trap of the double cylinder couette geometry was not sealed or secured to the geometry. To evaluate the accuracy of the data collected in this work, measurements were also taken using a system with a sealable solvent trap. Results, in Figure 4.34, revealed that as THF concentration was increased, there was a greater chance of receiving inaccurate data from an unsealed geometry. The sealed geometry measured constant viscosities for all samples, and the unsealed geometry measured constant viscosities for 220 mg/mL Ultem 1000 in DMAc and 3:1 DMAc/THF samples. However, in the open geometry, while measuring the 220 mg/mL, 1:1 DMAc/THF sample, THF evaporated over time from the top of the sample, causing the solution to solidify. This caused the rheometer's motor to measure an increasing viscosity, even though underneath the hardening surface the solution consistency was still intact. Differences in the actual viscosity magnitudes between rheometers were due to differences in measurement temperatures (25°C with the unsealed and 20°C with the sealed), as well as the extended time from dissolution to measurement with the sealed geometry. Samples were measured with the sealed geometry approximately one week after dissolution.

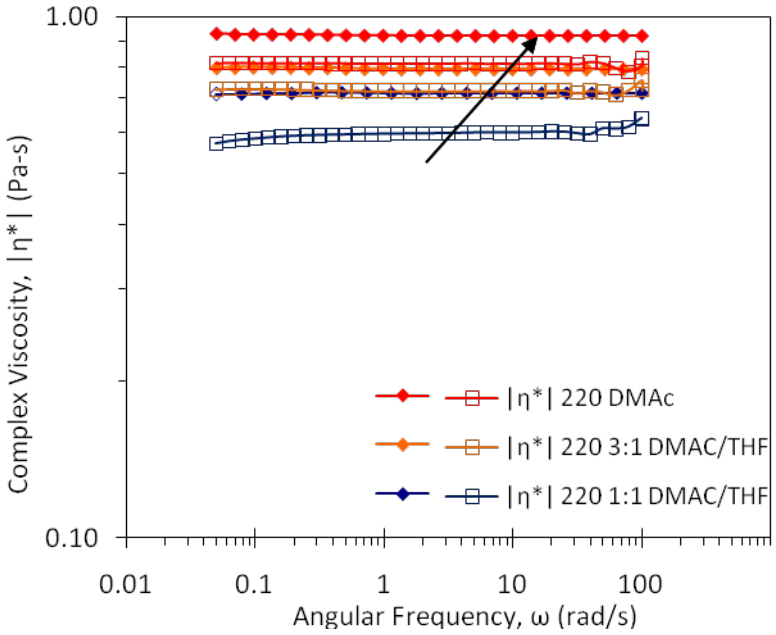

Figure 4.34 Complex viscosities of 220 mg/mL Ultem 1000 in DMAc, 3:1 DMAc/THF, and 1:1 DMAc/THF measured with the sealed and unsealed rheometer geometries. Data with open symbols are from the unsealed measurements. As THF content is increased, the viscosity decreases. The complex viscosities measured by the sealed geometry showed much more consistent viscosities, also revealing the effect which THF evaporation has on data. As the THF evaporates from the opening of the geometry, the polymer at the opening dries and causes the rheometer motor to require more torque to reach the set frequencies. This results in the rheometer interpreting the entire sample as being more viscous. This behavior is most evident in the viscosity trend of the 1:1 DMAc/THF sample.

Measurements were also taken of the 1:1 DMAc/THF solvent mixture with 180 and 130 mg/mL Ultem 1000. Results showed very similar magnitudes of moduli and viscosity when compared between the two geometries. However, the viscosities were again more constant with the sealed geometry. For the figures of these comparisons see Appendix C.

4.3.2 Effect of Polymer Molecular Weight

Table 4.3 outlines the estimated molar masses of the two PEI's used. With the estimated molar mass provided by GE, an approximate degree of polymerization was calculated, followed by a more exact molar mass, given the monomer molar mass.

Table 4.3 Molecular Properties for PEI: Molar mass estimate as reported by GE. (Equations acquired from Young and Lovell [19])

	Molar Mass (g/mol)			
PEI	**Monomer**	**Polymer est.**	$\overline{X}_n$ * **est.**	**Calculated Molar Mass (g/mol)**
Ultem 1000	594.62	41,000	69	41,029
Ultem 1010	594.62	33,000	55	32,704

* Degree of Polymerization

The viscosities of Ultem 1010 (33,000 g/mol) solutions are lower than the samples of Ultem 1000 (41,000 g/mol) with the same solution concentrations. From Figures 4.4 and 4.5, a significant difference in fiber formation between the two polymers was seen when they were electrospun with the same solvent ratios and PEI concentrations. Because there is a need for critical entanglement before fibers will form, [11, 13] it is evident that the critical entanglement concentration for Ultem 1010 is higher than that of Ultem 1000. In most solvent ratios tested in this project, fibrous electrospun morphologies do not even occur with the concentrations of Ultem 1010 that were tested, but do occur at all solvent ratios of Ultem 1000. The difference in molar mass between Ultem 1010 and 1000, while not enough to show a great difference in dynamic shear measurements, is enough to significantly affect the formation of nanofibers when electrospinning. The differences seen between polymer molecular

weights may also be due to the bad-good solvent effect. This is addressed in Section 4.4.1.

4.3.3 Effect of Polymer Concentration

Polymer concentration in the precursor solution is known to be a significant factor in the electrospinnability of a polymer. [12, 84, 85] In this project an increase in fiber formation was observed when the concentration of either Ultem 1010 or 1000 was increased, and the composition of solvents was constant. Both McKee *et al.* and Gupta *et al.* established that with increased polymer concentration there's an increased likelihood of fibers being formed, because there is an increase in chain to chain interaction, resulting in a higher viscosity (Figure 2.25). Shenoy *et al.* [86] established the relationship between the concentration of PS in the solution, and the PS morphology after electrospinning. By graphing the calculated viscosity of entanglement (akin to critical entanglement concentration) against the concentration of PS in solution, the authors were able to map the production of beads, beads-on-string, and uniform fibers at varied temperatures (Figure 4.35). Zong et al. [87] also concluded a progression of fiber formation with polymer concentration when they electrospun poly(d,l-lactic acid) (PDLA) (see Figure 4.36).

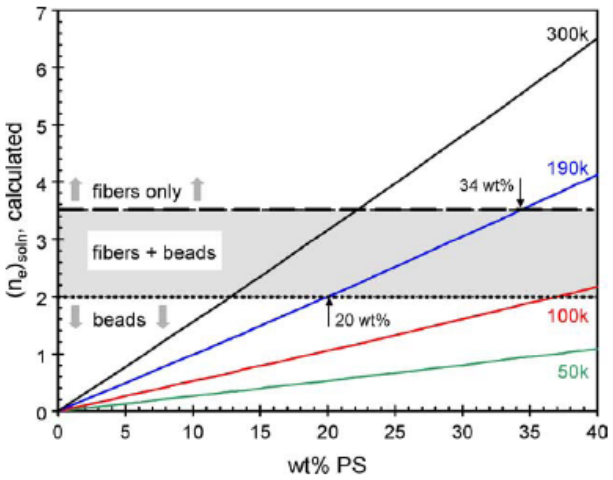

Figure 4.35 Regions of morphology for PS electrospun at various temperatures as the calculated viscosity of entanglement is graphed over PS concentration. [86] $(n_e)_{soln} = MW/(MW_e)_{soln}$, where $(MW_e)_{soln}$ is the entanglement molecular weight in solution.

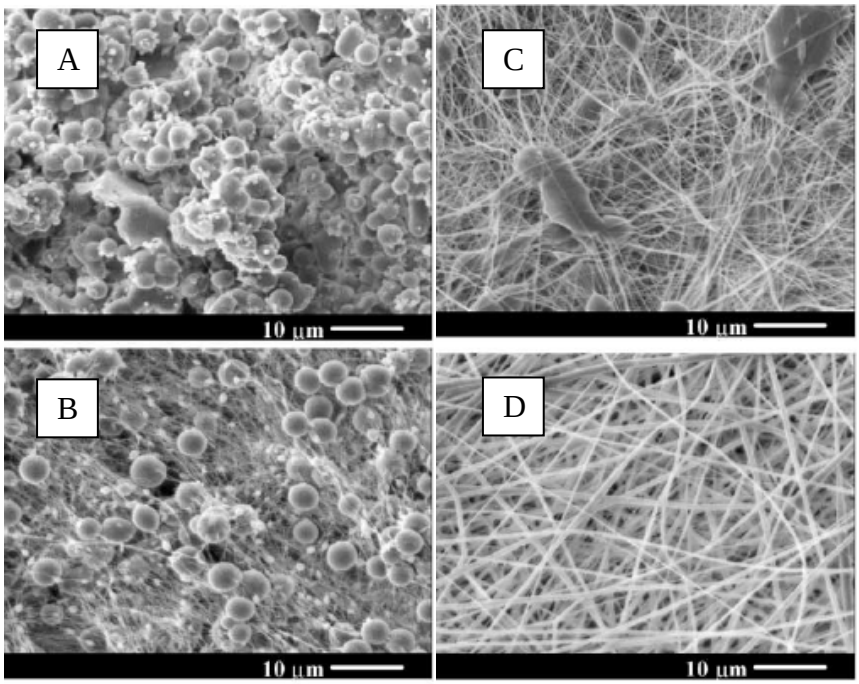

Figure 4.36 Electrospun PDLA by Zong et al. [87] at percent concentrations of A: 20%, B: 25%, C: 30% and D: 35%.

4.3.4 Statistical Analysis of Rheological Data

In the analysis of rheological data, first the viscosity data was modeled using PEI concentration, THF concentration, and molecular weight of the PEI as predictors. Both concentration predictors were converted to their solution weight percents in order to use specimen specific values. Then, the viscosity was log transformed (Figure 4.37).

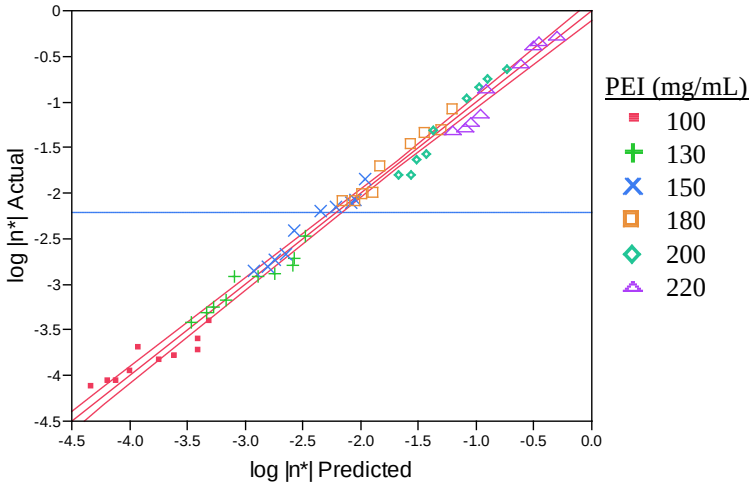

Figure 4.37 Actual viscosity data for both polymers against predicted viscosity data from a model with PEI molecular weight, weight percent THF, and weight percent PEI as the predictors. All predictors were significant, with p-values < 0.0001. The R^2 for the model, $\ln|\eta^*| = -9.37 + 7.13\text{x}10\text{-}5(MW) + 0.32(\%\ PEI) + -0.01(\%\ THF)$, was 0.986. This meant that the PEI molecular weight and concentrations of THF and PEI in solution explained 99% of the variability in viscosity. The red dashed lines represented the 95% confidence intervals about the mean of the model. Because all data points were very close to or within the CI bands, it was concluded that the solution parameters predicted viscosity with a good degree of accuracy.

The R^2 for this model was 0.986 and all predictors had significant p-values (< 0.0001). So, the model for log viscosity with solution parameters as predictors explained 98.6% of the variability in log viscosity. When molecular weight or PEI content are increased, the log viscosity increases. Molecular weight influences the log of viscosity at the slowest rate; an increase of molecular weight of one unit increases the

log viscosity by a factor of 7.13×10^{-5}. An increase of PEI amount by 1% increases the log viscosity by a factor of 0.32, and an increase in THF of 1% decreases the log viscosity by a factor of 0.01.

Several models were used to determine a good match of predictors with the fiber formation grading (Figure 4.38). The same three predictors as above were tested initially, and resulted in an R^2 of 0.78 and all predictors having p-values < 0.0001. The model, equation 42,

$$Fiber\ \ form = 12.89 - 1 \times 10^{-4}(MW) - 0.3(\%PEI) - 4.8 \times 10^{2}(\%THF), \qquad (42)$$

showed that with a 1% increase in the weight of PEI used, the fiber formation grade would decrease, or reduce in beadiness, by a factor of 0.3. This influence is very similar with both molecular weight and weight percent of THF. A 1% increase of THF would decrease the beadiness by a factor of 0.048, and a one unit increase in the molecular weight decreases the beadiness by a factor of 0.0001.

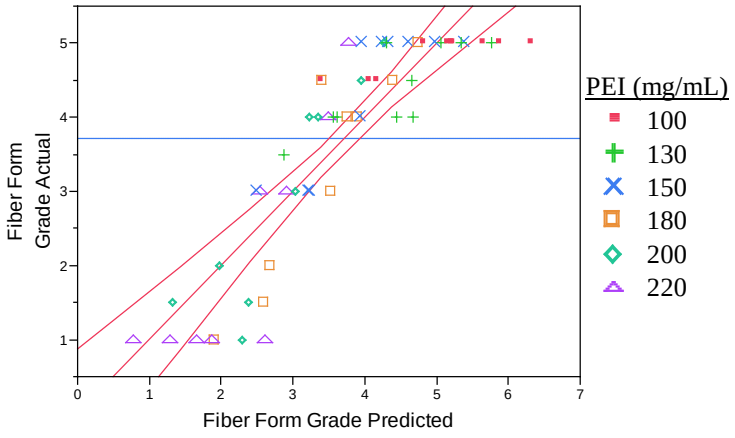

Figure 4.38 A model of fiber formation grade with PEI molecular weight, THF wt%, and PEI wt% as predictors gave an R^2 of 0.78 and all predictors were significant with p-values < 0.0001. Solution parameters and polymer molecular weight explain 78% of the variability in electrospun morphology.

To follow, a model was calculated separately for each PEI molecular weight, on fiber formation grading with THF wt%, PEI wt%, and ln |η*| as predictors (see Figure 4.39). No parameters were significant. Therefore, because polymer concentration had the most influence on change in viscosity, and is accounted for in the viscosity parameter, the PEI parameter was removed from the model.

Ultem 1000

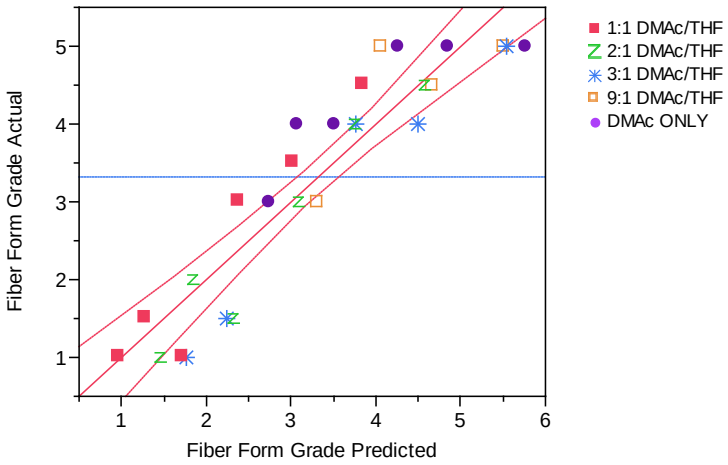

Ultem 1010

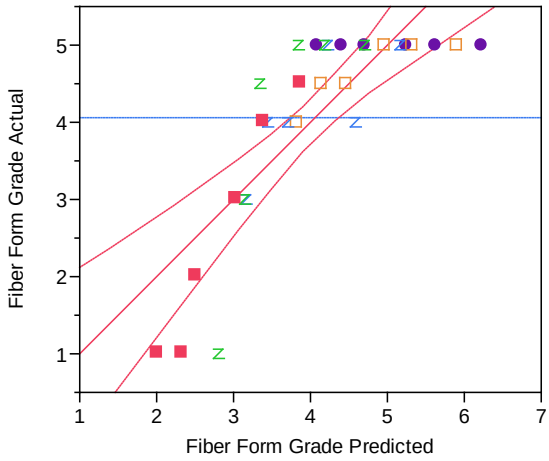

Figure 4.39 Actual fiber formation data graphed against predicted data from a model using weight percent of THF and the log of viscosity as predictors. Ultem 1000 was predicted fairly accurately, as the model had an R^2 of 0.86. Only 67% of the variation in Ultem 1010 fiber formation was predicted with the model. It was proposed that this was due to the lack of variation in morphologies of Ultem 1010 during electrospinning.

The resulting model for Ultem 1000 had an R^2 of 0.86 and both THF wt% and log|η*| had p-values < 0.0001. The Ultem 1010 model had a much lower fit (R^2 of 0.67), but both predictors were highly significant. The low R^2 in the Ultem 1010 model was caused by the lack of variation in morphology of the electrospun solutions. There was more variation in viscosity and THF% through the experimental range than there was variation of morphology.

Because the loss modulus was the dominant signal in the rheology measurements, this parameter was also tested as a predictor for fiber formation. Elastic modulus was negligible in lower frequencies and unreliable in higher, so it was not used in statistical analyses. A model of fiber grade with THF wt % and log(G″) as predictors showed both to be significant (p-value < 0.0001), and an R^2 for Ultem 1000 of 0.85 (Figure 4.40). The previous model, with log|η*| as the rheological component, instead of log(G″), had a greater fit to the fiber grade.

Because both G″ and G′ are additive to form ln |η*|,

$$\ln\left|\eta^*\right| = \left[\frac{G''}{\omega} + \frac{G'}{\omega^2}\right]^{1/2}, \tag{43}$$

the conclusion was that although G′ was unable to be interpreted directly, it did play at least a small part in the fiber grade.

To comprehensively analyze the effectiveness of fiber grading, the fiber grade scale was altered from a continuous variable to a categorical (ordinal) variable. In this way, the model assumes that fiber grades are ordered categories.

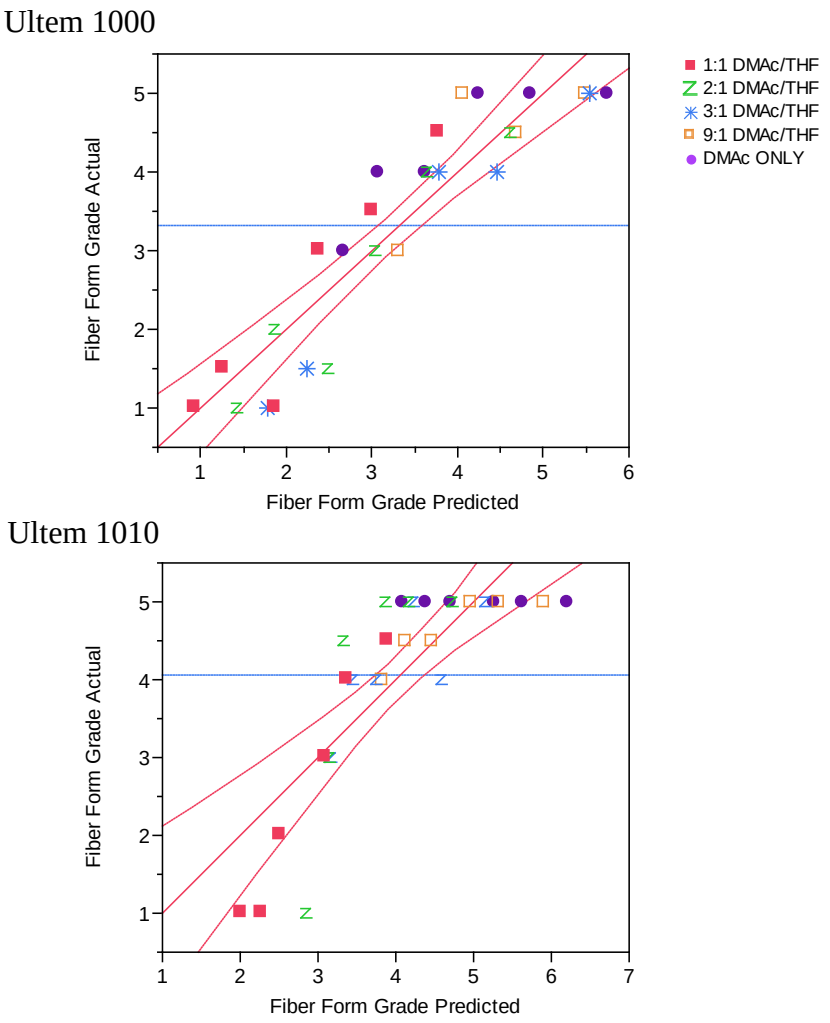

Figure 4.40 Actual fiber formation data graphed against predicted data from a model using weight percent of THF and the log of G˝ at 1 (rad/s) as predictors. The R^2 for Ultem 1000 was 0.85, and for Ultem 1010 was still 0.67. The model with G˝ does not predict the variability of either PEI as well as the model with viscosity as a predictor. This implies that G´, as a component of viscosity, contributes to the fiber formation, even though it could not be accurately evaluated from rheological measurements.

With fiber grade as an ordinal variable, a generalized ordered logit model was created. Predictors in the model were PEI molecular weight, weight percent of THF and weight percent of PEI in the solutions. Results of the model indicated that each predictor was significant with p-value < 0.001, and the model had a X^2 parameter of 90.922 and an

overall p-value < 0.001, indicating the model was a good fit to the ordinal fiber grades. The conclusion is that the creation of fiber form grades was an effective means of describing the electrospun morphologies and that the variation in polymer, solvent and viscosity are key predictors of the electrospun morphology of a solution.

4.4 Effect of Solvent Composition

Solvent choice is critical to the process of electrospinning. In this research work it is proposed that the DMAc-THF combinations influence the electrospun PEI's morphology by two mechanisms: a physical manipulation of chain orientation and evaporation during electrospinning. The rheological measurements show that PEI solutions exhibit Newtonian behavior. However, as previously stated, a certain amount of elasticity is needed to produce fibers when electrospinning. In solutions which include THF, better fiber formation is seen with higher % THF. THF, being a bad solvent for PEI, is thus producing two solution qualities which facilitate fiber formation. The first property involves the management of PEI chain volume within the solution. Because the complex viscosity distinctly changes when DMAc content is gradually replaced with THF, it is concluded that there is a change in the polymer chain distribution within the solution that leads to varied electrospun PEI morphologies. The second factor is the evaporation rate of THF. By evaporating much faster than the DMAc, THF leaves a highly concentrated PEI/DMAc solution in the initial jet, which significantly helps overcome the jet instabilities necessary to form electrospun fibers. [85]

4.4.1 Polymer-Solvent Interaction

In a binary solvent system, there will be differing rheological behaviors based on polymer molecular weight. An investigation by Y. Termonia [17] into the effects of solvent blends on polymer solubility revealed a behavior difference based on

molecular weight. If a polymer were dissolved into a mix of good and bad solvent, a large molecular weight chain would orient based on the average of the good-bad solvent system, while a small molecular weight chain will behave as if it is only in the good solvent (see Figure 4.41).

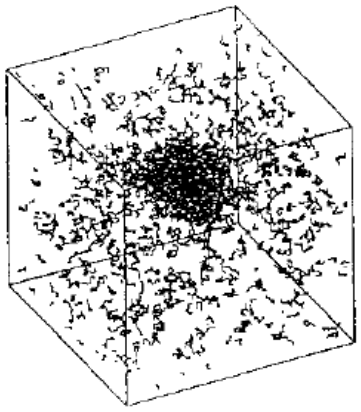

Figure 4.41 Mathematical modeling of polymer chain distribution in 50% good solvent and 50% bad solvent, by Termonia. [17] A 4000 unit chain was found to coil on itself, away from the bad solvent, while the 825 chains of 10 units each dispersed through the system as if they were only in good solvent.

This suggests that the Ultem 1010 and 1000 chains, at 55 and 69 units respectively, act similar to the short chains of Termonia's model and disperse through the solvent. Magda *et al.*[88] performed a simulation of a ternary system where the good and bad solvent had no interaction forces between them (attractive or repulsive), which is indicative of the miscible solvents used in this project. They found that in a solvent mix the affinity of the good solvent will cause it to surround the polymer chains at a high concentration, while the polymer chains themselves contract their occupying volume. This suggests that while in solution, THF acts as a dispersing agent to PEI chains which surround themselves in DMAc. The reduction in η^* observed when % THF is increased confirms this mechanism. The viscosity is also decreased because

THF has a viscosity 4 times lower than DMAc (viscosities acquired from material safety data sheets, MSDS), see Table 4.4.

Table 4.4 Viscosity of Solvents

	Viscosity, μ (Pa.s)
DMAc	1.956×10^{-3}
THF	4.8×10^{-4}

This, however, is not enough to cause the significant difference in viscosity compared to what PEI and DMAc would have without THF. In the presence of THF, according to Termonia, the PEI chains repel THF as they gather DMAc to surround themselves. However, in the 1:1 solvent ratio, there is 50% less DMAc than in the DMAc only solution. It is proposed that in order for PEI to continue dissolving as DMAc is replaced with THF, the chains must be reducing their occupying volume and clustering within pockets of DMAc that are then surrounded by THF. An illustration of this theory is shown in Figure 4.42.

Dynamic light scattering was performed on Ultem 1000 solutions with 220 mg/mL in DMAc and 1:1 DMAc/THF (Figure 4.43). The measurements were performed by Dr. Olivia Graeve's research group at the University of Nevada at Reno. These analyses revealed that the average polymer chain aggregate of Ultem 1000 in DMAc was approximately 6.77 nm, while the chain aggregate of Ultem 1000 in 1:1 DMAc/THF was an average of 9.70 nm.

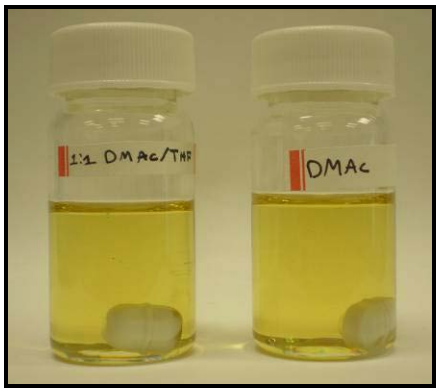

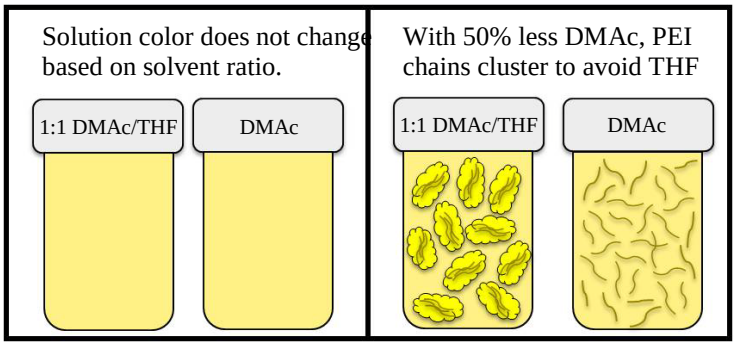

Figure 4.42 A: Color of solutions is unaffected by solvent ratio, at same PEI concentration (solutions become darker with added PEI). B: theory of how the same weight PEI can dissolve in 50% less good solvent. This is especially directed toward 220 mg/mL 1:1 DMAc/THF solutions, as this amount supersaturates DMAc when by itself, but not with the addition of THF. Preliminary dynamic light scattering data suggests that the proposed clustering mechanism is correct, as the average polymer chain aggregate in a DMAc solution was 6.77 nm, and the avg. chain aggregate for a 1:1 DMAc/THF solution was 9.70 nm.

Measurements of additional solvent systems are required to make a complete conclusion, but preliminary data suggested that while PEI chains do cluster in both extremes of solvent system, the clusters are bigger as THF is added to the solvent system as predicted.

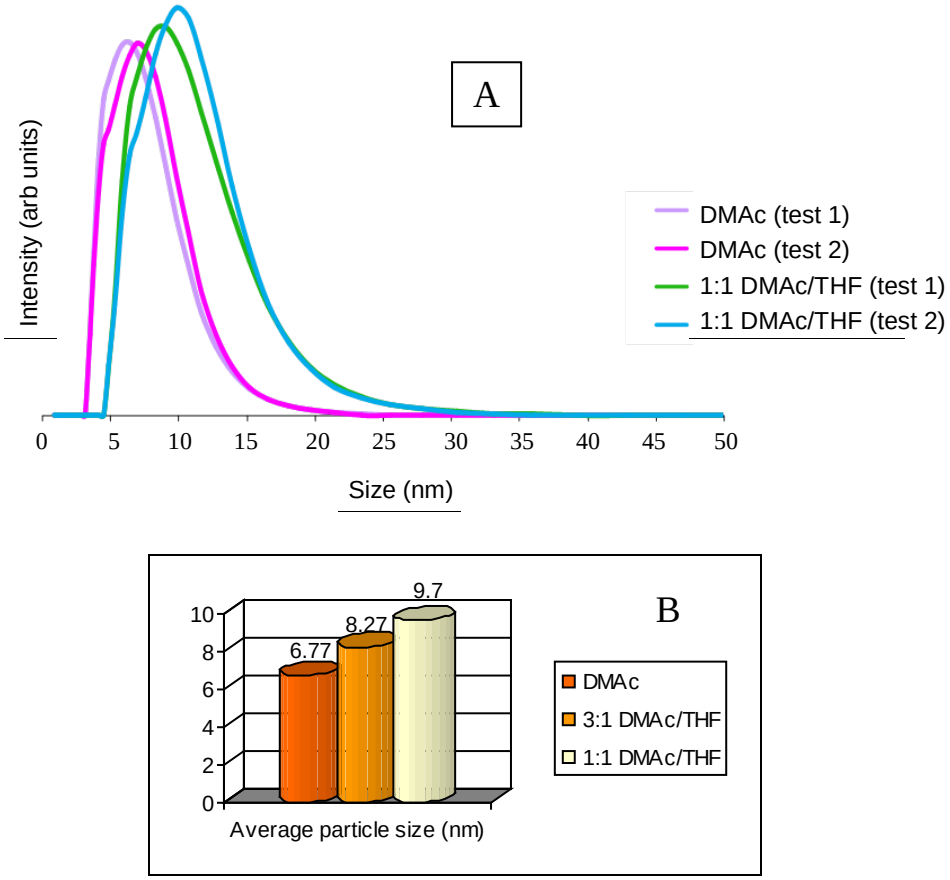

Figure 4.43 (A) Polymer chain aggregate size of Ultem 1000 measured by dynamic light scattering (DLS) from 220 mg/mL solutions in DMAc and 1:1 DMAc/THF. Two trials were averaged for each solution. The average chain aggregate in DMAc was 6.77 nm, while in 1:1 DMAc/THF the chain aggregate was 9.70 nm. While these numbers are too large to be individual PEI polymer chains, they do reveal that polymer chain aggregates do increase in size as THF is added. (B) Later, tests were run with 3:1 DMAc/THF as the solvent system. This graph shows the increase of aggregate size in solution as amount of THF in the solvent ratio is increased.

4.4.2 Solvent Evaporation

The solvent evaporation rate is key in fiber formation during electrospinning, and the influence of solvent evaporation was seen in the solution variations used through this project. The ASTM standard test method D3539-87(2004), Standard Test Methods for Evaporation Rates of Volatile Liquids by Shell Thin-Film Evaporometer,

shows how the evaporation of volatile liquids has been measured. When compared to butyl acetate = 1 as the standard, the evaporation rates > 3 (acetone = 5.6) are considered high and < 0.8 (water = 0.3) are considered low. THF has a relative evaporation rate of 8 and DMAc's relative evaporation rate is 0.17.

Shin *et al.* examined solvents of atactic polystyrene (a-PS) using solvents having different evaporation rates by analyzing the morphologies of the resulting electrospun a-PS. [89] THF and N,N-dimethylformamide (DMF), a solvent with similar evaporation rate to DMAc, were used. SEM results of the electrospun beaded a-PS showed that THF, with its higher evaporation rate, produced more irregularly shaped beads of a-PS while DMF produced more spherical beads, because it evaporated slower. In the study of electrospinning, evaporation rates in good-solvent combinations have also been investigated.

During electrospinning, THF evaporates 47 times faster than DMAc. As THF leaves the system, PEI's concentration in the total solution is increased because the slower evaporating DMAc is not yet leaving the system. In the most highly concentrated system electrospun in this thesis, 220 mg/mL, with the lowest starting amount of DMAc, 1:1 DMAc/THF, the percent of PEI is 19.2%, but relative to DMAc is 32%. In the DMAc only system 220 mg/mL PEI was 19.2%. To understand the evaporation importance during electrospinning, a DMAc only solution was created with 32% PEI. Figure 4.44 shows that in DMAc only, the solvent is super saturated. This solution would not electrospin. So, while THF is not a solvent for PEI, its presence does allow a much higher percentage of PEI (relative to DMAc) to be dissolved via chain clustering. This can be confirmed by Figure 4.42, in which the polymer chain aggregate size was found to be 6.77 nm in DMAc alone but 9.7 nm in 1:1 DMAc/THF.

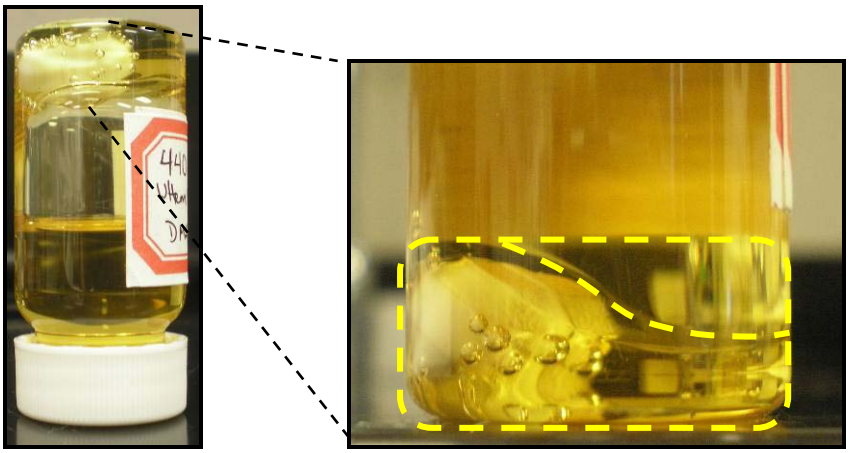

Figure 4.44 440 mg/mL Ultem 1000 partially dissolved in DMAc. Solution pictured upside down reveals the amount of PEI not dissolved and encasing the stir bar used for dissolution, while the yellow dashed line highlights the precipitated PEI containing the magnetic stir bar.

In order to confirm evaporation effects, Theron *et al.* added ethanol to an aqueous PEO solution. [18] They tracked the volume charge density through the electrospinning of the solutions and found that it did not increase with the addition of ethanol (Figure 4.45).

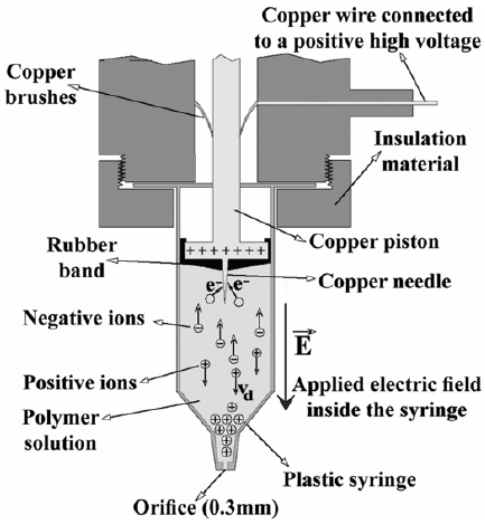

Figure 4.45 Electrospinning setup for measuring volume charge density used by Theron *et al.* [18]

They concluded that ethanol's effect in the electrospinning was primarily its evaporation rate being higher than water's; this higher evaporation rate aided in polymer jet solidification during electrospinning by leaving less water at the beginning of the jet and reducing the time the PEO jet took to dry.

In this work, the quick evaporation of THF influenced the electrospinning by leaving a higher concentrated PEI/DMAc system at the needle exit. This being the case, higher concentrations of PEI solutions were reached without the need to mix and transfer quite viscous solutions to the electrospinning setup. The increased viscosity enhanced fiber formation and perhaps elasticity.

CHAPTER 5

CONCLUSIONS

In this thesis it has been shown that with the combination of a good and bad solvent, a highly rigid polymer can be electrospun into nanofibers. Also, a bad solvent was used to dissolve polymer into good solvent at percentages past the good solvent super saturation point. Rheological analysis was performed to understand the influence of solvent ratio, polymer concentration and molecular weight. Finally, Dielectric spectroscopy was evaluated for its applicability in understanding the results of electrospinning.

There were no statistically significant differences in dielectric data over polymer content or solvent ratio. Also, the dielectric measurements in this project did not show trends across sample variation like those seen with rheology. The molecular dynamics which cause the signals in dielectric analysis and rheological analysis are, therefore, different. While the dielectric analysis showed only the ionic transport properties of the solvents, rheology showed variation in viscosity through sample variation of both solvent and polymer. The THF did not contribute to the dielectric signal, but only hampered ionic transport through the DMAc. Dielectric spectroscopy, although not conclusive in this system, has the potential to be related to the electrospinning of certain conductive polymers, like PVP, with more conductive solvents, like water.

Although THF lowered the viscosity of PEI/DMAc solutions, the solutions with THF produced better PEI nanofibers when electrospun. THF manipulated polymer chain clustering within the good solvent, because the polymer chains repelled the bad solvent, reduced their volume and surrounded themselves with good solvent. The addition of bad solvent also made less difficult the dissolution and handling of higher polymer concentrations relative to good solvent amount. This was so much the case

that PEI concentrations were achieved in 1:1 DMAc/THF that with only DMAc as the solvent would be super saturations (see Figure 4.43).

In the system used in this work, the addition of bad solvent was also effective because THF has a much higher evaporation rate than DMAc. While it was evaporating 47 times quicker than DMAc, THF left behind more and more concentrated PEI/DMAc solution at the Taylor cone. Along with facilitating the increased concentration at the Taylor cone, the solvent evaporation also allowed for quicker polymer jet solidification and less chance of jet breakup. Both of these factors resulted in the best fibers being formed when both PEI and THF concentrations were at their highest. Because of THF's effect of PEI chain volume and dissolution, and its high evaporation rate, it and other "bad" solvents may be a beneficial new technique in the manipulation of electrospinning and solution thermodynamics.

CHAPTER 6

RECOMMENDATIONS FOR FUTURE WORK

Dielectric spectroscopy did not prove to have a connection to electrospinning in this project as was originally hypothesized. PEI–solvent interactions were not detected with the dielectric measurements at 3V. It is recommend that before completely ruling out dielectric analysis' connection to electrospinning in this particular polymer-solvent system, that measurements first be done with a spectrometer that can measure with at least 10V. Also, the differences between dielectric signals of solutions and solvents should be investigated to understand what the actual effect of PEI was on the signal caused by the solvent, see Figure 4.9. In addition, several mathematical models do exist for the deconstruction of dielectric data that were not originally investigated. In the low frequency range used in this project, all ε″ data showed a kink and divergence from the -1 slope, as shown in Figure 6.1.

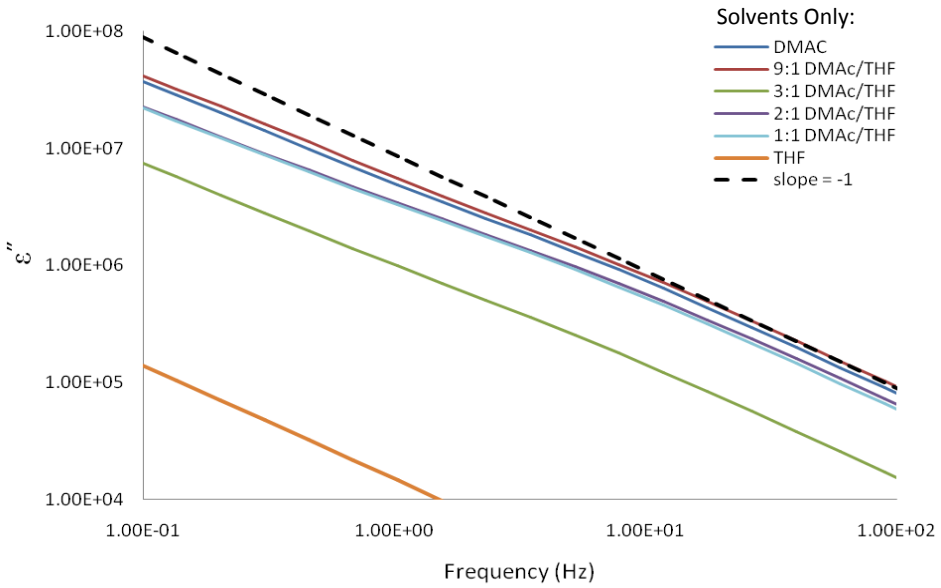

Figure 6.1 Divergence from the dominant slope (-1) of ε″ is seen in the lower frequencies of both solvent and solution measurements. The divergence is smaller when PEI is present. Further investigation is proposed in order to determine if there is more than a conductivity component in the signal.

Figure 6.1 (Continued)

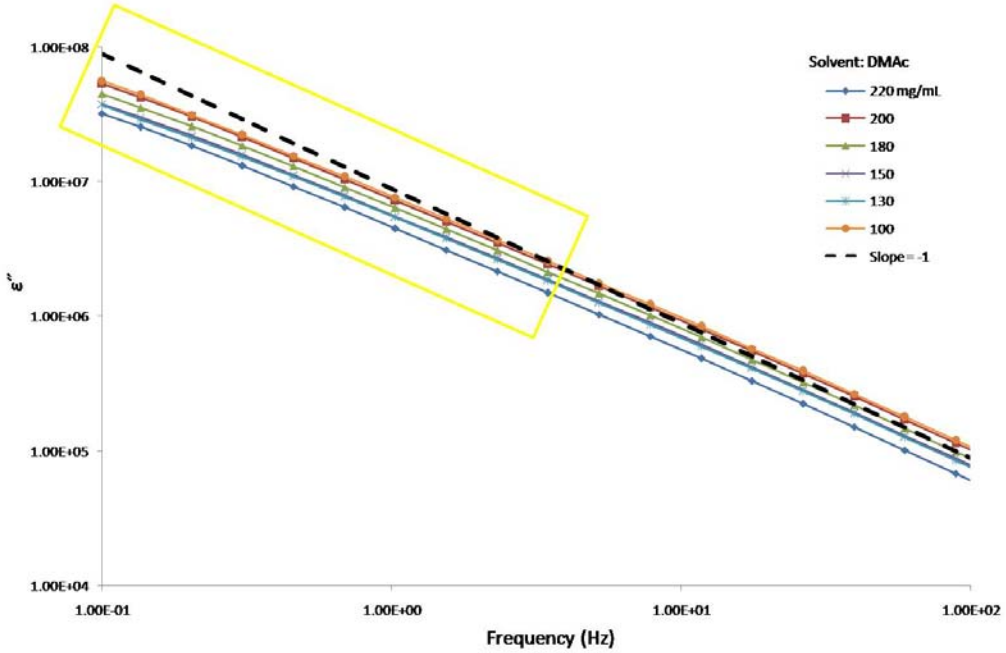

It is possible that this data could be isolated. It is recommended that the removal of the conductivity contribution at very low frequencies, where the slope of ε″ changes, be investigated by mathematical modeling laid out in Diaz-Calleja *et al.* and Bello *et al.* [4, 83]

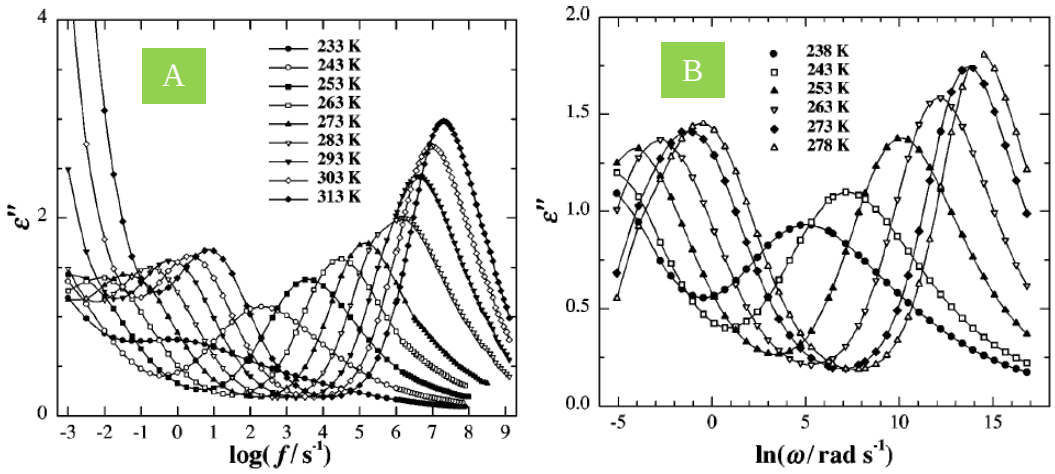

Figure 6.2 Bello et al. [83] removed the dc-conductivity component of the ε″ signal (from Figure A) of α-crystalline polyvinylidene fluoride (PVDF) at various temperatures by subtracting the conductivity expression $\sigma = \sigma_0 / \varepsilon_0 \omega$ (σ_0: dielectric conductivity data, ε_0: vacuum permittivity, ω: angular frequency) from ε″ data, Figure B.

The physical effects of THF can be further tested by dynamic light scattering (DLS). This is an especially important technique because the multicomponent instrument measures the real-time Brownian motion of the polymer. DLS can thus give a good understanding of the effects of solvent ratio on PEI orientation over time.[19] Further DLS research should be carried out in order to more fully understand the physical effects of THF. Also, in these experiments, no more than 50% THF was used in the solvent ratio. Increasing THF content past 50% could reveal more benefits for the electrospinning of PEI as well as the limitations. Because full understanding of the contribution of THF cannot be reached without further comparison, it is recommended that another miscible bad solvent, with a lower evaporation rate, be tested with the PEI/DMAc system. One option for this is ethanol. Finally, to better understand the effect of THF's evaporation on fiber formation, weight testing over THF evaporation time should be conducted. If the trends in fiber form over %THF are similar to the decrease in solution weight over time this could reveal the significance of evaporation rate to the system used in this project.

APPENDIX A

SEM Images of Electrospun PEI

Scanning electron micrographs of Ultem 1000 and 1010 electrospun from solutions in dimethylacetamide (DMAc) and ratios of DMAc with tetrahydrofuran (THF).

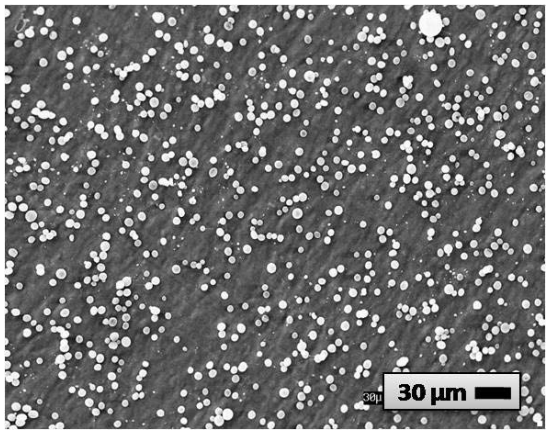

100 mg/mL Ultem 1000 in DMAc

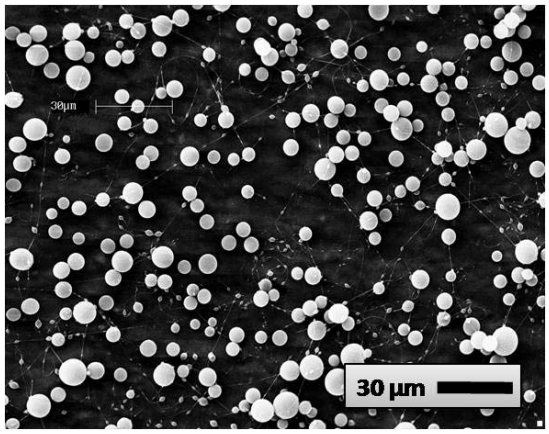

130 mg/mL Ultem 1000 in DMAc

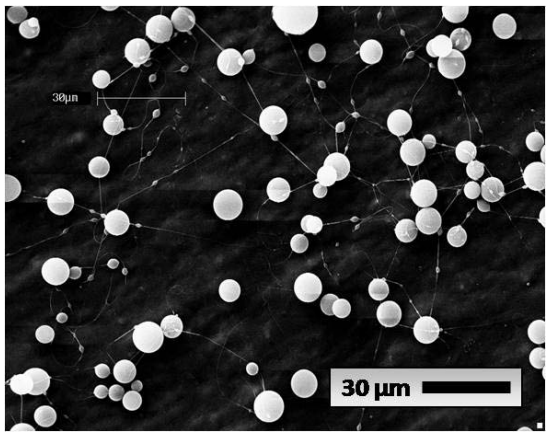

150 mg/mL Ultem 1000 in DMAc

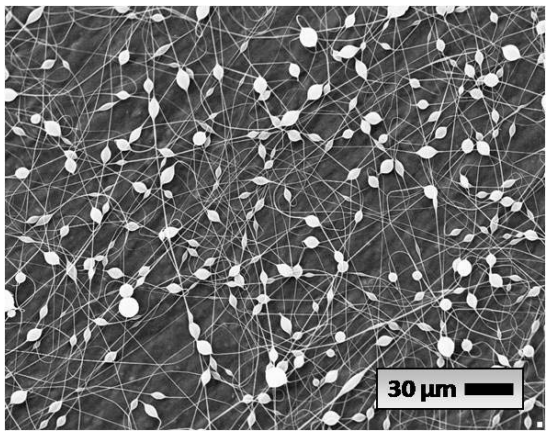

180 mg/mL Ultem 1000 in DMAc

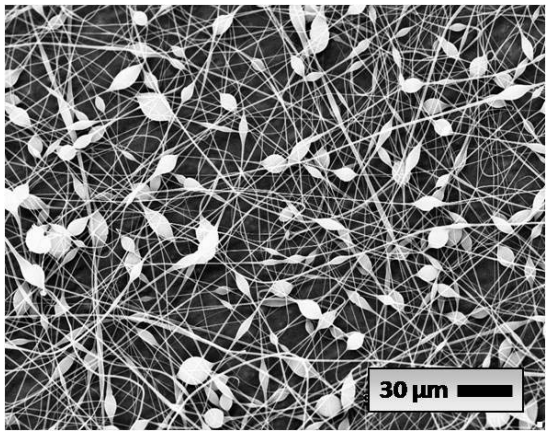

200 mg/mL Ultem 1000 in DMAc

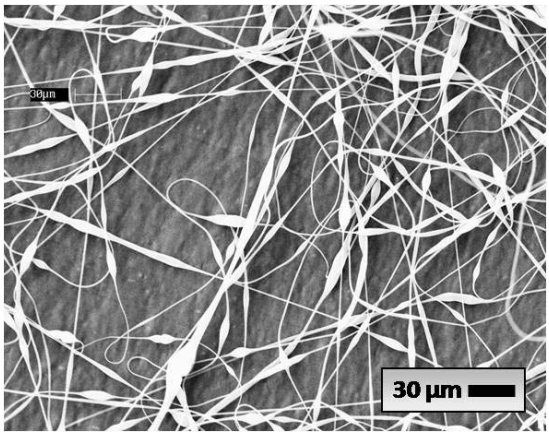

220 mg/mL Ultem 1000 in DMAc

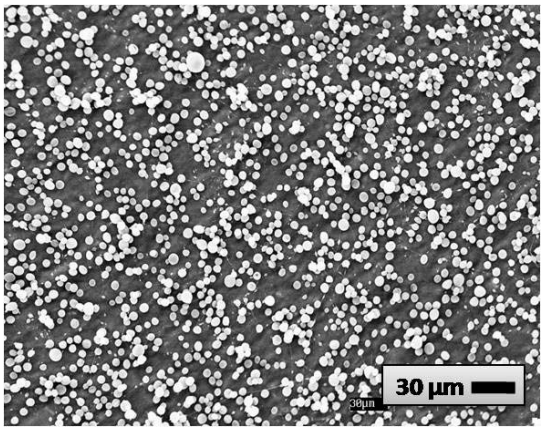

100 mg/mL Ultem 1000 in 9:1 DMAc/THF

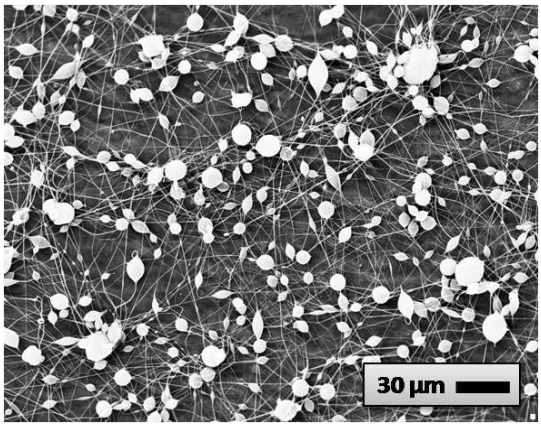

130 mg/mL Ultem 1000 in 9:1 DMAc/THF

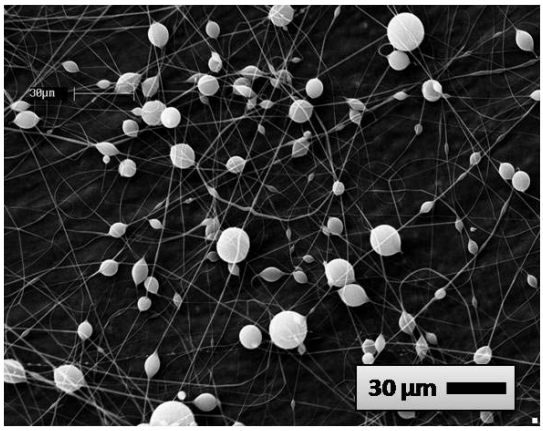

150 mg/mL Ultem 1000 in 9:1 DMAc/THF

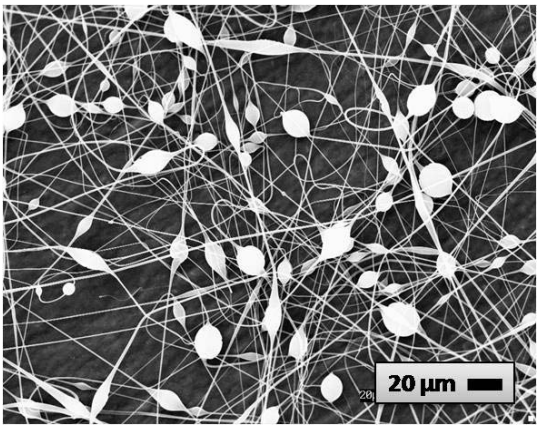

180 mg/mL Ultem 1000 in 9:1 DMAc/THF

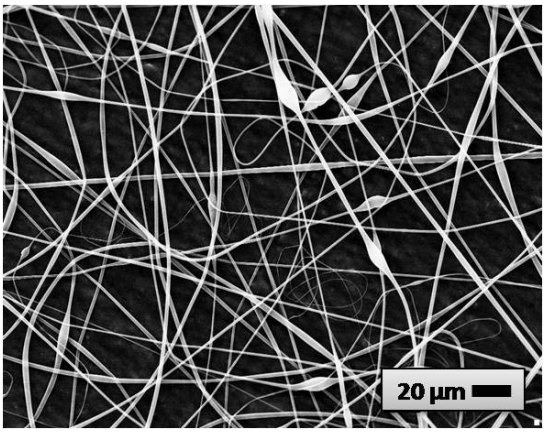

200 mg/mL Ultem 1000 in 9:1 DMAc/THF

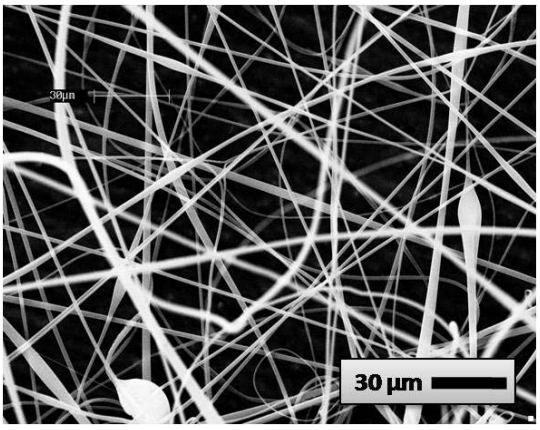

220 mg/mL Ultem 1000 in 9:1 DMAc/THF

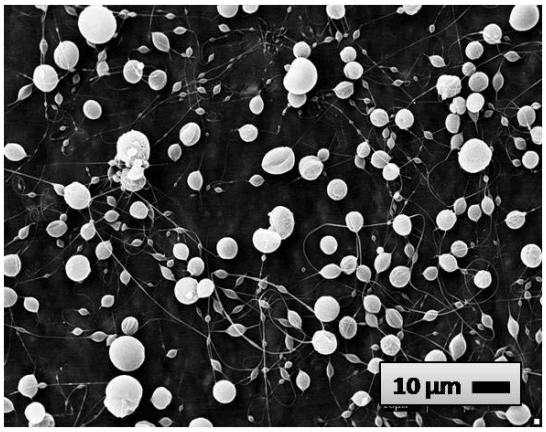

100 mg/mL Ultem 1000 in 3:1 DMAc/THF

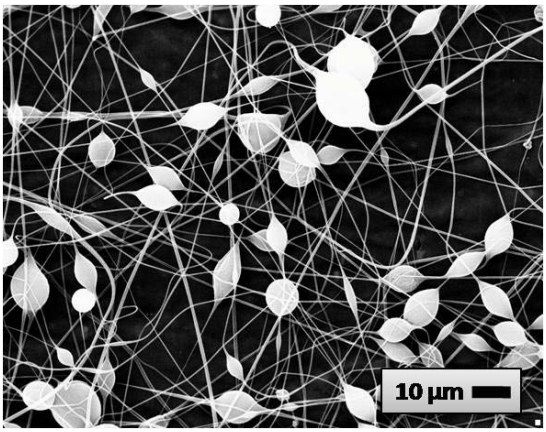

130 mg/mL Ultem 1000 in 3:1 DMAc/THF

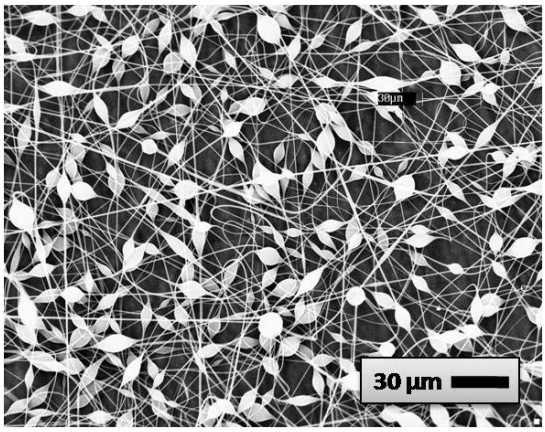

150 mg/mL Ultem 1000 in 3:1 DMAc/THF

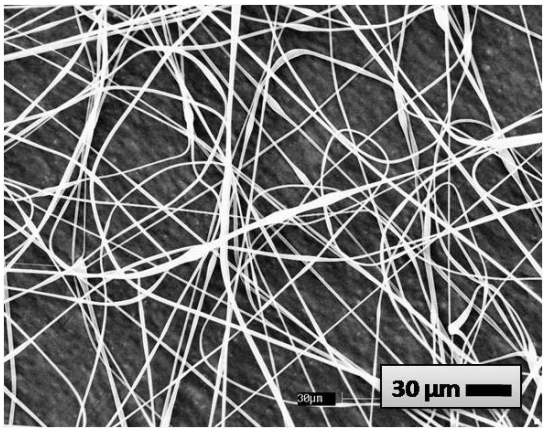

180 mg/mL Ultem 1000 in 3:1 DMAc/THF

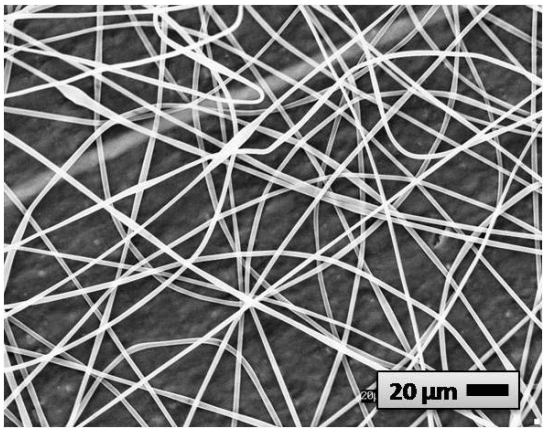

200 mg/mL Ultem 1000 in 3:1 DMAc/THF

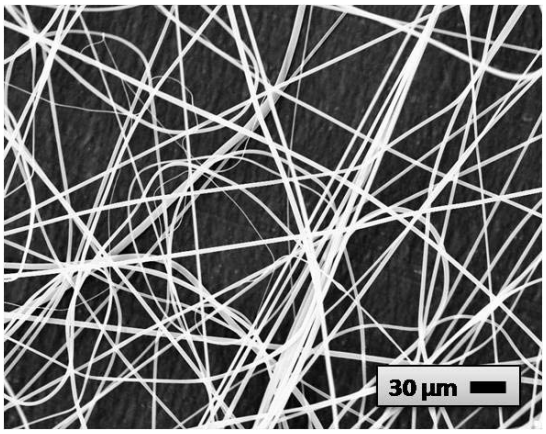

220 mg/mL Ultem 1000 in 3:1 DMAc/THF

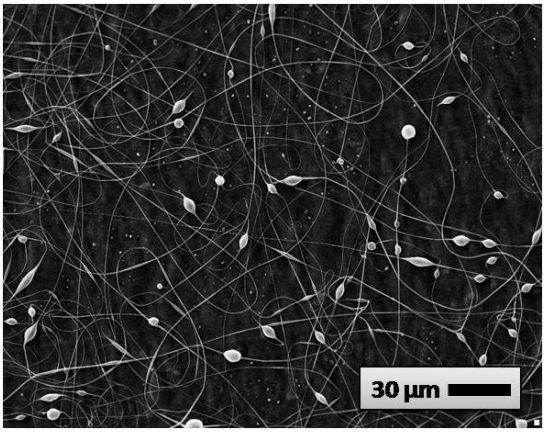

100 mg/mL Ultem 1000 in 2:1 DMAc/THF

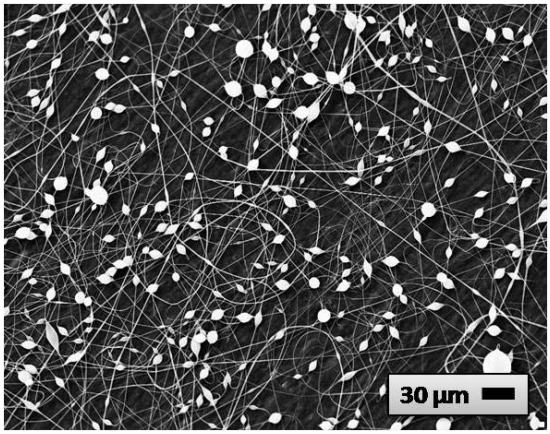

130 mg/mL Ultem 1000 in 2:1 DMAc/THF

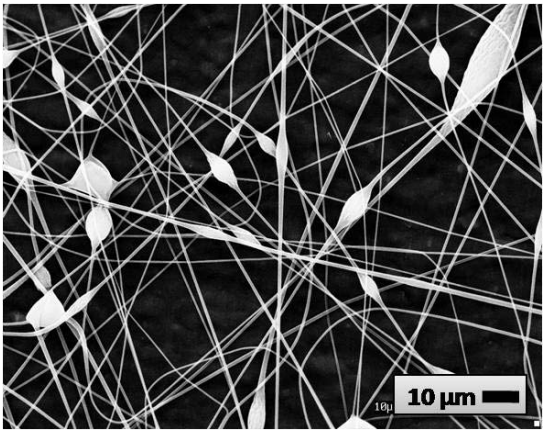

150 mg/mL Ultem 1000 in 2:1 DMAc/THF

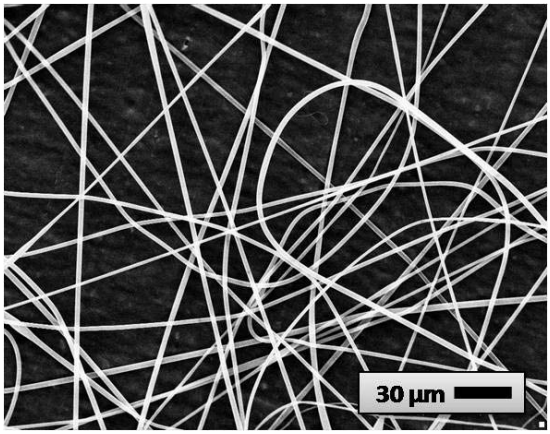

180 mg/mL Ultem 1000 in 2:1 DMAc/THF

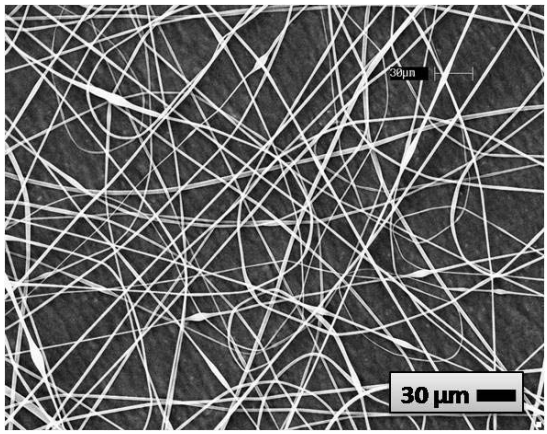

200 mg/mL Ultem 1000 in 2:1 DMAc/THF

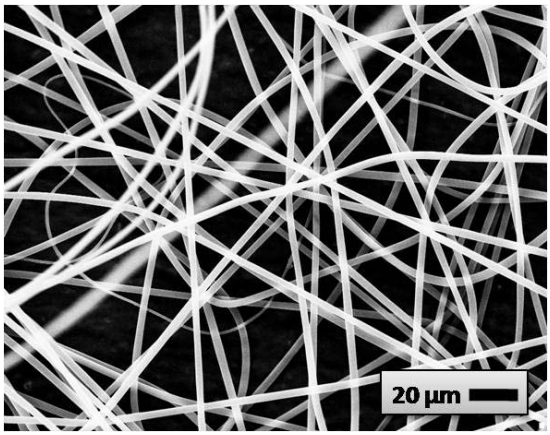

220 mg/mL Ultem 1000 in 2:1 DMAc/THF

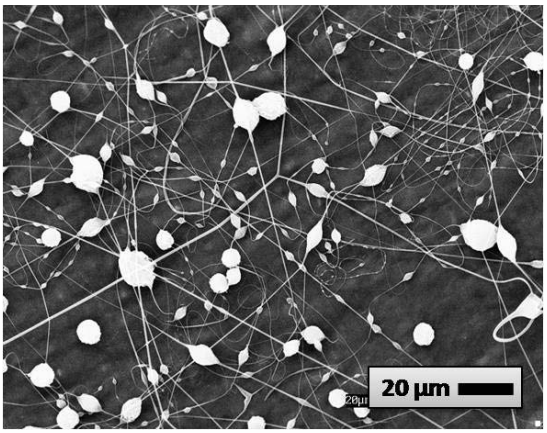

100 mg/mL Ultem 1000 in 1:1 DMAc/THF

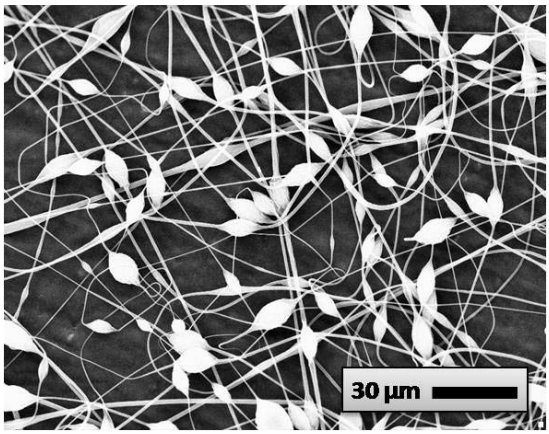

130 mg/mL Ultem 1000 in 1:1 DMAc/THF

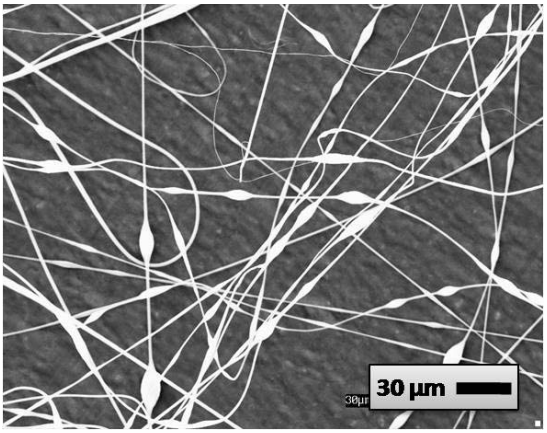

150 mg/mL Ultem 1000 in 1:1 DMAc/THF

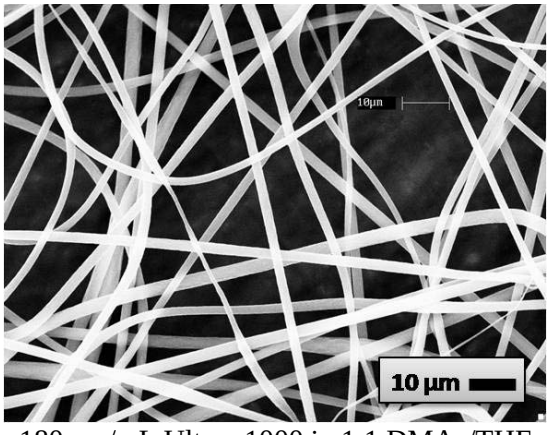

180 mg/mL Ultem 1000 in 1:1 DMAc/THF

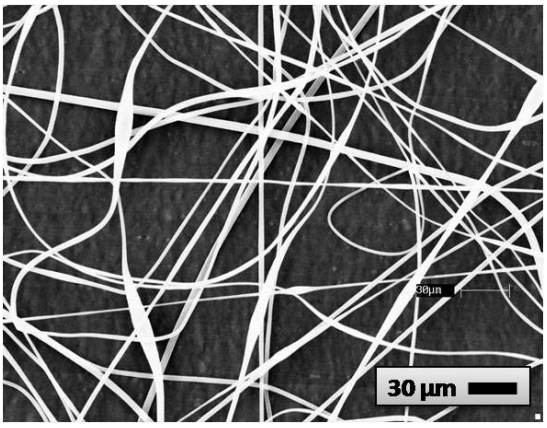

200 mg/mL Ultem 1000 in 1:1 DMAc/THF

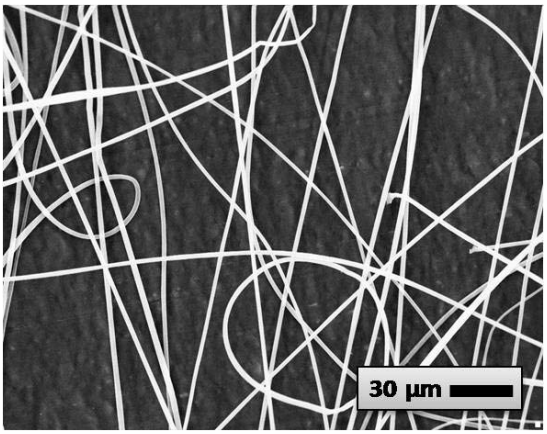

220 mg/mL Ultem 1000 in 1:1 DMAc/THF

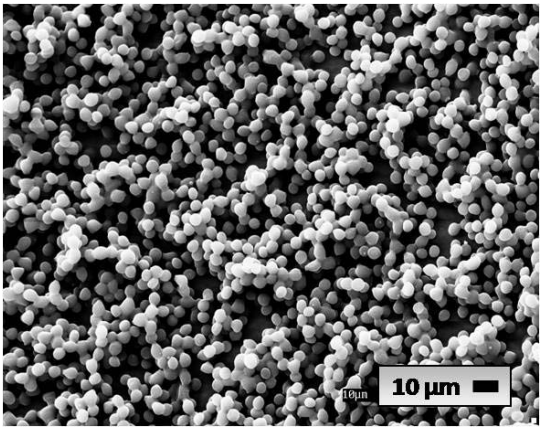

100 mg/mL Ultem 1010 in DMAc

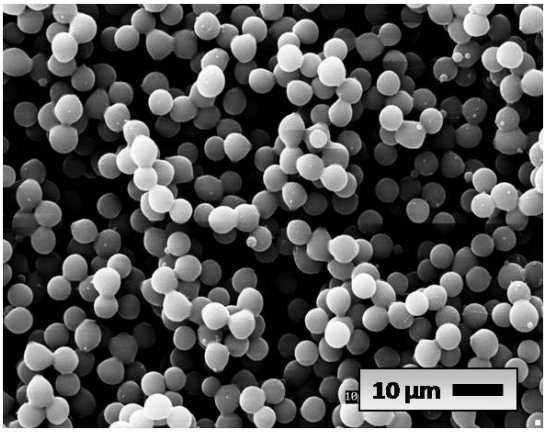

130 mg/mL Ultem 1010 in DMAc

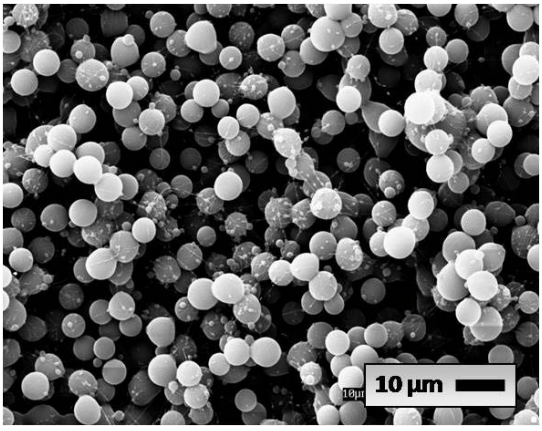

150 mg/mL Ultem 1010 in DMAc

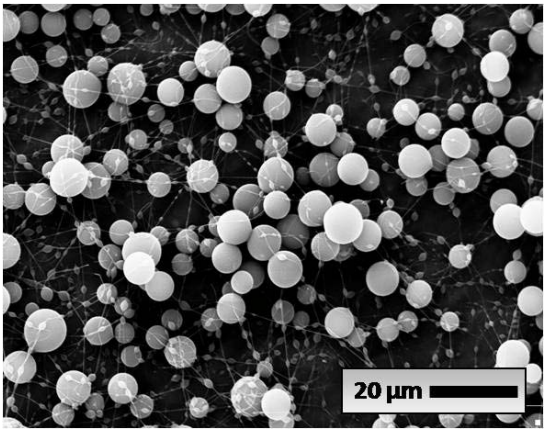

180 mg/mL Ultem 1010 in DMAc

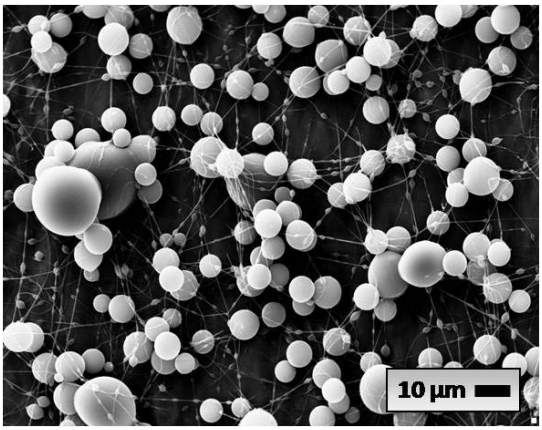

200 mg/mL Ultem 1010 in DMAc

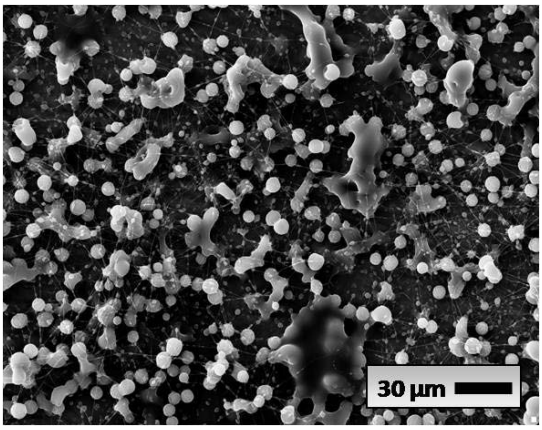

220 mg/mL Ultem 1010 in DMAc

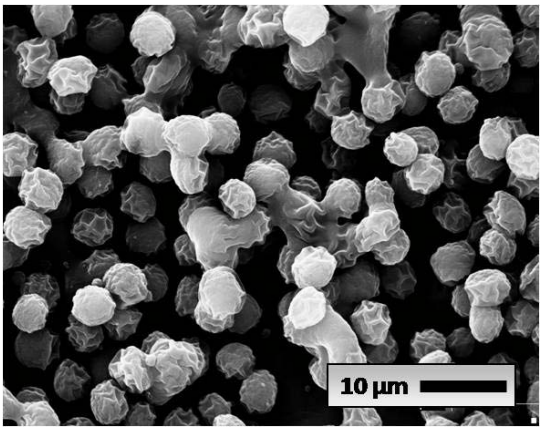

100 mg/mL Ultem 1010 in 9:1 DMAc/THF

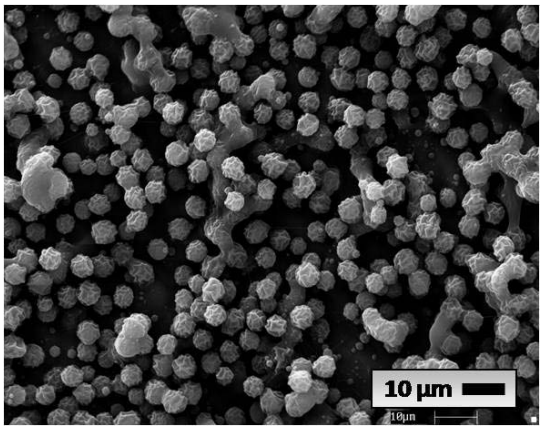

130 mg/mL Ultem 1010 in 9:1 DMAc/THF

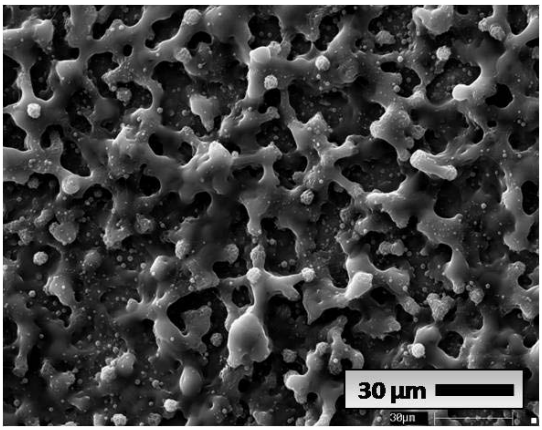

150 mg/mL Ultem 1010 in 9:1 DMAc/THF

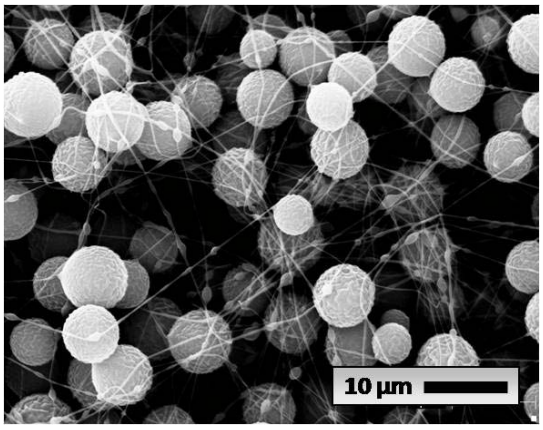

180 mg/mL Ultem 1010 in 9:1 DMAc/THF

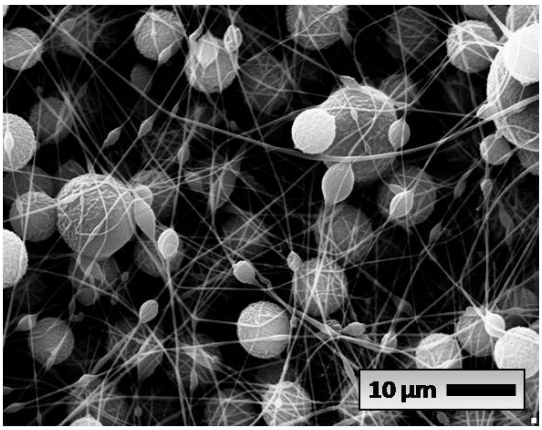

200 mg/mL Ultem 1010 in 9:1 DMAc/THF

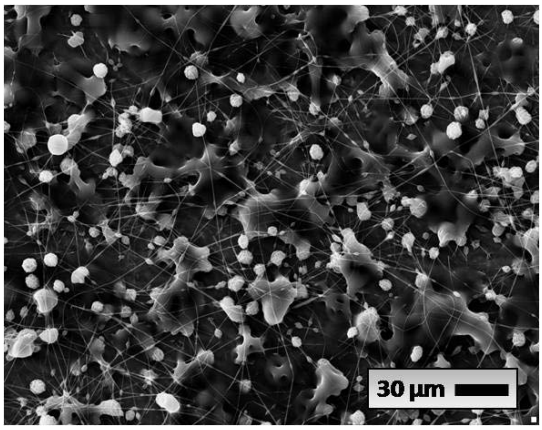

220 mg/mL Ultem 1010 in 9:1 DMAc/THF

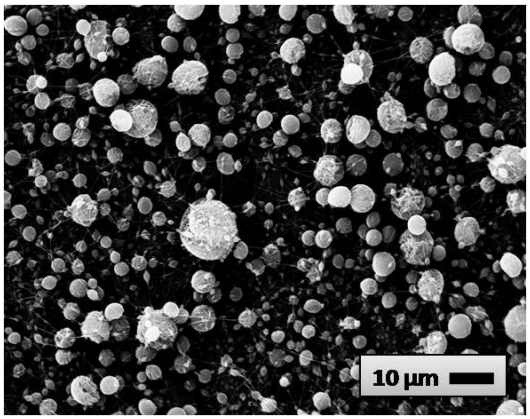

100 mg/mL Ultem 1010 in 3:1 DMAc/THF

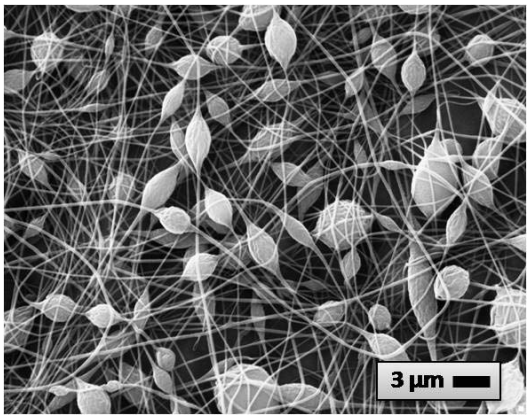

130 mg/mL Ultem 1010 in 3:1 DMAc/THF

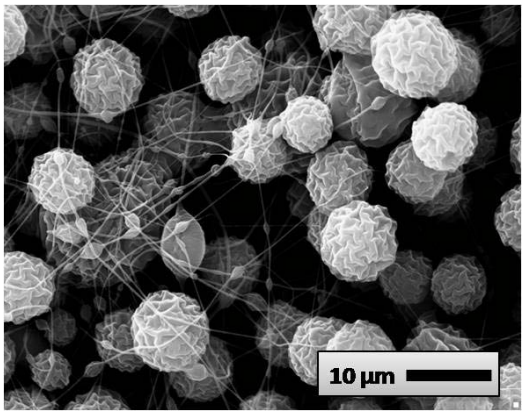

150 mg/mL Ultem 1010 in 3:1 DMAc/THF

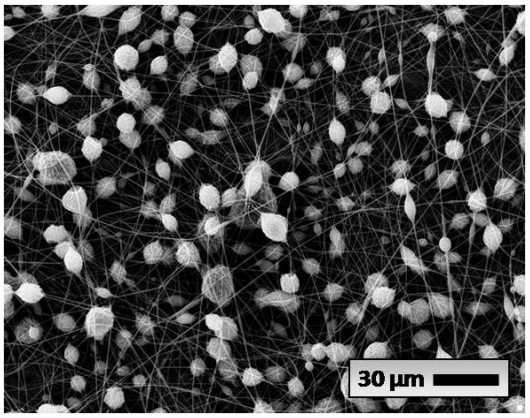

180 mg/mL Ultem 1010 in 3:1 DMAc/THF

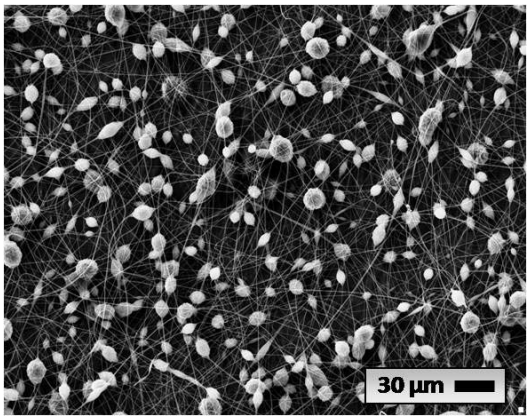

200 mg/mL Ultem 1010 in 3:1 DMAc/THF

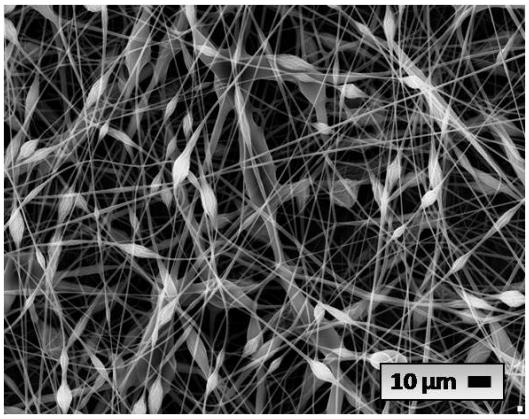

220 mg/mL Ultem 1010 in 3:1 DMAc/THF

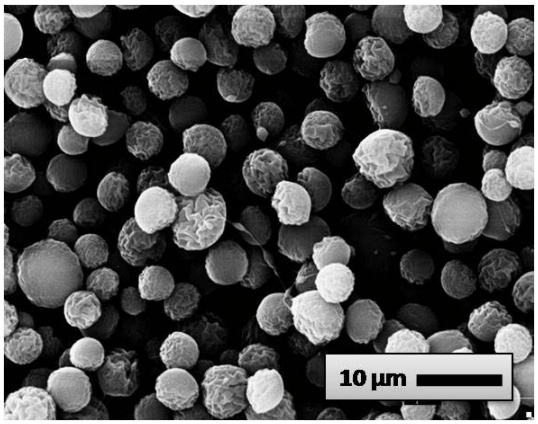

100 mg/mL Ultem 1010 in 2:1 DMAc/THF

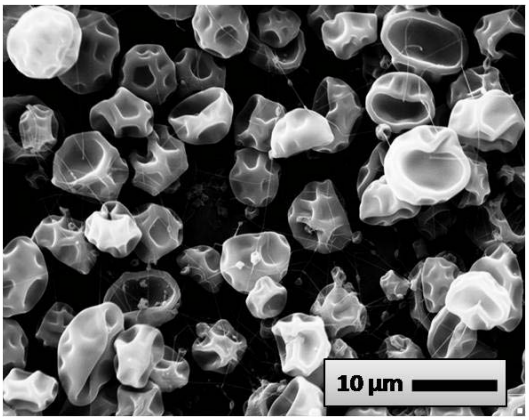

130 mg/mL Ultem 1010 in 2:1 DMAc/THF

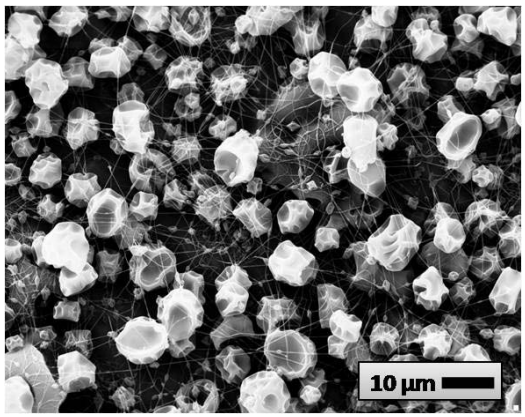

150 mg/mL Ultem 1010 in 2:1 DMAc/THF

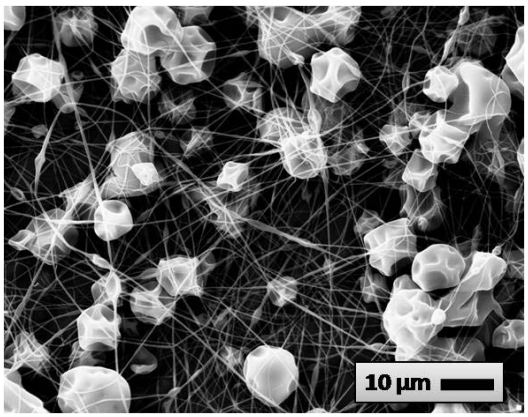

180 mg/mL Ultem 1010 in 2:1 DMAc/THF

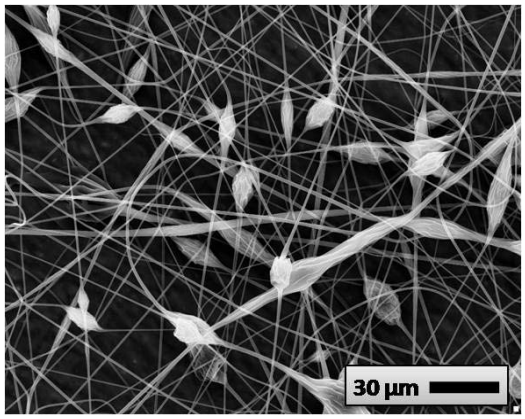

200 mg/mL Ultem 1010 in 2:1 DMAc/THF

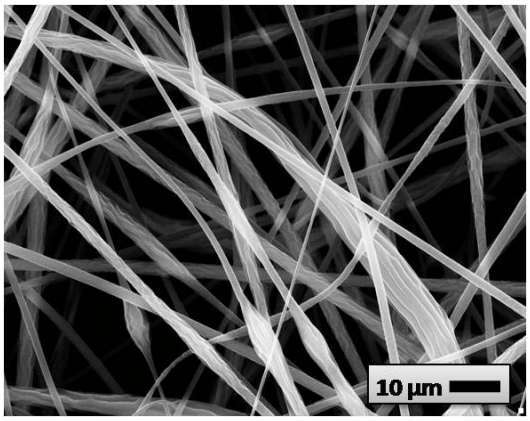

220 mg/mL Ultem 1010 in 2:1 DMAc/THF

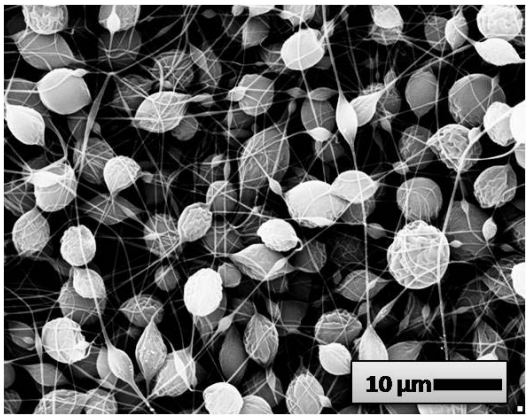

100 mg/mL Ultem 1010 in 1:1 DMAc/THF

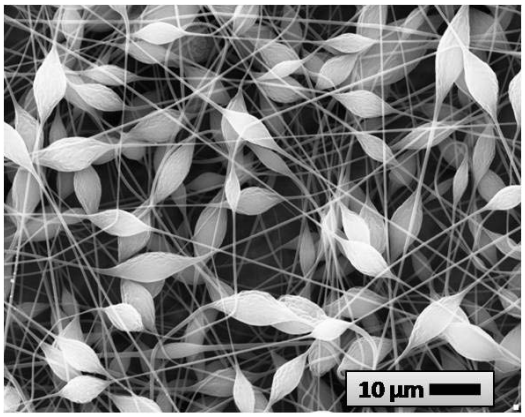

130 mg/mL Ultem 1010 in 1:1 DMAc/THF

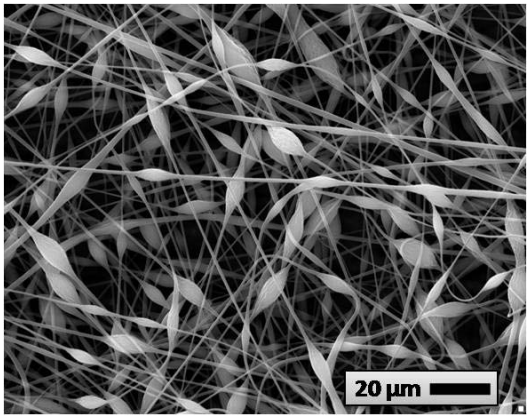

150 mg/mL Ultem 1010 in 1:1 DMAc/THF

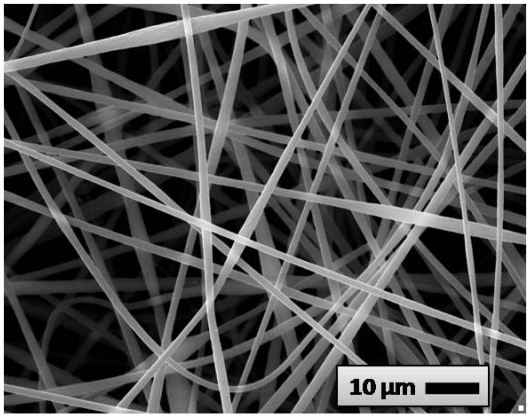

180 mg/mL Ultem 1010 in 1:1 DMAc/THF

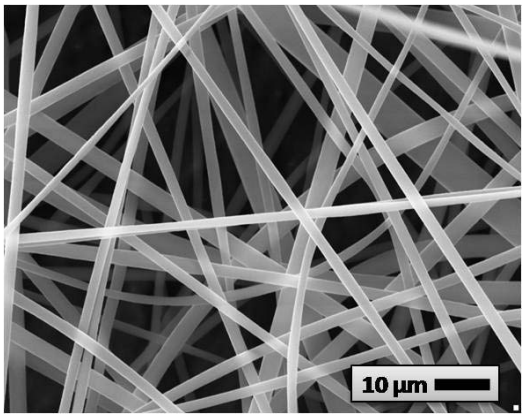

200 mg/mL Ultem 1010 in 1:1 DMAc/THF

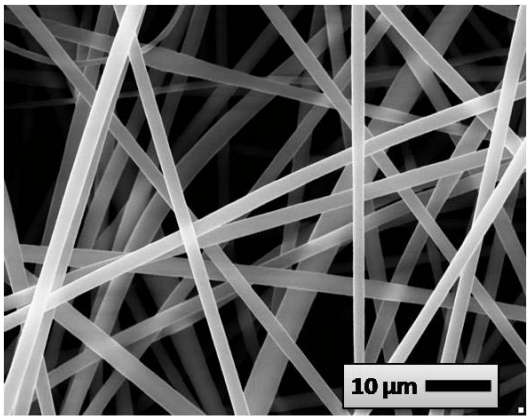

220 mg/mL Ultem 1010 in 1:1 DMAc/THF

APPENDIX B

Dielectric Spectroscopy Data of PEI Solutions

Ultem 1000 Dielectric Measurements

Ultem 1000 in 1:1 DMAc/THF:

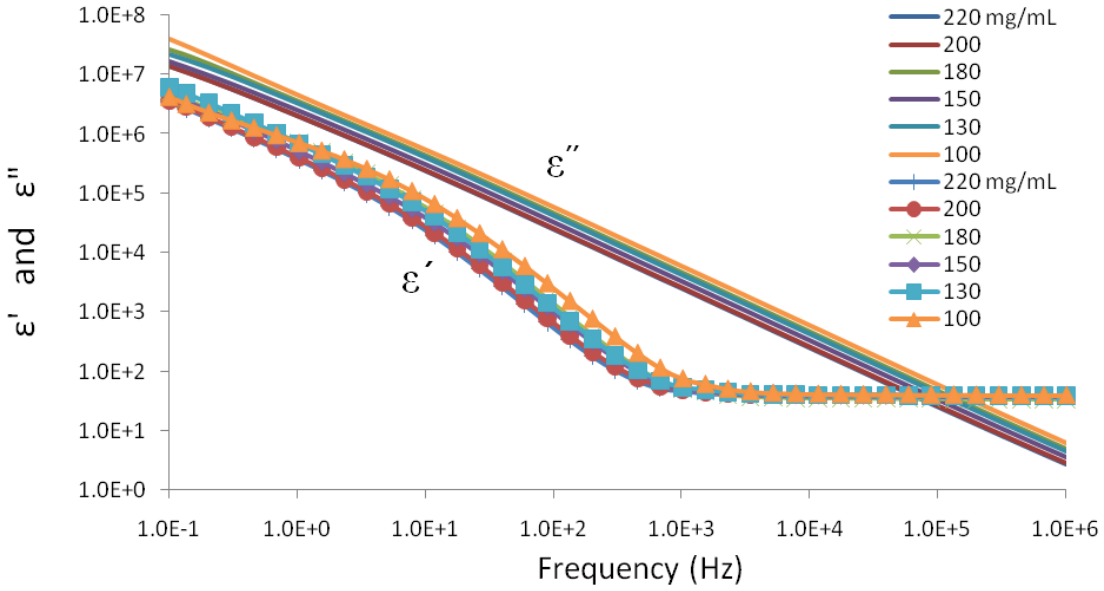

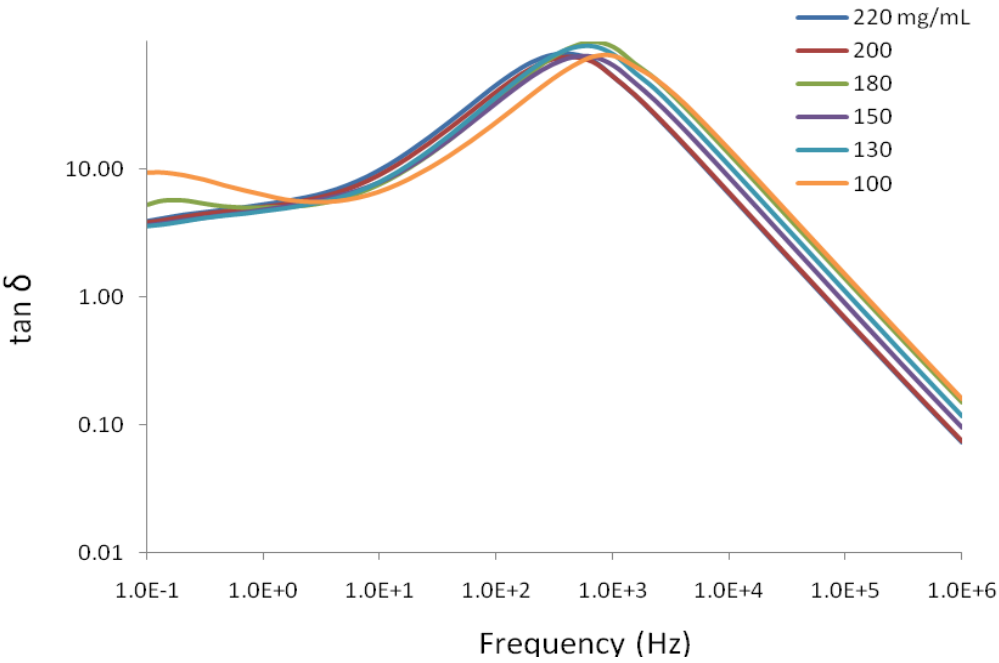

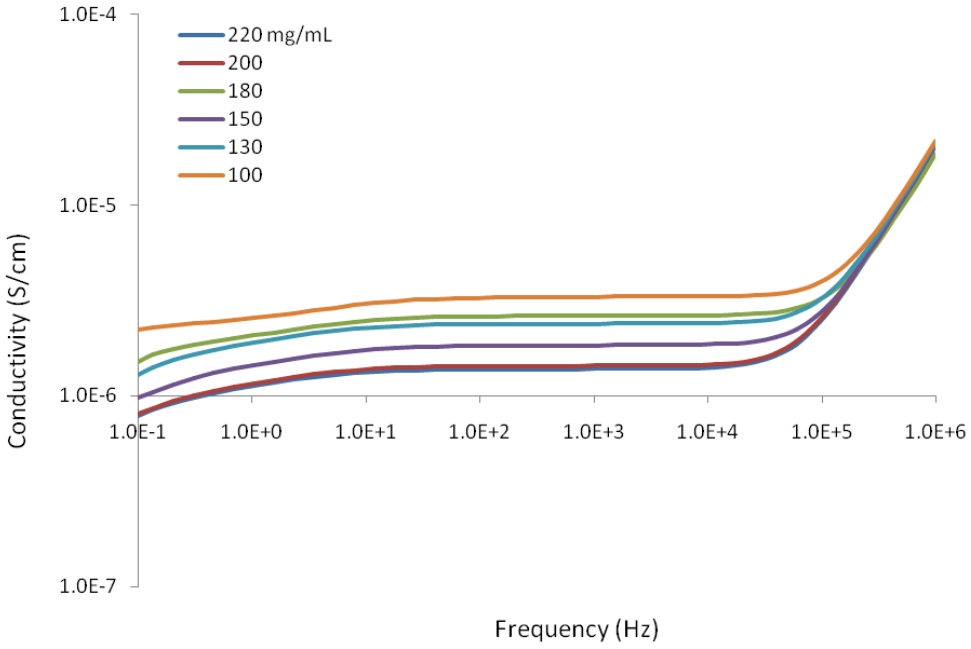

Ultem 1000 in 2:1 DMAc/THF:

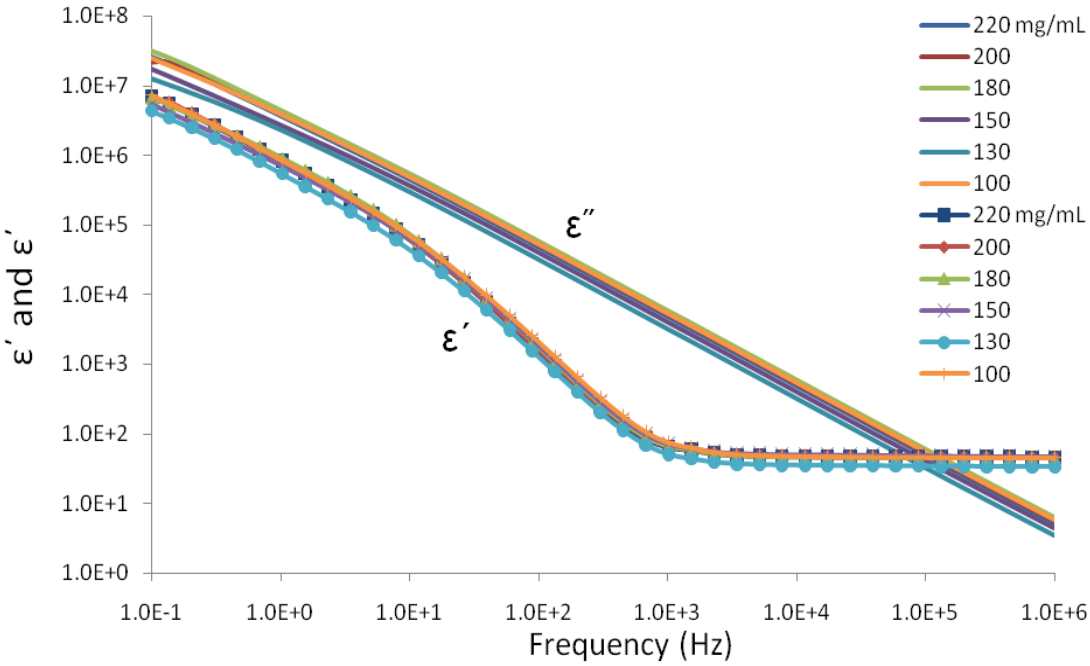

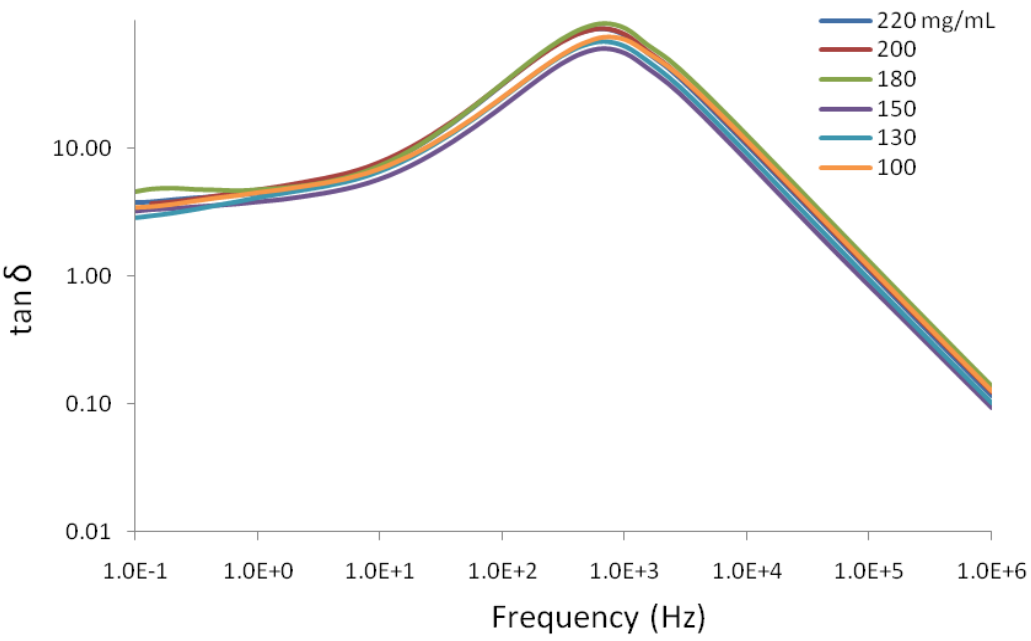
220 mg/mL
200
180
150
130
100
10.00
1.00
0.10
0.01
tan δ
1.0E-1
1.0E+0
1.0E+1
1.0E+2
1.0E+3
1.0E+4
1.0E+5
1.0E+6
Frequency (Hz)

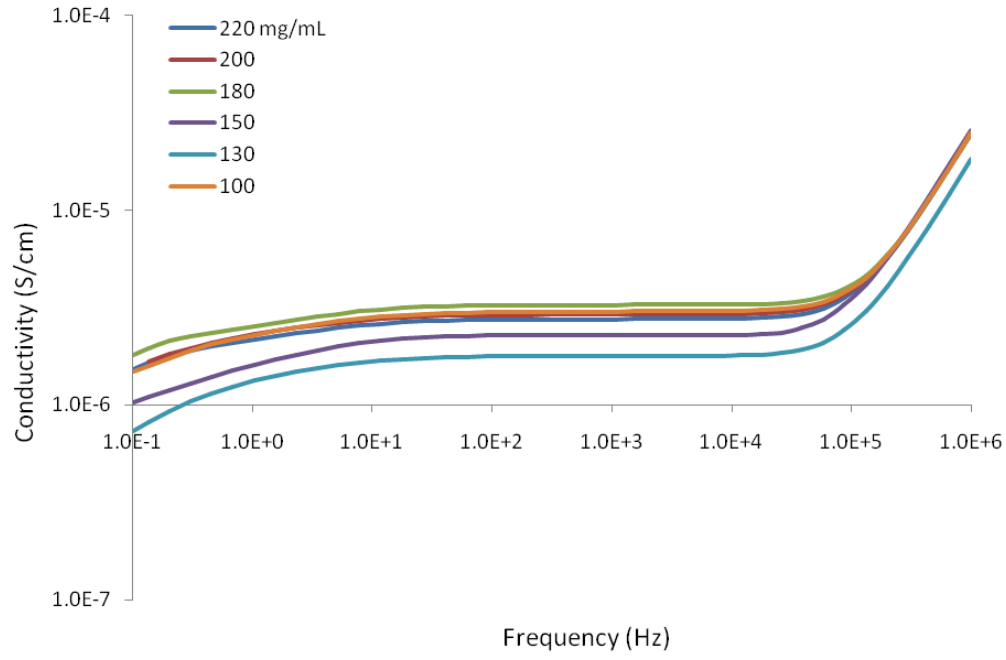
220 mg/mL
200
180
150
130
100
1.0E-4
1.0E-5
1.0E-6
1.0E-7
Conductivity (S/cm)
1.0E-1
1.0E+0
1.0E+1
1.0E+2
1.0E+3
1.0E+4
1.0E+5
1.0E+6
Frequency (Hz)

Ultem 1000 in 3:1 DMAc/THF:

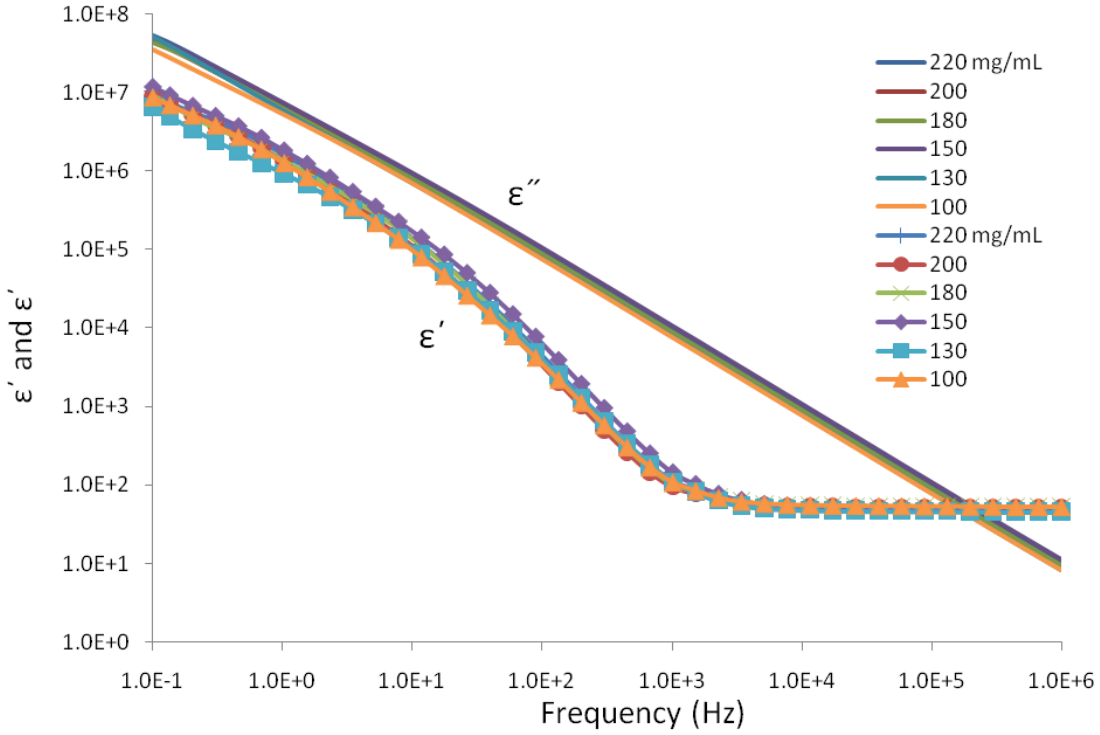

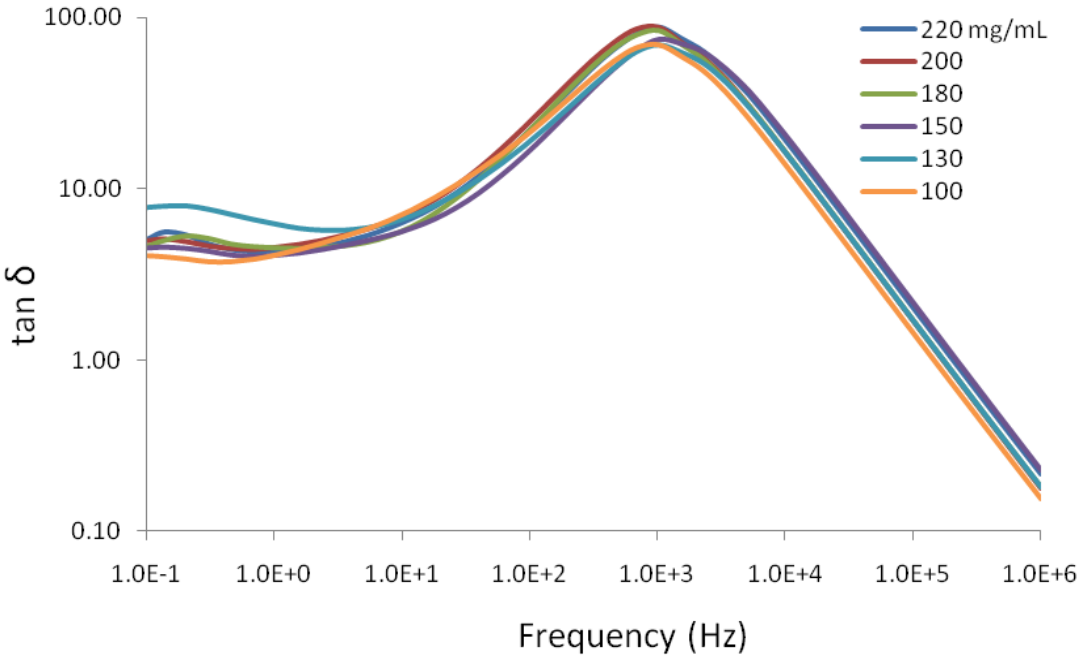

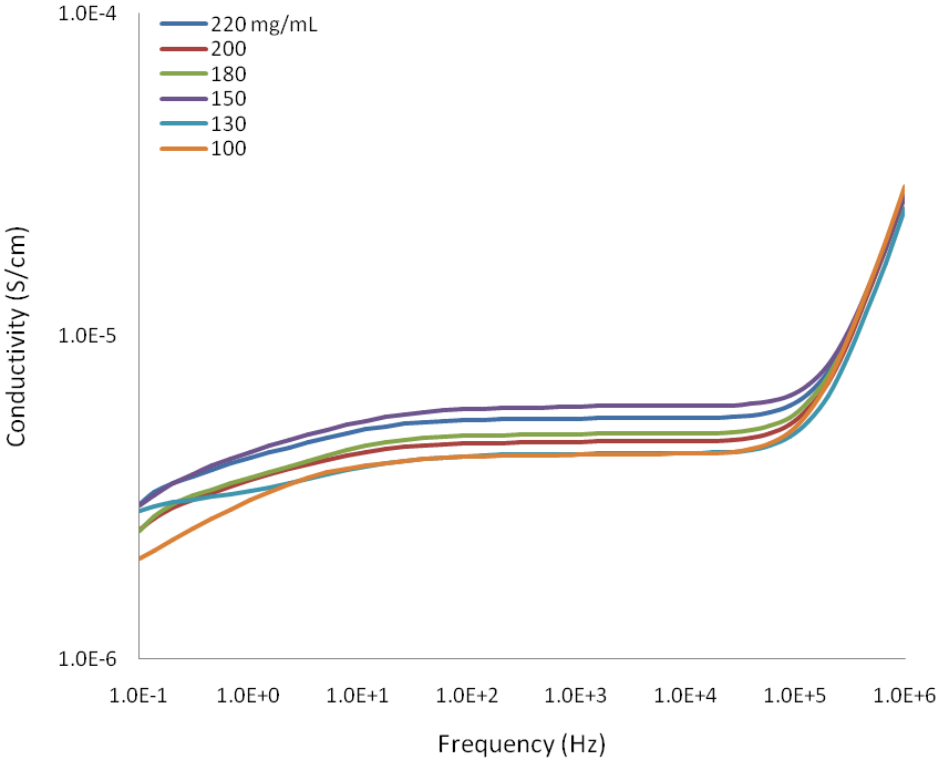

Ultem 1000 in 9:1 DMAc/THF:

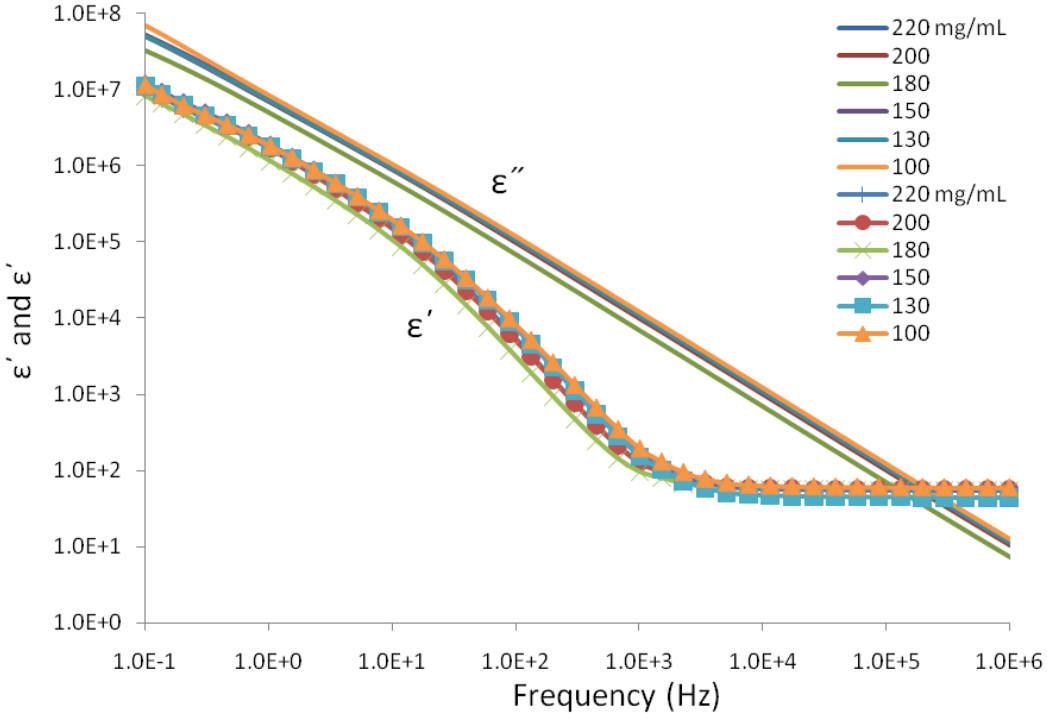

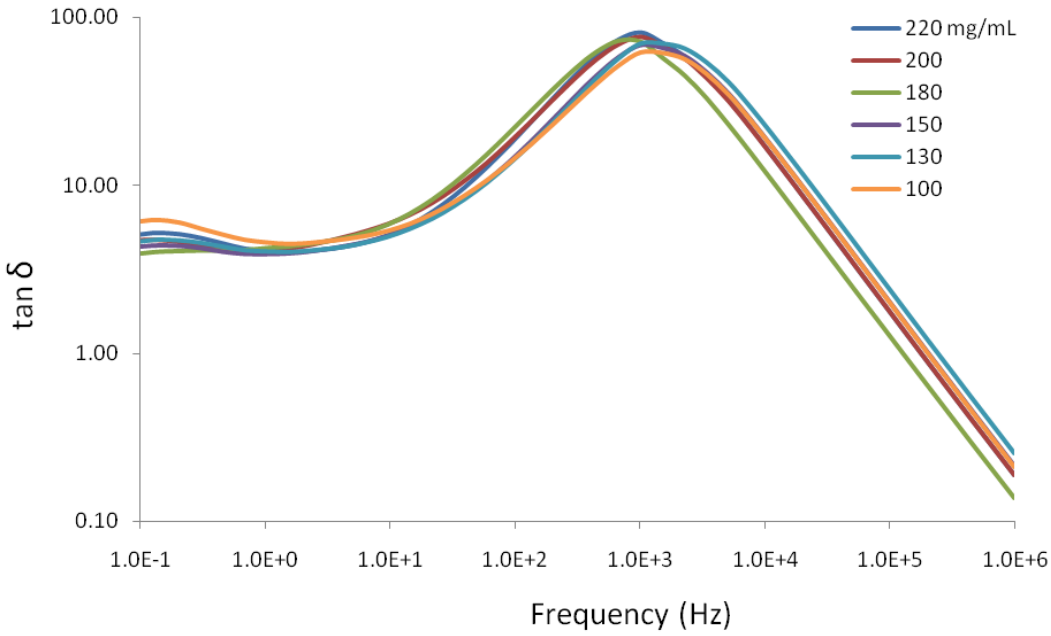
100.00
10.00
1.00
0.10
tan δ
1.0E-1
1.0E+0
1.0E+1
1.0E+2
1.0E+3
1.0E+4
1.0E+5
1.0E+6
Frequency (Hz)
220 mg/mL
200
180
150
130
100

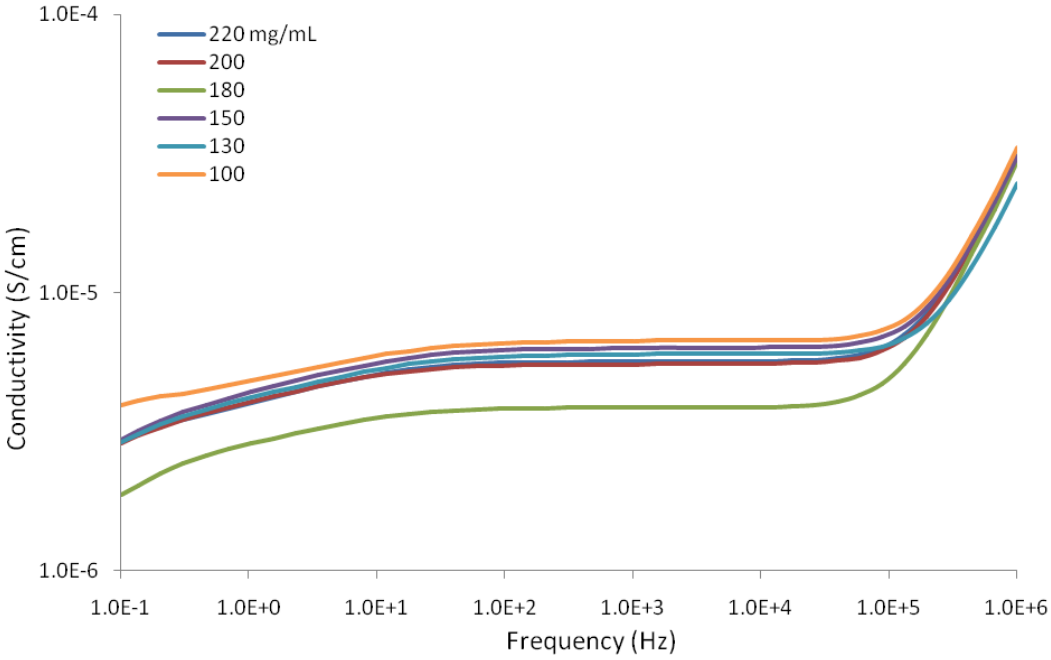
1.0E-4
1.0E-5
1.0E-6
Conductivity (S/cm)
1.0E-1
1.0E+0
1.0E+1
1.0E+2
1.0E+3
1.0E+4
1.0E+5
1.0E+6
Frequency (Hz)
220 mg/mL
200
180
150
130
100

Ultem 1010 Dielectric Measurements

Ultem 1010 in 1:1 DMAc/THF:

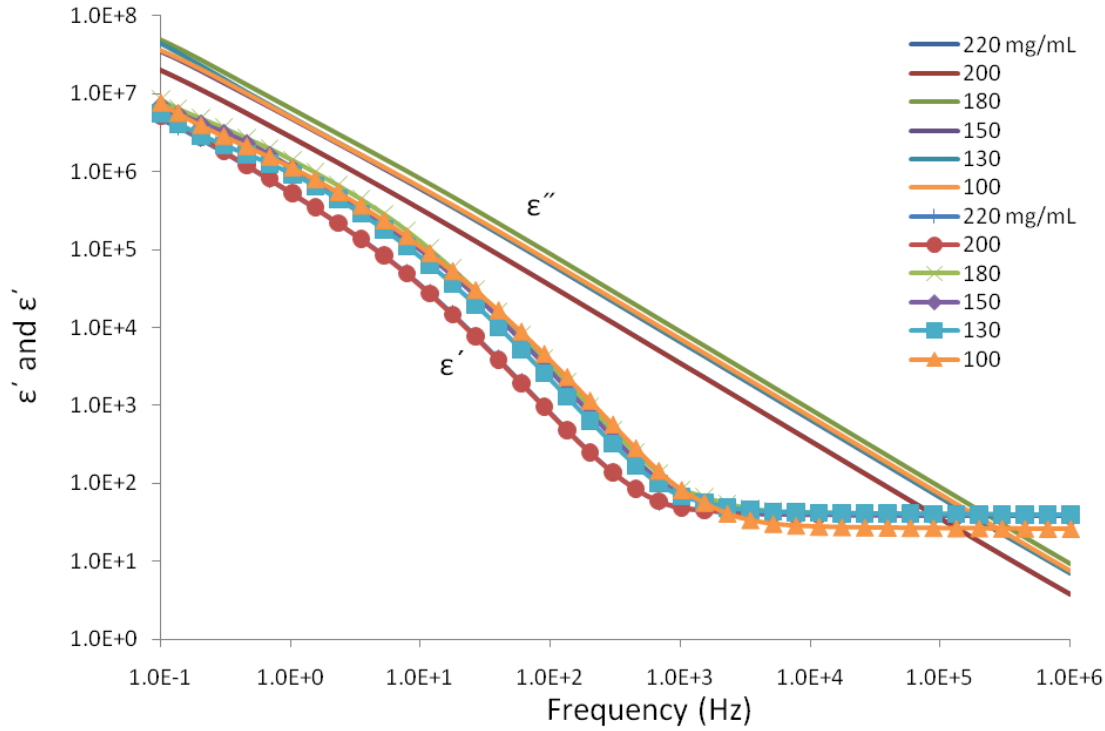

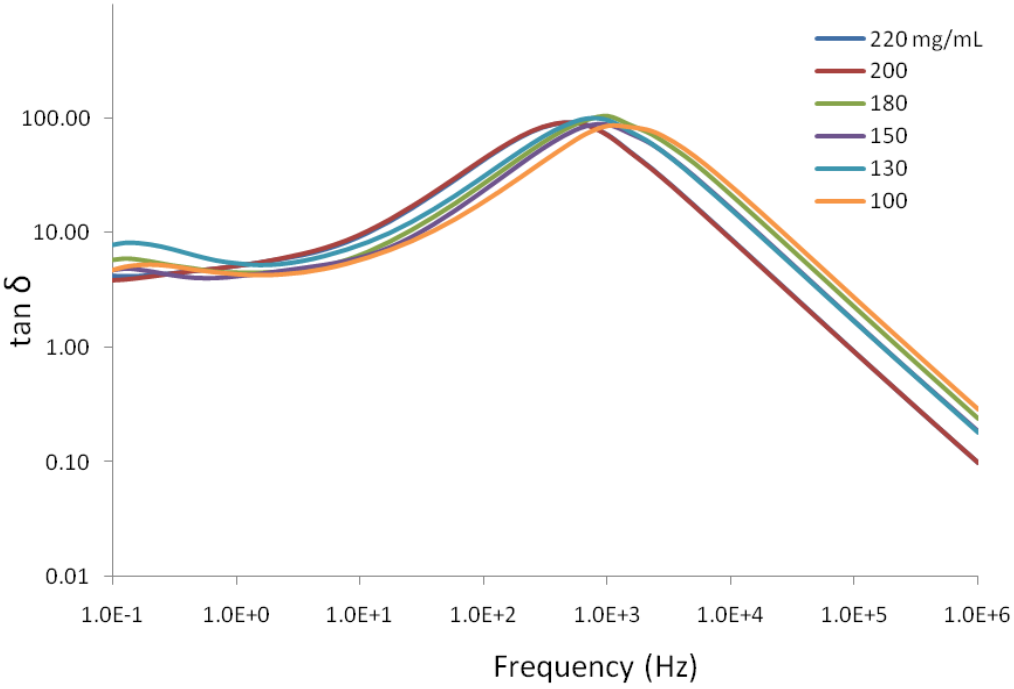
220 mg/mL
200
180
150
130
100
100.00
10.00
1.00
0.10
0.01
tan δ
1.0E-1
1.0E+0
1.0E+1
1.0E+2
1.0E+3
1.0E+4
1.0E+5
1.0E+6
Frequency (Hz)

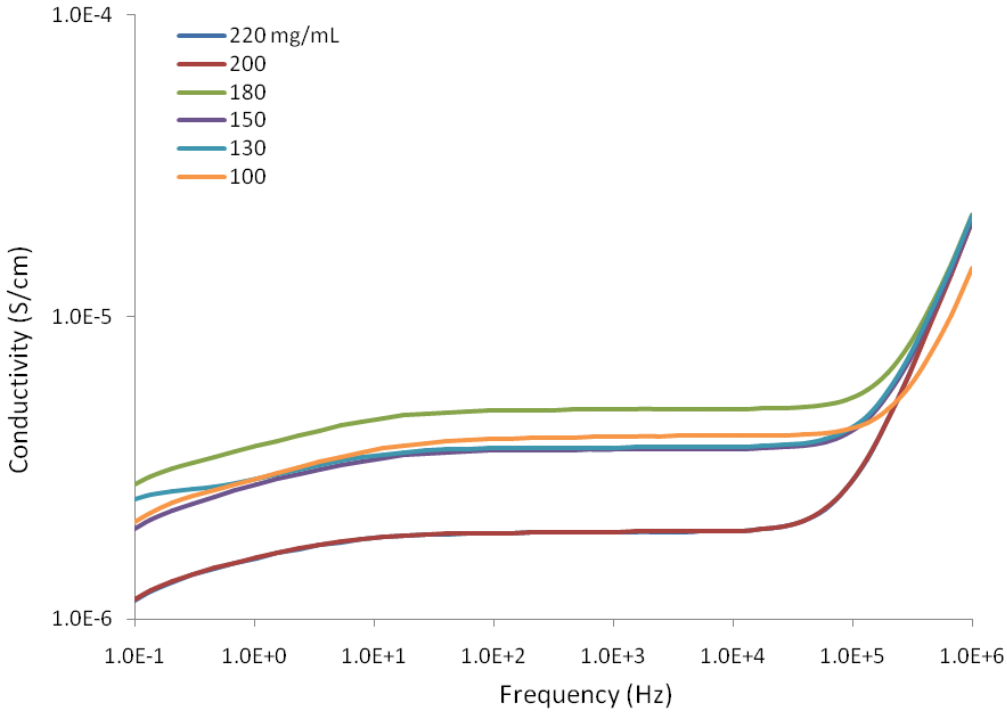
220 mg/mL
200
180
150
130
100
1.0E-4
1.0E-5
1.0E-6
Conductivity (S/cm)
1.0E-1
1.0E+0
1.0E+1
1.0E+2
1.0E+3
1.0E+4
1.0E+5
1.0E+6
Frequency (Hz)

Ultem 1010 in 2:1 DMAc/THF:

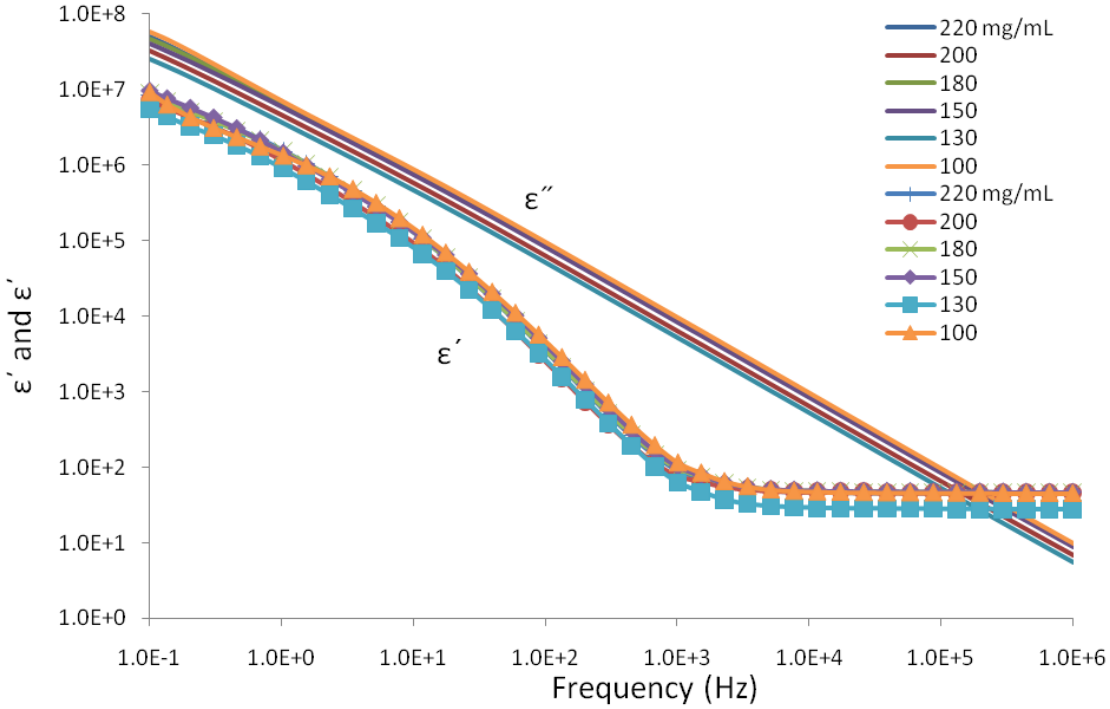

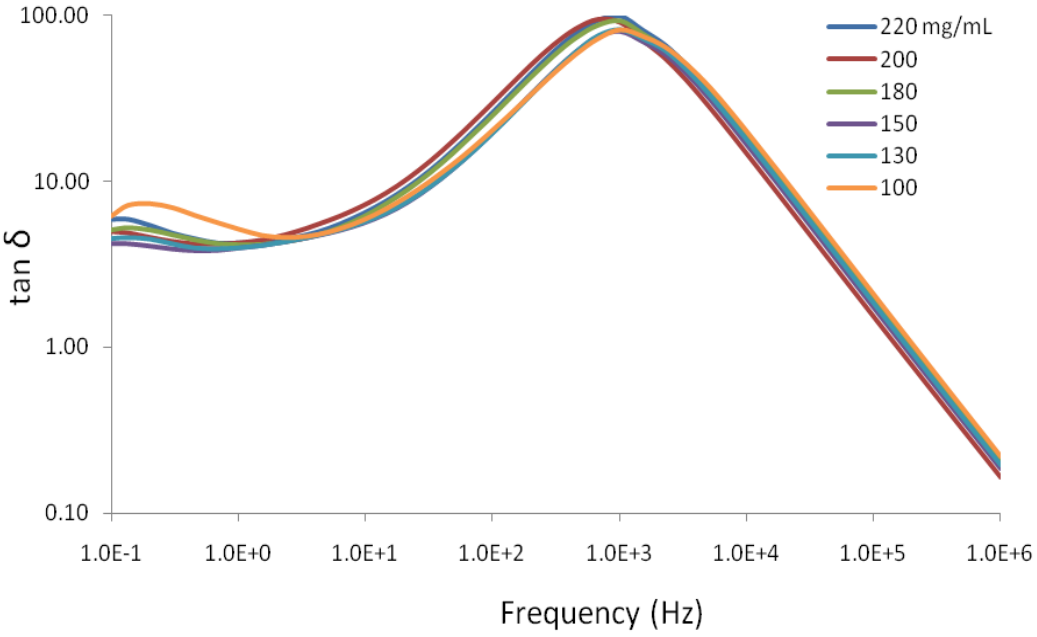

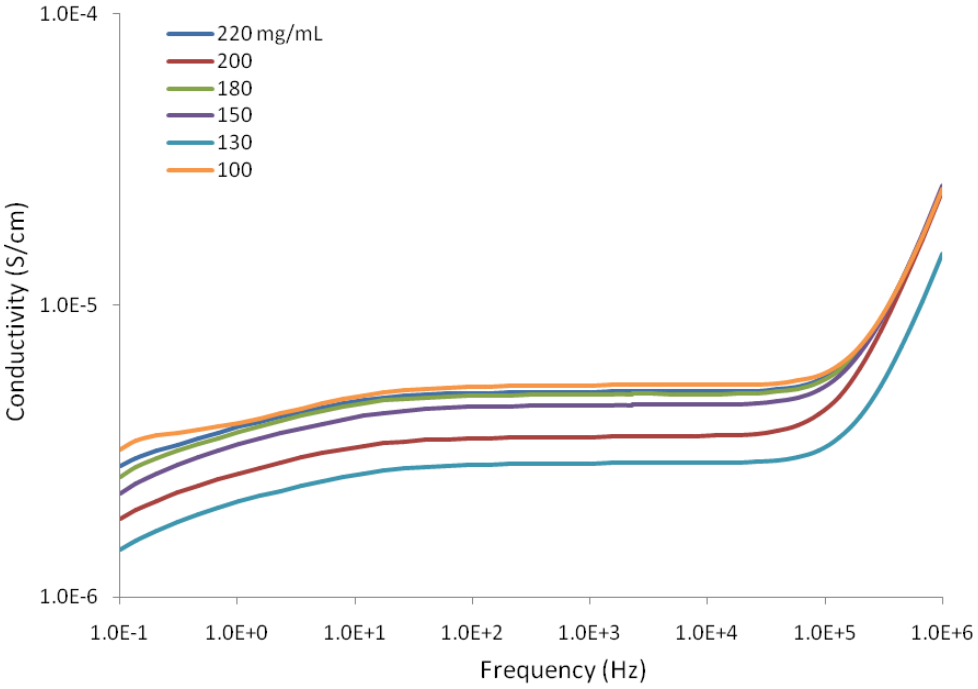
1.0E-4
1.0E-5
1.0E-6
Conductivity (S/cm)
220 mg/mL
200
180
150
130
100
1.0E-1
1.0E+0
1.0E+1
1.0E+2
1.0E+3
1.0E+4
1.0E+5
1.0E+6
Frequency (Hz)

Ultem 1010 in 3:1 DMAc/THF:

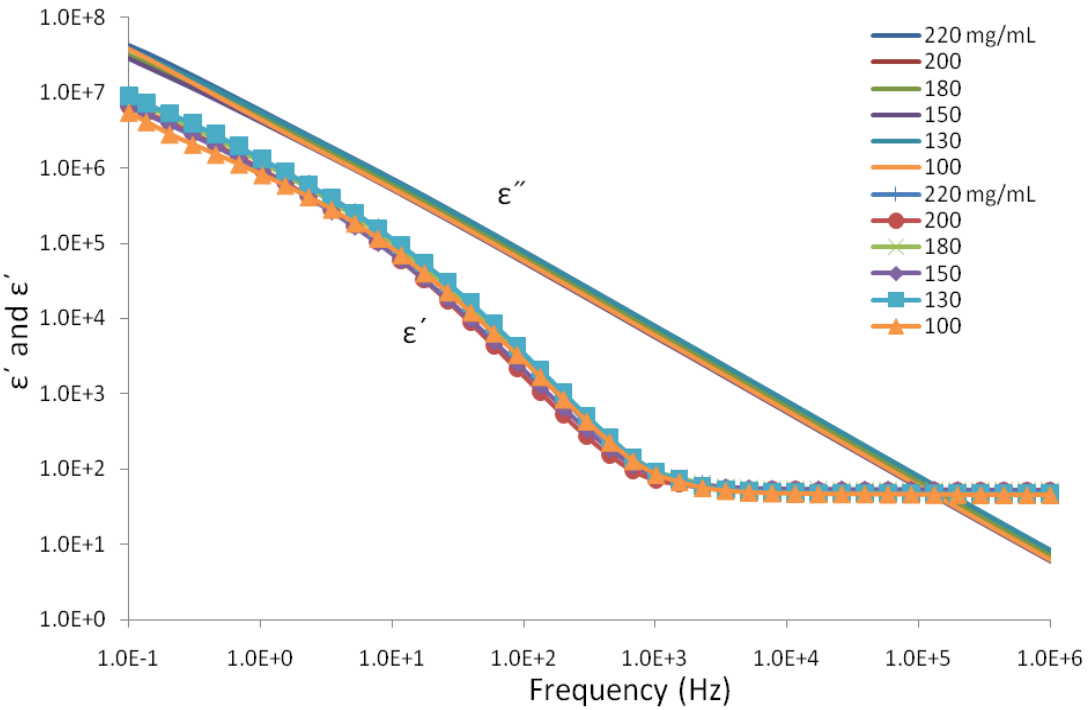

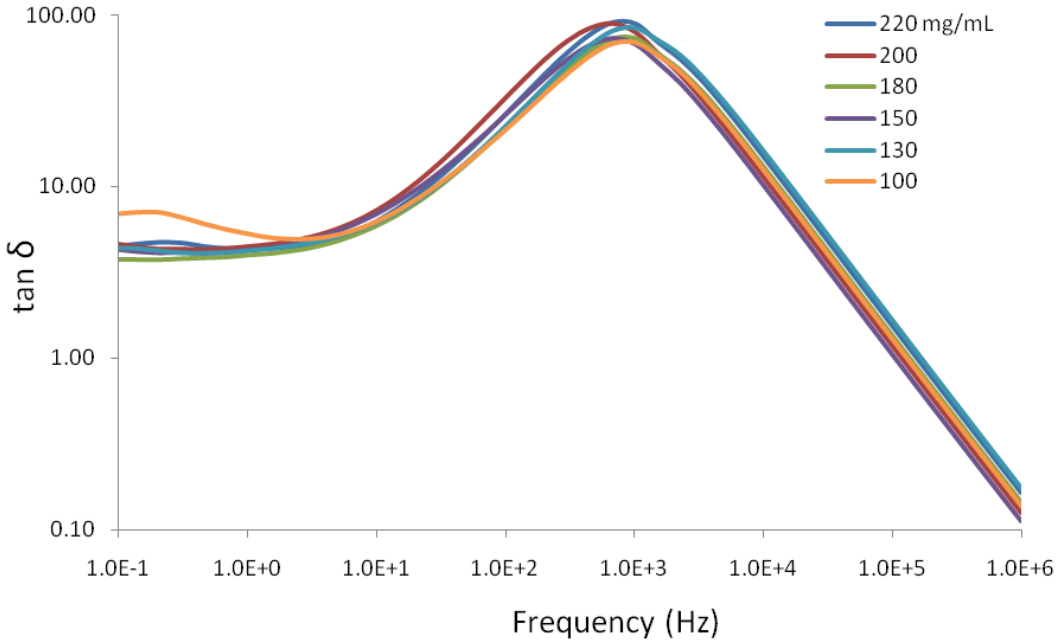

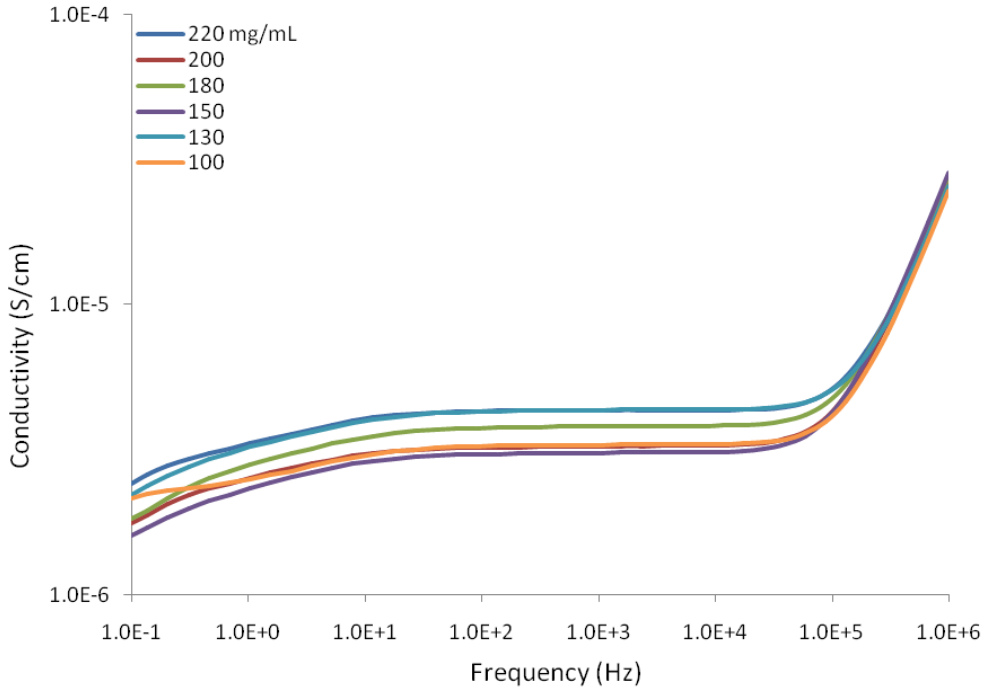

Ultem 1010 in 9:1 DMAc/THF:

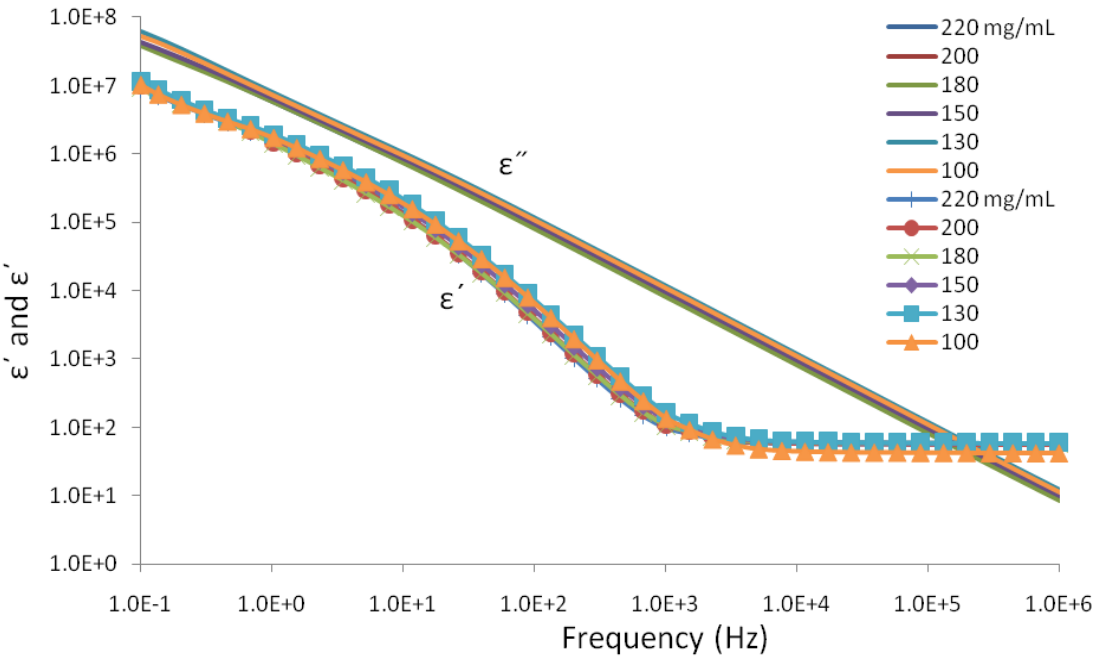

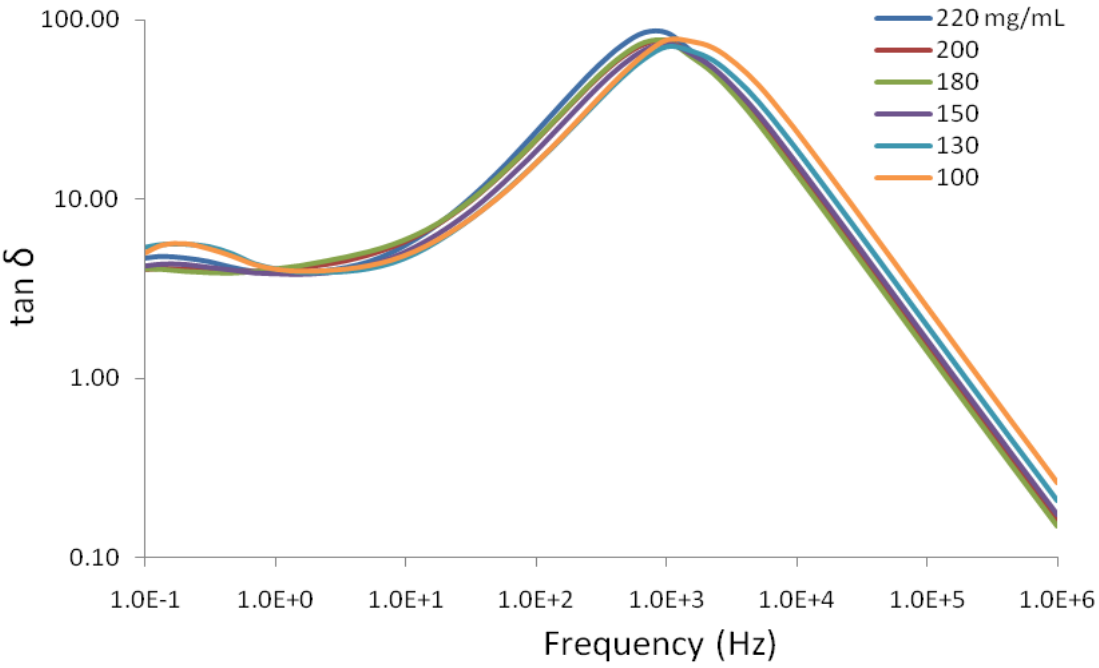
100.00
10.00
1.00
0.10
tan δ
220 mg/mL
200
180
150
130
100
1.0E-1
1.0E+0
1.0E+1
1.0E+2
1.0E+3
1.0E+4
1.0E+5
1.0E+6
Frequency (Hz)

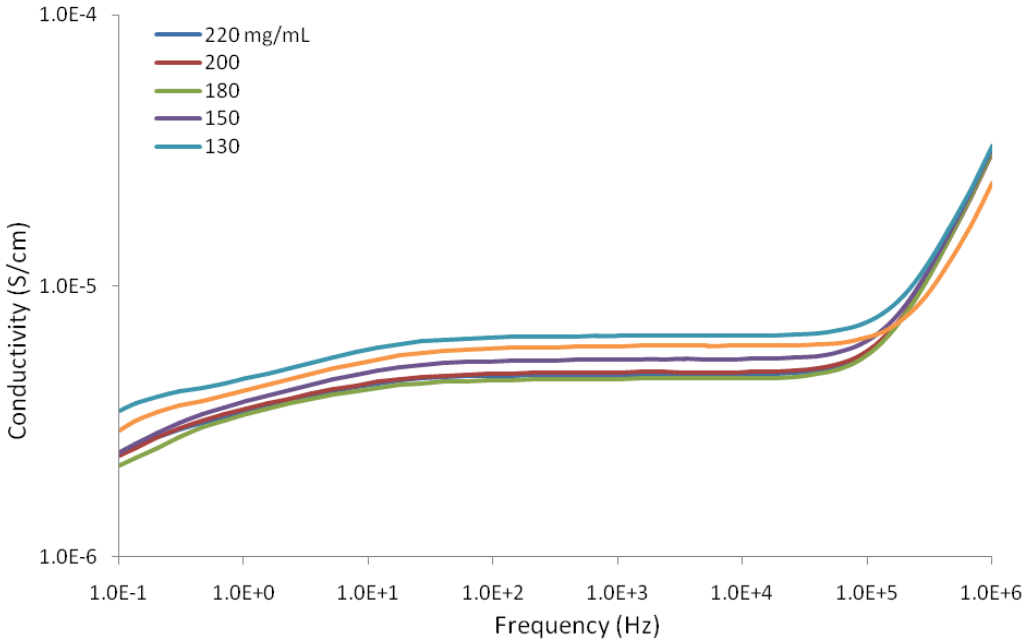
1.0E-4
1.0E-5
1.0E-6
Conductivity (S/cm)
220 mg/mL
200
180
150
130
1.0E-1
1.0E+0
1.0E+1
1.0E+2
1.0E+3
1.0E+4
1.0E+5
1.0E+6
Frequency (Hz)

220 mg/mL Ultem 1010:

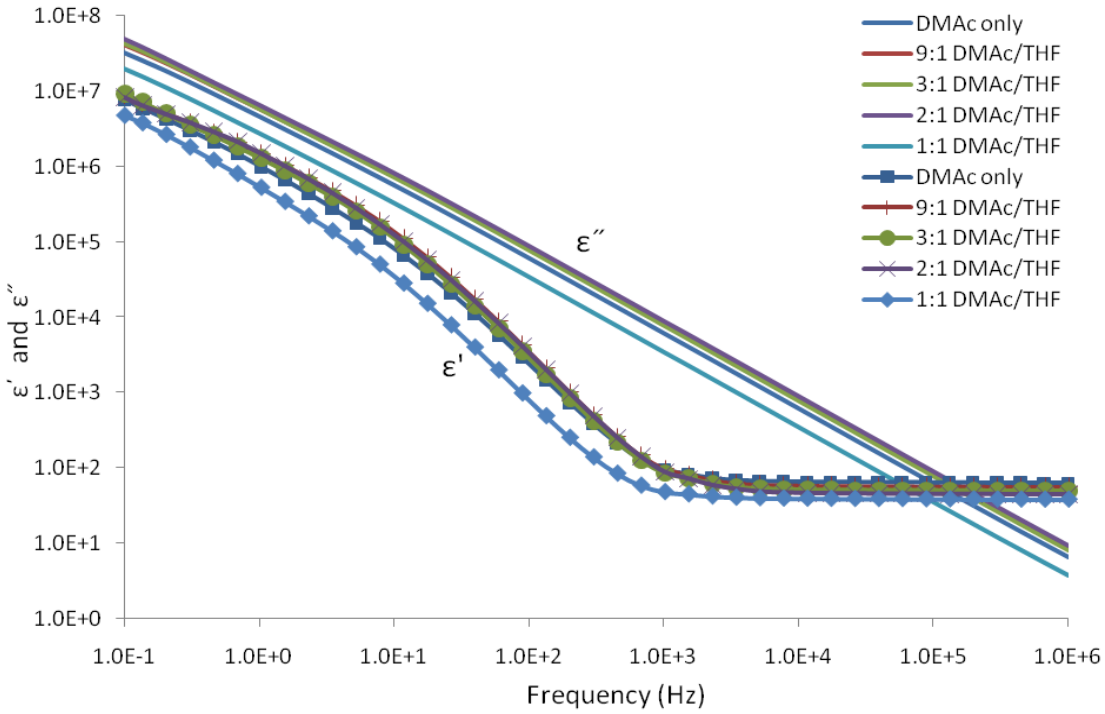

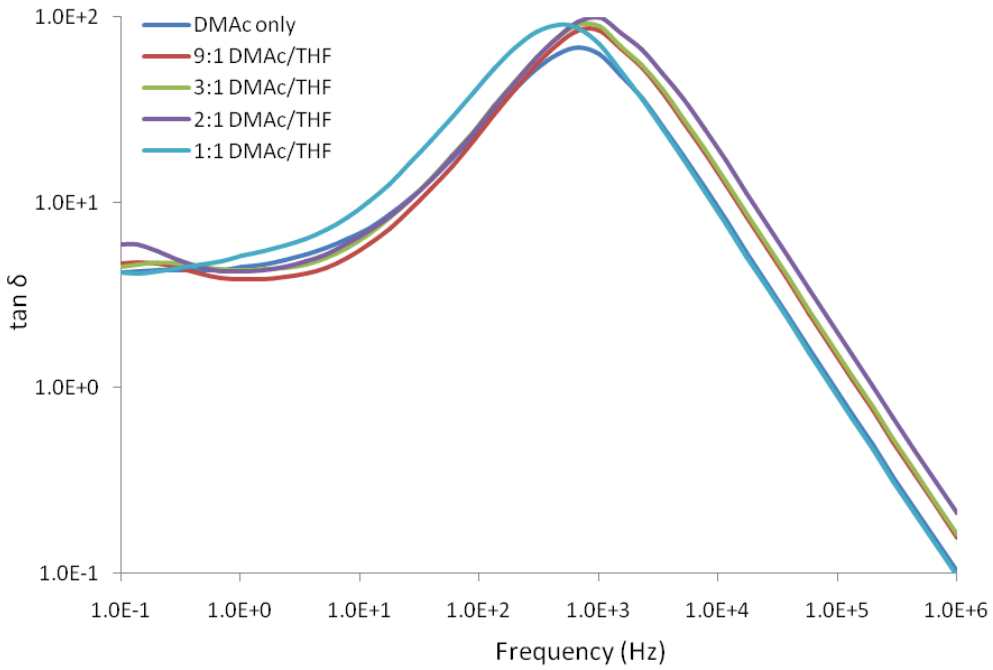

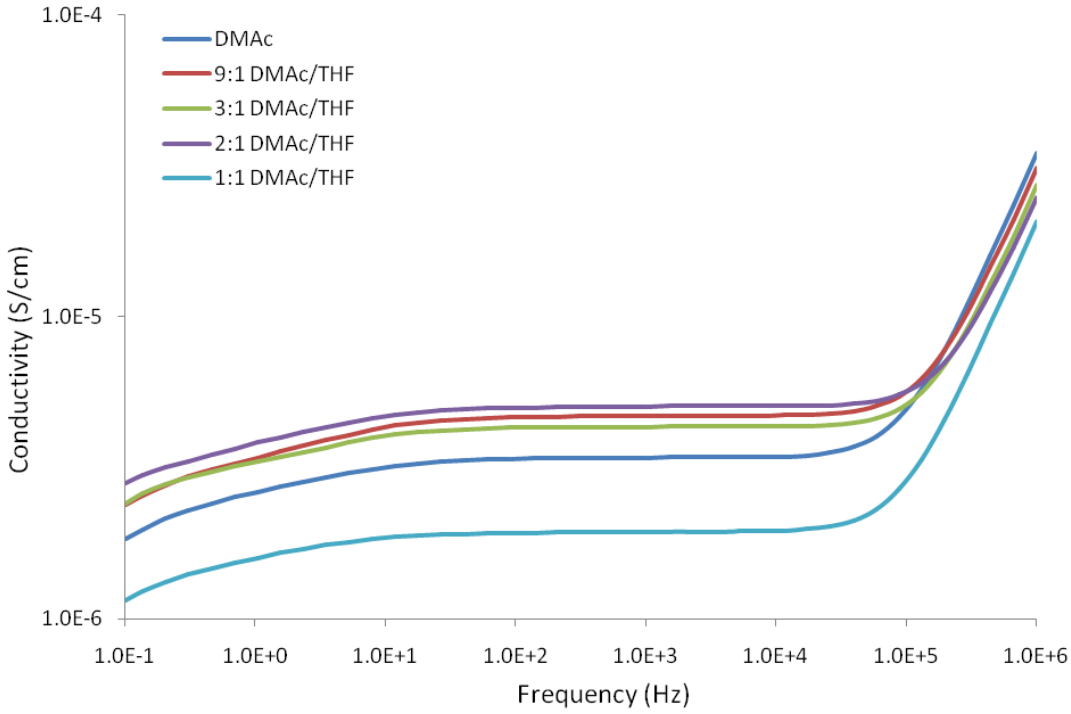

200 mg/mL Ultem 1010:

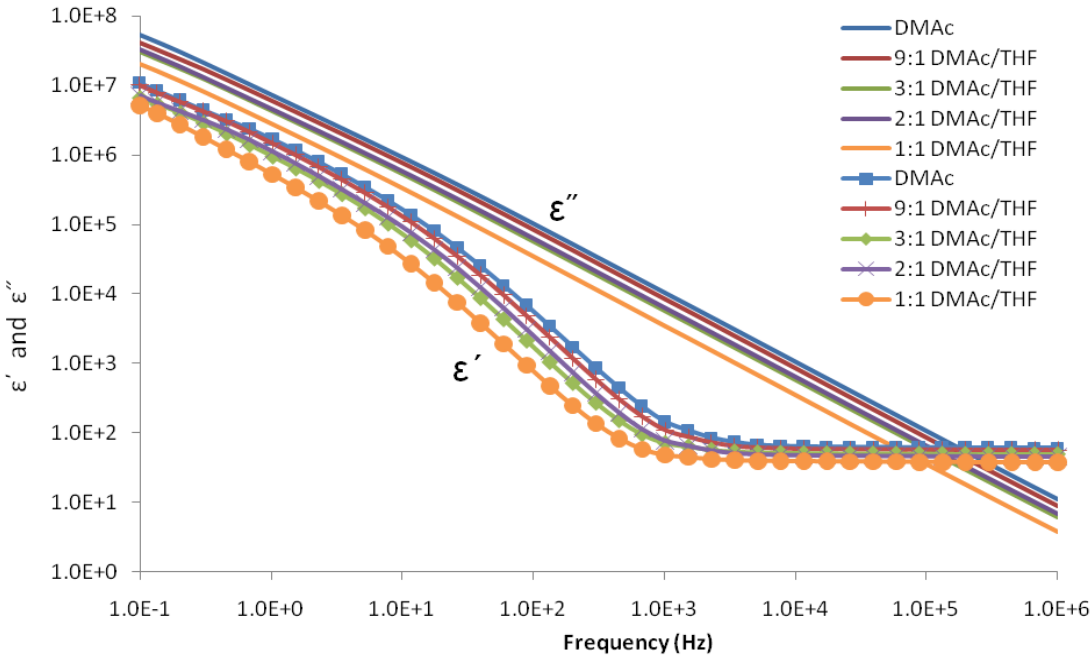

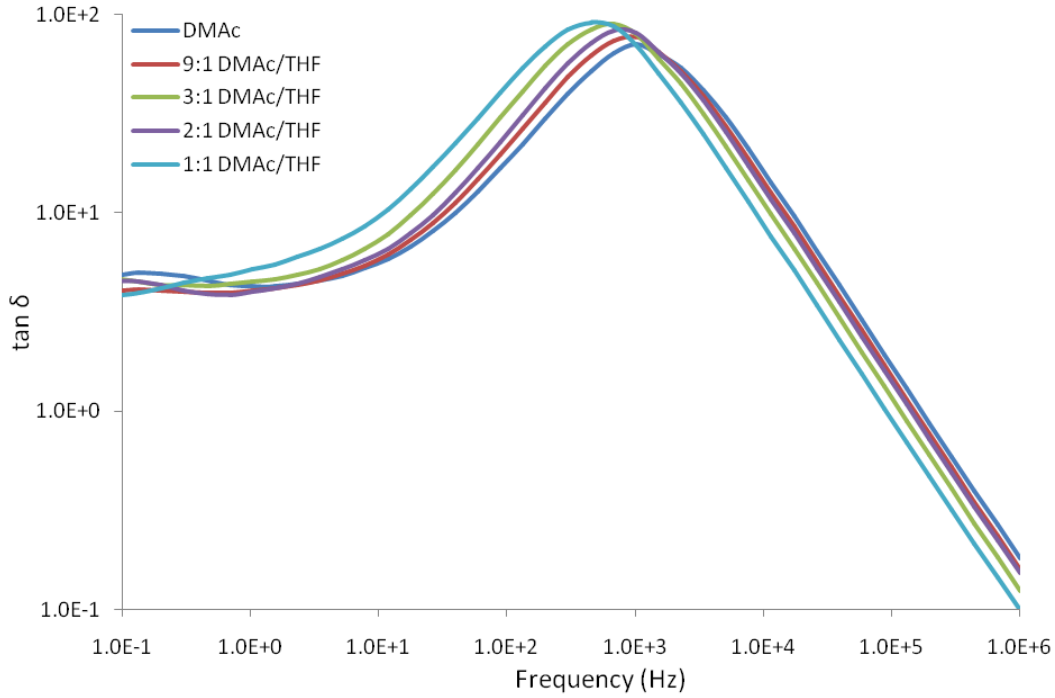
1.0E+2
1.0E+1
1.0E+0
1.0E-1
tan δ
DMAc
9:1 DMAc/THF
3:1 DMAc/THF
2:1 DMAc/THF
1:1 DMAc/THF
1.0E-1
1.0E+0
1.0E+1
1.0E+2
1.0E+3
1.0E+4
1.0E+5
1.0E+6
Frequency (Hz)

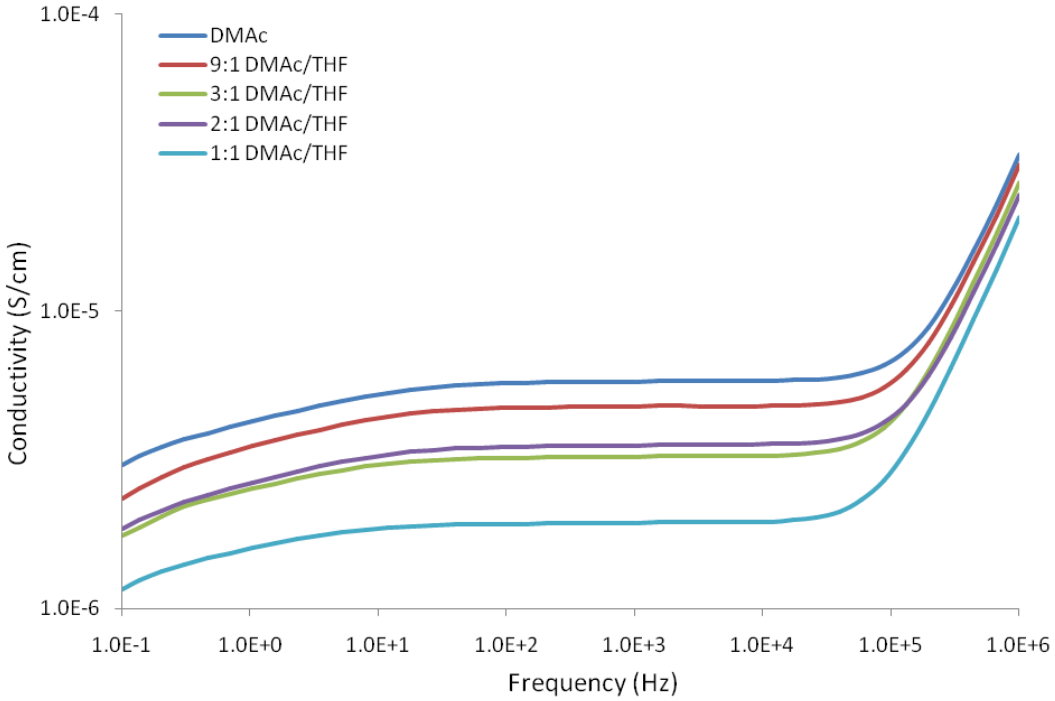
1.0E-4
1.0E-5
1.0E-6
Conductivity (S/cm)
DMAc
9:1 DMAc/THF
3:1 DMAc/THF
2:1 DMAc/THF
1:1 DMAc/THF
1.0E-1
1.0E+0
1.0E+1
1.0E+2
1.0E+3
1.0E+4
1.0E+5
1.0E+6
Frequency (Hz)

180 mg/mL Ultem 1010:

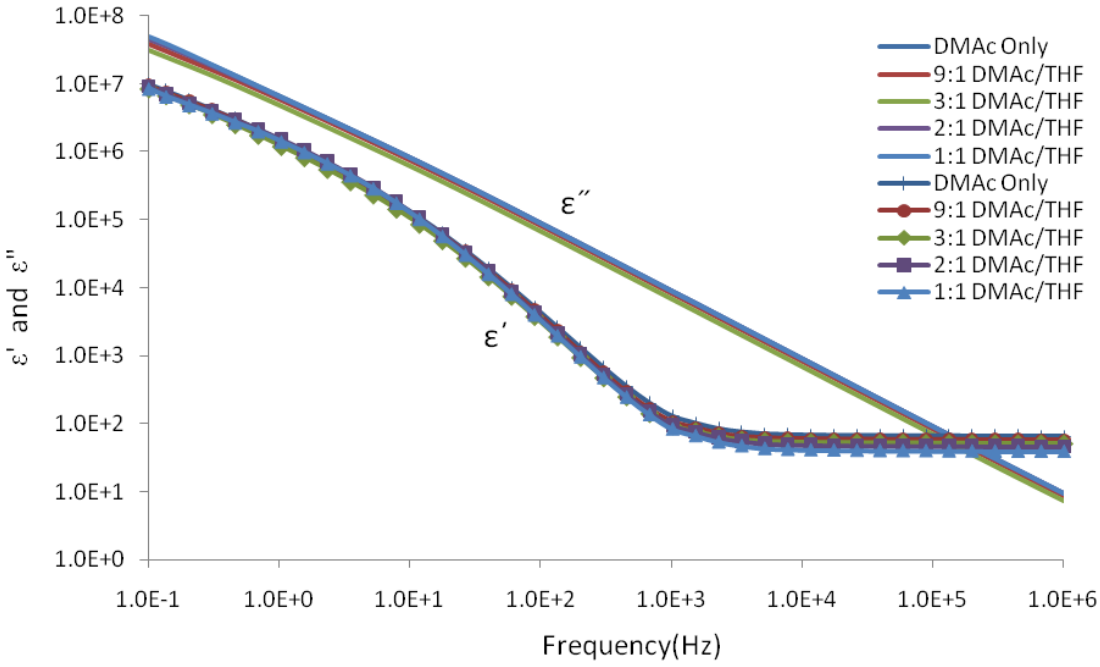

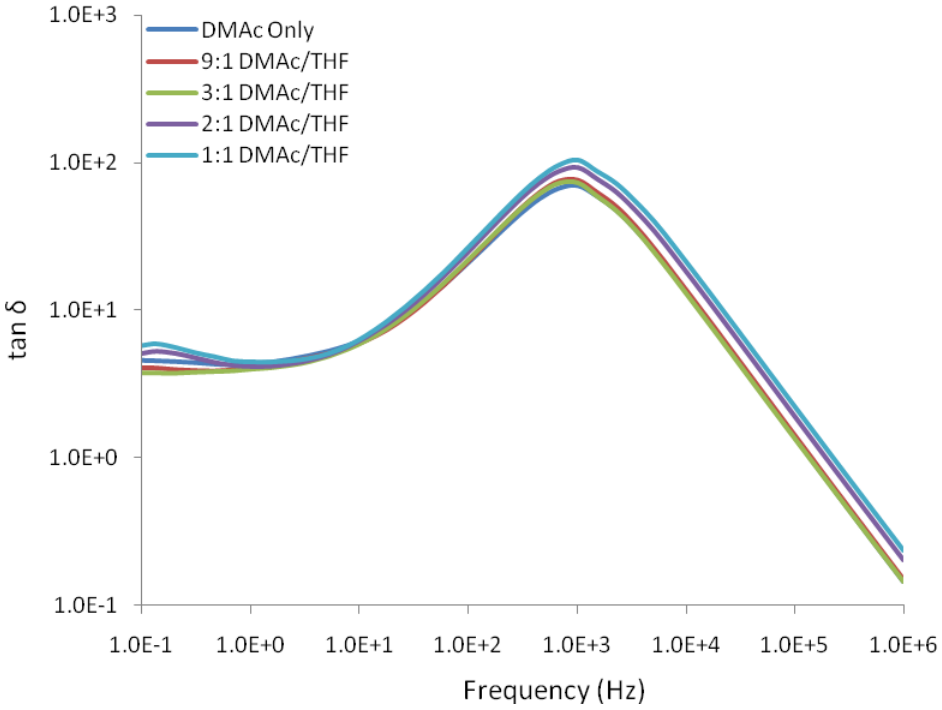

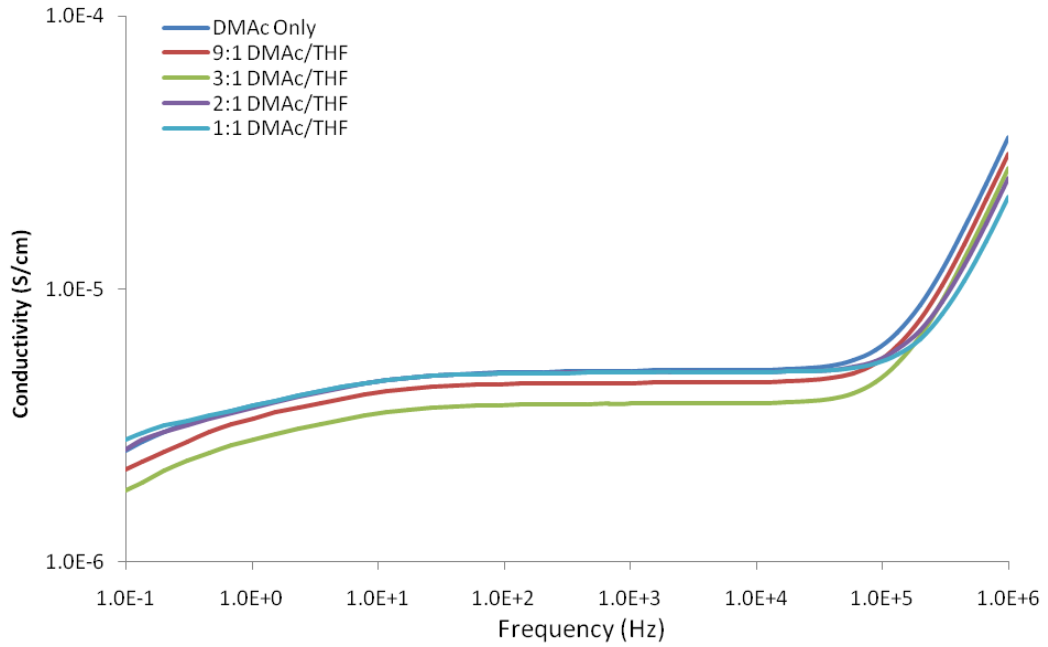

150 mg/mL Ultem 1010:

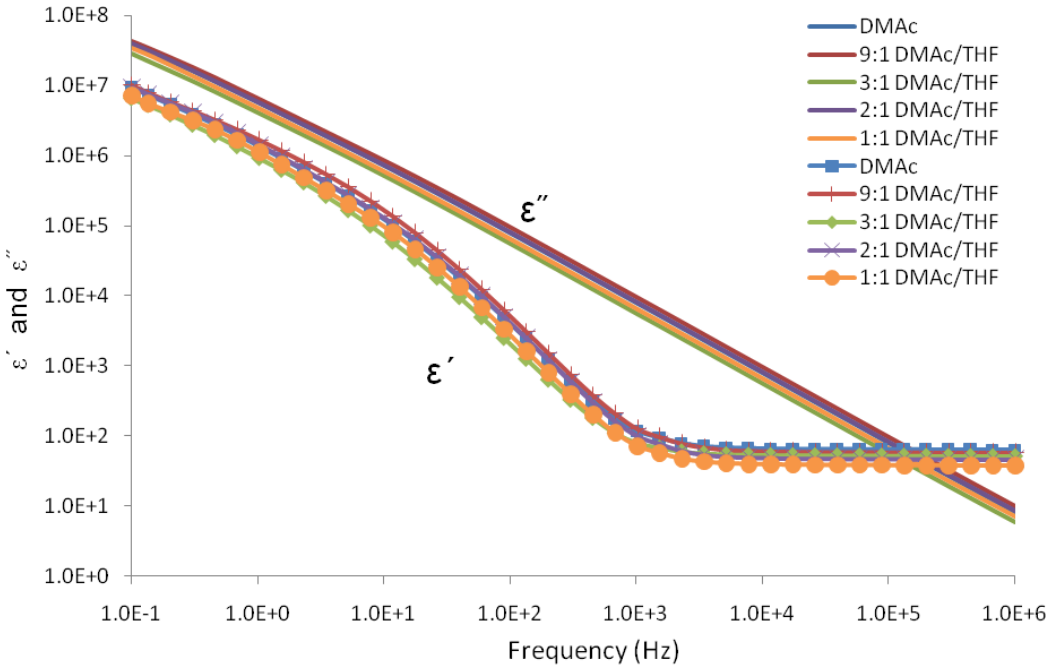

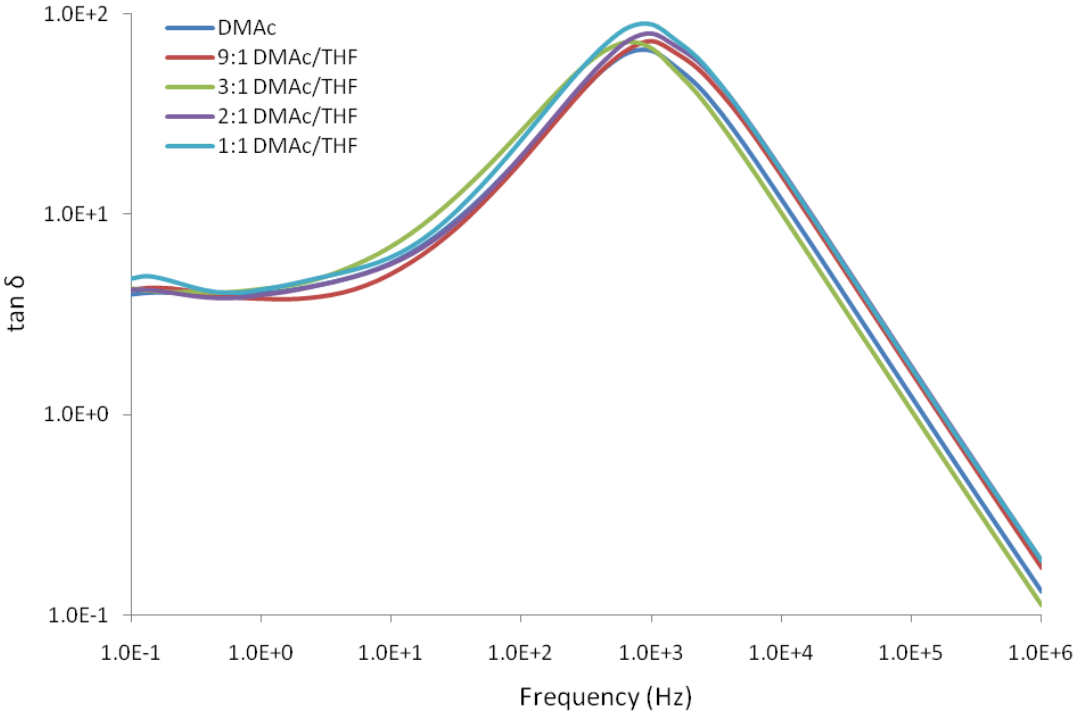
1.0E+2
1.0E+1
1.0E+0
1.0E-1
tan δ
DMAc
9:1 DMAc/THF
3:1 DMAc/THF
2:1 DMAc/THF
1:1 DMAc/THF
1.0E-1
1.0E+0
1.0E+1
1.0E+2
1.0E+3
1.0E+4
1.0E+5
1.0E+6
Frequency (Hz)

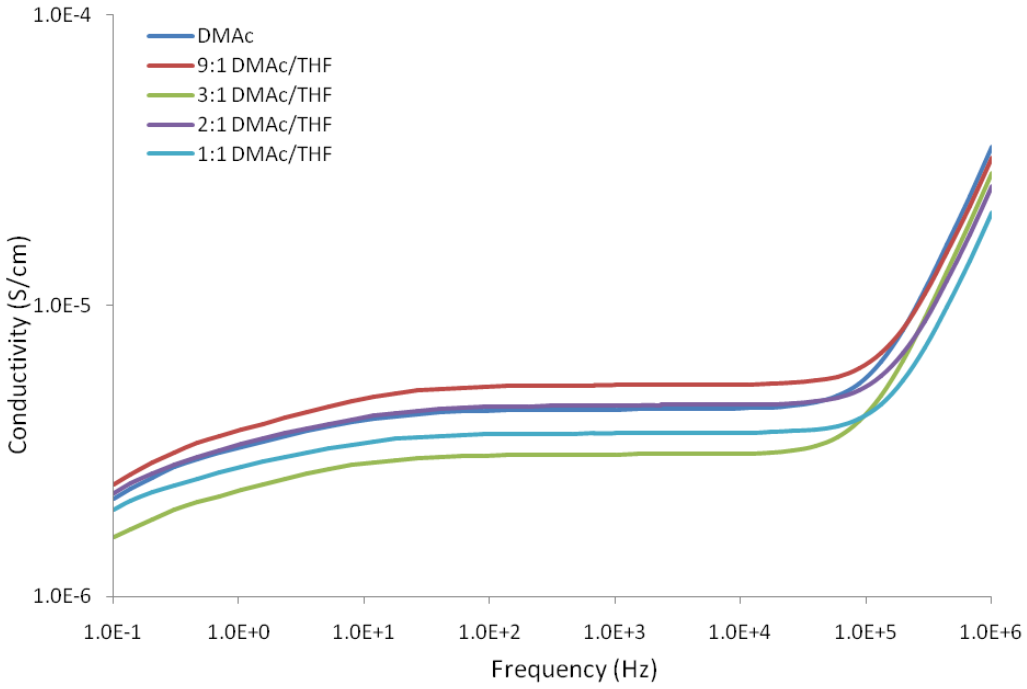
1.0E-4
1.0E-5
1.0E-6
Conductivity (S/cm)
DMAc
9:1 DMAc/THF
3:1 DMAc/THF
2:1 DMAc/THF
1:1 DMAc/THF
1.0E-1
1.0E+0
1.0E+1
1.0E+2
1.0E+3
1.0E+4
1.0E+5
1.0E+6
Frequency (Hz)

130 mg/mL Ultem 1010:

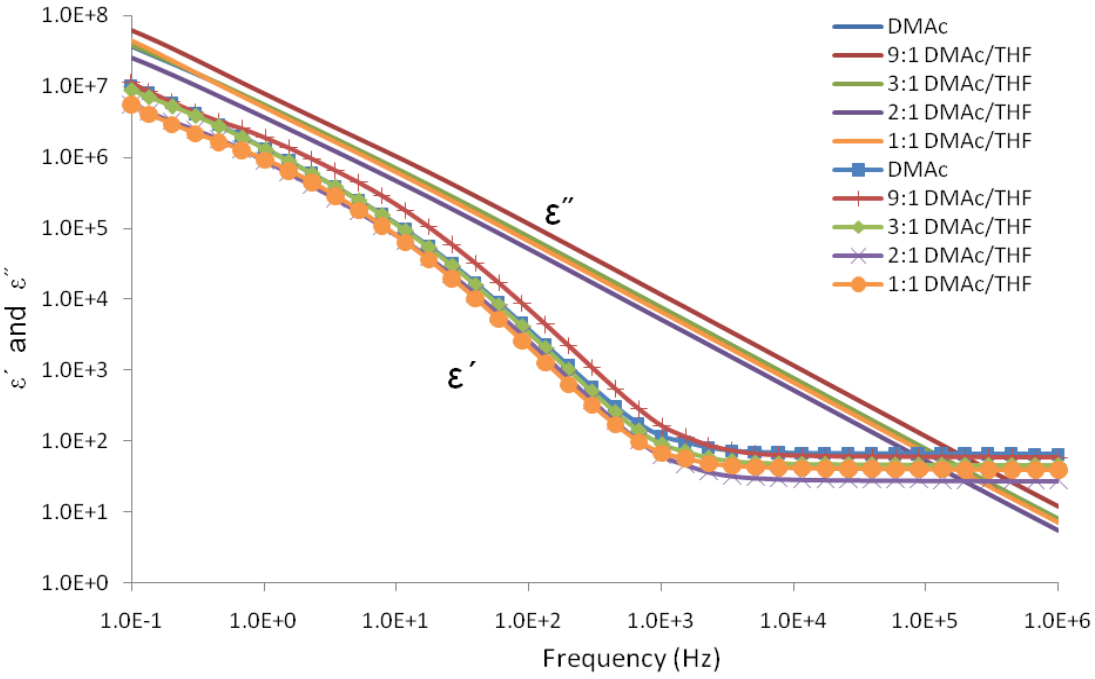

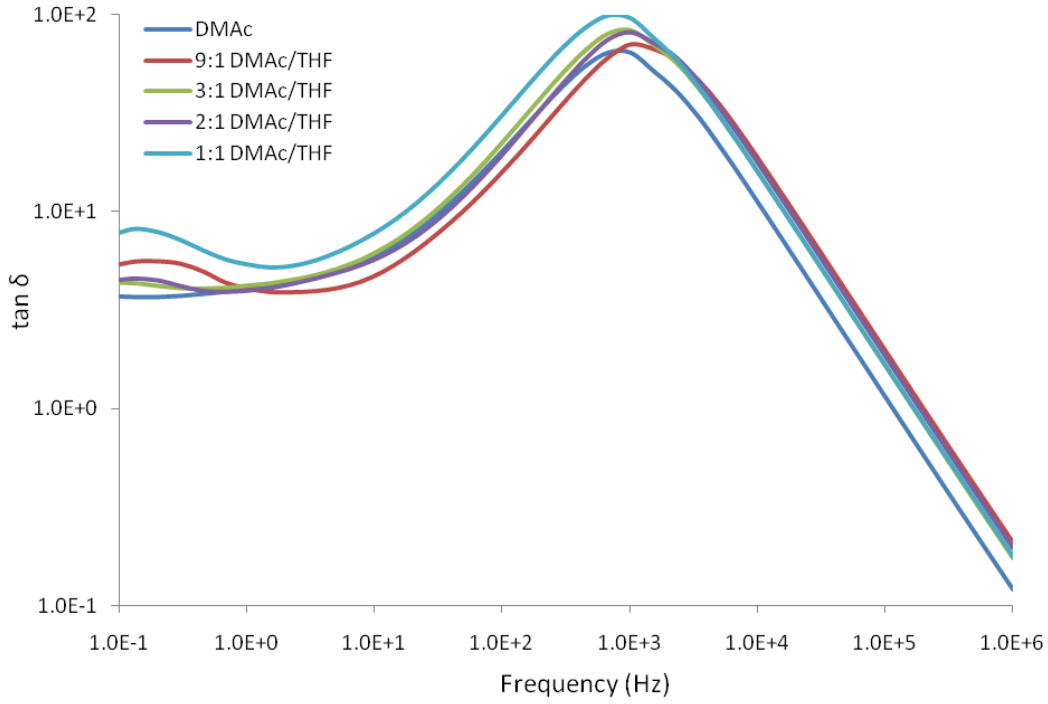

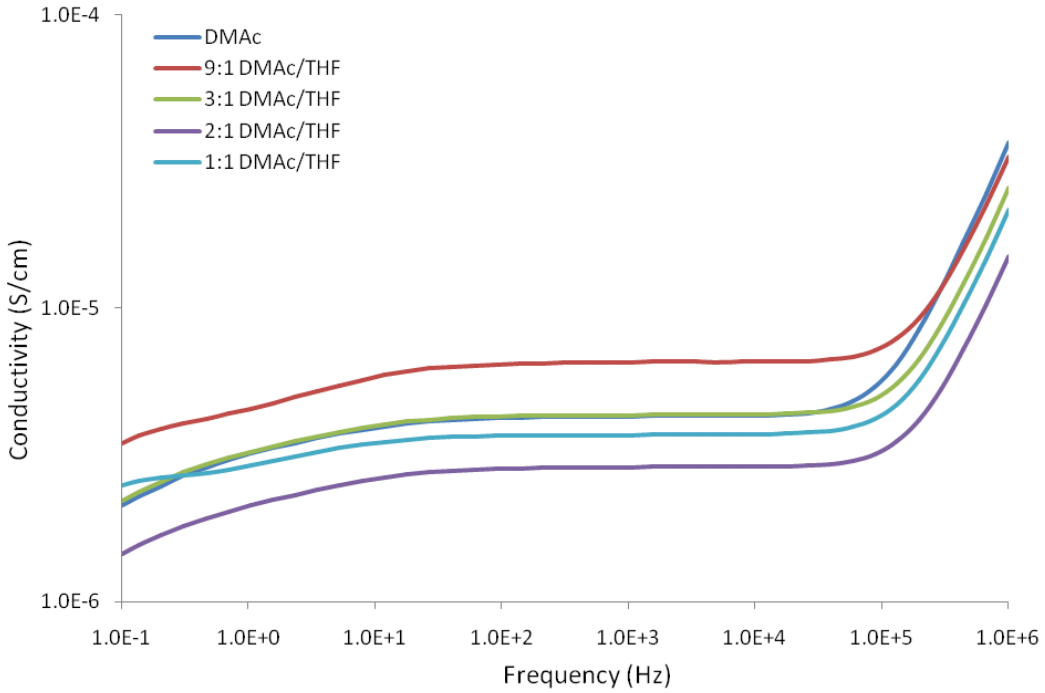

100 mg/mL Ultem 1010:

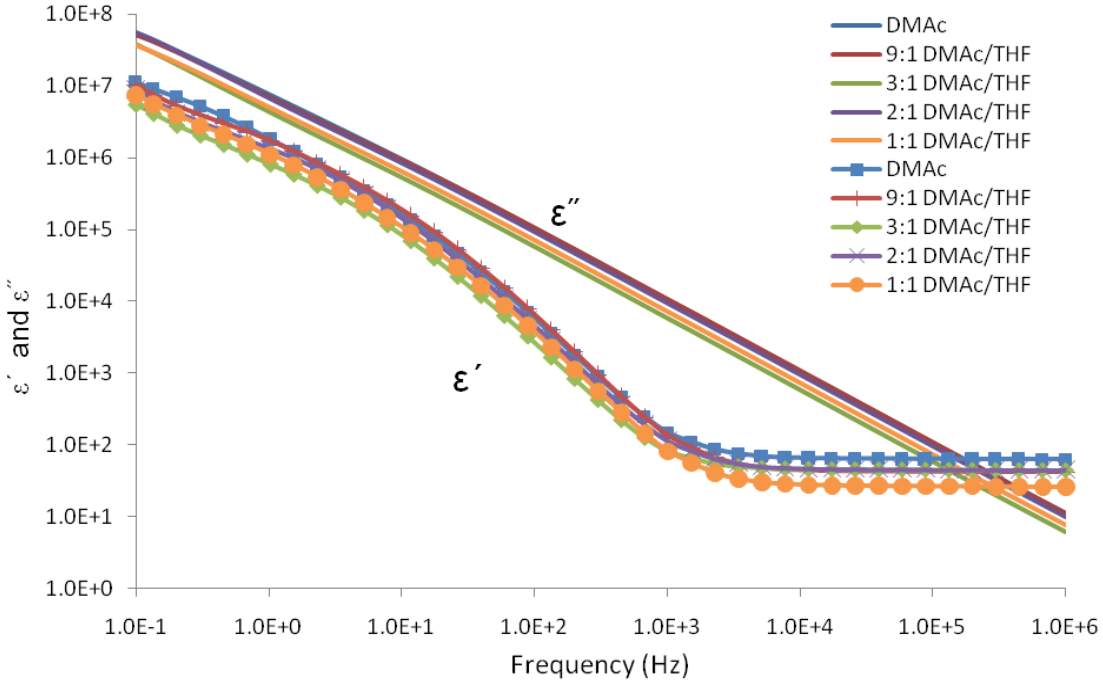

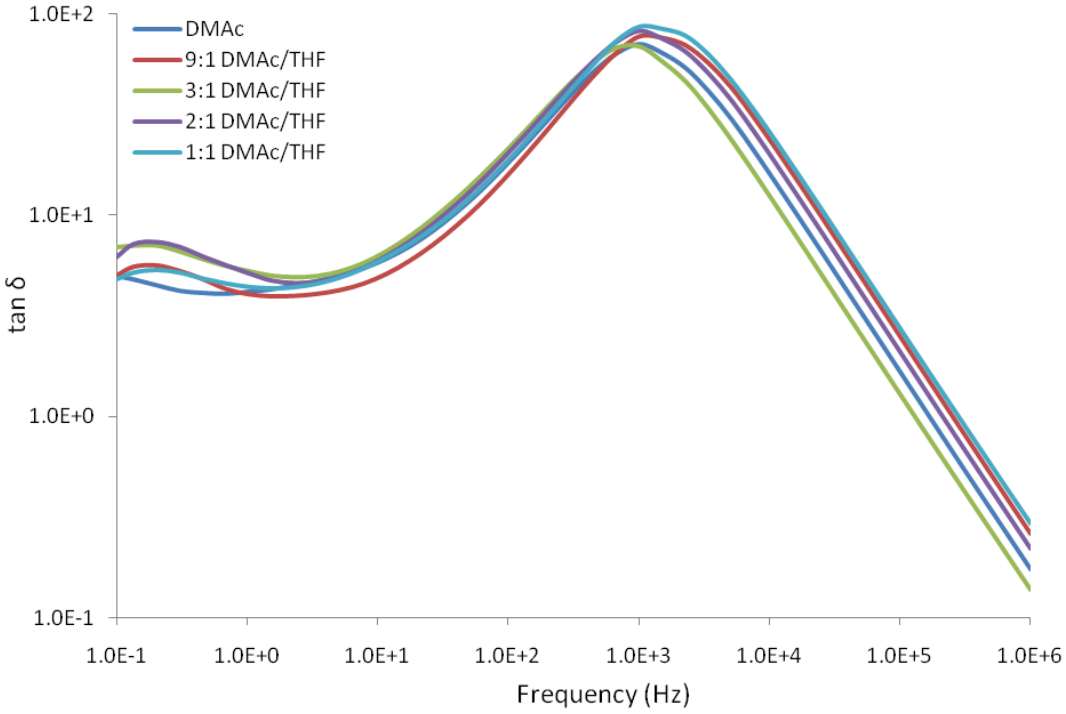
1.0E+2
1.0E+1
1.0E+0
1.0E-1
tan δ
DMAc
9:1 DMAc/THF
3:1 DMAc/THF
2:1 DMAc/THF
1:1 DMAc/THF
1.0E-1
1.0E+0
1.0E+1
1.0E+2
1.0E+3
1.0E+4
1.0E+5
1.0E+6
Frequency (Hz)

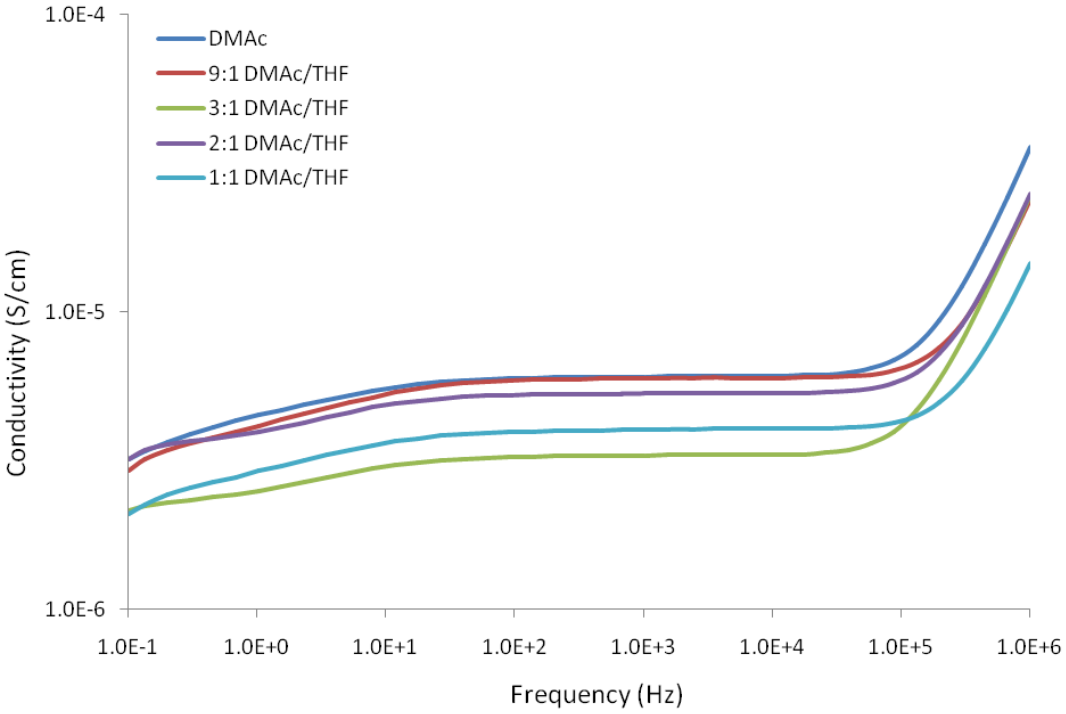
1.0E-4
1.0E-5
1.0E-6
Conductivity (S/cm)
DMAc
9:1 DMAc/THF
3:1 DMAc/THF
2:1 DMAc/THF
1:1 DMAc/THF
1.0E-1
1.0E+0
1.0E+1
1.0E+2
1.0E+3
1.0E+4
1.0E+5
1.0E+6
Frequency (Hz)

APPENDIX C

Rheological Data of PEI Solutions

Viscosities and loss moduli included are within the frequency range where all samples had a raw phase < 150 degrees. This ensures that the comparison of data is based on accurate, stable solution behavior. Full frequency range data of G´ is included for observation, but only data through 12 rad/s should be evaluated. Likewise, viscosities and G˝ full ranges are not included because sample instabilities caused non-linear data, inaccurate to actual sample properties, given low frequency behavior and steady shear viscosity measurements. Also, data was collected for all samples over the frequency range tested, but G´ curves appear incomplete because log plots do not include negative data.

Complex viscosities, loss moduli and storage moduli of Ultem 1010 solutions

In DMAc:

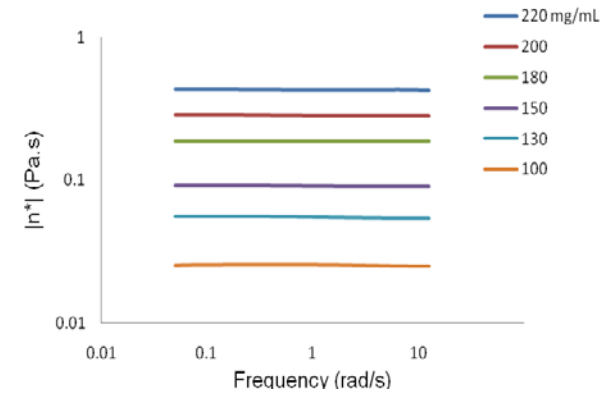

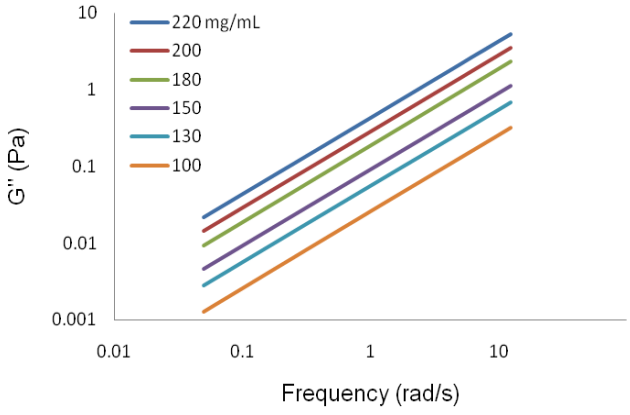

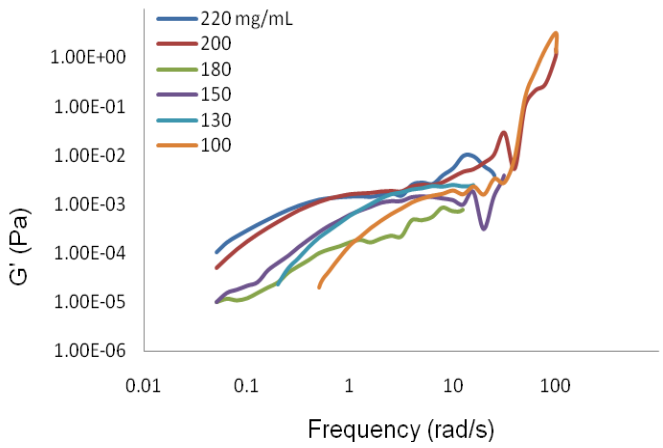

In 9:1 DMAc/THF:

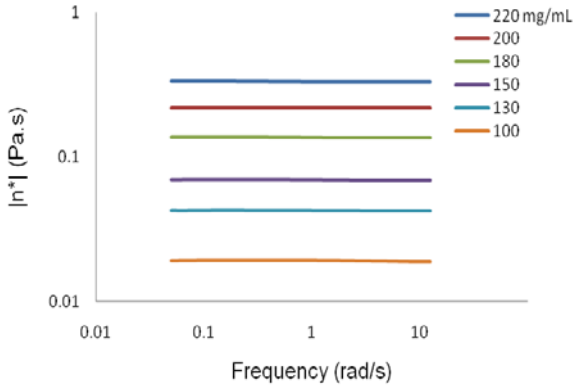

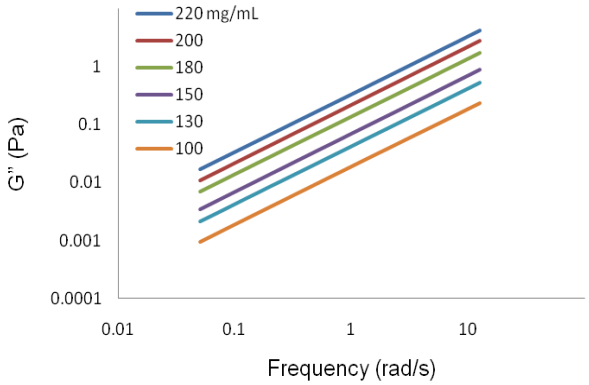

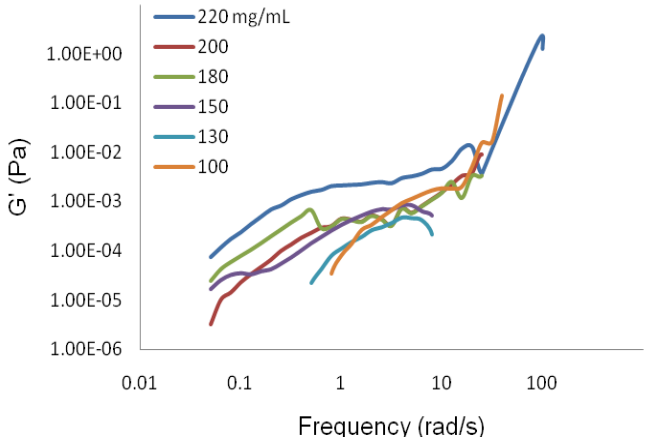

In 3:1 DMAc/THF:

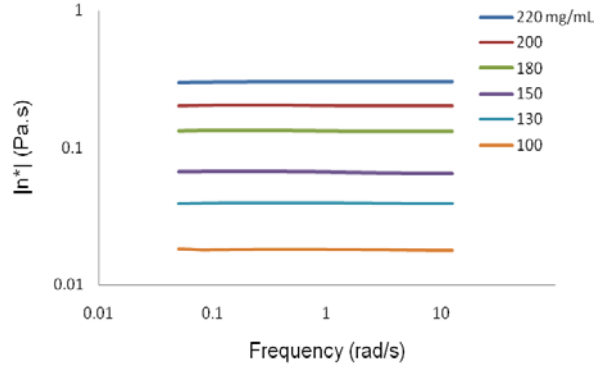

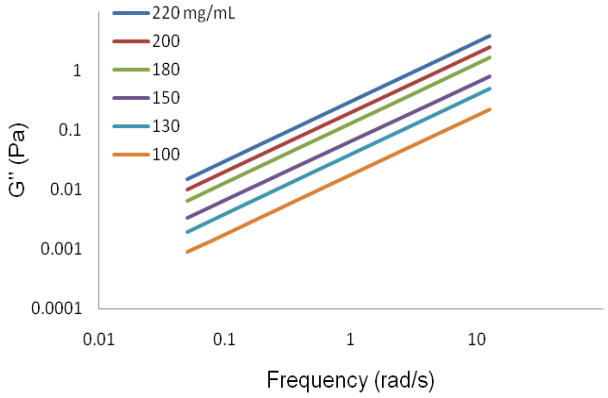

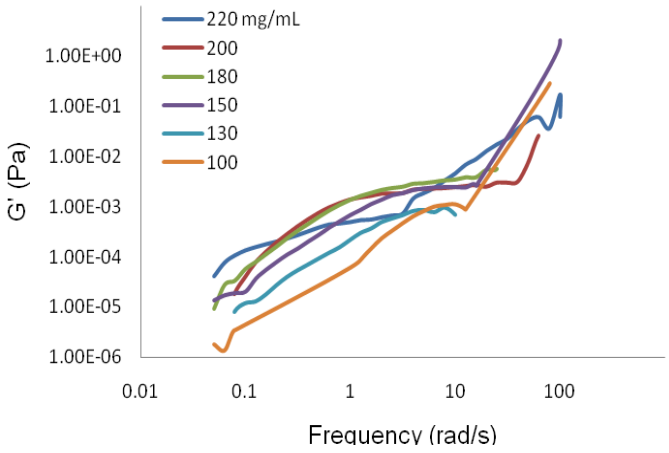

In 2:1 DMAc/THF:

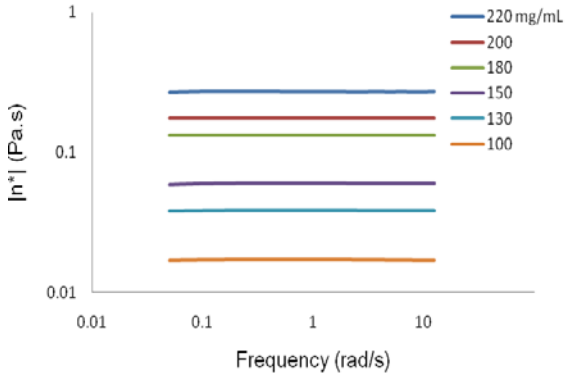

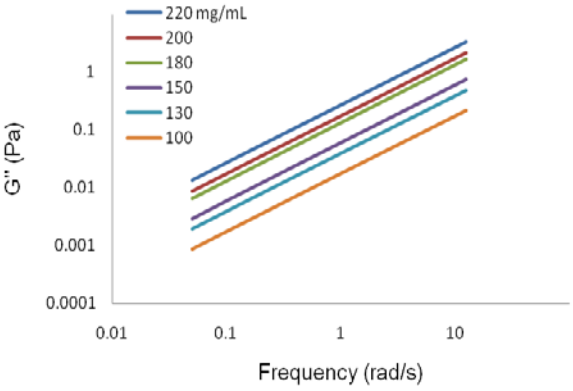

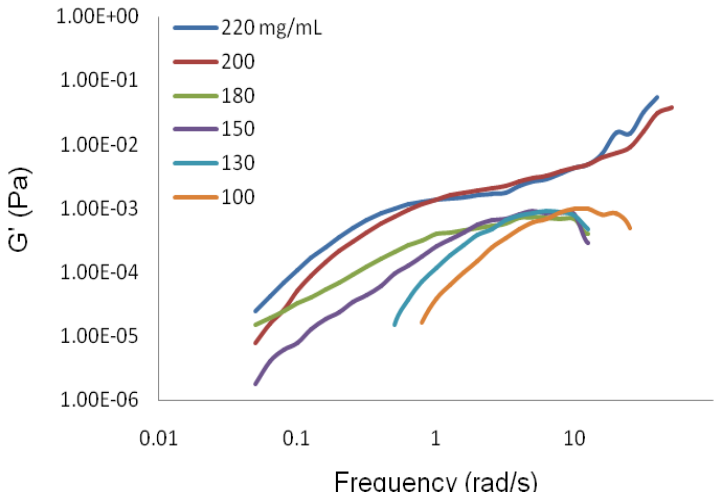

❖ **Ultem 1010 compared over solvent ratio**
100 mg/mL:

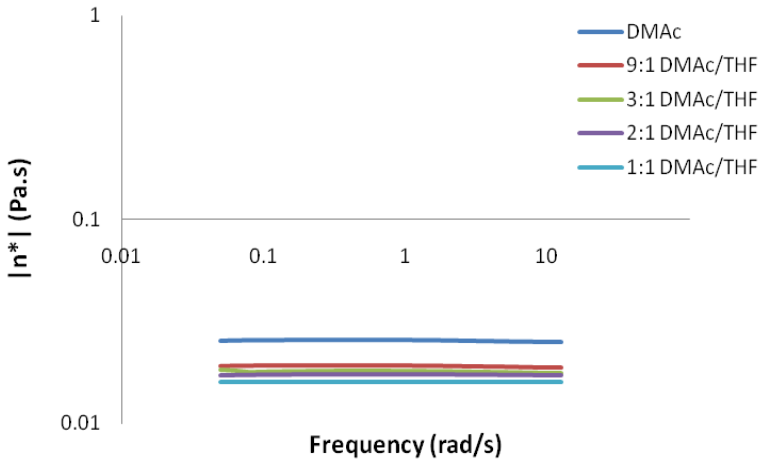

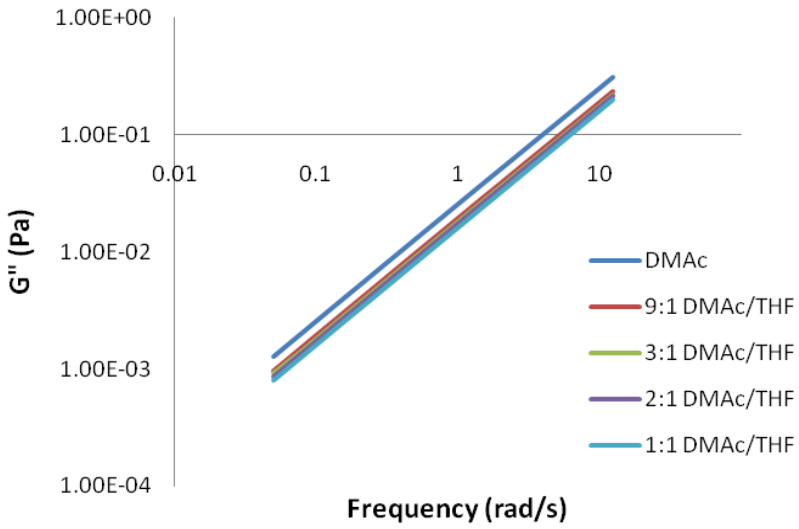
1.00E+00
1.00E-01
1.00E-02
1.00E-03
1.00E-04
0.01
0.1
1
10
G'' (Pa)
Frequency (rad/s)
DMAc
9:1 DMAc/THF
3:1 DMAc/THF
2:1 DMAc/THF
1:1 DMAc/THF

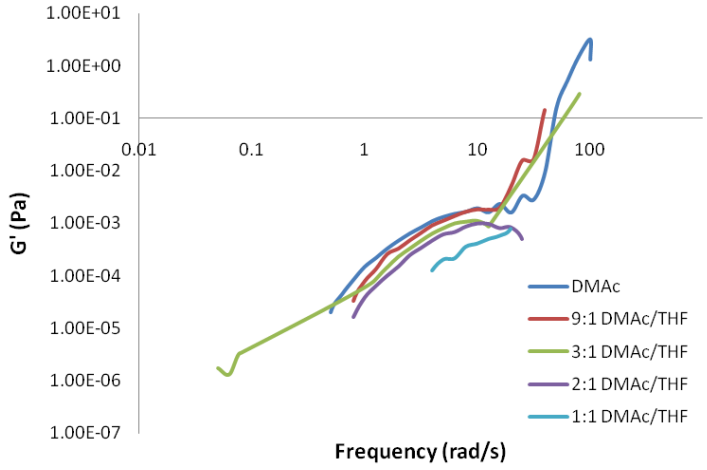
1.00E+01
1.00E+00
1.00E-01
1.00E-02
1.00E-03
1.00E-04
1.00E-05
1.00E-06
1.00E-07
0.01
0.1
1
10
100
G' (Pa)
Frequency (rad/s)
DMAc
9:1 DMAc/THF
3:1 DMAc/THF
2:1 DMAc/THF
1:1 DMAc/THF

130 mg/mL:

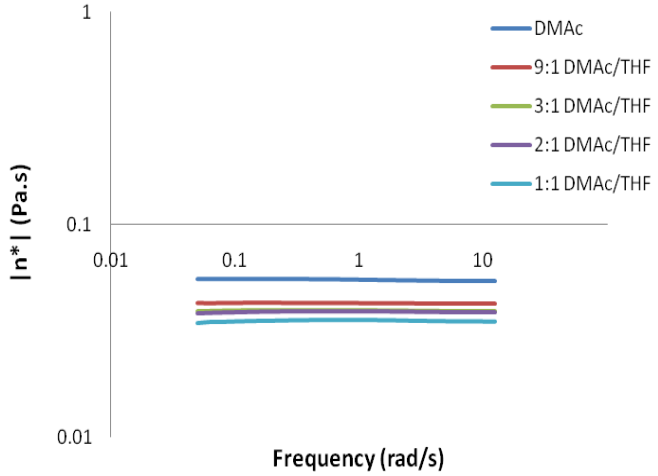
1
0.1
0.01
0.01
0.1
1
10
|n*| (Pa.s)
Frequency (rad/s)
DMAc
9:1 DMAc/THF
3:1 DMAc/THF
2:1 DMAc/THF
1:1 DMAc/THF

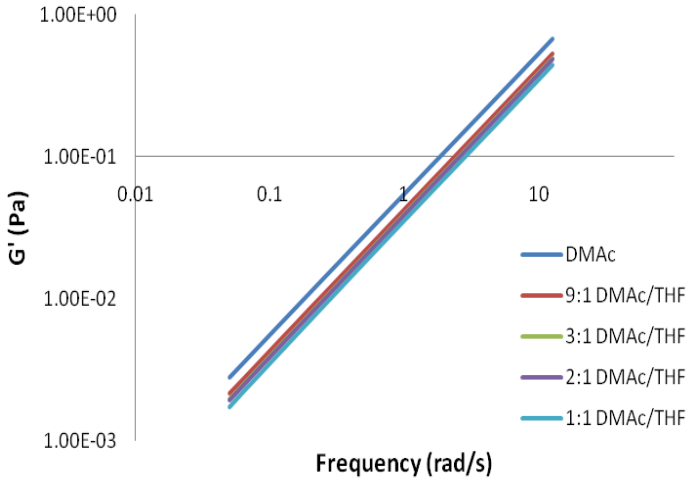
1.00E+00
1.00E-01
1.00E-02
1.00E-03
0.01
0.1
1
10
G' (Pa)
Frequency (rad/s)
DMAc
9:1 DMAc/THF
3:1 DMAc/THF
2:1 DMAc/THF
1:1 DMAc/THF

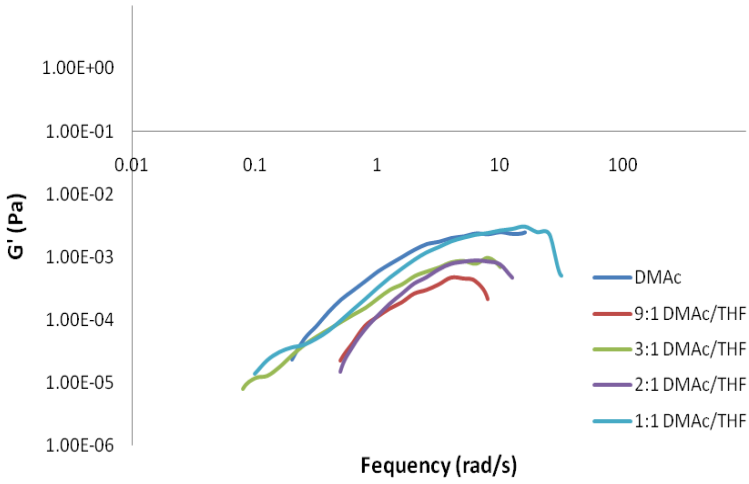
1.00E+00
1.00E-01
1.00E-02
1.00E-03
1.00E-04
1.00E-05
1.00E-06
0.01
0.1
1
10
100
G' (Pa)
Fequency (rad/s)
DMAc
9:1 DMAc/THF
3:1 DMAc/THF
2:1 DMAc/THF
1:1 DMAc/THF

150 mg/mL:

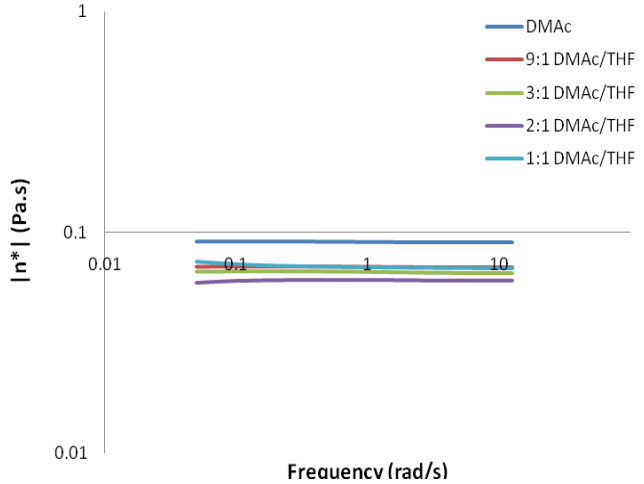
1
0.1
0.01
|n*| (Pa.s)
0.01
0.1
1
10
Frequency (rad/s)
DMAc
9:1 DMAc/THF
3:1 DMAc/THF
2:1 DMAc/THF
1:1 DMAc/THF

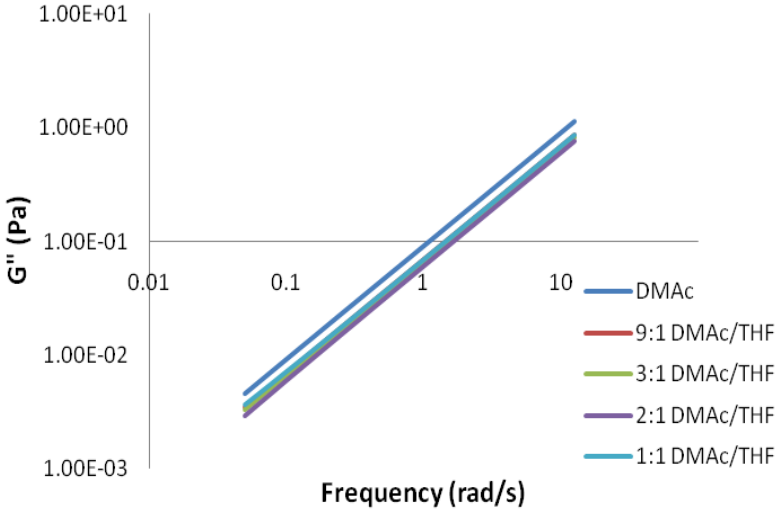
1.00E+01
1.00E+00
1.00E-01
1.00E-02
1.00E-03
G'' (Pa)
0.01
0.1
1
10
Frequency (rad/s)
DMAc
9:1 DMAc/THF
3:1 DMAc/THF
2:1 DMAc/THF
1:1 DMAc/THF

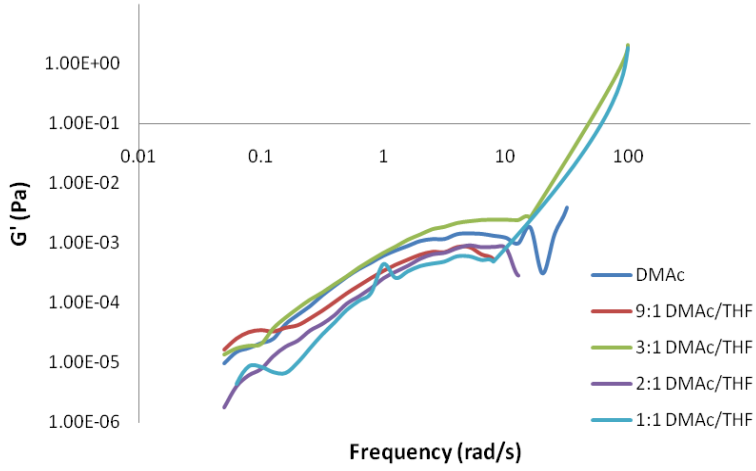
1.00E+00
1.00E-01
1.00E-02
1.00E-03
1.00E-04
1.00E-05
1.00E-06
G' (Pa)
0.01
0.1
1
10
100
Frequency (rad/s)
DMAc
9:1 DMAc/THF
3:1 DMAc/THF
2:1 DMAc/THF
1:1 DMAc/THF

180 mg/mL:

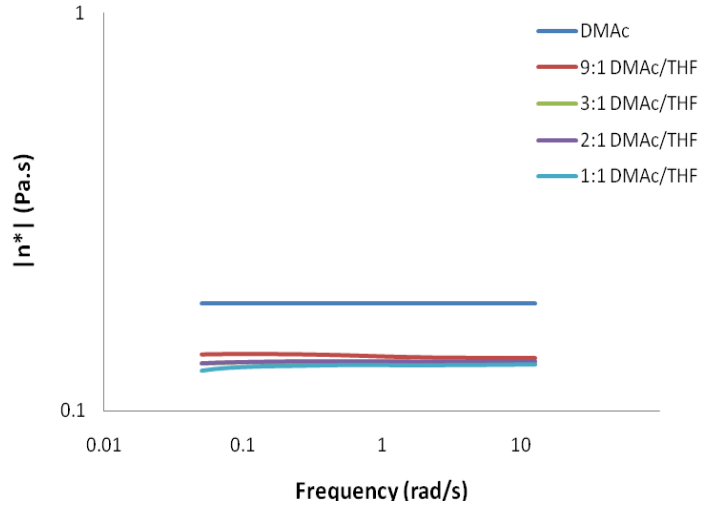
1
0.1
|n*| (Pa.s)
0.01
0.1
1
10
Frequency (rad/s)
DMAc
9:1 DMAc/THF
3:1 DMAc/THF
2:1 DMAc/THF
1:1 DMAc/THF

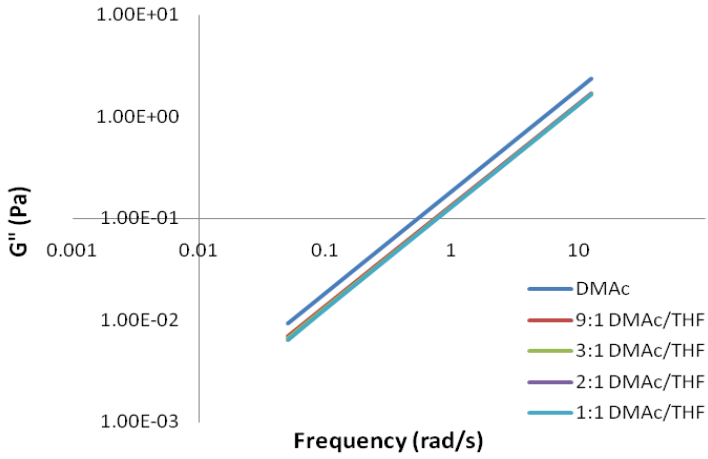
1.00E+01
1.00E+00
1.00E-01
1.00E-02
1.00E-03
G'' (Pa)
0.001
0.01
0.1
1
10
Frequency (rad/s)
DMAc
9:1 DMAc/THF
3:1 DMAc/THF
2:1 DMAc/THF
1:1 DMAc/THF

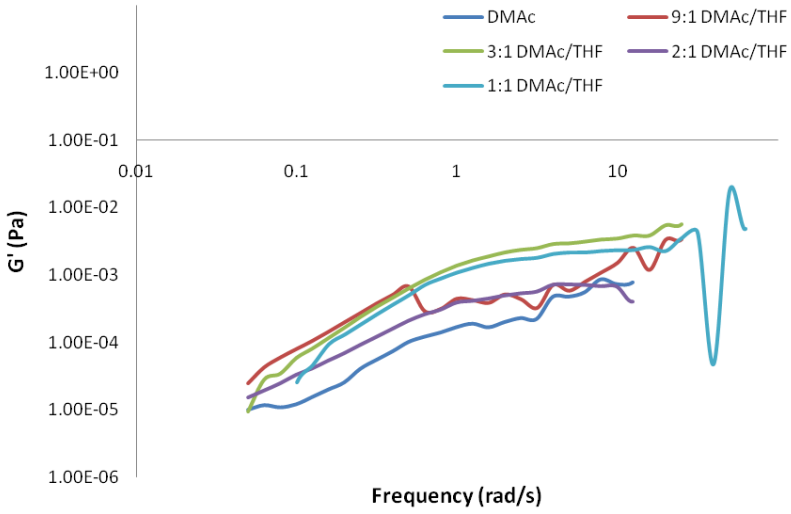
DMAc
9:1 DMAc/THF
3:1 DMAc/THF
2:1 DMAc/THF
1:1 DMAc/THF
1.00E+00
1.00E-01
1.00E-02
1.00E-03
1.00E-04
1.00E-05
1.00E-06
G' (Pa)
0.01
0.1
1
10
Frequency (rad/s)

200 mg/mL:

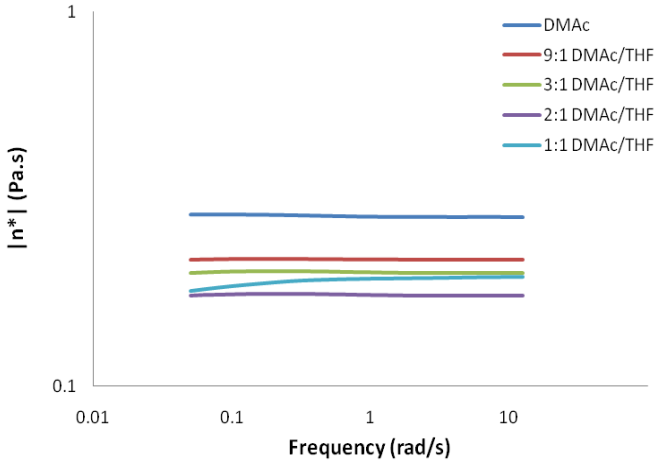
1
0.1
|n*| (Pa.s)
0.01
0.1
1
10
Frequency (rad/s)
DMAc
9:1 DMAc/THF
3:1 DMAc/THF
2:1 DMAc/THF
1:1 DMAc/THF

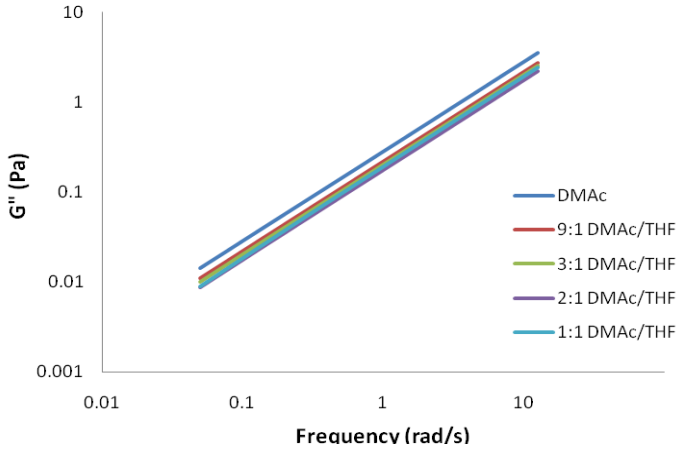
10
1
0.1
0.01
0.001
G'' (Pa)
0.01
0.1
1
10
Frequency (rad/s)
DMAc
9:1 DMAc/THF
3:1 DMAc/THF
2:1 DMAc/THF
1:1 DMAc/THF

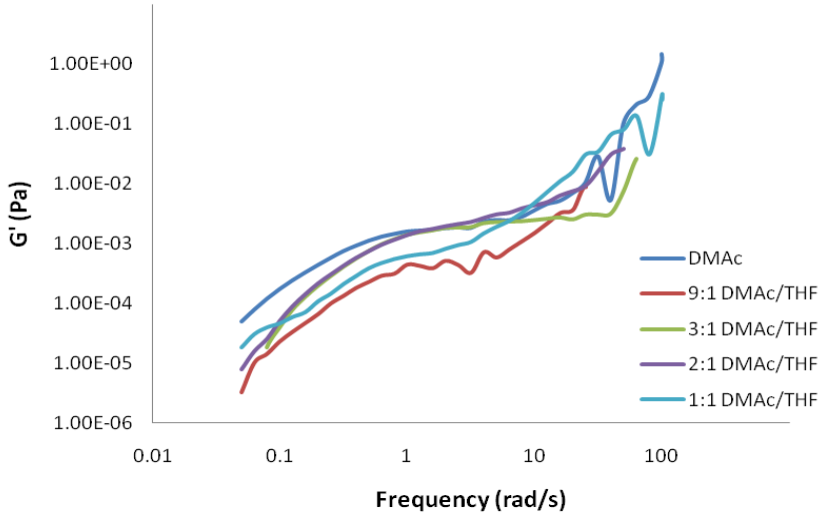
1.00E+00
1.00E-01
1.00E-02
1.00E-03
1.00E-04
1.00E-05
1.00E-06
G' (Pa)
0.01
0.1
1
10
100
Frequency (rad/s)
DMAc
9:1 DMAc/THF
3:1 DMAc/THF
2:1 DMAc/THF
1:1 DMAc/THF

220 mg/mL:

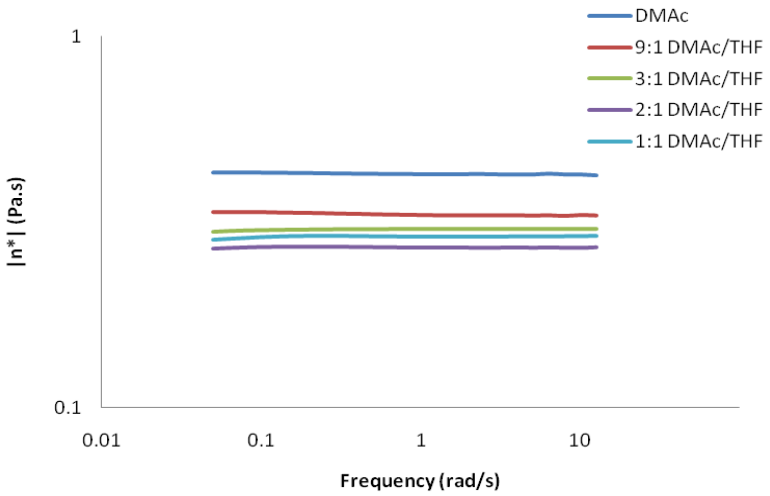
DMAc
9:1 DMAc/THF
3:1 DMAc/THF
2:1 DMAc/THF
1:1 DMAc/THF
|n*| (Pa.s)
1
0.1
0.01
0.1
1
10
Frequency (rad/s)

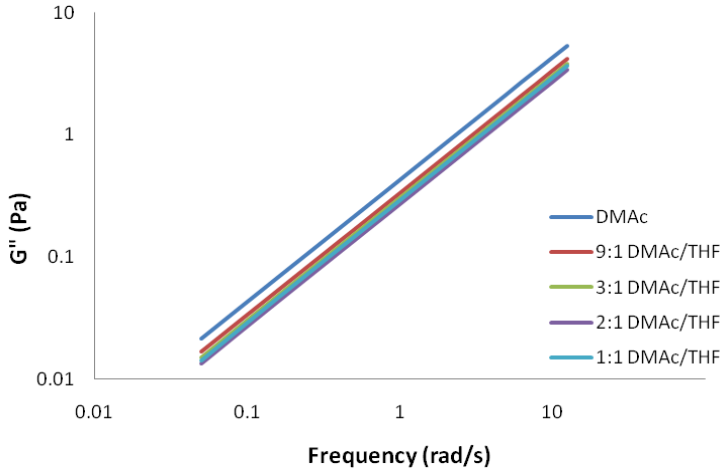
G'' (Pa)
10
1
0.1
0.01
0.01
0.1
1
10
Frequency (rad/s)
DMAc
9:1 DMAc/THF
3:1 DMAc/THF
2:1 DMAc/THF
1:1 DMAc/THF

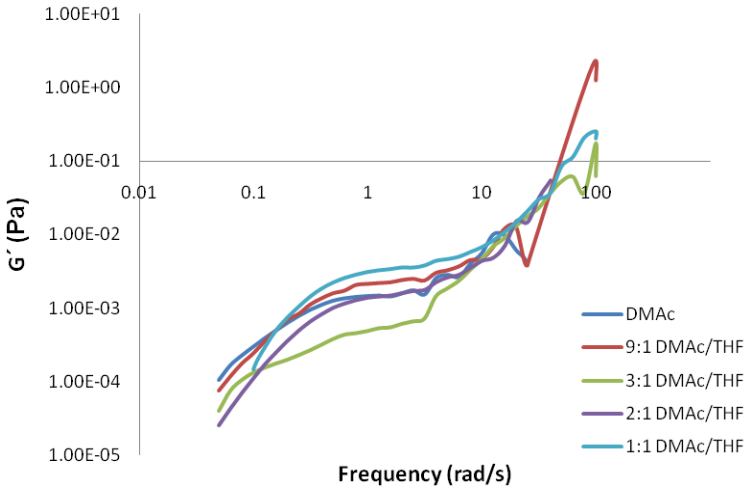
G´ (Pa)
1.00E+01
1.00E+00
1.00E-01
1.00E-02
1.00E-03
1.00E-04
1.00E-05
0.01
0.1
1
10
100
Frequency (rad/s)
DMAc
9:1 DMAc/THF
3:1 DMAc/THF
2:1 DMAc/THF
1:1 DMAc/THF

❖ Complex viscosities, loss moduli and storage moduli of Ultem 1000 solutions In DMAc:

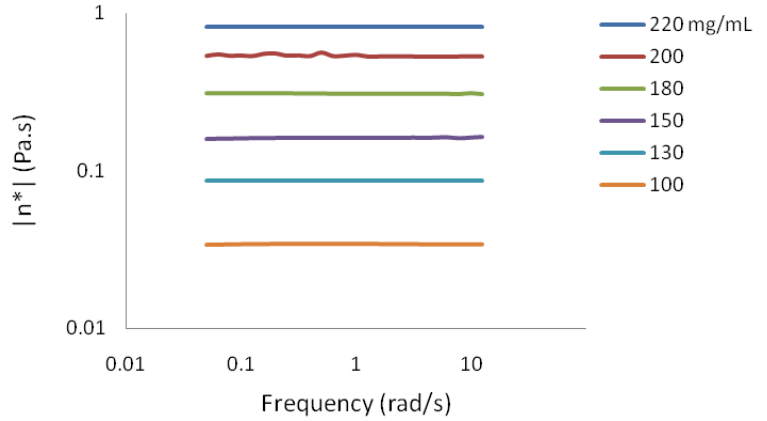

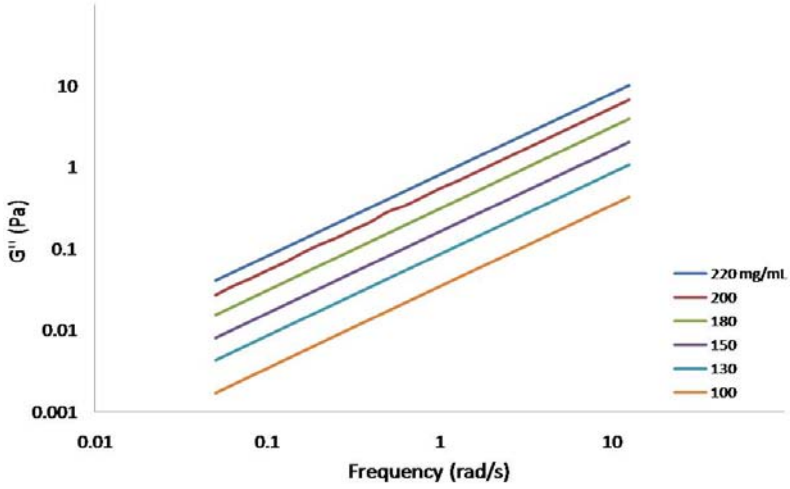

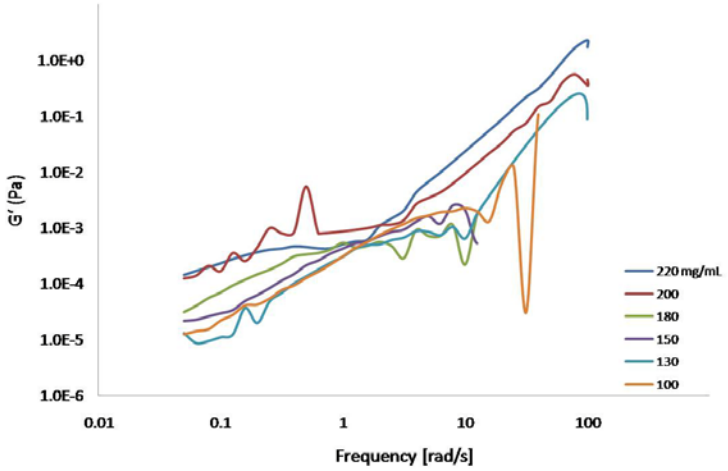

In 9:1 DMAc/THF:

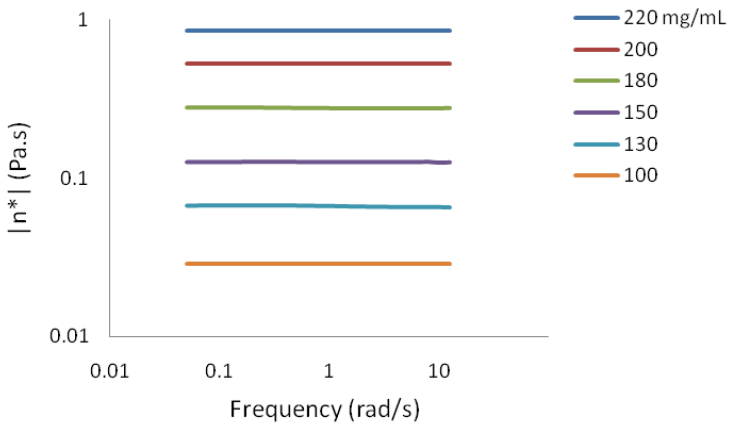

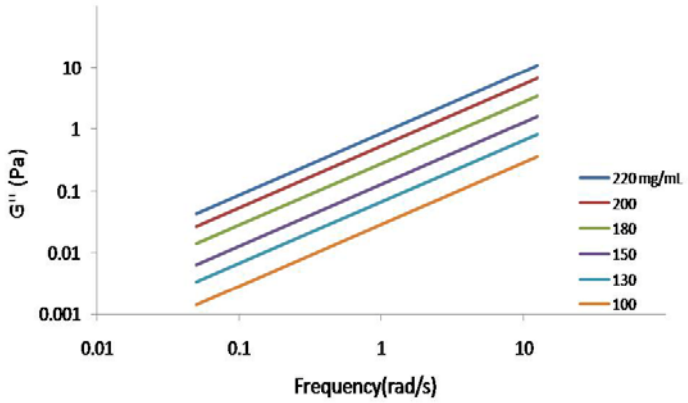

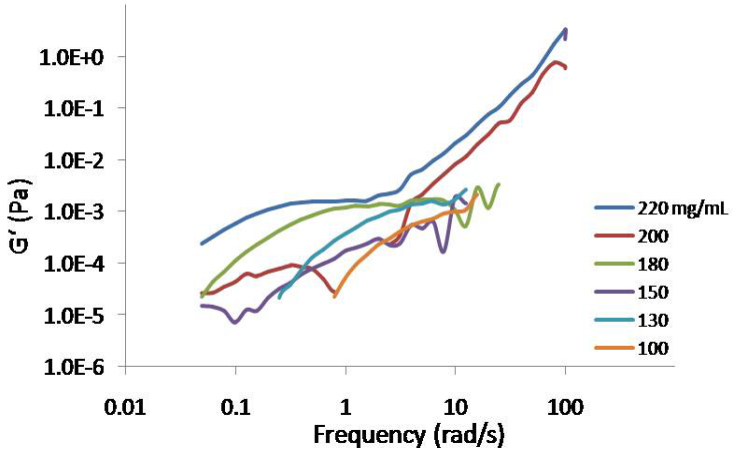

In 3:1 DMAc/THF:

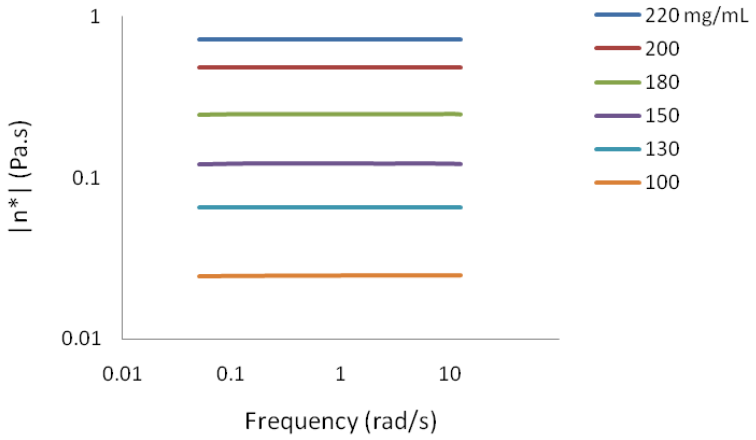

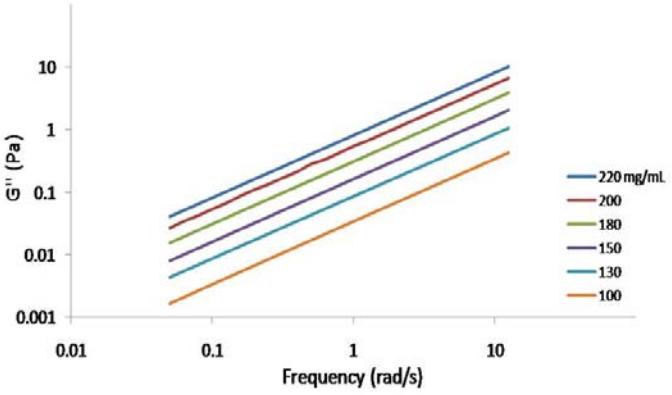

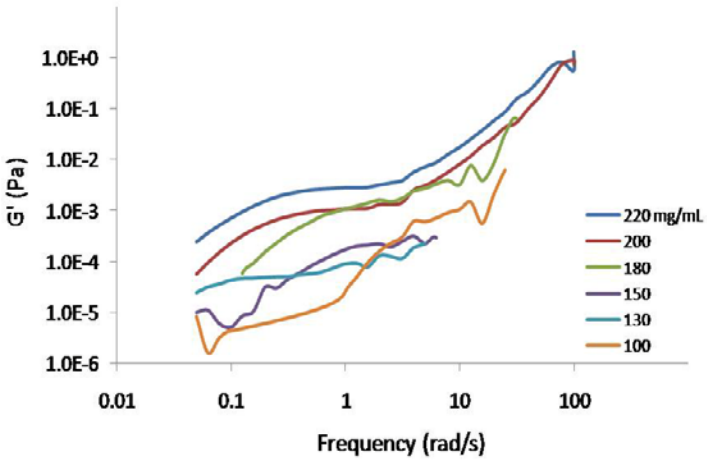

In 2:1 DMAc/THF:

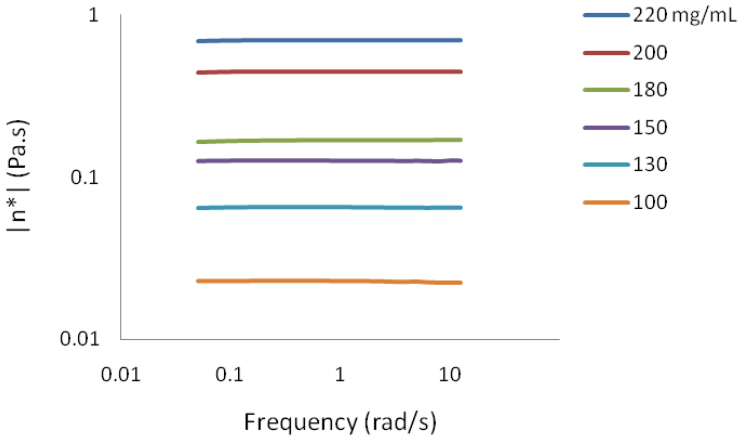

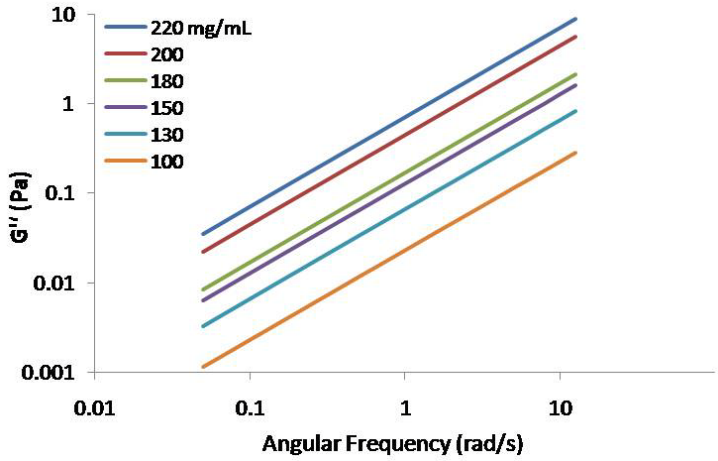

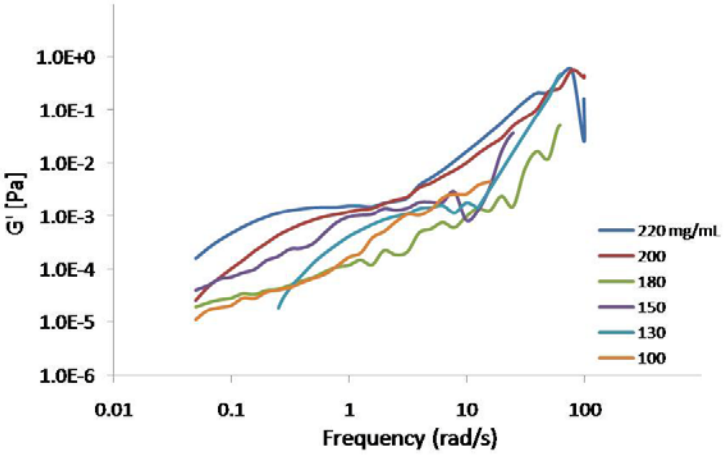

Comparison of measurements with sealed geometry and unsealed geometry

Results from the unsealed and sealed geometries revealed very similar results. However, the sealed geometry was able to more accurately measure viscosity due to the geometry's ability to prevent THF from evaporating out of the system. Included in this section are data comparisons which conclude that relationships between PEI concentrations as well as solvent ratios are quite similar with both geometries. Values from the sealed geometry were higher in magnitude due to an extended period, approximately one week between dissolution and measurement, as well as, vials being opened more than once to retrieve solution. Samples measured with the unsealed geometry were measured within two days of dissolution. All samples tested contained Ultem 1000.

- Comparison of solution measurements at varied PEI content
  - Closed symbols: sealed geometry
  - Open symbols: unsealed geometry

Complex Viscosity:

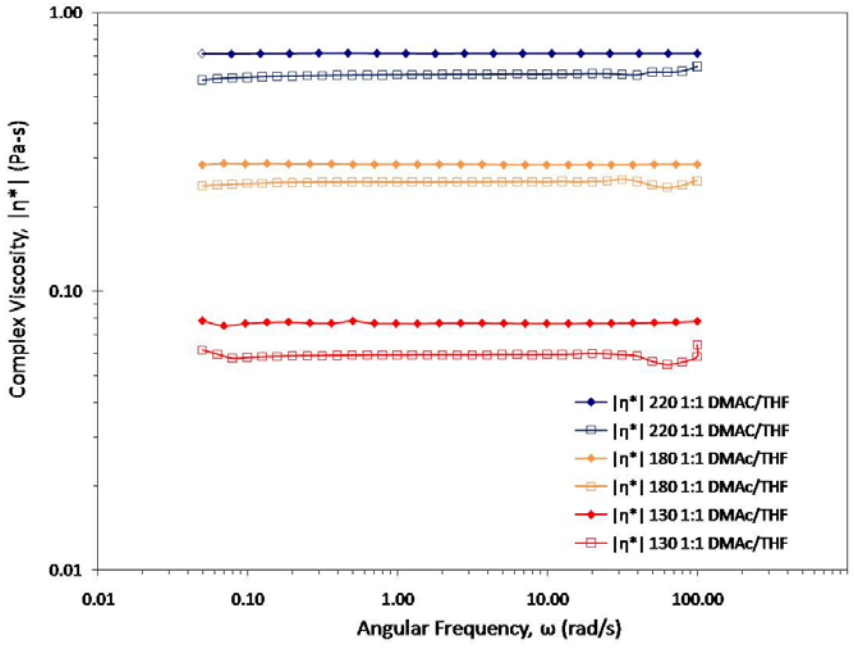

Loss Modulus:

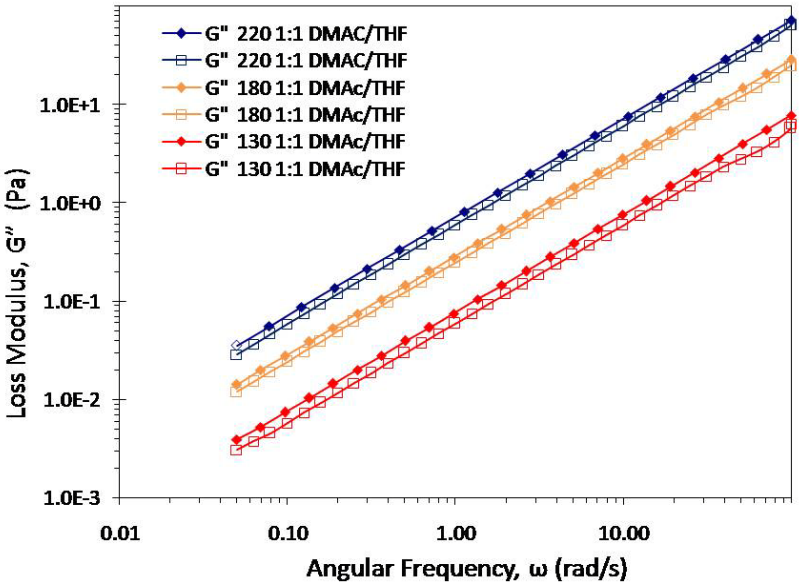

Storage Modulus:

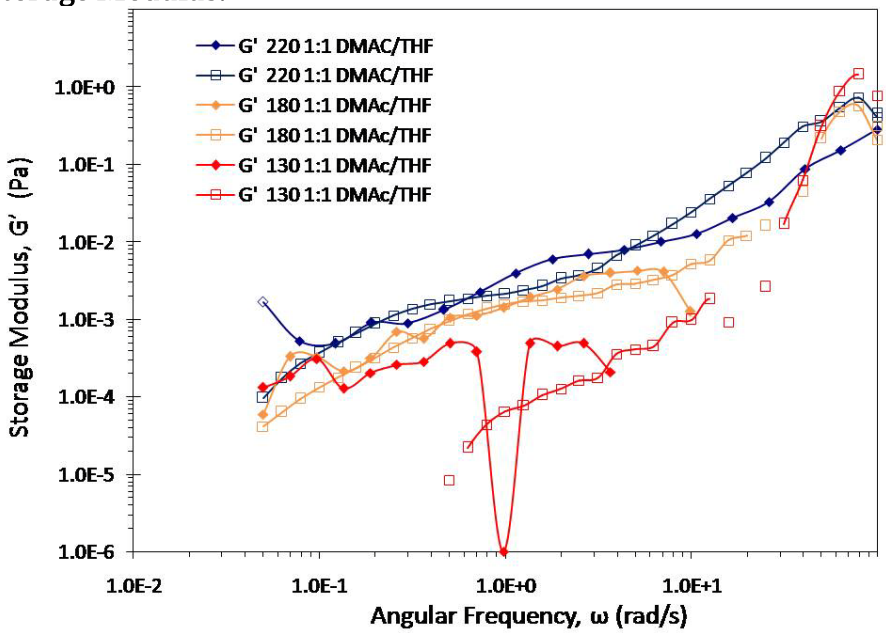

❖ **Comparison of measurements at varied solvent ratio (Ultem 1000)**

Loss Modulus:

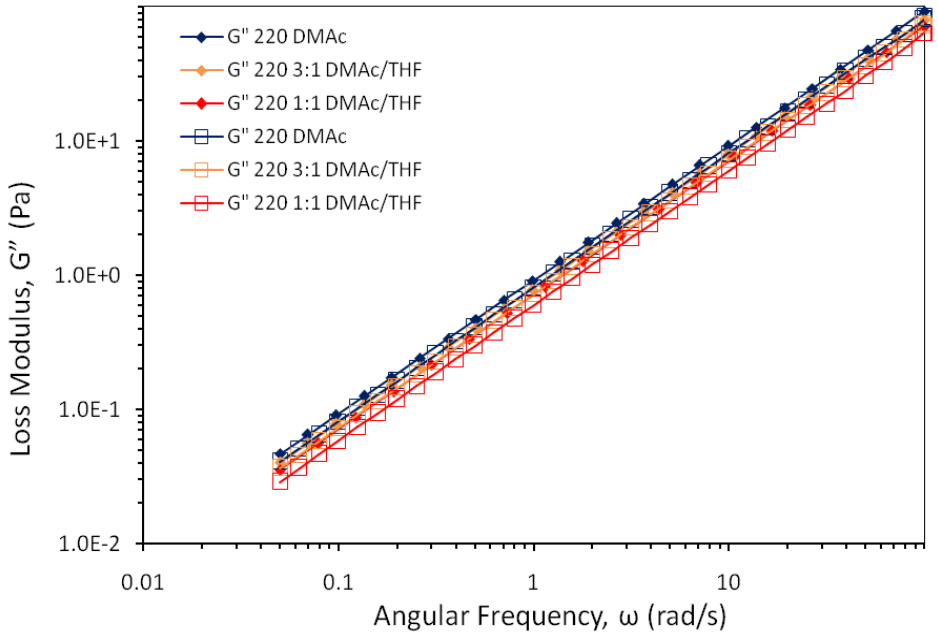

Storage Modulus:

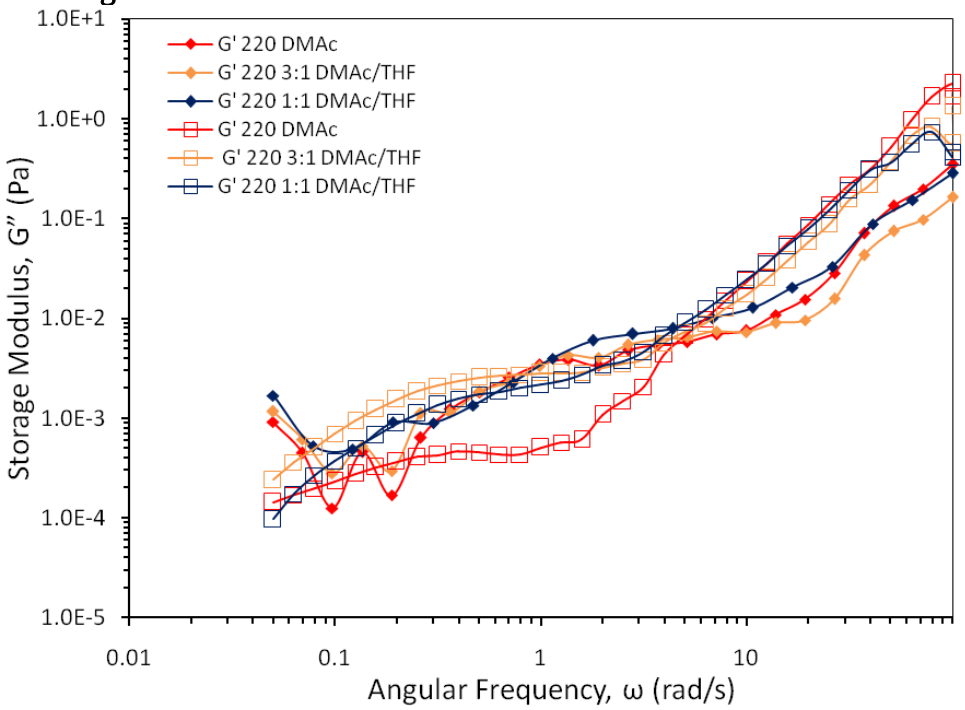

- Comparison of geometries with individual samples
  - Blue data is from sealed geometry on the Anton Paar rheometer
  - Orange data is from unsealed geometry on the AR2000 rheometer

220 mg/mL in 1:1 DMAc/THF:

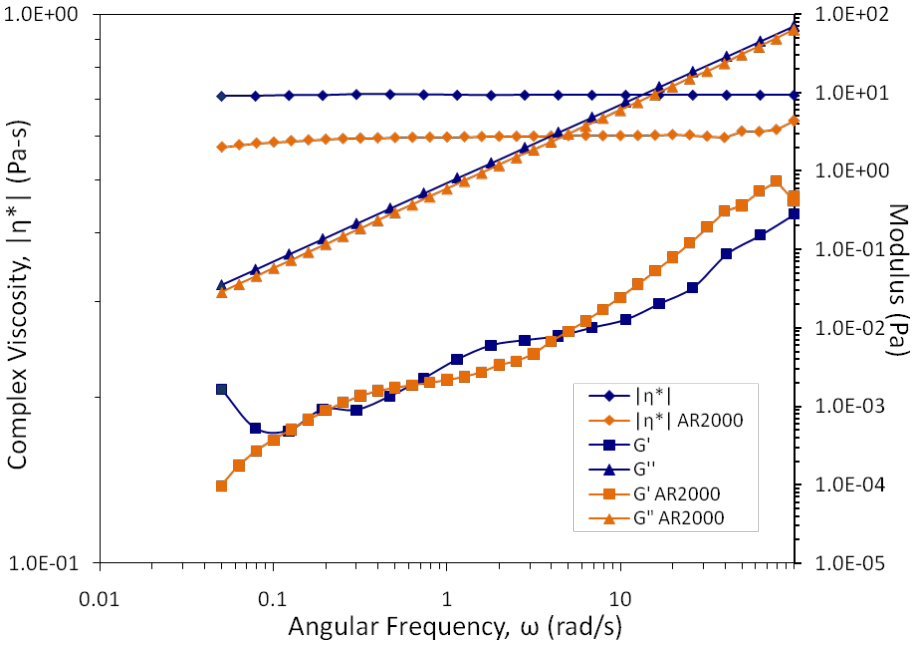

180 mg/mL in 1:1 DMAc/THF:

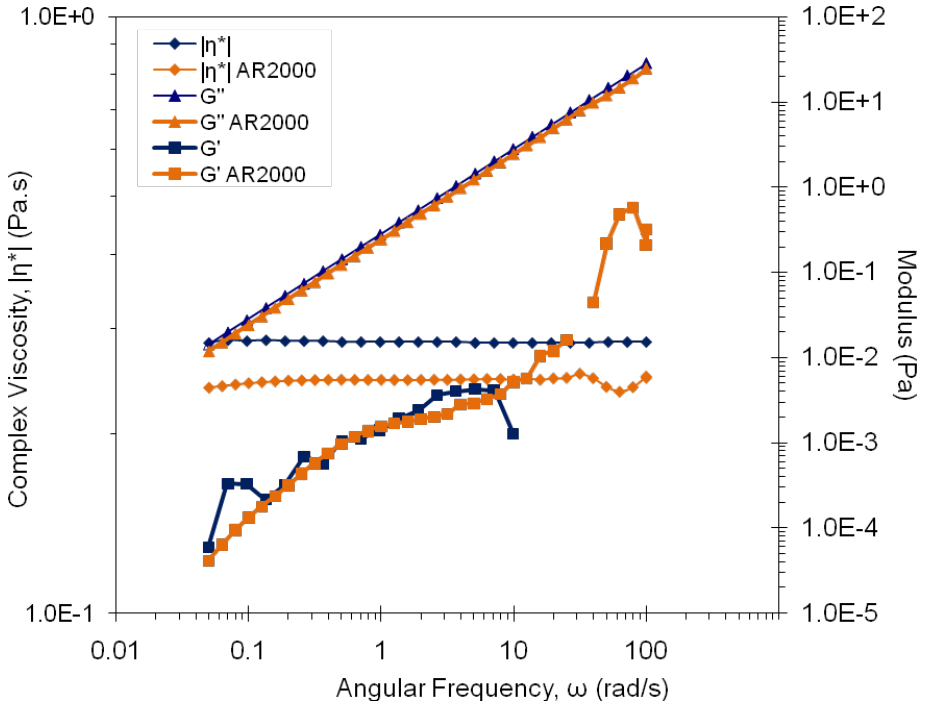

130 mg/mL in 1:1 DMAc/THF:

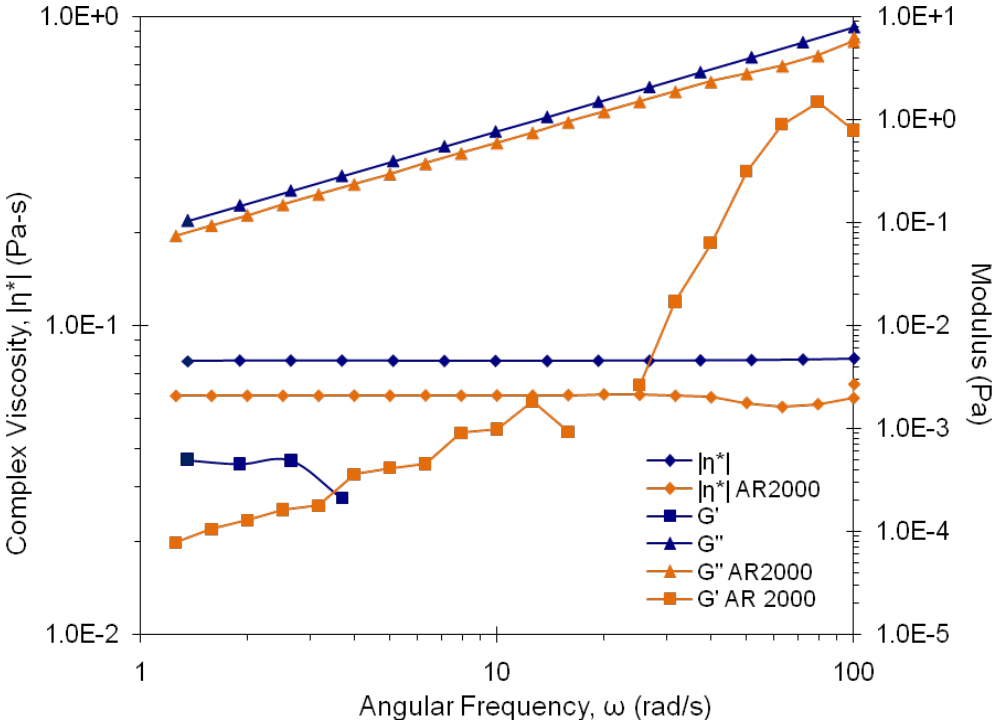

220 mg/mL in 3:1 DMAc/THF:

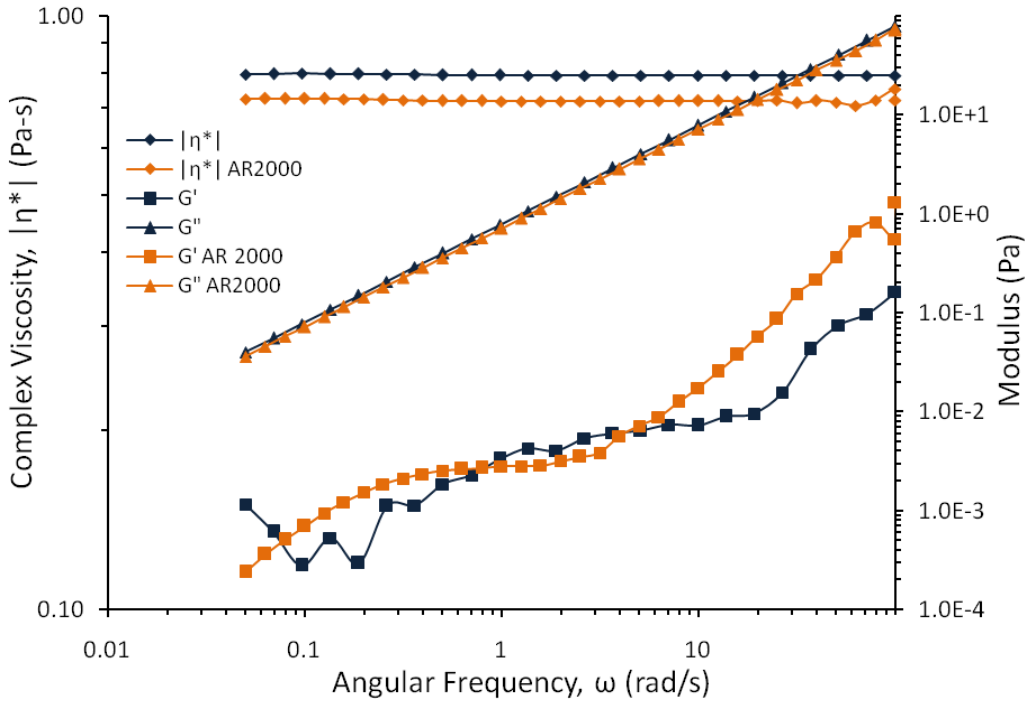

220 mg/mL in DMAc:

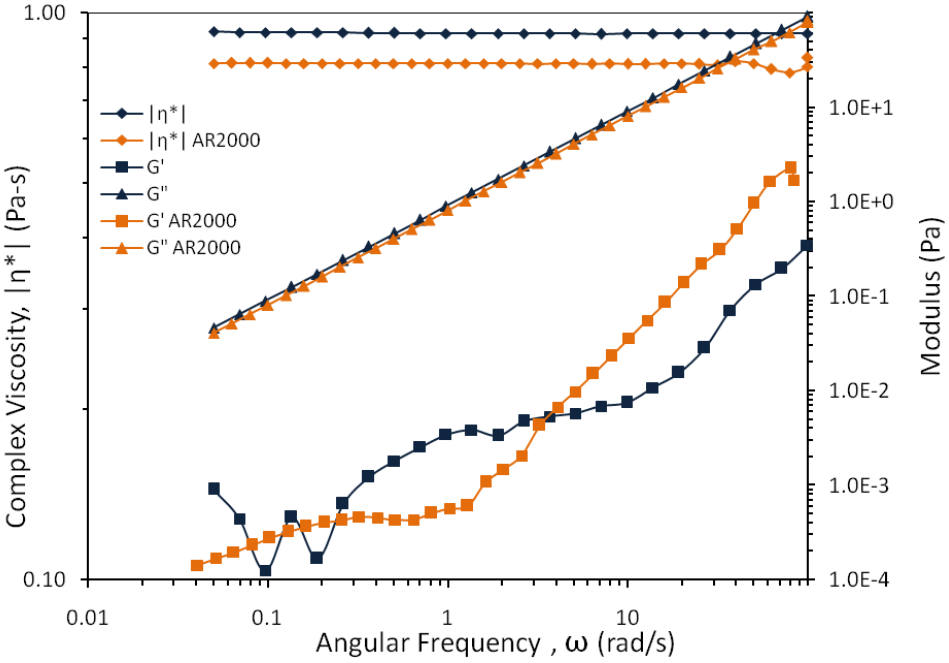

REFERENCES

(1) Belana, J.; Canadas, J. C.; Diego, J. A.; Mudarra, M.; Diaz-Calleja, R.; Friederichs, S.; Jaimes, C.; Sanchis, M. J. *Polym. Int.* **1998**, *46*, 11-19.

(2) Relles, H. M. *Comtemp. Top. Polym. Sci.* **1984**, *5*, 261-279.

(3) Choi, S. S.; Lee, S. G.; Joo, C. W.; Im, S. S.; Kim, S. H. *J. Mater. Sci.* **2004**, *39*, 1511-1513.

(4) Calleja, R. D.; Friederichs, S.; Jaimes, C.; Sanchis, M. J.; Belana, J.; Canadas, J. C.; Diego, J. A.; Mudarra, M. *Polym. Int.* **1998**, *46*, 20-28.

(5) Xu, Z. K.; Shen, L. Q.; Yang, Q.; Liu, F.; Wang, S. Y.; Xu, Y. Y. *J. Membr. Sci.* **2003**, *223*, 105-118.

(6) Koombhongse, S.; Liu, W. X.; Reneker, D. H. *J. Polym. Sci. Pt. B-Polym. Phys.* **2001**, *39*, 2598-2606.

(7) Han, S. O.; Son, W. K.; Cho, D. W.; Youk, J. H.; Park, W. H. *Polym. Degrad. Stab.* **2004**, *86*, 257-262.

(8) Blythe, A. R.; Bloor, D. *Electrical Properties of Polymers;* Cambridge University Press: New York, 2005.

(9) Hardy, L.; Fritz, A.; Stevenson, I.; Boiteux, G.; Seytre, G.; Schönhals, A. *J. Non-Cryst. Sol.* **2002**, *305*, 174-182.

(10) Morrison, F. A. *Understanding Rheology;* Oxford University Press: New York, 2001.

(11) McKee, M. G.; Wilkes, G. L.; Colby, R. H.; Long, T. E. *Macromolecules* **2004**, *37*, 1760-1767.

(12) Yu, J. H.; Fridrikh, S. V.; Rutledge, G. C. *Polymer* **2006**, *47*, 4789-4797.

(13) Gupta, P.; Elkins, C.; Long, T. E.; Wilkes, G. L. *Polymer* **2005**, *46*, 4799-4810.

(14) Thompson, C. J.; Chase, G. G.; Yarin, A. L.; Reneker, D. H. *Polymer* **2007**, *48*, 6913-6922.

(15) Wannatong, L.; Sirivat, A.; Supaphol, P. *Polym. Int.* **2004**, *53*, 1851-1859.

(16) McCrum, N. G. *Anelastic and dielectric effects in polymeric solids;* Read, B. E. W.,G., Ed.; J. Wiley: New York, 1967.

(17) Termonia, Y. *J. Polym. Sci. Pt. B-Polym. Phys.* **1999**, *37*, 2782-2787.

(18) Theron, S. A.; Zussman, E.; Yarin, A. L. *Polymer* **2004**, *45*, 2017-2030.

(19) Young, R. J.; Lovell, P. A. *Introduction to polymers;* New York : Chapman & Hall: 1991.

(20) White, D. M.; Takekoshi, T.; Williams, F. J.; Relles, H. M.; Donahue, P. E.; Klopfer, H. J.; Loucks, G. R.; Manello, J. S.; Matthews, R. O.; Schluenz, R. W. *J. Polym. Sci. Pol. Chem.* **1981**, *19*, 1635-1658.

(21) Chang, L.; Zhang, Z.; Zhang, H.; Friedrich, K. *Tribol. Int.* **2005**, *38*, 966-973.

(22) Xian, G. J.; Zhang, Z.; Friedrich, K. *J. Appl. Polym. Sci.* **2006**, *101*, 1678-1686.

(23) Yudin, V. E.; Otaigbe, J. U.; Gladchenko, S.; Olson, B. G.; Nazarenko, S.; Korytkova, E. N.; Gusarov, V. V. *Polymer* **2007**, *48*, 1306-1315.

(24) Crevecoeur, G.; Groeninckx, G. *Macromolecules* **1991**, *24*, 1190-1195.

(25) Extrand, C. W.; Bhatt, S.; Monson, L. *J. Mater. Sci.* **2001**, *36*, 4603-4609.

(26) Moon, S. I.; Monson, L. L.; Extrand, C. W. *J. Appl. Polym. Sci.* **2006**, *102*, 2362-2371.

(27) Morgan, A. B.; Gilman, J. W.; Jackson, C. L. *Macromolecules* **2001**, *34*, 2735-2738.

(28) Huang, J. C.; Zhu, Z. K.; Yin, J.; Qian, X. F.; Sun, Y. Y. *Polymer* **2001**, *42*, 873-877.

(29) Liang, Z. M.; Yin, J. *J. Appl. Polym. Sci.* **2003**, *90*, 1857-1863.

(30) Tong, Y. J.; Phang, I. Y.; Huang, J. C.; Shen, L.; Liu, T. X.; He, C. B. *Mat. Res. Innov.* **2005**, *9*, 46-47.

(31) Naskar, A. K.; Edie, D. D. *J. Composite Mater.* **2006**, *40*, 1871-1883.

(32) Runt, J. P.; Fitzgerald, J. J., Eds.; *Dielectric Spectroscopy of Polymeric Materials: Fundamentals and Applications;* American Chemical Society: Washington, D.C., 1997.

(33) Liu, R. X.; Qiao, X. Y.; Chung, T. S. *Chem. Eng. Sci.* **2005**, *60*, 6674-6686.

(34) Khulbe, K. C.; Feng, C. Y.; Hamad, F.; Matsuura, T.; Khayet, A. *J. Membr. Sci.* **2004**, *245*, 191-198.

(35) Ho, W. S. W. *J. Chin. Inst. Chem. Eng.* **2003**, *34*, 75-89.

(36) Feng, C. Y.; Khulbe, K. C.; Chowdhury, G.; Matsuura, T.; Sapkal, V. C. *J. Membr. Sci.* **2001**, *189*, 193-203.

(37) Wang, D. L.; Li, K.; Teo, W. K. *J. Membr. Sci.* **1998**, *138*, 193-201.

(38) Yalof, S.; Zika, K. *CHEMTECH* **1975**, *5*, 682-687.

(39) Kaatze, U.; Feldman, Y. *Meas. Sci. Technol.* **2006**, *17*, R17-R35.

(40) Feldman, Y.; Puzenko, A.; Ryabov, Y. *Chem. Phys.* **2002**, *284*, 139-168.

(41) Ryabov, Y. E.; Feldman, Y.; Shinyashiki, N.; Yagihara, S. *J. Chem. Phys.* **2002**, *116*, 8610-8615.

(42) Schonhals, A.; Kremer, F.; Hofmann, A.; Fischer, E. W.; Schlosser, E. *Phys. Rev. Lett.* **1993**, *70*, 3459-3462.

(43) Miura, N.; Yagihara, S.; Mashimo, S. *J. Appl. Phys.* **2002**, *91*, 4506-4510.

(44) Williams, G. *Chem. Soc. Rev.* **1978**, *7*, 89-131.

(45) Sperling, L. H. *Introduction to Physical Polymer Science;* Wiley-Interscience: Hoboken, NJ, 2006.

(46) Doi, M.; Edwards, S. F. *The Theory of Polymer Dynamics;* Clarendon Press: New York, 1986.

(47) Adachi, K.; Kotaka, T. *Macromolecules* **1988**, *21*, 157-164.

(48) Urakawa, O.; Adachi, K.; Kotaka, T. *Macromolecules* **1993**, *26*, 2042-2049.

(49) Williams, G. *Chem. Rev.* **1972**, *72*, 55-69.

(50) Feldman, Y. D.; Zuev, Y. F.; Polygalov, E. A.; Fedotov, V. D. *Colloid Polym. Sci.* **1992**, *270*, 768-780.

(51) Mopsik, F. I. *Rev. Sci. Instrum.* **1984**, *55*, 79-87.

(52) Garwe, F.; Schonhals, A.; Lockwenz, H.; Beiner, M.; Schroter, K.; Donth, E. *Macromolecules* **1996**, *29*, 247-253.

(53) Schiener, B.; Bohmer, R. *J. Non-Cryst. Solids* **1995**, *182*, 180-185.

(54) Goodwin, A. A.; Simon, G. P. *Polymer* **1996**, *37*, 991-995.

(55) Ngai, K. L.; Roland, C. M. *Macromolecules* **1993**, *26*, 6824-6830.

(56) Moscicki, J. K.; Williams, G.; Aharoni, S. M. *Macromolecules* **1982**, *15*, 642-651.

(57) Wurm, B.; Munsterer, M.; Richardi, J.; Buchner, R.; Barthel, J. *J. Mol. Liq.* **2005**, *119*, 97-106.

(58) Wurm, B.; Baar, C.; Buchner, R.; Barthel, J. *J. Mol. Liq.* **2006**, *127*, 14-20.

(59) Shames, I. H. *Mechanics of fluids;* McGraw-Hill: New York, 1982.

(60) Skelland, A. H. P. *Non-Newtonian flow and heat transfer;* Wiley: New York, 1967.

(61) Aris, R. *Vectors, tensors, and the basic equations of fluid;* Englewood Cliffs, N.J., Prentice-Hall, 1962.

(62) Bird, R. B. *Transport phenomena;* Stewart, W. E., Ed.; J. Wiley: New York, 2002.

(63) Crochet, M. J. *Numerical simulation of non-Newtonian flow;* Davies, A. R., Walters, K., Eds.; Amsterdam; New York: Elsevier, 1984, pp 352.

(64) Barnes, H. A. *A Handbook of Elementary Rheology;* The University of Wales Institute of Non-Newtonian Fluid Mechanics, Department of Mathematics, University of Wales Aberystwyth, Penglais, Aberystwyth, Dyfed, Wales: Aberystwyth, Wales, 2000.

(65) Levenspiel, O. *Engineering flow and heat exchange;* Plenum Press: New York, 1984.

(66) Bird, R. B. *Dynamics of polymeric liquids;* Armstrong, R. C., Ed.; J. Wiley: New York, 1987.

(67) Krieger, I. M.; Maron, S. H. *J. Appl. Phys.* **1954**, *25*, 72-75.

(68) Krieger, I. M.; Elrod, H. *J. Appl. Phys.* **1953**, *24*, 134-139.

(69) Dontula, P.; Macosko, C. W.; Scriven, L. E. *J. Rheol.* **2005**, *49*, 807-818.

(70) Bonnet, A.; Pascault, J. P.; Sautereau, H.; Camberlin, Y. *Macromolecules* **1999**, *32*, 8524-8530.

(71) Frigione, M.; Naddeo, C.; Acierno, D. *J. Polym. Eng.* **1997**, *16*, 217-229.

(72) Tao, Q. S.; Gan, W. J.; Yu, Y. F.; Wang, M. H.; Tang, X. L.; Li, S. J. *Polymer* **2004**, *45*, 3505-3510.

(73) Li, H.; Gan, W. J.; Zhao, L.; Li, S. J. *J. Macromol. Sci. -Pure Appl. Chem.* **2003**, *A40*, 833-846.

(74) Yu, Y. F.; Zhang, Z. C.; Gan, W. J.; Wang, M. H.; Li, S. J. *Ind. Eng. Chem. Res.* **2003**, *42*, 3250-3256.

(75) Cicala, G.; La Spina, R.; Recca, A.; Sturiale, S. *J. Appl. Polym. Sci.* **2006**, *101*, 250-257.

(76) Goodwin, A. A.; Simon, G. P. *Polymer* **1997/5**, *38*, 2363-2370.

(77) Teo, W. E.; Ramakrishna, S. *Nanotechnology* **2006**, *17*, R89-R106.

(78) Huang, Z. M.; Zhang, Y. Z.; Kotaki, M.; Ramakrishna, S. *Composites Sci. Technol.* **2003**, *63*, 2223-2253.

(79) Samatham, R.; Kim, K. J. *Polym. Eng. Sci.* **2006**, *46*, 954-959.

(80) Watanabe, K.; Sumio, S.; Ogata, S. *J. Fluids Eng.* **2006**, *128*, 95-100.

(81) Carroll, C. P.; Joo, Y. L. *Phys. Fluids* **2006**, *18*, 053102.

(82) Sengwa, R. J.; Sankha, S. *Polymer* **2007**, *48*, 2737-2744.

(83) Bello, A.; Laredo, E.; Grimau, M. *Physical Rev. B* **1999**, *60*, 12764-12774.

(84) Jayaraman, K.; Kotaki, M.; Zhang, Y. Z.; Mo, X. M.; Ramakrishna, S. *J. Nanosci. Nanotech.* **2004**, *4*, 52-65.

(85) Subbiah, T.; Bhat, G. S.; Tock, R. W.; Pararneswaran, S.; Ramkumar, S. S. *J. Appl. Polym. Sci.* **2005**, *96*, 557-569.

(86) Shenoy, S. L.; Bates, W. D.; Frisch H. L.; Wnek, G.E. *Polymer* **2005**, 46, 3372-3384.

(87) Zong, X.; Kim, K.; Fang, D.; Ran, S.; Hsiao, B. S.; Chu, B. *Polymer* **2002**, 43, 4403-4412.

(89) Magda, J. J.; Fredrickson, G. H.; Larson, R. G.; Helfand, E. *Macromolecules* **1988**, *21*, 726-732.

(90) Shin, D. S.; Lee, S. G.; Lyoo, W. S. *Polym. Polym. Compos.* **2006**, *14*, 755-765.